ABSTRACT

Title of Document: **DEPARTURE PHASE ABORTS FOR MANNED MARS MISSIONS**

Adam F. Dissel
Doctor of Philosophy, 2007

Directed By: Professor Mark J. Lewis
Department of Aerospace Engineering

NASA goals are set on resumption of human activity on the Moon and extending manned missions to Mars. Abort options are key elements of any system designed to safeguard human lives and stated requirements stipulate the provision of an abort capability throughout the mission. The present investigation will focus on the formulation and analysis of possible abort modes during the Earth departure phase of manned Mars interplanetary transfers. Though of short duration, the departure phase encompasses a mission timeline where failures have frequently become manifest in historical manned spacecraft necessitating the inclusion of a departure phase abort capability. Investigated abort modes included aborts to atmospheric entry, and to Earth or Moon orbit. Considered interplanetary trajectory types included conjunction, opposition, and free-return trajectory classes. All abort modes were analyzed for aborts initiated at multiple points along each of these possible departure trajectories across all launch opportunities of the fifteen-year Earth-Mars inertial period. The consistently low departure velocities of the conjunction

trajectories facilitated the greatest abort capability. An analysis of Mars transportation architectures was performed to determine the amount of available delta V inherent in each candidate architecture for executing departure aborts. Results indicate that a delta V of at least 4 km/s is required to achieve a continuous departure phase entry abort capability with abort flights less than three weeks duration for all transfer opportunity years. Less demanding transfer years have a corresponding increase in capability. The Earth orbit abort mode does not become widely achievable until more than 6 km/s delta V is provided; a capacity not manifest in any considered architecture. Optimization of the Moon abort mode resulted in slight departure date shifts to achieve improved lunar alignments. The Moon abort mode is only widely achievable for conjunction transfers during the optimum transfer years and delta V values greater than 4 km/s. A lesser delta V potential of 3 km/s is sufficient to enable entry aborts during the least demanding transfer opportunity years. Extensive abort capability is achievable for high delta V capable Mars architectures. Less propulsively capable architectures achieve moderate abort capability during favorable opportunity years.

DEPARTURE PHASE ABORTS FOR MANNED MARS MISSIONS

By

Adam F. Dissel

Dissertation submitted to the Faculty of the Graduate School of the
University of Maryland, College Park, in partial fulfillment
of the requirements for the degree of
Doctor of Philosophy
2007

Advisory Committee:
Professor Mark J. Lewis, Chair
Professor Darryll J. Pines
Associate Professor David Akin
Associate Professor Kenneth Yu
Associate Professor Derek C. Richardson

Dedication

To all the many wonderful members of my family, extended family and friends at school and church who have shown constant interest and sincere encouragement as I traversed this difficult and exciting path. One of the greatest blessings of this undertaking has been the realization of how blessed I am to have such true friends. A greater blessing still is the love and motivation of my one best friend Elizabeth and our children Caleb, Seth, and Kyra.

Acknowledgements

First, I would like to express my deep gratitude to my research advisor Dr. Mark Lewis whose encouragement and advice helped persuade me to remain at the University of Maryland and undertake my doctorate. My four years of graduate school have been extremely rewarding and enjoyable. I would also like to thank the other members of my committee for their direction and suggestions for this work.

I gratefully acknowledge the NASA funding that supported this work. This work was supported by the Space Vehicle Technology Institute under grant NCC3-989 jointly funded by NASA and DOD within the NASA Constellation University Institutes Project with Claudia Meyer as the project manager.

Finally, I would like to thank the rest of the graduate students and staff from the University of Maryland's Space Vehicle Technology Institute for their guidance and friendship. I am particularly indebted to Dr. Ryan Starkey and Joshua Johnson whose patient and professional interactions have greatly benefited both myself and the quality of my research.

Table of Contents

List of Tables

List of Figures

List of Symbols

A	=	constant used by universal variables
a	=	semi-major axis
C	=	universal variables function
c	=	foci separation parameter
DU	=	Solar canonical distance unit
E	=	eccentric anomaly
EDU	=	Earth canonical distance unit
ETU	=	Earth canonical time unit
e	=	eccentricity
$\boldsymbol{h}$	=	specific angular momentum vector
h	=	specific angular momentum
i	=	inclination
F	=	hyperbolic eccentric anomaly
f	=	linear combination function
G	=	universal gravitation constant
g	=	linear combination function
JD	=	Julian date
LDU	=	Moon canonical distance unit
LTU	=	Moon canonical time unit
M	=	mean anomaly
MDU	=	Mars canonical distance unit
MTU	=	Mars canonical time unit
m	=	mass
P	=	orbital period
p	=	semi-latus rectum or parameter
$\boldsymbol{R}$	=	Heliocentric position vector
R	=	Heliocentric position magnitude
$\boldsymbol{r}$	=	Geocentric position vector
r	=	Geocentric position magnitude
ROT	=	rotation matrix
S	=	universal variables function
t	=	time variable
TOF	=	time of flight
TR	=	transformation matrix
TT	=	J2000 epoch variable
TU	=	Solar canonical time unit
$\boldsymbol{V}$	=	Heliocentric velocity vector
V	=	Heliocentric velocity magnitude
$\boldsymbol{v}$	=	Geocentric velocity vector
v	=	Geocentric velocity magnitude
Δi	=	inclination change
$\Delta \boldsymbol{V}$	=	Heliocentric velocity change vector

ΔV	=	Heliocentric velocity change magnitude
$\Delta \boldsymbol{v}$	=	Geoocentric velocity change vector
Δv	=	Geocentric velocity change magnitude
x	=	independent universal variable
y	=	auxiliary variable used by universal variables
z	=	iterated universal variable
ξ	=	specific mechanical energy
ε	=	obliquity of the ecliptic
θ	=	transfer angle
Υ	=	vernal equinox direction
μ	=	gravitational parameter
Ω	=	right ascension of the ascending node
υ	=	true anomaly
λ	=	mean longitude
ϕ	=	flight path angle
ω	=	argument of periapse
$\tilde{\omega}$	=	longitude of periapse

Subscripts

A	=	condition at apoapse
Abort	=	refers to abort condition
Arr	=	condition at Mars arrival
C	=	condition of circular orbit
Dep	=	condition at Earth departure
E	=	refers to Earth
Est	=	estimated condition
Ex	=	condition at Earth sphere of influence exit
En	=	condition at Mars sphere of influence entrance
Final	=	final condition
IJK	=	Geocentric coordinates
ISS	=	refers to International Space Station
Initial	=	initial condition
Leo	=	low Earth orbit
M	=	refers to Mars
Moon	=	refers to Moon
P	=	condition at periapse
PQW	=	Perifocal coordinates
Plane	=	referring to the orbital plane(s)
S	=	refers to the spacecraft
Soi	=	refers to sphere of influence
Sun	=	refers to the sun
Syn	=	synodic period designation
Tot	=	total of preceding variable
Trans	=	refers to transfer trajectory
XYZ	=	Heliocentric coordinates
∞	=	condition at infinity, usually taken at sphere of influence

"The stringent requirement for crew safety dictates the necessity of as much or more contingency planning for abort situations as is provided for the nominal mission."

Apollo Experience Report[1]
Manned Spacecraft Center
National Aeronautics and Space Administration
June 1972

Chapter 1. Introduction

1.1. Moon-Mars Exploration Initiative

On January 14th, 2004, President George W. Bush announced an expansive new vision[2] for manned and robotic space exploration. Speaking from NASA headquarters, the President charged NASA with a new mandate to resume manned exploration missions beyond Earth orbit. "Today I announce a new plan to explore space and extend a human presence across our solar system. We will begin the effort quickly, using existing programs and personnel. We'll make steady progress, one mission, one voyage, one landing at a time." The efforts of the space agency were committed towards the attainment of several increasingly ambitious goals including:

- Completion of the International Space Station (ISS) by 2010.
- Development of a new spacecraft, the Crew Exploration Vehicle (CEV), by 2008, with first manned missions planned no later than 2014.
- Return to the Moon by 2020 and its use as a launching point for future missions.
- Human missions to Mars and beyond.

Encapsulated within these objectives is a shift in exploration focus from that of term-limited programs to one of continual emphasis and progress. As advocated by future NASA administrator Michael Griffin in testimony[3] before Congress, space activities will become a "way of life" instead of isolated episodic programs. As validation of such emphasis, Griffin stated on that occasion that, "The single overarching goal of human space flight is the human settlement of the solar system, and eventually

beyond. I can think of no lesser purpose sufficient to justify the difficulty of the enterprise, and no greater purpose is possible." With the announcement of the new Moon and Mars exploration initiatives, mankind is laying the foundation for its expansion into the final frontier. As affirmed by President Bush[2], "We do not know where this journey will end. Yet we know this: Human beings are headed into the cosmos."

The exploration initiative's focus for the next several decades is fixed on the resumption of human activity on Earth's moon, and the expansion of manned missions to the planet Mars. The Moon is viewed by some as the logical stepping stone into space, a place where new systems and experiences may be validated in a near-Earth setting. Mars is a locale of immense scientific interest and will be the proving ground for manned operations far removed from the haven of the home planet.

Powering the way towards the achievement of these early endeavors, NASA has envisioned two new launch vehicles derived from technologies and hardware used for the Space Shuttle program. The planned crew launcher has been designated as the Ares-I and consists of an elongated Shuttle solid rocket booster (SRB), and an upper-stage, atop which will sit the new crew exploration vehicle. The Ares-I (Figure 1.1) will be responsible solely for the transport of human crews to space abort the CEV. Mission cargo for the exploration initiative will be ferried to space aboard a heavy-lift cargo launcher, the Ares-V (Figure 1.2). The Ares-V will make use two of the enhanced SRB as well as the Shuttle external tank combined with a new upper-

stage. These two vehicles provide the lift capability necessary to resume lunar flights and landings and enable most candidate Mars architectures.

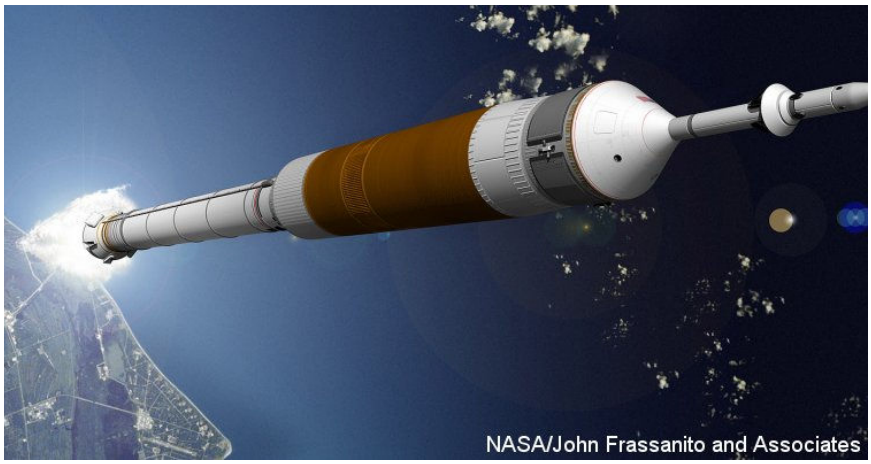

Figure 1.1 Ares-I Crew Launch Vehicle

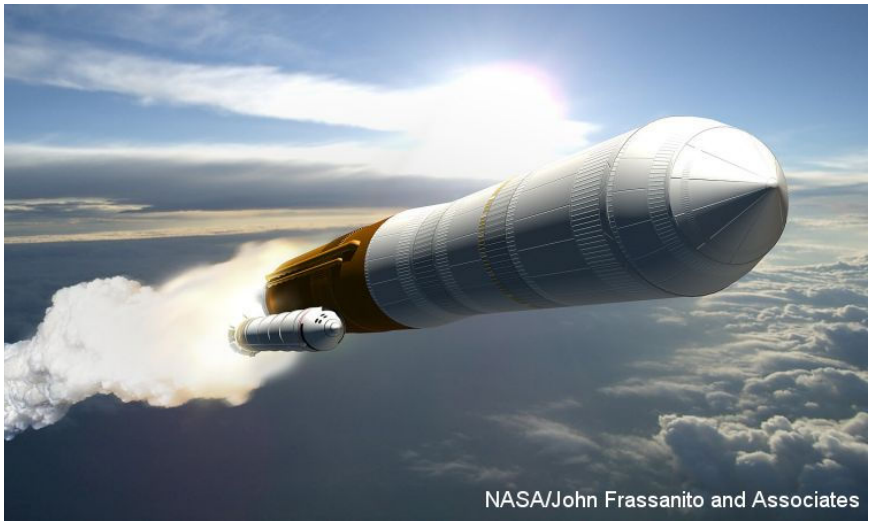

Figure 1.2 Ares-V Cargo Launch Vehicle

1.2. Motivation for Research

The goals of the exploration vision necessitate that the nation's current space capabilities, which permit but the periodic intrusion into the space environment, mature into the means and capacity of a great spacefaring nation. The mastery of space can only be achieved when humans have the freedom and ability to operate within the environment at will. Such operational ability and flexibility necessitates the emplacement of an effective logistics[4] infrastructure and knowledge base. An essential part of that operational knowledge is the understanding of contingency plans and abort options for every aspect of the total system.

Above all other requirements, manned exploration designs should preserve the life of the crew. Mercury astronaut Gordon Cooper[5] speaking of his responsibilities in abort planning said: "Some day, when space travel is more common than it is now, people will take this sort of thing as much for granted as they take firetrucks now at an airport." Indeed, many of the contingency features of modern well-developed transportation systems often escape public notice despite the frequency of their utility. An aviation example would be the multitude of airfields in existence which allow a troubled aircraft to abort to a closer location than its flight origin. Though implementing multiple safe ports in space is a more daunting objective, the safety benefits of such an abort option are just as real and desirable.

There are other practical reasons for having emplaced abort plans to guard against loss-of-crew failures in addition to the protection of human life. Apportioned funding and public support mechanisms are societal and political realities which frame space activities. It is a mater of historical fact that these political and public

sentiments can be severely injured by loss-of-crew failures. In the event of such failures, prudence demands that further flights be suspended pending failure investigations. The requisite review boards and recommended engineering and process modifications cause a backlog in future flights and stretch mission goal timelines. The Space Shuttle program endured a 32 month grounding following the *Challenger* trajedy[6] in 1986 and an additional 30 months hiatus after the loss of *Columbia* in 2003. Additionally, such failures re-ignite debate in the scientific and political communities concerning the justification, direction, and annual expense of the space endeavor as witnessed by the events following the 1967 Apollo I fire[7] and both Shuttle tragedies. Mars researcher Robert Zubrin observed that "every time a program goes before Congress for funds it is forced to play another game of Russian roulette."[8] An independent report[9] commissioned by the Planetary Society referring to the achievement of the proposed exploration goals stated: "Meeting these goals while remaining within realistic funding expectations is foreseen as the major difficulty in meeting this challenge." Simply stated, failures potentially jeopardize the budget and public support and delay the attainment of mission goals. Successfully executed contingency plans not only save the lives of the crew but mitigate the fallout of what would otherwise have been a catastrophic failure. Such was the case with the successful abort of Apollo 13 whose failure[10] caused but a single month delay in the launch of its successor Apollo 14, a reality that would not have been so timely had the Apollo 13 crew perished.

With an understanding of these concerns gained from experience, NASA has outlined several safety and abort planning expectations for the new exploration

systems. These requirements[11] from the Exploration Systems Mission Directorate (ESMD) stipulate:

- Crew survival capabilities intended to keep the crew alive must be considered early, and put in place regardless of the risks due to known failure modes.
- Separation of crew from cargo for launches of exploration mission. Launch of the crew element separate from cargo may facilitate design of a human rated launch system with more robust abort options and improved crew survival margins than offered by the current Shuttle system.
- Human spaceflight systems should provide for crew survival even when catastrophic events occur. The Columbia Accident Investigation Board (CAIB) report[12] states, "Future crewed-vehicle requirements should incorporate the knowledge gained from the *Challenger* and *Columbia* accidents in assessing the feasibility of vehicles that could ensure crew survival even if the vehicle is destroyed."

Crew safety has most appropriately been given top priority from the inception of this renewed space endeavor. The ESMD requirements above remain general as the details of the exploration systems have yet to materialize; though they were instrumental in the selection decisions of the Ares-I and Ares-V. The Planetary Society report[9] was more specific in its abort recommendations which included:

- Manned launch systems must provide a launch escape/abort capability throughout the flight envelope.
- Spacecraft should retain an abort capability to Earth or to a surface safe haven throughout their transit phase.
- Exploration infrastructure should evolve to maximize opportunities for redundant and emergency operations.

These recommendations envision a robust space transportation system whose operations are capable and adaptable in securing human life and mission objectives. One hallmark of the system shaped by these requirements is that abort options are accessible at any point in the mission eliminating mission phases or events where recovery of the crew is not possible, the so called "black zones".

1.3. Past Abort Work for Mars Missions

The previous section advocated the necessity of having a capable and continual abort capability for all manned spacecraft. Achieving this level of abort capability has been a major design constraint throughout all of the manned spacecraft programs of the past. During initial manned spaceflights, the primary concern was the rapid removal of the spacecraft from its booster rocket in the event of a catastrophic failure. For the Apollo Moon program, additional abort capabilities and trajectories were devised for returning the crew safely from a more distant and difficult objective. The means and methods used to obtain the discussed ascent and lunar abort capabilities will be detailed in Chapter 2. The lunar mission architectures and contingency plans of the past, of which the lunar free-return trajectory is the most well-known feature, were fairly successful in realizing extensive abort flexibility and will likely form the backbone of the contingency plans for NASA's renewed missions to the Moon in the coming decade. Consequently, in the decades since the conclusion of the Moon program there has been a flurry of activity in the abort analysis for the next established goal, manned missions to Mars. This large body of work focuses almost entirely on the provision of abort trajectory options during the heliocentric

interplanetary transfer with primary emphasis placed on achieving return to Earth aborts during the outbound half of that round-trip transfer. Abort options for the inbound return trajectories after leaving Mars are not usually considered as they are assumed to already be on track to return to Earth. The resulting Mars contingency plans are achieved primarily through Mars transfer trajectory selection and/or Mars spacecraft architecture design. Chapter 2 will discuss the development of the Mars trajectory work and the Mars spacecraft architecture designs and capabilities will be presented in Chapter 9.

1.4. Description of Present Work

Thorough reviews of investigated Mars abort trajectories and contingency options revealed an important mission segment of the outbound Mars transfer trajectory that has not received due attention. The segment is the relatively small portion of the transfer that proceeds at the beginning of the mission while the spacecraft is still strongly influenced by the Earth's gravity, referred to as the departure phase. The departure phase begins at the initiation of the Earth escape trajectory and continues until the spacecraft departs the Earth's gravitational sphere of influence. Though likely neglected due to its short duration, a handful of days compared to the several months of the heliocentric portions, the departure phase can nevertheless be of great importance because of its position at the very beginning of the entire transfer trajectory where many critical failures could be expected to occur. A high proportion of actual spacecraft failures are attributable to the operation of the propulsion systems, whether the engines themselves or related subsystems, and are

typically revealed quickly either during or after operation. Other likely failure propagations are associated with the first initialization and/or integration of a subsystem during actual flight conditions. There are clearly a significant number of potential failure modes that could manifest themselves at a very early stage of the mission. Though of short duration, the departure phase follows one of the mission's principal propulsion events, the Earth escape burn. As a consequence, though the spacecraft is still physically close to Earth, it has been placed on a high energy contour which potentially escalates the propulsive cost of contingency maneuvers as high as those considered for interplanetary aborts despite its proximity. In the event of an early-term emergency, it would be absurd to continue on whatever cycler orbit or free-return trajectory that had been embarked upon and which might not return the manned spacecraft back to Earth for many years. The manned spacecraft must therefore be capable of performing a powered abort from any point during the departure phase which will terminate the escape trajectory and return the crew in the event of an early failure. The present work will devise and analyze potential abort options during this flight segment. These departure phase abort capabilities need to be ascertained and integrated into the suites of contingency plans that have been established for application during other flight phases to ensure that manned Mars missions will have continuous abort options for all flight phases from Earth departure to Earth return.

1.5. Research Objectives

The principal aim of this study will be to investigate the availability and feasibility of abort maneuvers during the departure phase of a manned mission to Mars. The governing goal of the work is to preserve the lives of the crewmembers in the event of an emergency during departure. For the Apollo program, preserving the lives of the crew meant returning them to Earth via direct atmospheric entry. This was the only realistic survival option as there were no emplaced space assets; each mission was its own isolated excursion with no logistics train. Assuming the current progressive plan for exploration is utilized, a future Mars spacecraft would have several additional abort options. For example, in the event of a damaged or inoperative re-entry vehicle, the spacecraft might be aborted to low-Earth orbit to await rescue or possibly to dock with an orbiting habitat or space station. Additionally, the requirement for crew survival would no longer necessarily require an immediate return to Earth. Given the planned sequential building of Moon assets that will predate manned Mars missions, it may be in the crew's best interest to abort to either lunar orbit or the lunar surface. The addition of safe-havens beyond Earth will provide extra abort options and contribute tremendously to the reduction of crew risk. It is hoped that the considered abort options will provide the crew with a continuous abort capability throughout the departure phase of a Mars mission. In support of that goal, the research will proceed with the following objectives:

- Establish the propulsive requirements for performing a direct abort of the spacecraft to Earth atmospheric interface or to a low-Earth orbit from any position along the outbound trajectory of the departure phase.

- Contrast the above Earth abort cases with possible aborts to lunar orbit.
- Investigate requirement variation of Moon abort mode with respect to lunar position and determine resulting impact on interplanetary transfer requirements and launch window constraints for shifting departure dates.
- Apply the above investigations for mission opportunities from 2018 through 2033 to ensure continued abort access is possible for future planetary alignments across the complete fifteen-year Earth-Mars inertial period. Set abort requirements accordingly.
- For the expected spacecraft configurations of candidate mission architectures, apply abort requirements to define exclusion zones and abort options for each architecture.

In support of these research goals, a computational program is needed to calculate the planetary and Moon positions, create the various trajectories, and to implement and analyze the specified abort options for any date of interest. The program must be accurate in time and space if confidence is to be had in the output abort maneuvers.

1.6. Thesis Overview

This thesis consists of 11 chapters and several appendices.

- Chapter 2 contains an overview of both historical and future abort planning activities. This chapter will highlight the abort modes and strategies used by the manned space programs of the past and present with special emphasis on the

Apollo and Space Shuttle programs. A discussion of the successes and failures of these plans are given from which valuable lessons will be extracted for application in future abort planning.

- Chapter 3 gives treatment to many fundamental and required concepts which must be defined and understood before consideration of the interplanetary trajectories and abort modes can proceed. The successful execution of the planned research objectives necessitates proper application of coordinate and date transformations. This chapter also presents the employed trajectory methods.
- Chapter 4 utilizes the tools of Chapter 3 to construct patched conic interplanetary trajectories and to iterate the various trajectory phases until space and time continuity is achieved at the patch interfaces. The various trajectory phases and associated parameters are illustrated and defined.
- Chapter 5 varies the parameters of Julian departure date (JDD) and time of flight (TOF) to search hundreds of interplanetary trajectory opportunities for Mars transfers for any given year. The chapter also presents an overview of the different classes of Mars trajectories and rationale for the trajectories selected for consideration in this study.
- Chapter 6 contains the problem setup for performing departure phase aborts resulting in direct atmospheric entry at Earth. The delta V requirement behavior is characterized and evaluated for abort initiations all along the outbound track.
- Chapter 7 presents the problem setup for executing aborts to Earth orbit and Earth orbiting assets. The delta V requirements for these abort destination possibilities are analyzed. An additional investigation is conducted into methods

to reduce the potentially high propulsive cost of aborting to existing Earth orbital assets.

- Chapter 8 begins with a presentation of the peculiarities of the Moon's orbital motion and the implied considerations when electing to execute a lunar abort. The chapter then presents the problem setup for the performance of aborts to lunar orbit and characterizes the behavior of the resulting abort requirements. The delta V requirements of these aborts are then contrasted with the results from the Earth return aborts of the previous chapters.
- Chapter 9 introduces the types of mission architectures that may find application in future manned Mars missions. Three candidate architectures are extracted for use in evaluating the achievability of a departure phase abort capability.
- Chapter 10 analyzes the selected candidate architectures individually to ascertain the extent of the resulting abort capability for each of the developed abort modes and likely trajectory classes of the previous chapters. The influence on mission propulsive requirements due to optimization of the Moon abort mode through launch date variation is also investigated.
- Chapter 11 summarizes the principal findings of the departure phase abort investigation and provides recommendations concerning the transfer classes, abort modes, and propulsive requirements needed to achieve a robust departure phase abort capability for a manned Mars mission.

Chapter 2. Abort Planning: Historical and Prospective Applications

The Apollo program defined an abort[1] as "the recognition of an intolerable situation and the performance of the activities necessary to terminate the mission and return the crew to Earth." The discussion of the previous chapter proposed that there may be future abort situations for which, given sufficient logistical emplacement, it may be more advantageous for the crew to abort to the Moon or to some other orbital location. However, regardless of abort destination, the sentiment remains the same, recover the crew safely. Abort planning is the process of preparing and evaluating abort options and contingencies subject to the capabilities of the spacecraft hardware and operational constraints of the mission. Crew safety is the prime directive of abort planning but other considerations are also included such as, in the case of less-severe failures, options for mission continuation with reduced mission objectives. The Apollo Experience Report[1] observed the following: "Because of the large number of constraints that must be considered, abort plans and techniques must be kept as simple as possible." The importance of the abort planning process coupled with its potential impact on the requirements of the final spacecraft design mandate that abort planning be integrated into the design analysis from the very beginning of system definition. The following sections will discuss the abort planning process for historical, current, and future human spaceflight systems.

2.1. Historical Abort Plans

The technological hurdles that characterized the early American manned spaceflight programs stimulated great developmental strides in abort planning. Unlike previous unmanned rocket vehicles, the integration of man and machine required for the first time extensive abort methods to ensure crew survival. The abort plans that emerged from the buzz of activity were innovative, simple, and effective with capabilities ranging from capsule extraction in the event of an explosion to the creation of new trajectory classes. These abort methods were successfully proven several times in the course of the Mercury, Gemini, and Apollo programs and remain relevant to current and future abort planning.

2.1.1. Mercury, Gemini, and Apollo Ascent Aborts

Crew abort capability was not a luxury during the Mercury program, it was an absolute necessity. Rocket technology was a new field and the booster vehicles were prone to explosive failures. This was particularly true for the Atlas booster that was designed to power the orbital Mercury missions. The possibility of explosion and vehicle breakup were time critical events that required launch escape hardware that was capable of immediately removing the astronauts from danger. The launch escape tower, Figure 2.1, was conceived by Mercury capsule designer Max Faget and consisted of a tractor rocket designed to rapidly separate and pull the manned capsule away from the booster. At a safe distance and altitude, the tractor rocket disconnected and the capsule would descend under its own parachute. This escape maneuver was possible during ascent and even while the booster was still on the pad.

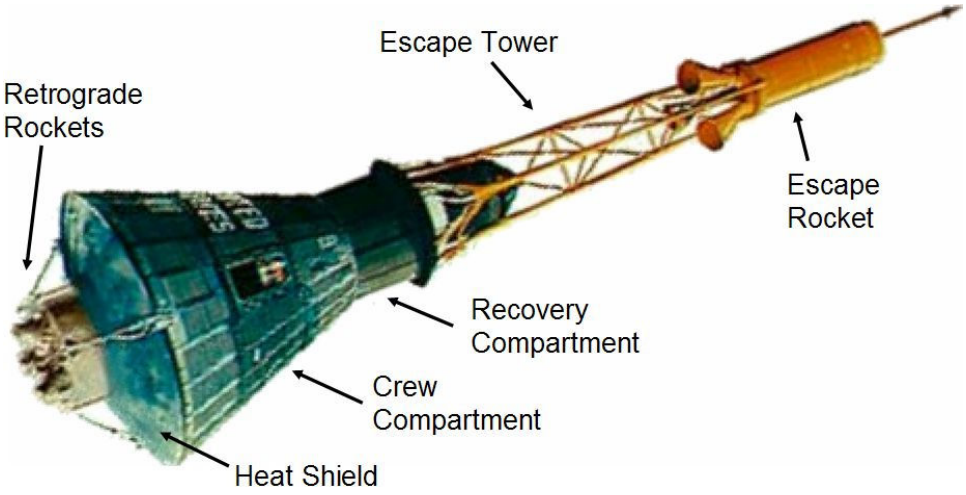

Figure 2.1 Mercury Capsule and Launch Escape Tower (NASA)

For the two-man Gemini capsule, the escape tower was replaced with dual ejection seats (Figure 2.2). The seats could quickly distance the astronauts at least 800 feet from the booster and were functional on the launch pad or during ascent and re-entry.

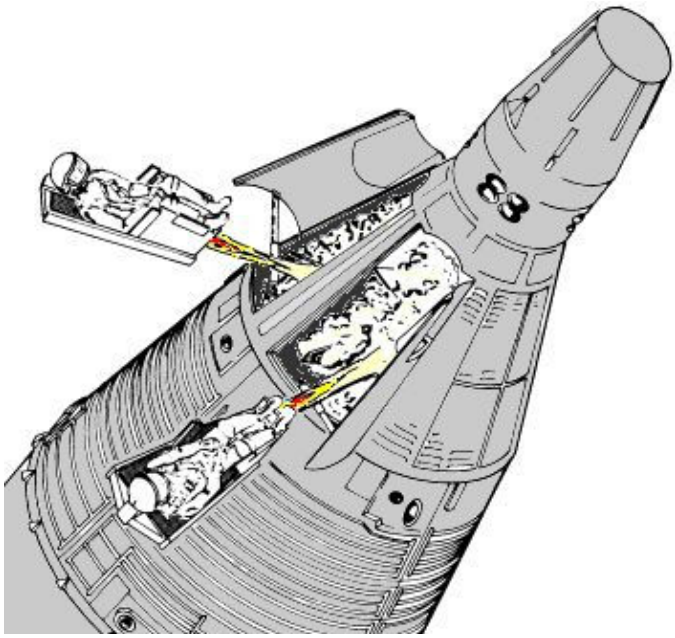

Figure 2.2 Gemini Capsule Crew Ejection Seats[13]

The Apollo launch escape system[14] returned to a greatly scaled up version of the tower tractor rocket design (Figure 2.3). The scaling was necessary as the three-man Apollo capsule was many times the mass of the Mercury one-man capsule.

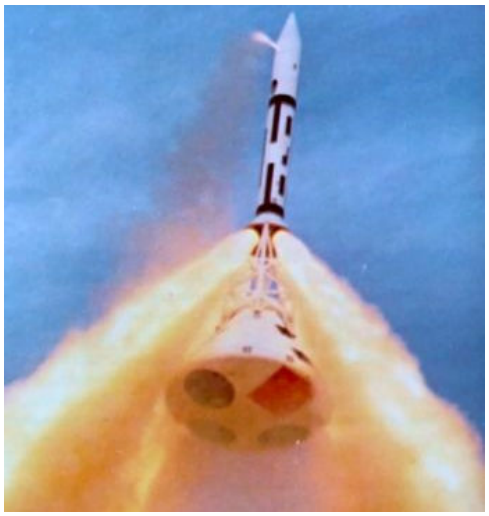

Figure 2.3 Apollo Launch Escape Tower Test Fire (NASA)

The Apollo architecture enabled more expansive ascent abort options than either Mercury or Gemini. Besides the launch escape system (LES) tower attached to the command module capsule, the service module was also available for possible use in contingency plans. This was significant because the service module had its own main engine which could be used to great effect to enable four categories of abort modes[1].

- Mode I: LES executes time-critical escape from an impending launch-vehicle explosion during atmospheric flight. The capsule parachutes into the Atlantic.
- Mode II: For above-atmosphere aborts, the spacecraft simply separates from the launch vehicle, orients for entry, and lands in the Atlantic Ocean.
- Mode III: Similar to Mode II, but utilizes the propulsion of the service module to more precisely control the entry point and landing zone.

- Mode IV: For aborts during the last two minutes of the launch phase, the spacecraft may separate from the launch vehicle and independently attain orbit from which the craft may perform entry at any desirable point. (All modes shown in Figure 2.4)

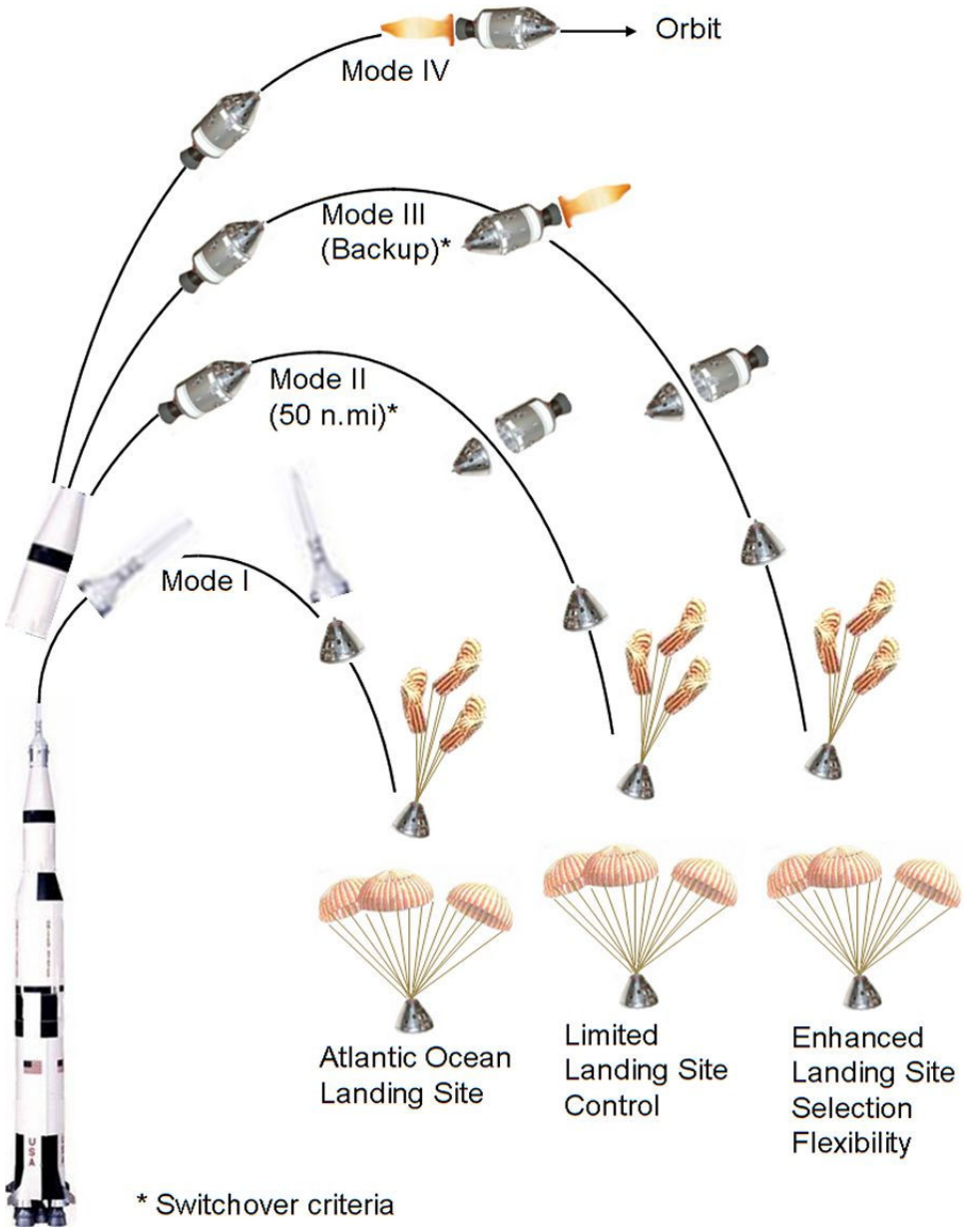

Figure 2.4 Apollo Spacecraft Launch Abort Modes[1]

The four ascent abort modes represent a significant improvement in abort planning because they provide multiple layers of abort options which may be selected to adapt to a variety of situations and achieved without adversely affecting the scaling of the vehicle. The benefits of having abort flexibility options were realized in other phases of the Apollo mission and were designed into the Space Shuttle program that followed. The lessons learned from Apollo will be specifically relevant again as NASA returns to capsule designs for the CEV.

2.1.2. Russian and Chinese Spacecraft Abort Systems

The United States is not the only authority on the subject of human-rated spacecraft. The Russian Vostok became the first human spacecraft[15] when it successfully carried Major Yuri Gagarin into space on April 12, 1961. Like the later Gemini spacecraft, the Vostok capsule was equipped with an ejection seat/parachute system. For Vostok, the ejection seat was also employed nominally during the descent phase of the spacecraft to remove the cosmonaut from the capsule before its hard landing. The successor to the Vostok, the larger and more capable Soyuz spacecraft, was outfitted with a launch escape tower similar to those of Mercury and Apollo. In fact the only actual execution of a launch escape tower abort occurred on the launch pad of the Soyuz T-10-1 mission[16] on September 26, 1983. The Soyuz escape tower safely hoisted its cosmonaut occupants away from the explosion of the booster rocket.

China became the third nation[17] capable of placing humans in space on October 15, 2003 with the launch of taikonaut Yang Liwei aboard the Shenzou 5

spacecraft. Launched atop a Long March 2F rocket, the Shenzou spacecraft closely resembles the design layout of the Russian Soyuz capsule. Shenzou launch aborts are also executed through the use of a launch escape tower.

2.1.3. Lunar Free Return Trajectories

One of the major abort mandates[14] of the Apollo architecture was that the spacecraft travel on a free return trajectory. A free return trajectory is one in which the spacecraft is returned to the primary body after gravitational interaction with a secondary body (e.g. the Moon). The idea of such a possibility was first conceived by science fiction author Jules Verne in 1865. A true free return proceeds without the need of additional propulsive maneuvers and was therefore ideally suited to the first missions to the Moon when there was little in-flight experience with the spacecraft engines. Apollo 11 was the last Apollo mission to fly a true free return trajectory. Later missions began as such but were modified through midcourse maneuvers in order to achieve non-equatorial landing sites that are inaccessible with a free-return trajectory. The well-known Apollo 13 mission therefore required a maneuver soon after the accident in order to resume a free return trajectory. Future lunar explorations may use these trajectories, but the associated landing limits may hinder the goal for global lunar surface access.

2.1.4. Apollo Abort Trajectories

In addition to the baseline free return trajectory, the Apollo abort planning processes identified many other less well known abort trajectory needs. During the transit to the Moon, the service module main engine was capable of performing a

direct abort that would put the spacecraft on a trajectory back to Earth without continuing to the Moon. This option would return the astronauts in a shorter amount of time than the eventual arrival on the free return trajectory. A direct abort was not exercised on Apollo 13 despite the time-critical nature of the failure because of doubts about the integrity of the service module engine after the explosion. Additional classes of abort trajectories were devised for use inside the Moon's gravitational sphere of influence. Upon arrival at the Moon, the Apollo spacecraft performed a lunar orbit injection (LOI) maneuver to reduce speed and be captured into lunar orbit. If this burn was insufficient the spacecraft could enter on a host of possible orbits[1] from unsteady near-escape orbits to elliptical orbits that would lead to lunar surface impact as shown Figure 2.5. Conversely, too much of a velocity change would result in insufficient orbital speed and lead to a direct impact with the Moon's surface. Abort capabilities had to be devised to recover from a failed LOI maneuver. Similarly, future exploration missions will need to provide a set of contingency trajectory options for each critical maneuver or phase of the mission.

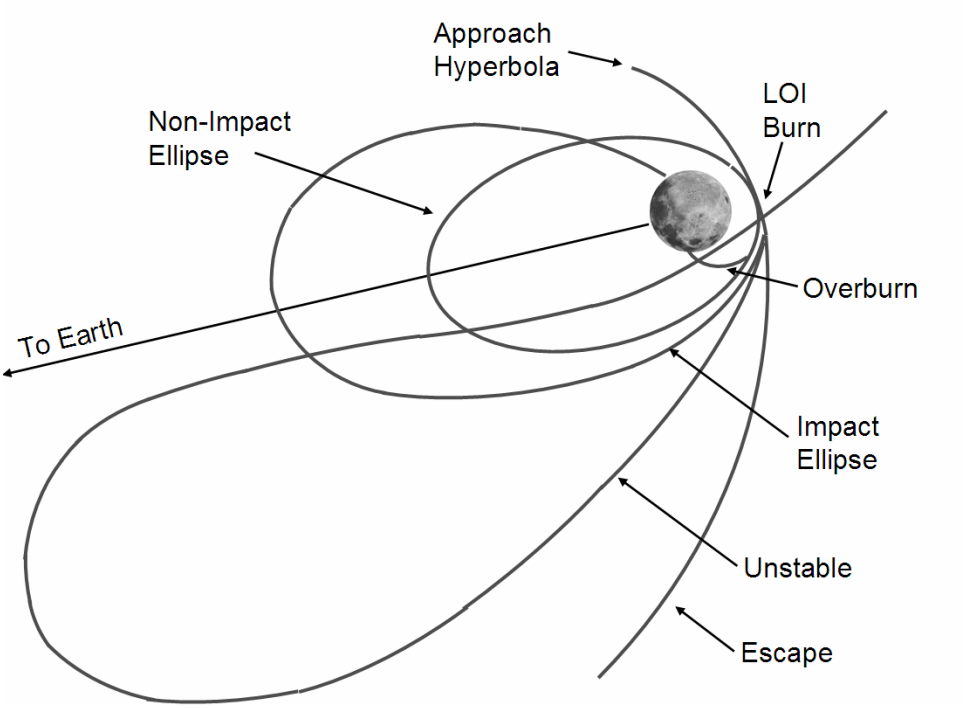

Figure 2.5 Premature and Overdue LOI Shutdown Trajectories[1]

2.1.5. Space Shuttle Abort Possibilities

The Space Transportation System (STS) continued the practice established by its predecessors of providing multiple overlapping abort options for different flight phases. On-pad aborts were accomplished by emergency egress slidewires leading from the gantry to underground bunkers 1,200 feet distant. Though not as rapid as the launch escape tower, it was quite impractical to quickly separate the entire Shuttle Orbiter from the remainder of the stack in the event of a pad emergency. The Shuttle uses a combination of liquid fueled Space Shuttle Main Engines (SSME) and solid propellant rocket motors (SRB). An operational limitation of a solid propellant motor is that once ignited it may not be shut down prematurely as a liquid engine may be. A safety measure established for all Shuttle launches is the ignition of the three SSME

engines several seconds before liftoff. This event allows the flight engineers to quickly evaluate the health of the SSME engines before committing to a definite liftoff with the ignition of the two SRBs. If anomalies are manifest, the flight is aborted resulting in the shutdown of the SSMEs and the termination of the SRB ignition sequence. The use of this contingency option has been exercised several times to prevent launches with a faulty SSME. Assuming a successful ignition and liftoff, there are four overlapping ascent abort modes[18].

- Return to Launch Site (RTLS): For main propulsion failures in the first few minutes of flight, an RTLS abort (Figure 2.6) is initiated after the SRBs separation. The Orbiter and external tank combination continues downrange under the power of the remaining SSMEs. When just enough propellant remains to reverse flight direction, the stack rotates until it is headed back to the launch site. The Orbiter separates and glides back to a landing on the runway near the launch site.

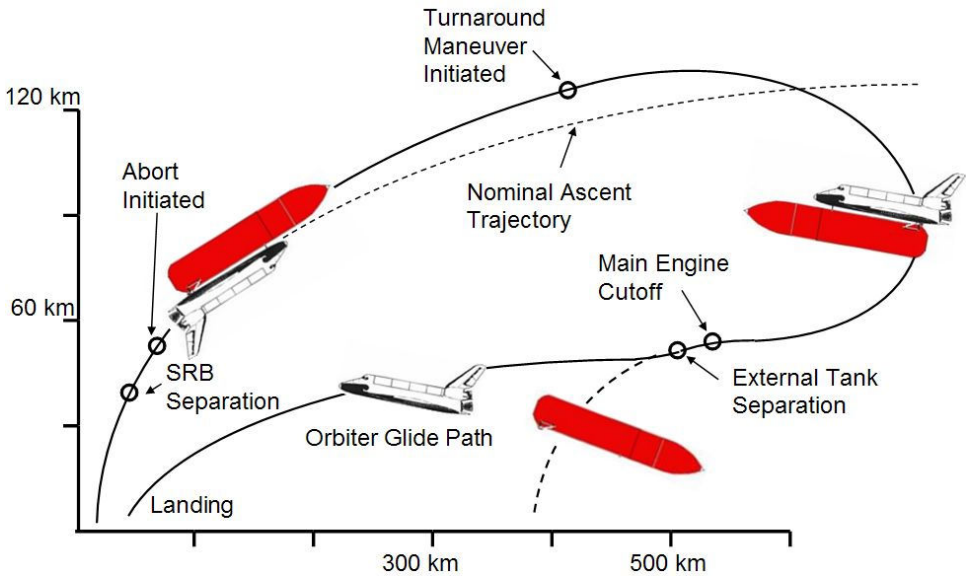

Figure 2.6 Shuttle Return to Launch Site Abort Profile[18]

- Trans-Atlantic Abort (TAL): The next abort option is for an emergency landing at a prepared runway in Spain, Morocco, Senegal, or West Germany with site selection dependant on launch azimuth. The execution of the TAL abort becomes available a few minutes into the flight when the Orbiter can successfully cross the Atlantic.
- Abort Once Around (AOA): An AOA option becomes available after the SRB burnout. The stack continues under the power of all remaining engines until propellant is exhausted. The Orbiter then continues on a suborbital trajectory four-fifths of the way around the Earth to entry and landing at White Sands, New Mexico.
- Abort to Orbit (ATO): Aborting to orbit becomes possible if the SSME failure occurs later in the ascent. As with the other options, the stack continues under the power of the remaining engines. The final orbit will differ from the planned mission orbit, but hopefully many mission goals will still be achievable.

Of the four ascent abort modes, only the ATO mode has ever been executed. The abort profiles of these modes are presented in Figure 2.7. The availability of the different ascent abort options often overlap, enabling selection of the most advantageous mode adapted to particular circumstance. The abort mode availability is shown as a function of flight time in Figure 2.8. The figure shows multiple TAL aborts for each available trans-Atlantic runway for two different mission launch inclinations.

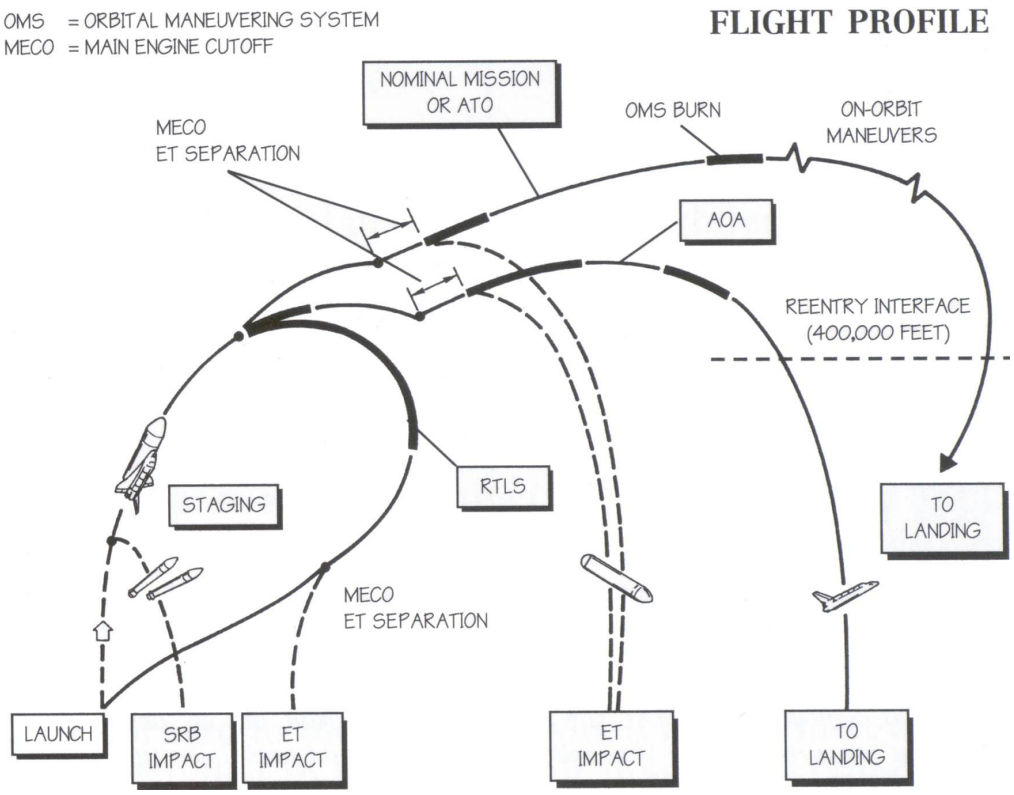

Figure 2.7 Shuttle Abort Profiles[6]

There have been several efforts to enhance the capability of the Space Shuttle to eliminate the need for the RTLS abort segment as it is considered to have the greatest inherent risk. This desire motivated the development of the five-segment booster (FSB)[19] by SRB contractor Thiokol. The integration of the FSB would permit an off-the-pad TAL abort capability effectively eliminating the need for the RTLS option. Additionally, the extra power imparted by the FSBs would make the AOA and ATO options available earlier in the flight. The FSB has recently found fortuitous application as the booster propulsion for the planned Ares-I and Ares-V launch vehicles.

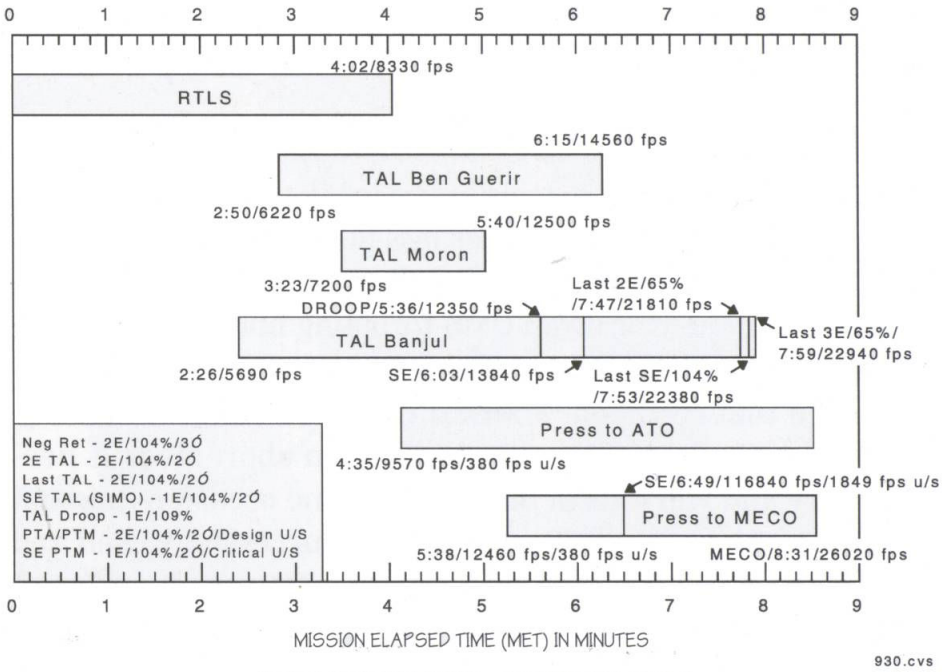

ABORT MODE BOUNDARIES – 28.5-DEGREE MISSION

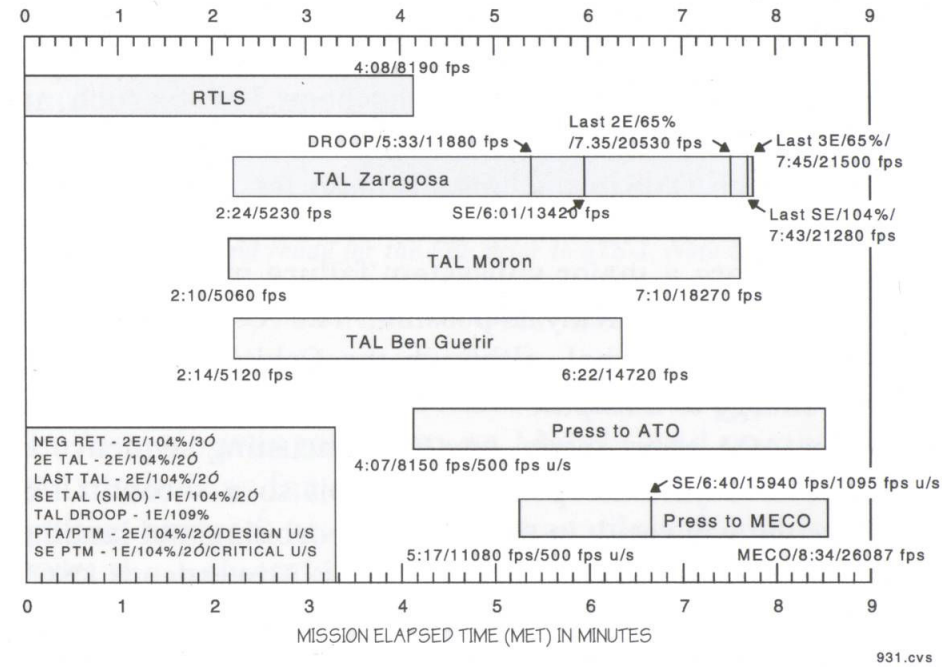

ABORT MODE BOUNDARIES – 57.0-DEGREE MISSION

Figure 2.8 Space Shuttle Abort Mode Boundaries Circa 2000[6]

Once in orbit, the re-entry capabilities of the Shuttle Orbiter permit the quick return of the crew in the event of an on-orbit failure or emergency. The suite of abort trajectories exhibited by Apollo for transfer and lunar insertion were not required for the Shuttle as it remained in Earth orbit. Return possibilities require only a de-orbit burn to bring the Shuttle to Earth. The Orbiter has the capability to abort to either Edwards Air Force Base in California, or to the Kennedy Space Center (KSC) in Florida. The Orbiter has no capability for crew abort during the heating of the re-entry sequence as was disastrously shown by the thermal protection system (TPS) failure that precipitated the loss of *Columbia* in 2003.

The operational history of the Space Shuttle program abounds with instances that prove beyond disputation the absolute necessity of abort planning for any manned mission. The abort modes and strategies that have been presented were called upon many times to save the crew during the first 113 flights of the STS. The most critical of these failures are tabulated in Table 2.1. Some of the failures are quite dramatic such as the quick shutdown of a failed SSME seconds before launch. Others are less dramatic such as the cutting short of a mission because of an on-orbit system problem. These failures only appear unexciting because they occurred on a spacecraft that was at most a few hundred kilometers from the Earth. Had they occurred on a spacecraft even a few days time of flight away from the planet (to say nothing of years away), they could have been catastrophic instead of mundane. The important fact that the data demonstrate is that these failures do happen and occur routinely in the first few days of a manned mission.

.

Table 2.1 Critical Failures Experienced by Space Shuttle Program[6]

Flight #	Mission	Result of Failure	Description of Failure
2	STS-2	Early Mission Termination	failure of fuel cell #1 shortened planned five-day flight by three days
7	STS-7	Early Mission Termination	failure of APU #3 forced quick landing at Edwards AFB two orbits after a KSC landing attempt was waved off due to weather
12	STS-16,41-D	Abort after Ignition	aborted at T-4 seconds due to SSME#3 fuel valve failure on Discovery's first mission
19	STS-25/51-F	Abort after Ignition	aborted at T-3 seconds due to SSME#2 coolant valve failure
19	STS-25/51-F	Abort to Orbit	SSME#1 shut down at T+5min 45 sec after overheating. Flight controller action prevented a faulty temperature sensor from commanding the shutdown of an additional SSME shortly thereafter.
25	STS-33/51-L	Loss of Vehicle and Crew	*Challenger* destroyed 73 seconds after launch on January 28, 1986
44	STS-44	Early Mission Termination	failure of an IPU shortened planned ten day mission by three days
55	STS-55	Abort after Ignition	aborted at T-3 seconds due to SSME#3 ignition failure
57	STS-51	Abort after Ignition	aborted at T-3 seconds due to SSME#2 fuel sensor failure
65	STS-68	Abort after Ignition	aborted at T-2 seconds due to overheating in SSME#3 oxidizer turbopump
83	STS-83	Early Mission Termination	failure of fuel cell #2 shortened planned fifteen day flight by eleven days
113	STS-107	Loss of Vehicle and Crew	*Columbia* destroyed during re-entry on February 1, 2003

The Shuttle has exercised the abort after ignition option five times, approximately 4% of flights. Presumably a small number of events until one considers that the crew would have been severely endangered and potentially lost in each of those cases in the absence of the emplaced procedure. Another discouraging fact illustrated by these aborts is that they continued to occur even up to the 65th Shuttle mission. That means that after hundreds of full-up ground tests and 192 actual flight tests (3 per mission) of the SSME there was still the very real possibility of serious engine glitches. Abort options never cease to be relevant, even after confidence is attained through experience. The Shuttle has often exercised its abort to

Earth capability to prematurely terminate a mission after an on-orbit failure. The seriousness of such failures when applied to Moon or Mars missions has already been discussed. Once again, these failures continue to occur at intervals even after dozens of flights. Perhaps the most dramatic of all the failures were those on STS 25/51-F[6]. The 19th shuttle flight was first delayed by an abort before ignition event. After it was finally launched, an SSME overheated and was shut down nearly six minutes into the flight. With two healthy engines, an ATO was instigated (the first and only exercise of a Shuttle ascent abort mode). However, a temperature sensor on a different SSME also began to register a heating problem with its engine and was on the verge of shutting it down as well. A flight controller determined that the sensor was giving faulty information and prevented it from commanding a shutdown. Otherwise, the Shuttle's ascent energy at that stage was such that both the AOA and ATO abort modes were unachievable with only a single operative SSME and the Shuttle would have been forced to attempt a TAL abort to the Zaragoza, Spain landing site. Considering all the listed failures, it is interesting to note that most occur in the liquid rocket engines or fluid-related power and life support systems.

2.2. Abort Planning for Manned Mars Missions

This section will present a summary of the abort planning that has occurred with respect to planned Mars missions. As advocated in previous sections, such abort plans should include the methodologies and ideas that have been successfully realized in previous programs as well as learning from their shortcomings. While a mission to Mars is markedly different from the programs of the past, the need for multi-faceted,

effective and continual abort ability is the same. Possibly foremost among the differences between a Mars mission and all other manned missions to date is the magnitude of the time involved, as much as a hundred times or more the duration of an Apollo mission. Many of the abort modes discussed thus far are for rapid, time-critical events and equally quick abort response or recovery. During the Apollo 13 abort, the combined ingenuity of NASA was required to maintain the crew for a handful of days until they could be recovered. Mars abort plans will need to be capable of much longer duration recoveries. The long flight times necessitate a paradigm shift in planning for Mars missions where an abort procedure may extend for months.

2.2.1. Human Factors of Long-Duration Spaceflight

Flight time becomes a critical parameter when humans are included in the system. Unlike the sensors or propulsion systems, the humans may not be turned off or kept in standby mode during the long duration voyage. Their presence will require continual operation of the life support and communication systems. During a potentially multi-year flight, the human crew will process prodigious amounts of material, from water to oxygen, while producing significant amounts of carbon dioxide and other waste. Provisioning the spacecraft for such long durations is one of the hurdles in achieving manned Mars missions and is the reason for the push towards closed-loop life support and short duration transfer missions.

Besides nourishment and life support, there are other pressing physiological consequences to long duration transfer flights. Chief among them are the radiation and gravity considerations of the space environment. Microgravity physiological

deconditioning is a serious outcome of long-duration spaceflight with consequences on human performance when the crew must operate in the gravity environment of the Mars surface. To avoid cosmic and solar radiation the spacecraft must be well shielded with additional capability during solar flare events. The Planetary Society report[9] estimated an uncertainty factor of four for the biological effects of space radiation. In a NASA study[20] of 39 astronauts who had developed cataracts, 36 of them had flown high-radiation missions such as those of Apollo. Much research remains to be done in this area. Faster flight times obviously help mitigate the detrimental effects of microgravity and radiation by reducing exposure. These human factors issues also highlight why long transfer trajectories using low-thrust engines are likely unacceptable for manned spaceflight.

2.2.2. Mars Cycler and Free-Return Trajectories

Defining the best transfer trajectory to meet mission and human safety requirements is an active research area. Titus[21] was among the first to recognize that a very important criterion in the selection of a mission to Mars is "the ability of the spacecraft to abort a mission in heliocentric space between Earth and the target planet and return to Earth at an earlier date." His 1969 paper showed that the addition of an abort capability to the ballistic flyby trajectories increased the required system mass significantly, while multiple impulse flybys could provide an "inherent abort capability with no mass penalty." Another novel idea that was conceived about this time was that of cyclic trajectories between Earth and Mars. These trajectories became known as "cyclers" and were developed initially in the late 1960's by

Rall[22,23] and Hollsister[24,25] with subsequent work by Aldrin[26] in 1985. These cycler orbits transition between the two planets perpetually aided by planetary gravity assists, and occasional moderate mid-course correction propulsive maneuvers. The abort advantages of such trajectories are in the eventual return of the spacecraft to an Earth encounter. The magnitude of the correction maneuvers is one of the principle disadvantages of a cycler orbit though improvement has been shown[27] by optimization results. Another major issue with cyclers is the fact that that they never stop in orbit around either planet which necessitates high-energy shuttling to get on or off of such a trajectory. Numerous cycler concepts have been spawned by the initial efforts, many of which have been conveniently compared and contrasted by Walberg[28], by Bonin[29] and by Linder and Vasile[30]. Besides cyclers, there has also been considerable desire to establish the Mars equivalent of a lunar free-return trajectory. Mars free return trajectories[31] have been identified with associated times of flight between 1.4 years up to 3 years. Free return trajectories; however, may not be the trajectory of choice for the various mission time and propulsive constraints of manned missions. Tartabini[32] et. al. have determined that up to 85% of nominal missions may be aborted as powered aborts without increasing the planned propulsive capability of the spacecraft and without utilizing a slower free-return trajectory.

2.2.3. Departure Phase Abort Capability Justification

The growing body of trajectory research has yet to include a detailed analysis of the abort options during the departure phase of the outbound trajectory. The previous sections of this chapter have provided further justification for this analysis in

addition to that of providing continuous abort capability. The great body of experience gained during the Shuttle program has demonstrated that abort situations arise repetitively throughout the life of a system. Additionally, the number of pre-SRB ignition aborts confirms that failures often become manifest at the beginning of the mission when the major systems are first put into cooperative operation. These data suggest that in a sustained Mars exploration program, departure phase aborts will almost certainly be required in some cases. An additional benefit of departure phase abort capability is the freedom given to delay the commitment to proceed with interplanetary transit from before the departure escape burn until after the spacecraft exits the Earth gravitational sphere of influence several days later. This allows the crew several days to conduct a short "shakedown cruise" of their spacecraft on its maiden voyage before committing themselves to a multi-year voyage aboard it. The value of this period is enhanced by the fact that it follows one of the major events of the mission, the departure burn, a time when many hidden failure modes would possibly be revealed by the full-on system operation.

Chapter 3. Fundamental Astrodynamic Concepts

This chapter will present the essential concepts and techniques that constitute the basis for the development of various interplanetary trajectories connecting the selected departure planet to the specified destination planet. Brief overviews of orbit and date specifications are presented as well as definitions of the utilized coordinate systems. Methods are then given for the estimation of planetary positions and velocities as well as for the determination of appropriate transfer trajectories between two known positions for a desired time of flight.

3.1. Julian Date

The Julian date[33] is the standard measurement used in astrodynamics for the representation of date and time. It was conceived by Joseph Scaliger in 1582 by combining elements of several previous solar cycle conventions which all shared a common point in the year 4713 B.C. which therefore became the epoch date for the start of the Julian cycle. The Julian date is measured in units of days from January 1, 4713 B.C. at 12:00 noon. The decision to cycle the days at noon allowed night-working astronomers to use the same date for all their same-night observations. The basic time scale for Julian date is coordinated Universal Time (UTC). The Julian date is especially convenient for computer applications as it contains all date and time information in a single variable. A common double-precision variable can achieve millisecond resolution. The U.S. Naval Observatory is considered the preeminent authority in the provision of precise time and astrometry data for navigation and

maintains a Julian date converter[34] application on its website. Julian date values for several dates of interest are tabulated in Table 3.1.

Table 3.1 Julian and Gregorian Dates for Selected Historical Events

Julian Date	Gregorian Date	UTC	Historical Event
2451545.00000	January 1, 2000	12:00:00	J2000 Epoch
2446459.19390	January 28, 1986	16:39:13	Challenger Disaster
2440423.34560	July 20, 1969	20:17:40	First Moon landing
2416466.14931	December 17, 1903	15:35:00	First Powered Flight
2266296	October 12, 1492	--:--:--	Columbus Discovers America
1871046	August 24, 410	--:--:--	Fall of Rome
786384	2560 B.C.	--:--:--	Great Pyramid at Giza Completed

3.2. Orbital Elements

Orbital elements[35] are the parameters required to specify a particular two-body orbit. Six such elements are necessary to uniquely define an orbit as the problem has six degrees of freedom corresponding to the three Cartesian coordinates. The first five elements describe the size, shape and orientation of the orbit while the sixth pinpoints the position of the satellite within that orbit at a given time. While there are several sets of six independent parameters that fulfill this purpose, the following set contains those utilized throughout this study.

- *a* *semi-major axis* --- a constant that defines the size of any conic orbit
- *e* *eccentricity* --- a constant that defines the shape of any conic orbit

- i *inclination* --- angle between the **Z** coordinate unit vector (**K** unit vector if geocentric) and the angular momentum vector **h**. It ranges from 0° to 180°.
- Ω *longitude of the ascending node* --- angle in the coordinate system fundamental plane between the **X** unit vector (**I** unit vector if geocentric) and the point on the satellite's orbit where it transits through the fundamental plane in an upwards (ascending direction). The angle is measured counter-clockwise when observed from the upper side of the fundamental plane and ranges from 0° to 360°.
- ω *argument of periapse* --- angle between the ascending node and the point of periapse measured in the satellite's orbital plane in the direction of the satellite's orbital motion and ranges from 0° to 360°.
- υ *true anomaly* --- angle between the satellite's position and the orbital periapse as measured in the orbital plane from 0° to 360° with the orbital apoapse located at 180°.

This orbital element set is depicted graphically for the geocentric coordinate system in Figure 3.1 and Figure 3.2.

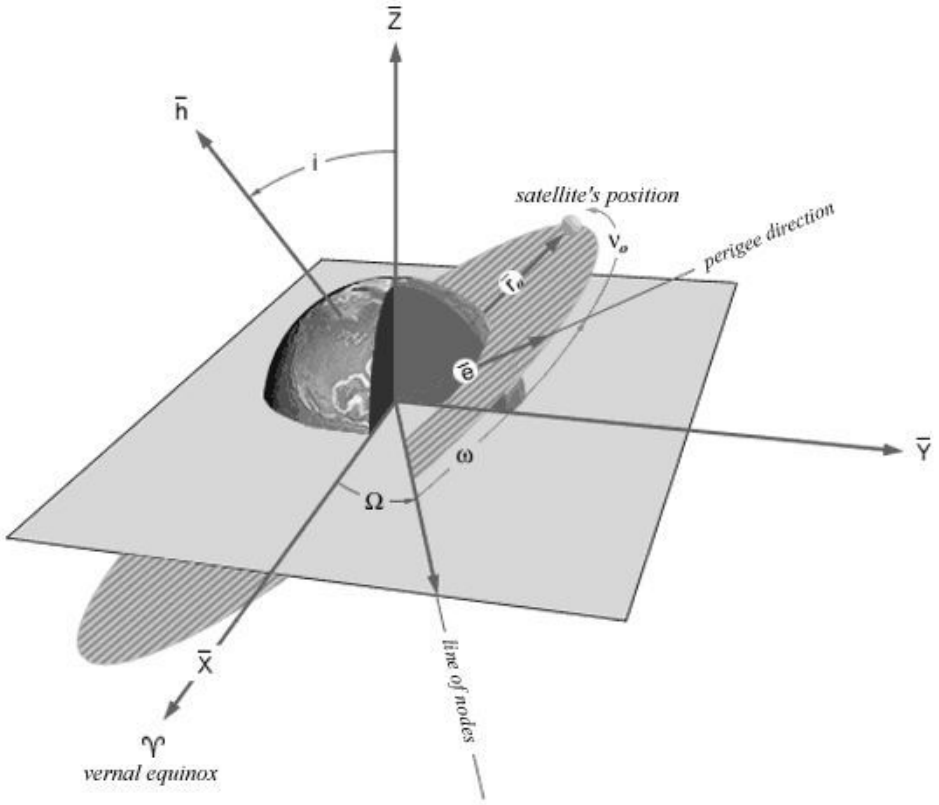

Figure 3.1 Orbital Elements - Geocentric coordinates (NASA[36])

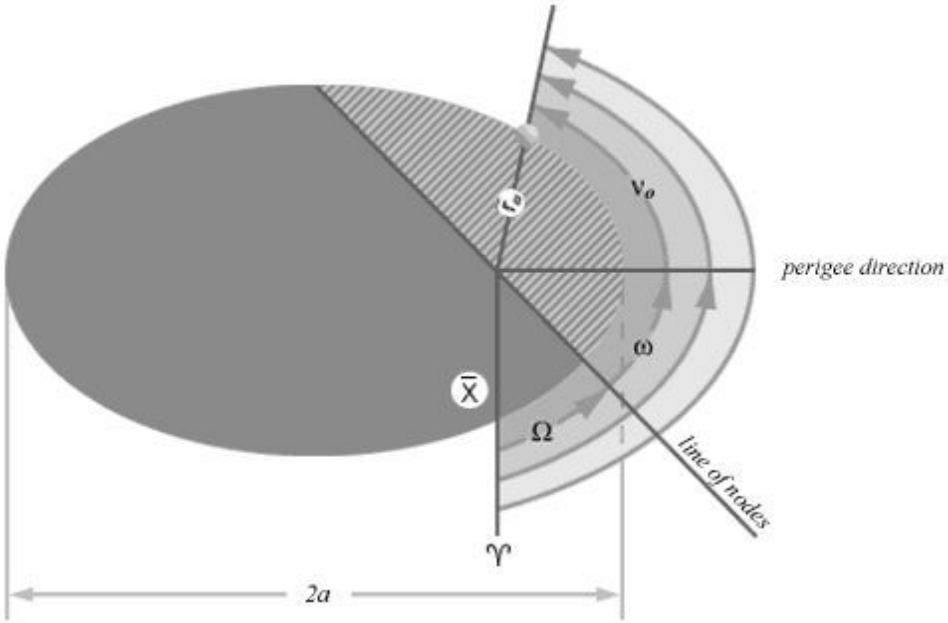

Figure 3.2 Orbital Elements - Orbital Plane (NASA[36])

3.3. Coordinate Systems

In seeking to describe an orbit one must first describe the reference frame. There were two basic inertial coordinate systems used during this analysis (an inertial coordinate system is one that does not rotate with the body but remains fixed with respect to the stars). For orbital motion about the sun, the heliocentric-ecliptic coordinate system is used. The standard axes notation for this coordinate system is **XYZ** where **X** and **Y** define the fundamental plane which is taken to be the ecliptic (the Earth orbital plane). The positive **X** axis points in the direction of a line joining the centers of the Earth and the Sun at the time of the vernal equinox. This direction is called the first point of Aries after the constellation at which the axis points and is designated as Υ. The heliocentric coordinate system is shown in Figure 3.3.

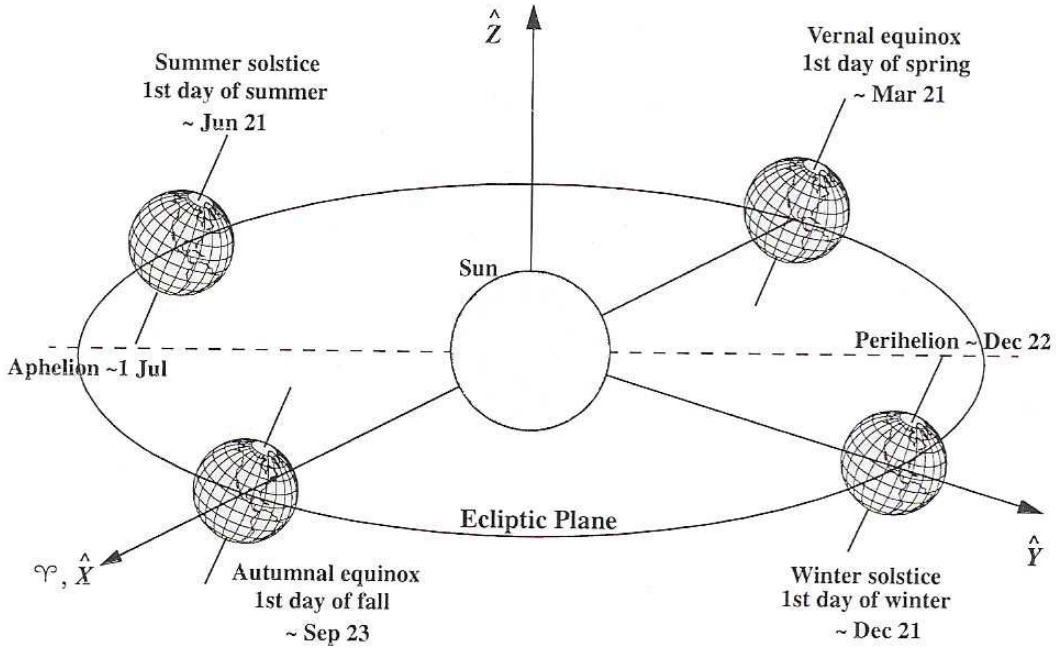

Figure 3.3 Heliocentric-Ecliptic Inertial Coordinate System (Vallado[33])

For orbital motion about the Earth, the geocentric-equatorial coordinate system was employed. This inertial system is normally designated by the coordinates **IJK** where the fundamental plane is the Earth equatorial plane defined by **I** and **J** with the **I** axis unit vector pointing in the same vernal equinox direction as the heliocentric **X** axis. This coordinate system, shown in Figure 3.4, is the reference frame of choice for calculation of Earth orbits and departure trajectories as well as the position of Earth's Moon.

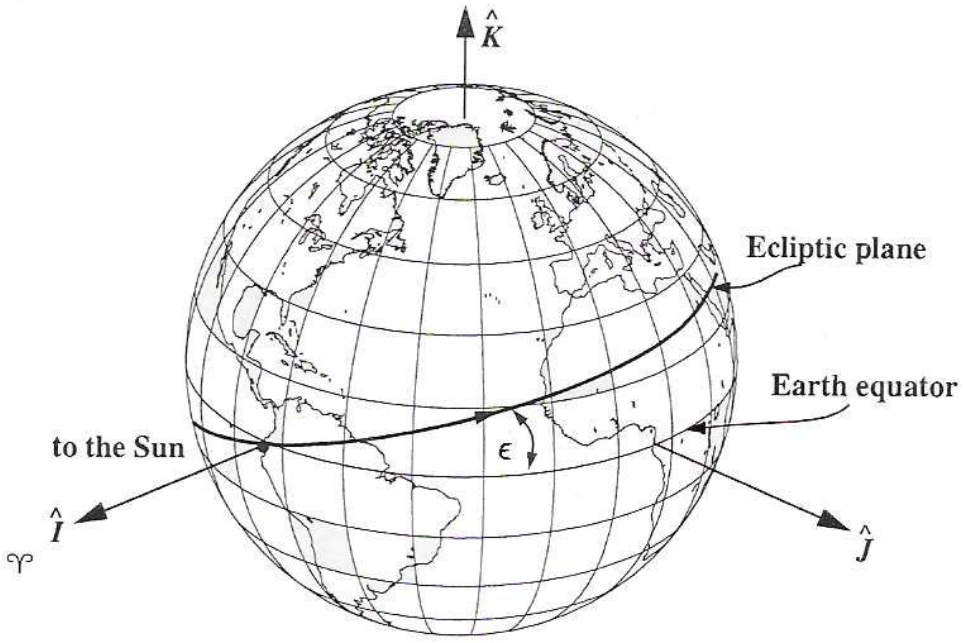

Figure 3.4 Geocentric Equatorial Inertial Coordinate System (Vallado[33])

Also shown in Figure 3.4 is the Earth obliquity angle ε which defines the tilt angle between the Earth equatorial plane and Earth ecliptic plane. The Earth's obliquity[37] is not constant but varies between 22.1° and 24.5° with a period of approximately 41,000 years. The value was taken to be 23.5° throughout the present work. The obliquity is the necessary parameter required to transform vectors from heliocentric

coordinates to geocentric coordinates. Recalling that the **X** and **I** axes are aligned, this transformation is simply a rotation about that common axis as expressed by Eq. 3.1.

$$ROT1(\varepsilon) = \begin{bmatrix} 1 & 0 & 0 \\ 0 & \cos(\varepsilon) & \sin(\varepsilon) \\ 0 & -\sin(\varepsilon) & \cos(\varepsilon) \end{bmatrix} \tag{3.1}$$

Rotations follow a right-hand rule about the axis of rotation. Thus, when converting a vector from heliocentric to geocentric coordinates, the rotation angle (the obliquity in this case) will be negative.

$$\vec{r}_{IJK} = ROT1(-\varepsilon) \cdot \vec{r}_{XYZ} \tag{3.2}$$

In addition to the sun-based and earth-based inertial frames of reference, a satellite-based frame of reference was used called the perifocal coordinate system. The fundamental plane of the perifocal system is the satellite's own orbital plane. The axes are denoted as **PQW** with the **P** unit vector in the direction of the periapse and the **Q** axis perpendicular to it and positive in the direction of the satellite's orbit. This system is represented in Figure 3.5. The figure presents a convenient opportunity to illustrate several other important basic orbital parameters including the periapse and apoapse distances, (r_A and r_P), the true anomaly υ, the flight path angle φ, and the satellite position and velocity vectors ***r*** and ***v***.

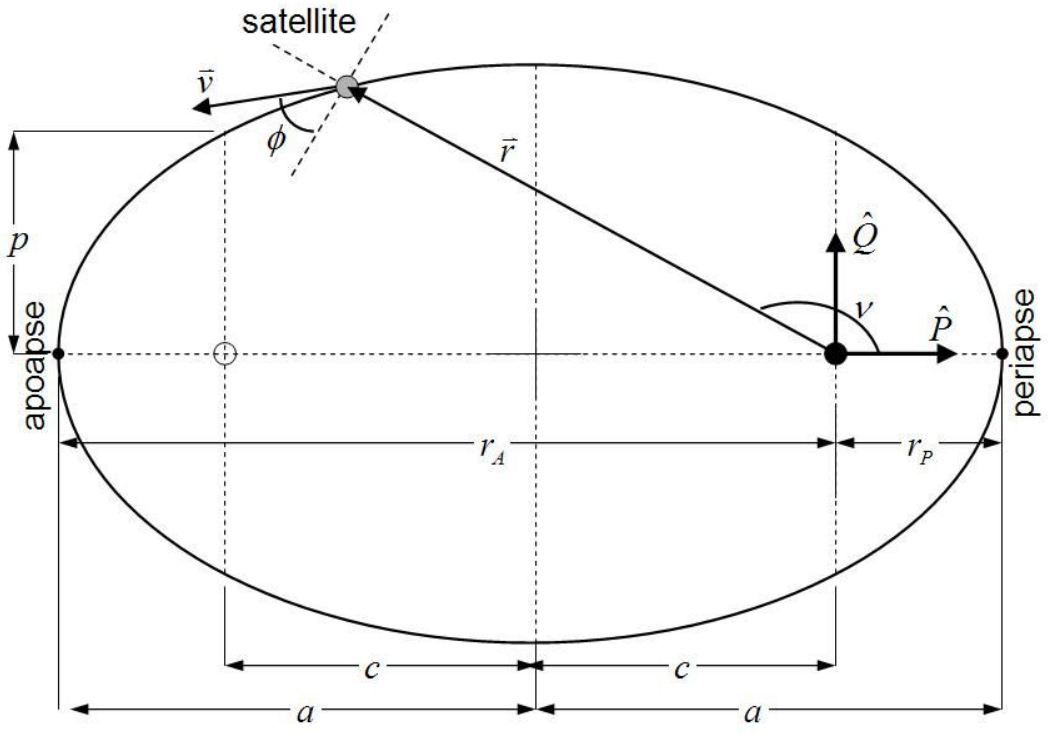

Figure 3.5 Perifocal Coordinate System and Orbital Parameters

The perifocal system is ideal for simple orbital calculations as all orbital motion occurs in the fundamental plane and is two-dimensional. The angular momentum vector ***h***, which is perpendicular to the orbital plane, is therefore in the same direction as the **W** unit vector. The satellite position may be defined in this system by the semi-major axis *a*, the eccentricity *e*, and the true anomaly *υ*; however the other three orbital elements will be required to convert from the two-dimensioinal perifocal plane to a three-dimensional inertial system.

Unlike the heliocentric-geocentric single rotation transformation already discussed, transforming the **PQW** system to either **XYZ** or **IJK** coordinates will require three successive rotations for alignment. An additional rotation matrix will be required with the vertical **Z** direction as the rotation axis.

$$ROT3(\omega) = \begin{bmatrix} \cos(\omega) & \sin(\omega) & 0 \\ -\sin(\omega) & \cos(\omega) & 0 \\ 0 & 0 & 1 \end{bmatrix} \tag{3.3}$$

The transformation begins by rotating the orbit about the **Z** axis through the angle Ω thus aligning the orbital plane's line of nodes with the **X** axis (see Figure 3.1). The orbital plane is then rotated about the **X** axis through the inclination angle i. A final **Z** rotation aligns the periapse direction with the **X** axis through the angle ω. Recalling that the positive angle directions are given by the right-hand rule for each rotation axis, the transformation is expressed thus:

$$\vec{r}_{XYZ} = ROT3(-\Omega)ROT1(-i)ROT3(-\omega)\cdot\vec{r}_{PQW} \tag{3.4}$$

It must be remembered that matrix multiplication is not commutative and therefore knowledge of the multiplication order of successive matrices is essential. Combining the rotation matrices yields a single matrix for this transformation:

$$TR = \begin{bmatrix} \cos(\Omega)\cos(\omega) - \sin(\Omega)\sin(\omega)\cos(\mathrm{i}) & -\cos(\Omega)\sin(\omega) - \sin(\Omega)\cos(\omega)\cos(\mathrm{i}) & \sin(\Omega)\sin(\mathrm{i}) \\ \sin(\Omega)\cos(\omega) + \cos(\Omega)\sin(\omega)\cos(\mathrm{i}) & -\sin(\Omega)\sin(\omega) + \cos(\Omega)\cos(\omega)\cos(\mathrm{i}) & -\cos(\Omega)\sin(\mathrm{i}) \\ \sin(\omega)\sin(\mathrm{i}) & \cos(\omega)\sin(\mathrm{i}) & \cos(\mathrm{i}) \end{bmatrix} \tag{3.5}$$

The coordinate transformation from **PQW** to **XYZ** then becomes:

$$\vec{r}_{XYZ} = TR\cdot\vec{r}_{PQW} \tag{3.6}$$

Reversing the direction of the transformation is a simple process because the rotation matrices are orthonormal since the rows are mutually independent. The matrix inverse of an orthonormal matrix is the transpose and the reverse transformation is then:

$$\vec{r}_{PQW} = TR^{T}\cdot\vec{r}_{XYZ} \tag{3.7}$$

The perifocal transformation to **XYZ** is equally applicable for transformation from **PQW** to **IJK** provided the orbital elements used in the rotation are measured with respect to the proper coordinate system.

3.4. Canonical Units

The distances involved in interplanetary calculations are immense if expressed in either English or metric units as are a few other orbital terms such as the gravitational parameter μ. Though all these terms are quite large, they also vary by orders of magnitude from each other when switching from sun-centered orbits to planetary or lunar orbits and coordinate systems. As conversion between various frames of reference is a repeated and necessary occurrence, the constant unit transformation and tracking becomes burdensome and increases the potential for error. Canonical units assuage these difficulties by scaling the basic units involved in the orbital parameters and solution process with respect to the current coordinate system. This enables the creation of single routines that, when given input values in canonical units, may be used universally in the performance of oft repeated calculations for any stellar or planetary system. At termination, the scaled results need only be multiplied by their corresponding canonical units to retrieve the information in the original units. The most advantageous modification is to select values for the canonical units that render the gravitational parameter μ equal to unity. In practice, a convenient value of the canonical distance unit DU is selected. The time unit is then solved assuming $\mu = 1$.

$$\mu = \frac{DU^3}{TU^2} = 1 \tag{3.8}$$

A set of canonical distance and time units can be determined for each body of interest. The distance unit selected for the Sun system is the Sun-Earth distance (1 *AU*). The planetary and lunar scaling distances typically correspond to the radius of the body. Table 3.1 lists the distance and time units for the principal celestial bodies of interest of this study presented in both canonical and metric forms.

Table 3.2 Canonical Distance and Time Units

	Distance Units		Time Units		μ
	Canonical	Metric *(km)*	Canonical	Metric *(s)*	Metric *(km^3/s^2)*
Sun	1 *DU*	$1.4959965*10^8$	1 *TU*	$5.0226757*10^6$	$1.327154*10^{11}$
Earth	1 *EDU*	6,378.145	1 *ETU*	806.811	398,602
Moon	1 *LDU*	1,738.1	1 *LTU*	1,035.176	4,900
Mars	1 *MDU*	3,397.0	1 *MTU*	956.686	42,830

The scale of the Sun's units clearly dwarfs that of the planets and the Moon. While the selection of the distance unit is consistent, the table shows no discernible pattern to the value of the resulting time constant obtained by scaling the gravitational parameter equation to unity using the decided upon value of the distance unit. The given table canonical unit notation (*DU*, *EDU*, etc) will be utilized throughout the remainder of this present work. The canonical value of the gravitational parameter was not listed as it is equal to unity in conformance with Eq. (3.8).

3.5. Planetary Ephemerides

The first basic problem in finding an interplanetary trajectory is obtaining an accurate estimate of the planet's position and velocity on a given date. A planetary ephemeris (from the Greek word *ephemeros* meaning daily) was historically a reference table that cataloged the positions of celestial bodies of interest tabulated by date. In modern times, algorithms have been developed which are capable of accurate estimation of planetary orbital elements as a function of Julian date. The orbital elements may then be used to determine planetary position and velocity. These algorithms are typically reliable for several centuries preceding and following the current year. This investigation used the formulations of Meeus[38]. The orbital elements are given as a function of Julian date. The date variable *TT* in the algorithm is however, referenced to the J2000 epoch and the Julian century (100 years of 365.25 days each) and is calculated using a given Julian date in the following manner:

$$TT = \frac{JD - 2{,}451{,}545.0}{36{,}525} \tag{3.9}$$

The orbital element data for the first five planets are given in Appendix A: Planetary Ephemerides but will require some calculation to convert the longitude of periapse $\tilde{\omega}$ and mean longitude λ orbital elements into argument of periapse ω and true anomaly υ. The argument of periapse is obtained simply by subtracting the right ascension of the ascending node from the longitude of periapse:

$$\omega = \tilde{\omega} - \Omega \tag{3.10}$$

The true anomaly calculation will first require the value of the mean anomaly which may be obtained from the mean longitude.

$$M = \lambda - \tilde{\omega} \tag{3.11}$$

The eccentricity and mean anomaly are then combined to iteratively solve Kepler's equation for the eccentric anomaly E.

$$M = E - e\sin(E) \tag{3.12}$$

The true anomaly υ may then be determined from the following equation:

$$\tan\left(\frac{\upsilon}{2}\right) = \sqrt{\frac{1+e}{1-e}}\tan\left(\frac{E}{2}\right) \tag{3.13}$$

The desired orbital element set is thus obtained for whichever planet is specified.

3.6. Lambert Problem

In determining an interplanetary trajectory, the position vectors of the departure and arrival planets are known quantities. Theoretically, an infinite number of orbits (see Figure 3.6) could be determined that connect these two vectors; however, there are only two such solutions for a specified time of flight between the two positions.

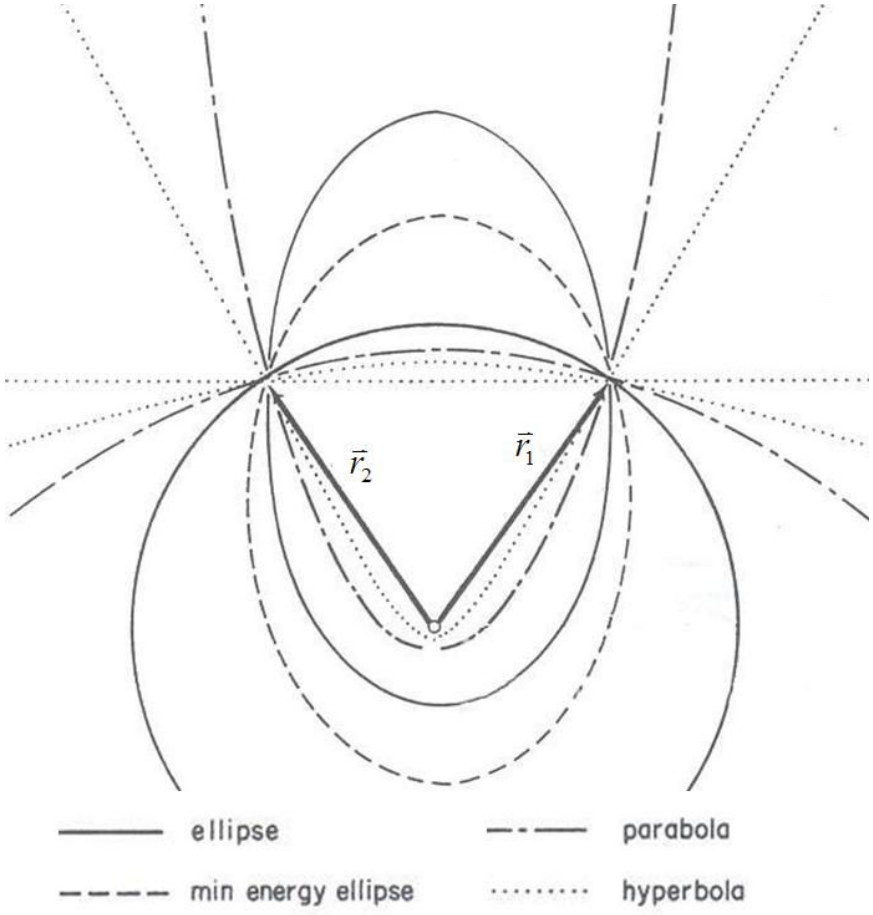

Figure 3.6 Family of Possible Transfer Orbits (Bate[35])

Determining the transfer orbit for a particular time of flight between two position vectors is known as Lambert's problem[33] because he was the first to form a solution. For a given time of flight, the two possible transfer trajectories are designated as either the short or long trajectories. The short trajectory experiences a change of true anomaly $\Delta\upsilon$ of less than 180° from point of departure until arrival while the long trajectory follows a different orbit and passes through a $\Delta\upsilon$ of greater than 180° in an orbital direction opposite of that of the short trajectory as shown in Figure 3.7

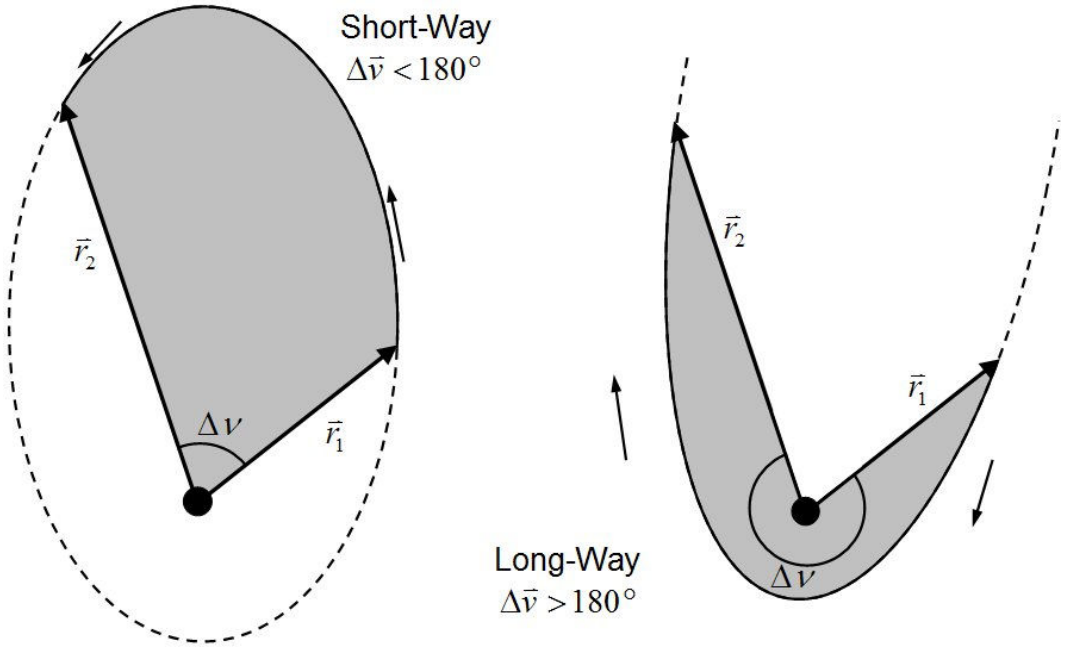

Figure 3.7 Lambert Problem Transfer Trajectory Possibilities

The solution will be unique for a specified transfer type. The problem is alternatively referenced in the literature[35] as Gauss's problem so named because of his famous solution to the problem and subsequent prediction of the orbital position of the asteroid Ceres.

3.6.1. General Solution Methods

The primary data needed for the formulation of the transfer trajectory are the initial and final velocity vectors. The two position vectors uniquely define the plane of the orbit (provided they are not collinear) which plane will also contain the unknown velocity vectors. It is therefore possible to express the vectors as linear combinations of the others using the variables *f* and *g*.

$$\vec{r}_2 = f\vec{r}_1 + g\vec{v}_1 \tag{3.14}$$

This expression may be differentiated to obtain the following:

$$\vec{v}_2 = \dot{f}\vec{r}_1 + \dot{g}\vec{v}_1 \tag{3.15}$$

The *f* and *g* quantities and their derivatives are scalar variables of which only three are independent because the v_1 may be expressed as a function of the other three. Bate[35], Mueller, and White give relations for *f* and *g* in terms of the transfer angle, the change in eccentric anomaly, the transfer time of flight, and the orbital parameter and semi-major axis.

$$f = 1 - \frac{r_2}{p}\left(1 - \cos(\Delta\nu)\right) = 1 - \frac{a}{r_1}\left(1 - \cos(\Delta E)\right) \tag{3.16}$$

$$g = \frac{r_1 r_2 \sin(\Delta\nu)}{\sqrt{\mu p}} = t - \sqrt{\frac{a^3}{\mu}}\left(\Delta E - \sin\Delta E\right) \tag{3.17}$$

$$\dot{f} = \sqrt{\frac{\mu}{p}}\tan\left(\frac{\Delta\nu}{2}\right)\left(\frac{1-\cos(\Delta\nu)}{p} - \frac{1}{r_1} - \frac{1}{r_2}\right) = \frac{-\sqrt{\mu \cdot a}}{r_1 r_2}\sin(\Delta E) \tag{3.18}$$

Of the seven variables in these expressions, three are unknown: the change in eccentric anomaly ΔE, the semi-major axis *a*, and the parameter *p*. Direct solution is impossible as the functions are transcendental so guess values must be iterated until the time *t* equals the desired time of flight. There are many methods in the literature for the execution of this solution which vary from each other in application, convergence rate, and stability as well as in the unknown variable that is utilized for iteration. Methods based on iteration of the semi-parameter are not as robust because the selection of the axis *a* does not guarantee unique values of *p* or ΔE. The universal variables solution iterates the eccentric anomaly *E* (or *F* for hyperbolic orbits) and was the method chosen throughout the present work for the solution of Lambert's problem.

3.6.2. Universal Variables Solution

Unlike many other solutions to Lambert's problem, the universal variables solution is valid for the solution of any type of conic transfer orbit. The method was selected for use in the present work because of its robustness and ability to solve both hyperbolic and elliptic orbits. Original methods for iterating solutions using E or F suffered from instability and inaccuracy if the orbit was near parabolic. This problem was corrected with the formulation of a general "universal" variable different than the eccentric anomaly that would overcome the previous problems. The universal variable also allows for a single time of flight calculation that is acceptable for any type of orbit. The method development is extensive and will only be summarized here in order to establish a basis from which to present the modifications and applications made to the method to incorporate it into this investigation. The summary follows the full development as given by Bate[35], Mueller, and White.

First, the independent universal variable x is created. This variable relates energy and the angular momentum and is here expressed in terms of the yet-to-be defined function C and variable y. The derivative of x; however, may be given in terms of known quantities as shown.

$$x = \sqrt{\frac{y}{C}} \tag{3.19}$$

$$\dot{x} = \frac{\sqrt{\mu}}{r} \tag{3.20}$$

Several of the known problem parameters may be lumped into a single convenient variable A.

$$A = \sqrt{r_1 r_2 \left(1 + \cos\left(\Delta\nu\right)\right)} \tag{3.21}$$

An additional universal variable z is defined which relates to the square root of the distance traveled between the transfer endpoints and corresponds to the change in eccentric anomaly. This variable is the iterated quantity in the solution process starting with a guess value and modified until the calculated time of flight equals the desired flight time. Elliptical orbits will have positive values of z while hyperbolas will have negative values.

$$z = \frac{x^2}{a} = (\Delta E)^2 \tag{3.22}$$

In the full expansion of the equations in the literature, it is helpful to consolidate some common terms into two functions designated C and S. These expressions involve the square root of the universal variable z and therefore it is necessary to provide an alternative formulation in terms of the hyperbolic sine and cosine for instances when z is negative.

$$C = \frac{1-\cos\left(\sqrt{z}\right)}{z} = \frac{1-\cosh\left(\sqrt{-z}\right)}{z} \tag{3.23}$$

$$S = \frac{\sqrt{z}-\sin\left(\sqrt{z}\right)}{\sqrt{z^3}} = \frac{\sinh\left(\sqrt{-z}\right)-\sqrt{-z}}{\sqrt{(-z)^3}} \tag{3.24}$$

The auxiliary variable y is now defined which relates to the area swept through during the transfer.

$$y = r_1 + r_2 - A \cdot \frac{(1-zS)}{\sqrt{C}} \tag{3.25}$$

For a guessed value of z, the variables C, S, and y can be determined. Combined with the constant A, the universal variable x presented at the beginning of this section can

now be calculated. Once the universal variables are determined, they are used in a modified time equation to determine the resulting time of flight for the guess value.

$$t = \frac{x^3 S + A\sqrt{y}}{\sqrt{\mu}} \tag{3.26}$$

The general form of the solution via universal variables will be to iterate z until this value of t equals the desired time of flight. Numerical solution methods will be addressed in the next section. Once the variables have converged, the previously defined f and g functions, modified for use with the universal variables, may be calculated.

$$f = 1 - \frac{y}{r_1} \tag{3.27}$$

$$g = A\sqrt{\frac{y}{\mu}} \tag{3.28}$$

$$\dot{g} = 1 - \frac{y}{r_2} \tag{3.29}$$

These functions are then employed to finally determine the initial and final velocity vectors which correspond to the trajectory connecting the two position vectors and traversing between the two in the specified amount of time.

$$\vec{v}_1 = \frac{\vec{r}_2 - f\vec{r}_1}{g} \tag{3.30}$$

$$\vec{v}_2 = \frac{\dot{g}\vec{r}_2 - \vec{r}_1}{g} \tag{3.31}$$

3.6.3. Solution Implementation

The universal variables solution was conceived for application to the solution of a broad collection of orbits. In obtaining the results presented later in this work, the universal variables solution process is employed many thousands of times. As such, a method with quick convergence was desired. Newton's method[39] is a speedy solution routine that approximates the desired root by taking the derivative of the functions at the evaluation point. Implementing the method will require the derivatives of the *C* and *S* functions and the time equation with respect to the iterated universal variable *z*.

$$\frac{dC}{dz} = \left(\frac{1}{2 \cdot z}\right) \cdot \left(1 - z \cdot S - 2 \cdot C\right) \tag{3.32}$$

$$\frac{dS}{dz} = \left(\frac{1}{2 \cdot z}\right) \cdot \left(C - 3 \cdot S\right) \tag{3.33}$$

$$\frac{dt}{dz} = \left[x^3 \cdot \left(\frac{dS}{dz} - \frac{3 \cdot S \cdot \dfrac{dC}{dz}}{2 \cdot C} \right) + \frac{A}{8} \cdot \left(\frac{3 \cdot S \cdot \sqrt{y}}{C} + \frac{A}{x} \right) \right] \cdot \left(\sqrt{\mu}\right)^{-1} \tag{3.34}$$

For the problem of matching interplanetary trajectories, Newton's method was robust and produced tightly convergent answers in approximately five iterations. For the problem of matching departure trajectories leaving Earth, Newton's method was not as robust. While convergence was achieved for these orbits in over 99% of cases, the method would often crash for high-energy hyperbolic trajectories, especially for short times of flight (several hours). These solutions occur in regions where the functions are often quite flat. Another solution routine was created to attempt the problem by

using the secant method[39]. When first applying this routine it was noticed that the method was occasionally attempting solutions with much larger z values than normal. The C and S functions were therefore plotted across a large range of possible z values to ascertain the solution behavior (Figure 3.8).

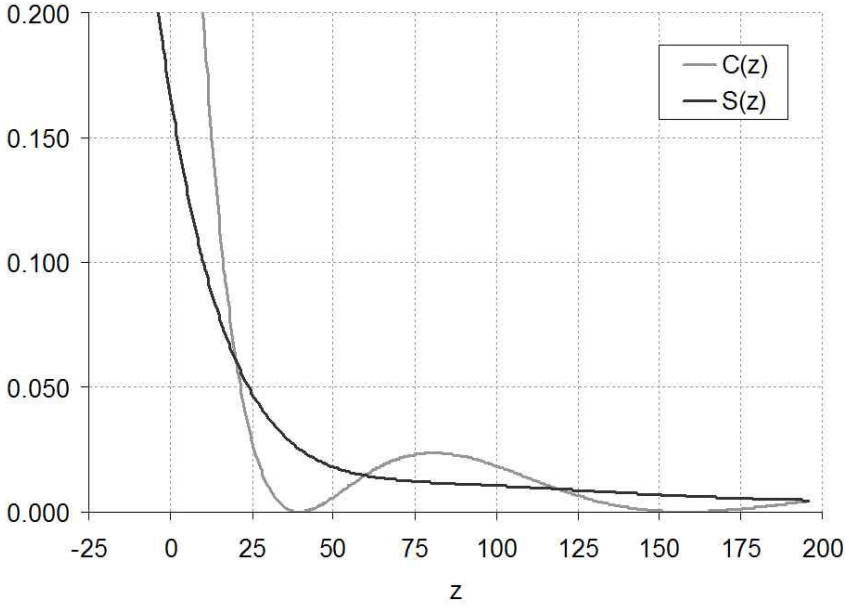

Figure 3.8 Universal Functions C(z) and S(z)

The C function is zero at a z value of $4\pi^2$ (~39.5) and again at $16\pi^2$ (~158). This periodicity corresponds to multiple elliptical transfer solutions. Values of z greater than $4\pi^2$ are for ellipses with times of flight greater than one period. To prevent the secant method from stumbling upon the undesired multi-period solutions, a bi-section method was added to limit the value of z to less than $4\pi^2$. With these modifications, the approach was entirely successful for use with the short departure orbits. Convergence was usually obtained in about eight iterations. The final version of the solution method is contained in Appendix B: Lambert's Problem Solution Algorithm.

Chapter 4. Development of Interplanetary Trajectories

This chapter builds upon the basic elements of the previous chapter to construct realistic three-dimensional interplanetary trajectories. The methods for determining these trajectories progresses from simple generalized two-body solutions up through converged three-body solutions utilizing the assumption of patched-conics. The final trajectories are divided into three phases by the boundaries of planetary spheres of influence. Methods are offered for finding the orbital parameters of the various trajectory segments.

4.1. Two-Body Trajectories

Precisely defining an interplanetary trajectory theoretically requires that all forces acting on the spacecraft be accounted for. These real forces include the mutual gravitational attractions of all the bodies in the Solar system as well as solar pressure and other non-gravitational forces. Overcoming such a problem setup would require a numerical solution approach which is extensive in both its formulation and use of computing resources making it difficult to analyze multitudes of trajectory possibilities. Fortunately, one of the forces dwarfs the others in terms of its magnitude, the gravitational influence of the Sun. Gravity varies as the inverse square of the distance and is proportional to mass. Thus, while the much less massive planets (compared to the Sun) may wield considerable gravitational influence over a nearby spacecraft, the strength of that influence decreases quickly with distance until

only the attraction of the Sun remains significant. During a standard interplanetary transfer between planets, the spacecraft may be considered to be proceeding under the sole influence of the Sun for a great majority of the transfer. The simplicity and relative accuracy of implementing these two-body calculations is very attractive when performing large numbers of trade studies comparing different transfers and was used as the first step in determining more refined interplanetary trajectories.

4.1.1. Point to Point Transfers

Employing the above assumption, the interplanetary transit trajectory becomes a simple transfer from the location point of the Earth on the date of the launch to the location point of the destination planet on the date of arrival. The planetary ephemeris data for the respective dates give the initial and final desired heliocentric position and velocity vectors but the planets themselves have no bearing in the solution at this stage. Clearly, solutions for different transit flight times on a specific launch date will result in different arrival dates. The solution of the transit trajectory is the straightforward application of the universal variables solution to Lambert's problem as detailed in the previous chapter. The method yields the required initial and final velocity vectors needed to travel between the locations. Figure 4.1 presents a sketch of the transfer trajectory to Mars and calls out the various position and velocity vectors.

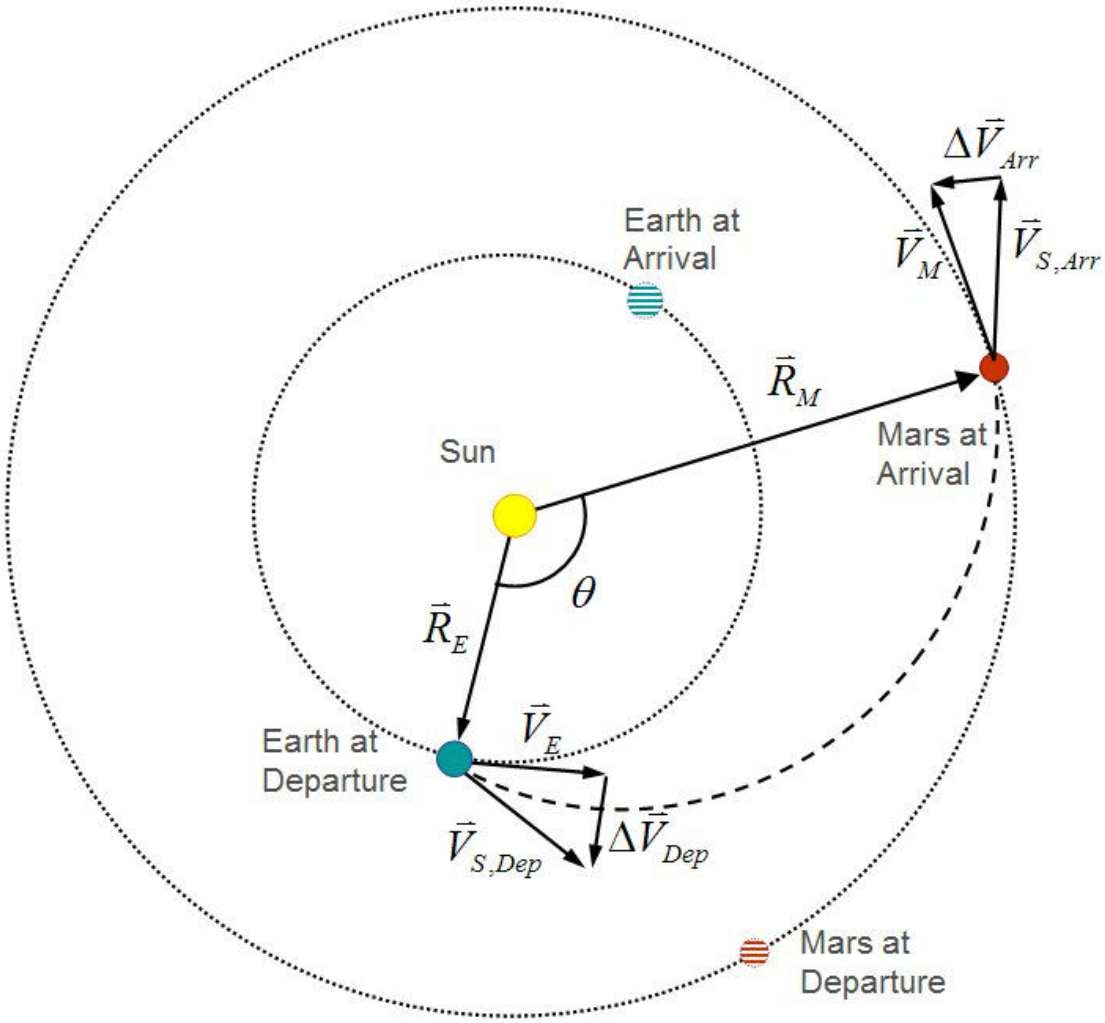

Figure 4.1 Point to Point Interplanetary Transfer Trajectory

Because the spacecraft is assumed to be moving at the speed of the Earth immediately before departure, the actual velocity change required of the craft will be the vector subtraction of the initial transfer velocity solution and the Earth's velocity. (A note on notation convention: heliocentric vectors are designated in this work as capital letters, while geocentric position and velocity vectors will be lower-case letters.)

$$\Delta\vec{V}_{Dep} = \vec{V}_{S,Dep} - \vec{V}_E \tag{4.1}$$

Similarly, once completing the interplanetary transfer the spacecraft will perform a maneuver to change its velocity from that of the final velocity of the transfer solution to that of the arrival planet (Mars in this case).

$$\Delta\vec{V}_{Arr} = \vec{V}_{M} - \vec{V}_{S,Arr} \tag{4.2}$$

The Earth's orbital speed, 30 km/s, is contributed towards the total velocity required of the transfer trajectory. For this reason, when attempting trajectories between Earth and the outer planets, it normally will be desirable to enter upon a transfer trajectory that has the same orbital direction as the Earth. To do otherwise would result in a substantial increase in the spacecraft propellant requirements. Another observation of interest is the position of Mars at departure. As shown in Figure 4.1, at the time of Earth departure, Mars is in a substantially different location than it will be by the time of the spacecraft's arrival some months in the future. Additionally, the Earth quickly separates itself from the location of the spacecraft's transfer path by the time of arrival. This is one of the principal difficulties in a direct return to Earth during the interplanetary transfer without incurring large propulsive expenditures.

4.1.2. Planetary Alignments

The greater the distance a planet, or any other body, is from the body it orbits, the slower the required orbital speed and the larger the distance traveled to complete one revolution (year). Therefore, in the sequence of its year, a farther planet will be lapped at intervals by more interior planets during the course of its orbit around the Sun. Consequently, for a specified planetary transfer alignment, the angular geometry of the two planets will only be available periodically. The synodic period is the elapsed time between successive occurrences of a given planetary orientation and

is derived from the orbital periods of the respective planets. The synodic formula from the Earth relative to a superior (farther from Sun) planet is computed as follows:

$$P_{Syn} = \frac{P_{Planet} P_E}{P_{Planet} - P_E} \tag{4.3}$$

Calculations for inferior planets will be of opposite sign than that given by the above expression. Table 4.1 shows the calculated synodic periods between the Earth and the other planets. The table also contains information on the orbital periods, velocities, and inclinations of the various planetary orbits. More detailed planetary information is presented in Appendix C: Planetary Physical and Orbital Data.

Table 4.1 Orbital and Synodic Periods of the Planets

	Orbital Period *(days)*	Orbital Period *(years)*	Orbital Velocity *(km/s)*	Orbital Inclination *(deg)*	Synodic Period *(days)*
Mercury	88.00	0.24	47.90	7	115.9
Venus	224.70	0.62	35.00	3.4	583.9
Earth	365.25	1.00	29.80	0.0	N/A
Mars	687.00	1.88	24.10	1.9	779.9
Jupiter	4,331.00	11.86	13.10	1.3	398.9
Saturn	10,747.00	29.4	9.70	2.5	378.1
Uranus	30,589.00	84	6.80	0.8	369.7
Neptune	59,800.00	164	5.40	1.8	367.5
Pluto	90,588.00	248	4.70	17.2	366.7

Launch opportunities from the Earth to Mercury happen with the greatest frequency as the small planet completes four revolutions in the time Earth completes one. The synodic period is greater than that fraction however, because in the course of one mercury year, the Earth has moved a quarter of its orbit and it takes Mercury an additional 28 days to catch up to it. With a synodic period of 116 days, Mercury laps the Earth approximately three times each Earth year. Venus and Mars alignments are

the least frequent of all the planets as their orbital periods are the most similar in magnitude to the Earth's. The outer planets all have synodic periods of approximately one year. With orbital periods many times greater than one Earth year, these planets, especially the farthest ones, do not change significantly in angular position in a single Earth year. As such, periodic realignments occur roughly as often as the Earth can return again to some desired position. The present study will be examining Earth-Mars trajectories. The synodic period indicates that for a specified planetary alignment scenario, Martian launch opportunities will recur roughly every other year.

4.1.3. Non-Coplanar Trajectories

This investigation did not make the simplifying assumption of circular coplanar planetary orbits. The planetary ephemerides are of real elliptical orbits whose planes are inclined to the ecliptic (see Table 4.1). Propulsive maneuvers to change inclination when effecting a transfer between two non-coplanar planetary orbits are significant and could not be neglected for this type of study without incurring a loss of realism and usefulness of the generated data. In addition to the planes of the Earth and arrival planet, the transfer orbit will be contained in its own orbital plane. This plane is defined by three points: the attracting body (the Sun in this case) and the two endpoints of the transfer orbit. The velocity vectors obtained from the universal variables solution will also both lie in this transfer orbit plane. The vector subtraction used in the propellant usage calculations will account for the required propellant expenditure for both velocity magnitude and direction/inclination

alterations for the departure and arrival. Figure 4.2 highlights the orientation of the transfer orbit as well as the inclination changes.

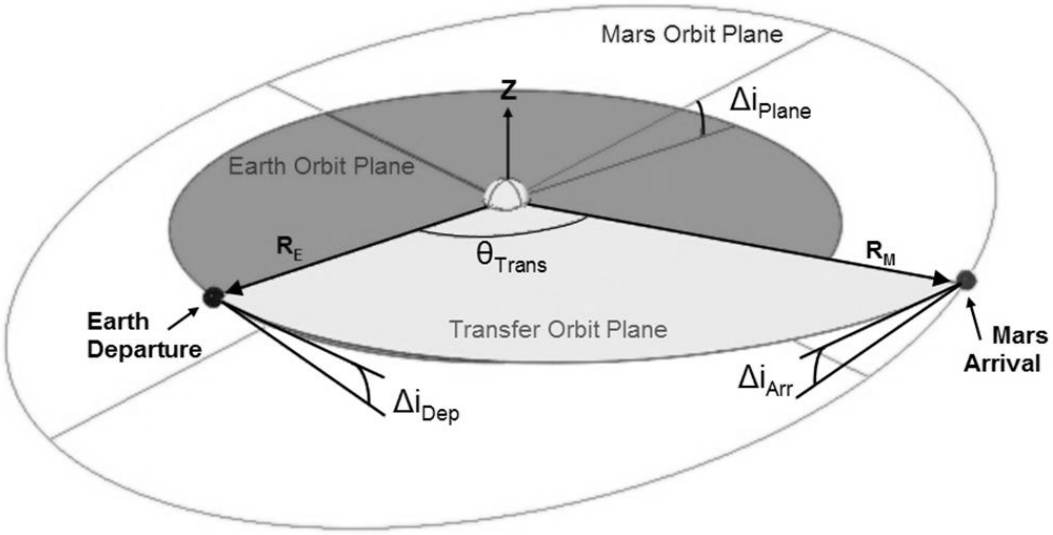

Figure 4.2 Inclinations of Orbital Planes for Non-Coplanar Transfers

4.2. Patched-Conic Approximation

The point-to-point solution previously considered generates a first-order trajectory approximation sufficient for obtaining a general understanding of the propulsive requirements as well as an appreciation of the impact of various planetary alignments. However, the specific departure and abort trajectories that are the focus of this body of work demand a more rigorous trajectory method capable not only of estimating the global propulsive requirements but of generating accurate and realistic position and velocity data for any point of the trajectory. Accomplishing such accuracy during the initial and terminal phases of the mission mandates that the gravitational influences of the associated planets be included. The patched-conic

approximation is a widely utilized method for including the influence of a planet on the trajectory without transforming the question into a three-body problem. The basis for the approximation is the assumption that the spacecraft initially moves under the sole gravitational influence of the departure planet. Then, at some distance, when the magnitude of that influence has decreased substantially, the departure planet is "turned off" and the Sun's influence is "turned on." The stellar gravitational attraction will be the sole influence until the spacecraft has approached the arrival planet at which time the Sun's influence is deactivated and the planet's gravitational attraction is activated.

4.2.1. Sphere of Influence

The fundamental element of the patched conic approximation is the gravitational sphere of influence (SOI). The radius of the sphere of influence is the distance at which the spacecraft transits from planetary motion to heliocentric motion. In actuality, the transition between the two frames of motion is a gradual one, but is adequately approximated with the sphere of influence assumption. The SOI is obtained by equating the equations of motion as viewed from the Sun frame to those of the planetary frame. Laplace suggested the following formulation[35]:

$$r_{SOI} = \left(\frac{m_{Planet}}{m_{Sun}} \right)^{2/5} r_{Planet} \tag{4.4}$$

Increasing planetary mass and/or distance will increase the extent of the planet's sphere of influence. The spheres of influence of the different planets are presented in Table 4.2 tabulated alongside the mass, sun distance, and diameter data[40] of each.

Table 4.2 Spheres of Influence: Planets

	Orbital Distance *(km)*	Mass *(10^{24} kg)*	Diameter *(km)*	Sphere of Influence *(km)*
SUN	0	1989100	1,392,000	N/A
Mercury	57,909,176	0.33	4,879.0	112,380
Venus	108,208,926	4.87	12,104.0	616,328
Earth	149,597,888	5.97	12,756.0	924,384
Mars	227,936,637	0.64	6,794.0	577,252
Jupiter	778,412,027	1899.00	142,984.0	48,212,192
Saturn	1,426,725,413	568.00	120,536.0	54,527,688
Uranus	2,870,972,220	86.80	51,118.0	51,757,612
Neptune	4,498,252,900	102.00	49,528.0	86,501,032
Pluto	5,906,376,272	0.01	2,390.0	3,094,728

The general trend seen from the table is the increasing size of planetary spheres of influence with distance. Two notable exceptions are Mars and Pluto. Mars has a smaller SOI than the Earth even though Mars has 1.5 times the Earth's orbital distance. This occurs because Mars has only one tenth of the Earth's mass which reduces the mass ratio part of the equation enough to reduce the SOI despite the increasing distance. The same trend occurs even more drastically for Pluto leaving Neptune with the largest SOI of any Solar planet with a sphere more than ninety times the extent of the Earth's SOI.

In addition to Sun-planet frames of reference, spheres of influence may also be defined for planet-moon systems. Table 4.3 catalogs the SOI values for the major moons of the Solar system as well as their masses, orbital distances, and diameters. The distances are given with respect to the parent planet of each moon. The table includes the Earth's moon Luna, the four Galilean moons of Jupiter, and the largest

moon each of Saturn, Uranus, Neptune, and Pluto. Figure 4.3 presents the relative sizes of the largest of these moons for comparison.

Table 4.3 Spheres of Influence: Major Moons

	Orbital Distance *(km)*	Mass *(10^{24} kg)*	Diameter *(km)*	Sphere of Influence *(km)*
Luna	384,403	0.0730	3475.0	66,028
Io	421,700	0.0893	3642.6	7,834
Europa	671,034	0.0480	3121.6	9,724
Ganymede	1,070,400	0.1482	5262.4	24,348
Callisto	1,882,700	0.1076	4820.6	37,677
Titan	1,221,931	0.1345	5150.0	43,331
Titania	435,910	0.0035	1577.8	7,637
Triton	354,800	0.0215	2706.8	12,003
Charon	19,571	0.0015	1212.0	8,425

Figure 4.3 Relative Sizes of Select Planets and Largest Moons

One difference which must be noted in the interpretation of the moon SOI table is that the moons listed do not all orbit the same planet. That means that the mass in the denominator of the mass ratio term in the SOI equation is not constant as it was for the planet SOI calculations. This behavior is readily apparent when comparing the spheres of Luna and Io. Both moons are approximately the same size, mass, and orbit their parent planets at about the same orbital distance. However, Luna has a SOI more than eight times larger than Io because the planet it orbits (Earth) is 300 times less massive than Io's parent planet (Jupiter). Though Ganymede and Titan are the most massive moons in the Solar system, Luna (third largest mass) has the largest SOI. This fact will become important when discussing transfer or abort trajectories to the Earth's moon. (When discussed in the context of other moons, the Earth's moon is designated by its Latin name Luna, otherwise it will referred to simply as the Moon.)

4.2.2. Trajectory Phases

Employing the sphere of influence formulation divides the interplanetary trajectory into three segments. The first is the escape trajectory from the departure planet, the second is the heliocentric transit trajectory, and the third is the arrival trajectory at the destination planet. The departure trajectory begins with the departure propulsive maneuver that alters the spacecraft from an assumed circular orbit around the departure planet and places it on an escape trajectory. The departure trajectory ends when the spacecraft exits the planet's sphere of influence. The heliocentric

interplanetary transfer is then patched from the exit point on the departure planet's sphere of influence to some entrance point on the arrival planet's sphere. The arrival phase lasts from that entrance until the spacecraft reaches a desired altitude and circularizes its orbit. These phases and the associated Sun-centered and planet-centered position vectors are shown in Figure 4.4 for an Earth-Mars transfer.

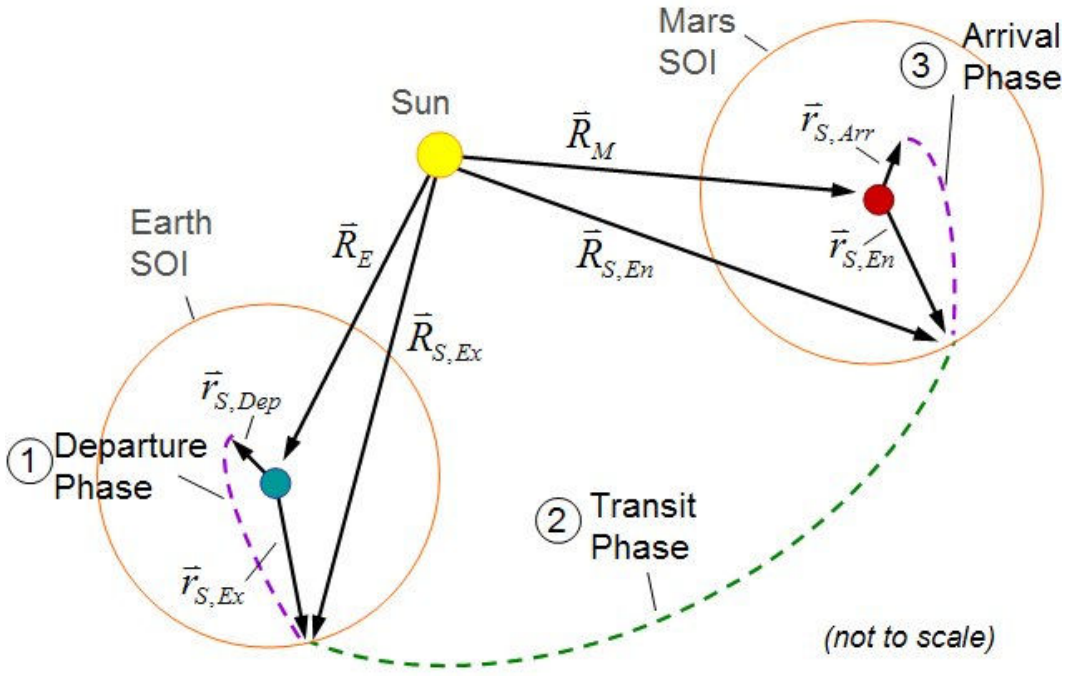

Figure 4.4 Interplanetary Trajectory Phases and Position Vectors

When within the SOI of a planet (during the departure or arrival phases), the spacecraft is assumed to be moving as part of the particular planetary system. The spacecraft position and velocity vectors will be accordingly referenced to the planet's coordinate system until crossing the SOI after which they must be transposed to the heliocentric coordinate system. Hence, the heliocentric spacecraft position at the SOI exit point is given by the following expression:

$$\vec{R}_{S,Ex} = \vec{R}_{E,Ex} + \vec{r}_{S,Ex} \tag{4.5}$$

The trajectory segmentation brought about by the application of the patched conic approximation also divides the total flight time of the mission into three segments. The Earth position in the above equation is consequently taken at the Julian date corresponding to the spacecraft exit of the Earth sphere of influence. The departure trajectory is developed in the next section.

4.3. Departure Phase: Earth-Centered

This section details the solution process used to determine the Earth departure orbit. The solution methods that are presented assume that a point-to-point trajectory between the departure and arrival planets has already been made and a rough estimate of the Julian date of departure and the direction and magnitude of the required velocity change has been obtained. This information is utilized to construct the departure hyperbolic orbit. The departure segment begins on the Julian date of Earth departure and ends when the spacecraft exits the Earth SOI.

4.3.1. Outbound Hyperbolic Orbit

The departure orbit is an escape trajectory meaning the spacecraft has enough orbital energy to leave the gravitational bounds of Earth. A hyperbolic orbit does not revolve around a planet repeatedly. If approaching the planet from infinity, the spacecraft will accelerate as it approaches the planet, experience a single orbital pass with the closest approach at periapse, and then be accelerated on a course which will

take it away from the planet. The general geometry of such a hyperbolic orbit is shown in Figure 4.5.

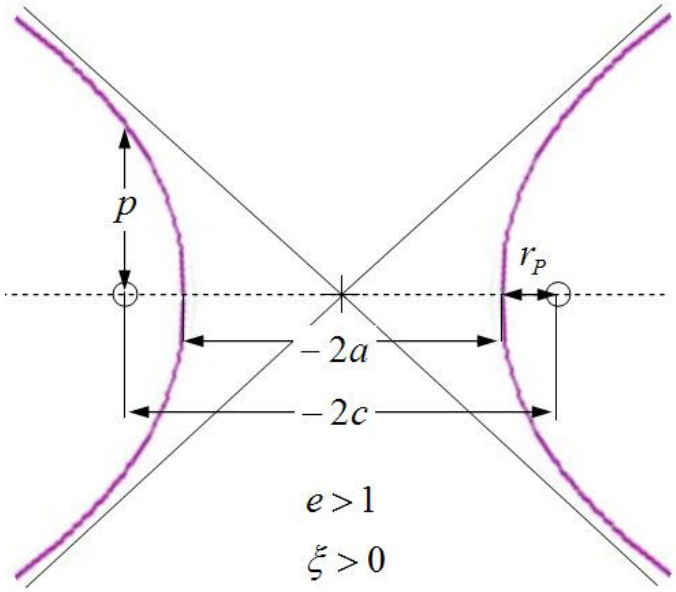

Figure 4.5 Hyperbolic Orbit

The departure orbit in this study begins, not at infinity, but at some specified circular low-Earth orbit. A propulsive maneuver is then performed which increases the velocity of the spacecraft sufficiently to send it on a one-way course out of the planetary system. Accordingly, the departure trajectory begins at the periapse of the hyperbolic orbit, which periapse has the same radius magnitude as the initial LEO orbit. The rationale behind the assumption of the parking orbit stems from the standard architecture expectation of a manned Mars mission. The vehicle and propellant mass requirements are anticipated to be quite large, necessitating at least minimal assembly of the spacecraft in Earth orbit before embarkation.

A few more parameters of the departure orbit must be identified before a solution is possible. Besides the altitude of this orbit, this study also specified the

orbital inclination relative to the **IJK** frame and used the provided value of the Earth obliquity given in the previous chapter. To maximize payload capability to LEO, it is extremely desirable to have the parking orbit at the same inclination as the latitude of the launch site. Propulsive maneuvers to alter inclination are costly in terms of mass both for the placement of material in LEO and for the hyperbolic departure from LEO. For this reason, the inclination of both the parking and departure orbit were specified at 28.5°, the inclination corresponding to a launch from Kennedy Space Center (KSC) in Florida.

The initial point-to-point solution of the previous section (see Figure 4.1) provided the velocity vector $\Delta \boldsymbol{V}_{Dep}$ which was taken for that approximation to represent the velocity change required of the spacecraft to achieve $\boldsymbol{V}_{S,Dep}$ which was the heliocentric spacecraft velocity vector of the transfer connecting the departure and destination planets. With the application of the more accurate patched conic approximation, $\Delta \boldsymbol{V}_{Dep}$ is no longer the velocity change required of the departure burn maneuver, rather, it is the velocity at which the spacecraft must be moving with respect to the Sun at the SOI exit. The excess velocity of the spacecraft after exiting the SOI is called the infinity velocity. Therefore, $\Delta \boldsymbol{V}_{Dep}$ becomes $\boldsymbol{V}_{S,\infty}$. After exiting the Earth SOI, the total heliocentric velocity, $\boldsymbol{V}_{S,Ex}$, is the sum of the infinity velocity and the Earth velocity vectors $\boldsymbol{V}_{S,\infty}$ and $\boldsymbol{V}_{E,Ex}$. The hyperbolic departure orbit must be designed to provide both the magnitude and direction of $\boldsymbol{V}_{S,\infty}$ at the SOI exit. As the departure orbit is Earth-centered and assumed to be inside the Earth SOI, the infinity vector must be transformed from the heliocentric $\boldsymbol{V}_{S,\infty}$ to the geocentric $\boldsymbol{v}_{S,Ex}$ using the coordinate transformations of the previous chapter. The layout of the departure phase

and the patching of the outbound hyperbolic orbit at the SOI interface are sketched in Figure 4.6

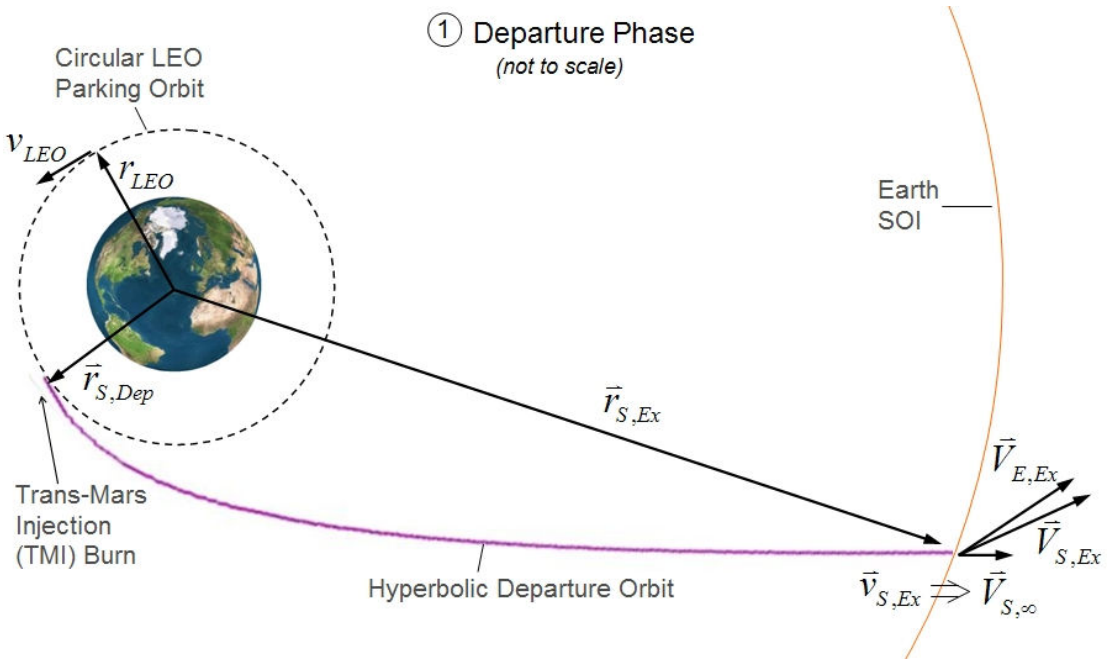

Figure 4.6 Departure Phase Position and Velocity Vectors

Note again that the infinity velocity direction is called out for both Geocentric and Heliocentric coordinates. The parking orbit is circular; therefore the radius and velocity magnitudes shown are constants of that orbit.

4.3.2. Establishing the Departure Orbit in Perifocal Coordinates

At this point of the solution, the known orbital parameters are the geocentric exit velocity vector and magnitude, the magnitude of the hyperbolic periapse, and the inclination of the hyperbolic departure orbit. Specifying Earth as the departure planet, values are available for the obliquity, gravitational parameter, and radius of

the sphere of influence. Using the magnitudes of the exit velocity and the radius of the SOI allows for the determination of the specific mechanical energy ξ.

$$\xi = \frac{v_{S,Ex}^2}{2} - \frac{\mu_E}{r_{SOI}} \tag{4.6}$$

The specific mechanical energy, though calculated here at the exit point, is a constant for a given orbit and therefore will be the same value along the trajectory from periapse departure to SOI exit. Consequently, the above expression may be rearranged and solved for the periapse velocity by using the mechanical energy and the periapse radius r_P.

$$v_P = \sqrt{2\left(\xi + \frac{\mu_E}{r_P}\right)} \tag{4.7}$$

Utilizing the energy further, the semi-major axis of the orbit may also be found[35].

$$a = -\frac{\mu_E}{2\xi} \tag{4.8}$$

The solution of the two-dimensional orbit in the perifocal plane does not require orienting that plane in space. Further, though the geocentric vectors of many of the orbital parameters are yet unknown, their magnitudes may be used to great effect in forming the perifocal trajectory. For example, the specific angular momentum, which is another constant of an individual orbit, is obtained from the position and velocity vectors. However, the magnitude of that momentum is simply the product of the magnitudes of the position and velocity and the cosine of the flight path angle. The periapse point is the ideal place to determine this constant for a hyperbola as the flight path angle at periapse is zero by definition. Calculating the magnitude of the specific angular momentum:

$$h = r_P v_P \tag{4.9}$$

The angular momentum is useful for obtaining the parameter of the orbit.

$$p = \frac{h^2}{\mu_E} \tag{4.10}$$

With the parameter defined, an expression for the orbital eccentricity may be formulated.

$$e = \frac{p}{r_P} - 1 \tag{4.11}$$

The angle between the spacecraft position and the orbital periapse is known as the true anomaly *v*. The true anomaly of the spacecraft at the SOI exit may be found from this relation:

$$\cos(\nu_{Ex}) = \left(\frac{1}{e}\right)\left(\frac{p}{r_{SOI}} - 1\right) \tag{4.12}$$

With the value of true anomaly for the spacecraft position at the SOI exit, the spacecraft position at that location may now be defined in the **PQW** perifocal coordinate system using the geometry of the orbit. Note the expression is good for finding the perifocal position vector, but requires the magnitude of that position (the SOI radius in this case) and true anomaly.

$$\vec{r}_{PQW,S,Ex} = \begin{bmatrix} r_{SOI}\cos(\nu_{Ex}) \\ r_{SOI}\sin(\nu_{Ex}) \\ 0 \end{bmatrix} \tag{4.13}$$

A different expression is used to give the two-dimensional perifocal velocity vector. Unlike the previous expression, only the true anomaly is required in addition to the constants of the orbit.

$$\bar{v}_{PQW,S,Ex} = \begin{bmatrix} \sqrt{\frac{\mu_E}{p}} \cdot \left(-\sin\left(\nu_{Ex}\right)\right) \\ \sqrt{\frac{\mu_E}{p}} \cdot \left(e + \cos\left(\nu_{Ex}\right)\right) \\ 0 \end{bmatrix} \tag{4.14}$$

Finally, with the assumption that the departure orbit and parking orbit are coplanar (same inclination), the propellant expenditure for initiating the interplanetary transit may be calculated. Making the reasonable assumption that the velocity change occurs over a very short time, the propellant ΔV is simply the difference between the velocity of the hyperbolic orbit at periapse, and the circular orbit speed of the parking orbit.

$$\Delta v_{Dep} = v_P - v_{LEO} = v_P - \sqrt{\frac{\mu_E}{r_{LEO}}} \tag{4.15}$$

The perifocal orbit is now completely defined both in orbital elements and by position and velocity vectors.

4.3.3. Determination of Unknown Orbital Elements

The objective of this section is to discover the departure orbit that yields the desired infinity velocity vector at the sphere of influence boundary. The exit position vector of that orbit must be found in order to facilitate the eventual patching of the trajectories across the sphere of influence. The size and shape of the orbit, along with the spacecraft's angular position from periapse have all been determined by the perifocal orbit. Orienting the perifocal orbital plane with respect to the geocentric **IJK** coordinate system requires the final three angular orbital elements; the inclination i, the argument of periapse ω, and the right ascension of the ascending

node (RAAN) Ω (see Figure 3.1). The desired inclination was already selected. The final departure orbit solution then becomes one of finding the values of ω and Ω that, when used to transform the orbit from the **PQW** to the **IJK** system, returns the correct exit velocity vector and provides the as-yet-unknown exit position vector. Considering the perifocal-to-geocentric transformation matrix of section 3.3, it is possible to use each of the three rows of that matrix to compute each component of the transformed velocity vector independently. The estimated **K** component of velocity for a guess value of ω would therefore be given by the following expression:

$$v_{K,Est} = \begin{bmatrix} \sin(\omega)\sin(i) \\ \cos(\omega)\sin(i) \\ \cos(i) \end{bmatrix}^T \cdot v_{PQW} \tag{4.16}$$

The difference between the desired **K** component of the exit velocity vector and the estimated component from the above equation is then simply:

$$D_K = \left| v_K - v_{K,Est} \right| \tag{4.17}$$

Considering this difference as the objective function, a basic numerical bracketing method can be applied to minimize the difference variable by changing ω. The method follows the direction of decreasing slope until the minimum has been bracketed. The bracketed interval is then searched at higher resolution for the actual minimum difference. Searching arguments of perigee over a range of 360° revealed that there are actually two values of ω that result in the desired velocity **K** component. Figure 4.7 shows the behavior of the objective function for a test case departure on June 8, 2003.

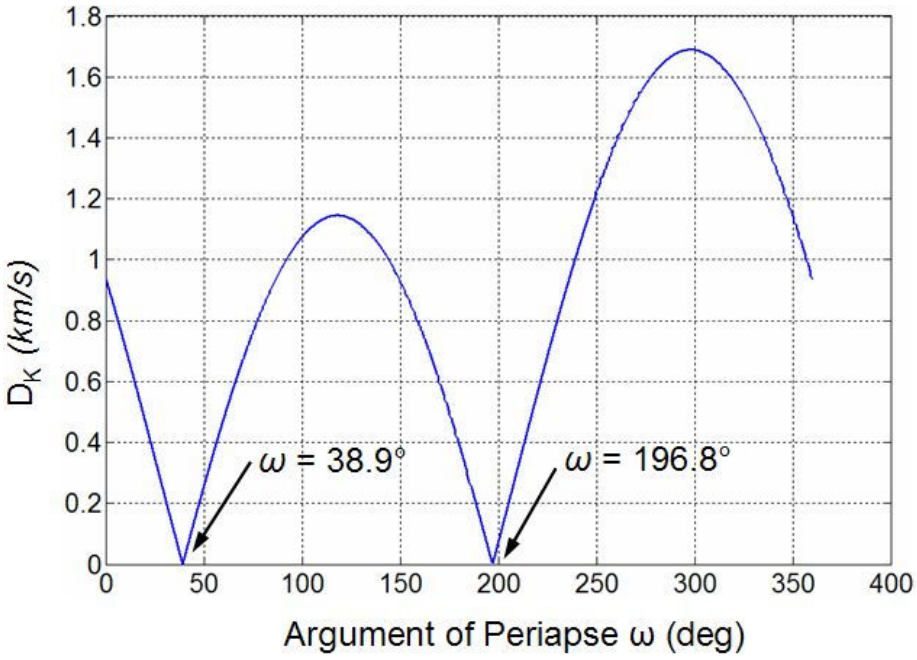

Figure 4.7 Argument of Periapse Values for K Component Matching

As shown by the figure, the **K** component of velocity is a periodic function which, when formulated as an absolute difference, provides two local minima. Only the **K** component has been matched. Establishing the correct set of orbital elements will necessitate matching the other two components of the exit velocity vector. The **J** component is a function of all three angular elements and an estimate is obtained thus:

$$v_{J,Est} = \begin{bmatrix} \sin(\Omega)\cos(\omega)+\cos(\Omega)\sin(\omega)\cos(i) \\ -\sin(\Omega)\sin(\omega)+\cos(\Omega)\cos(\omega)\cos(i) \\ -\cos(\Omega)\sin(i) \end{bmatrix}^T \cdot v_{PQW} \tag{4.18}$$

The search process for correct values of RAAN Ω is more complicated than for ω because values of Ω must be found for each of the two solutions of ω. The numerical

solution of Ω was setup in the same way as for ω with the formulation of a difference between the desired and estimated velocity components.

$$D_J = \left| v_J - v_{J,Est} \right| \tag{4.19}$$

The behavior of the Ω solutions for the two different ω values is shown in Figure 4.8.

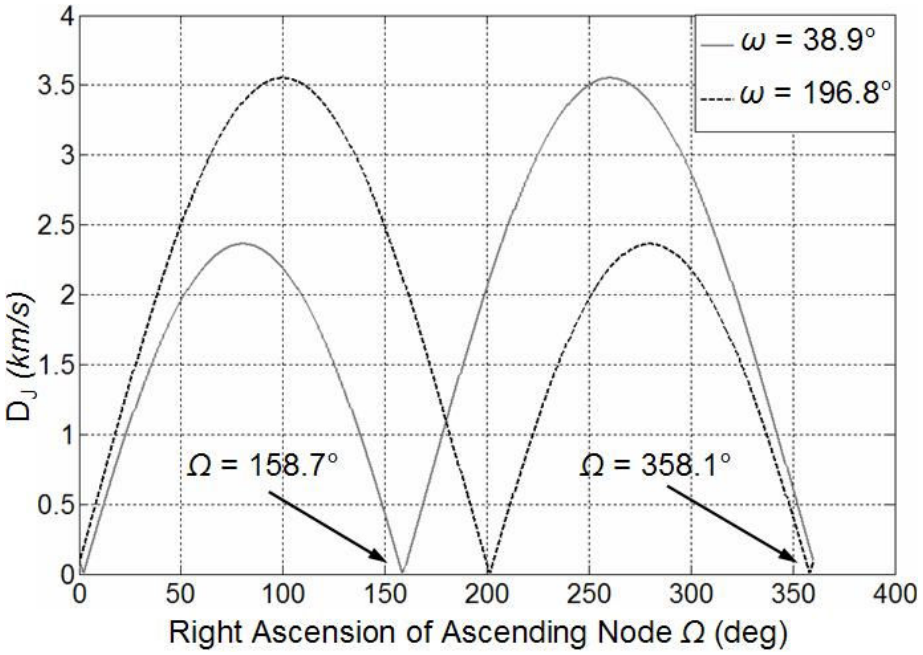

Figure 4.8 RAAN values for J Component Matching

Each Ω function also has two points where the difference between the estimated **J** component velocity and the desired velocity component is minimized. To discover which of the four candidate Ω values are acceptable, they must be substituted in along with the two solutions of ω to obtain an estimate of the **I** velocity component.

$$v_{I,Est} = \begin{bmatrix} \cos(\Omega)\cos(\omega) - \sin(\Omega)\sin(\omega)\cos(i) \\ -\cos(\Omega)\sin(\omega) - \sin(\Omega)\cos(\omega)\cos(i) \\ \sin(\Omega)\sin(i) \end{bmatrix}^T \cdot v_{PQW} \tag{4.20}$$

Substituting all the values into the expression reveals that, while all four values of Ω result in the correct **I** velocity component magnitude, only two of them give the correct sign of the component. The locations and values of these correct Ω solutions are those labeled in Figure 4.8. There are therefore two possible outbound hyperbolic trajectories for this example case which will deliver the desired velocity vector at the SOI exit. The now established orbital element sets are then used to specify the exit position vectors of each orbit. The orbital elements and position vectors of these two departure trajectories are given in Table 4.4 along with the example exit velocity vector that was matched (data from the June 8, 2003 test case).

Table 4.4 Orbital Parameters of Dual Departure Orbits for Sample Case

	$\boldsymbol{r}_{S,Ex,1}$	$\boldsymbol{r}_{S,Ex,2}$	$\boldsymbol{v}_{S,Ex}$
	924,384 *km*	**924,384 *km***	**2.969 *km/s***
I	898,003 *km*	895,884 *km*	2.8960 *km/s*
J	-206,864 *km*	-206,429 *km*	-0.5940 *km/s*
K	-72,693 *km*	-96,250 *km*	-0.2714 *km/s*
a (km)	-50,132.33	-50,132.33	
e	1.1309	1.1309	
i (deg)	28.5	28.5	
ω (deg)	38.927	196.837	
Ω (deg)	158.674	358.142	
v (deg)	150.559	150.559	

The two exit points of the above trajectories are almost 24,000 km apart. Though that seems a large separation distance, it is less than two Earth diameters. The trajectories are both plotted from LEO departure to SOI exit in Figure 4.9.

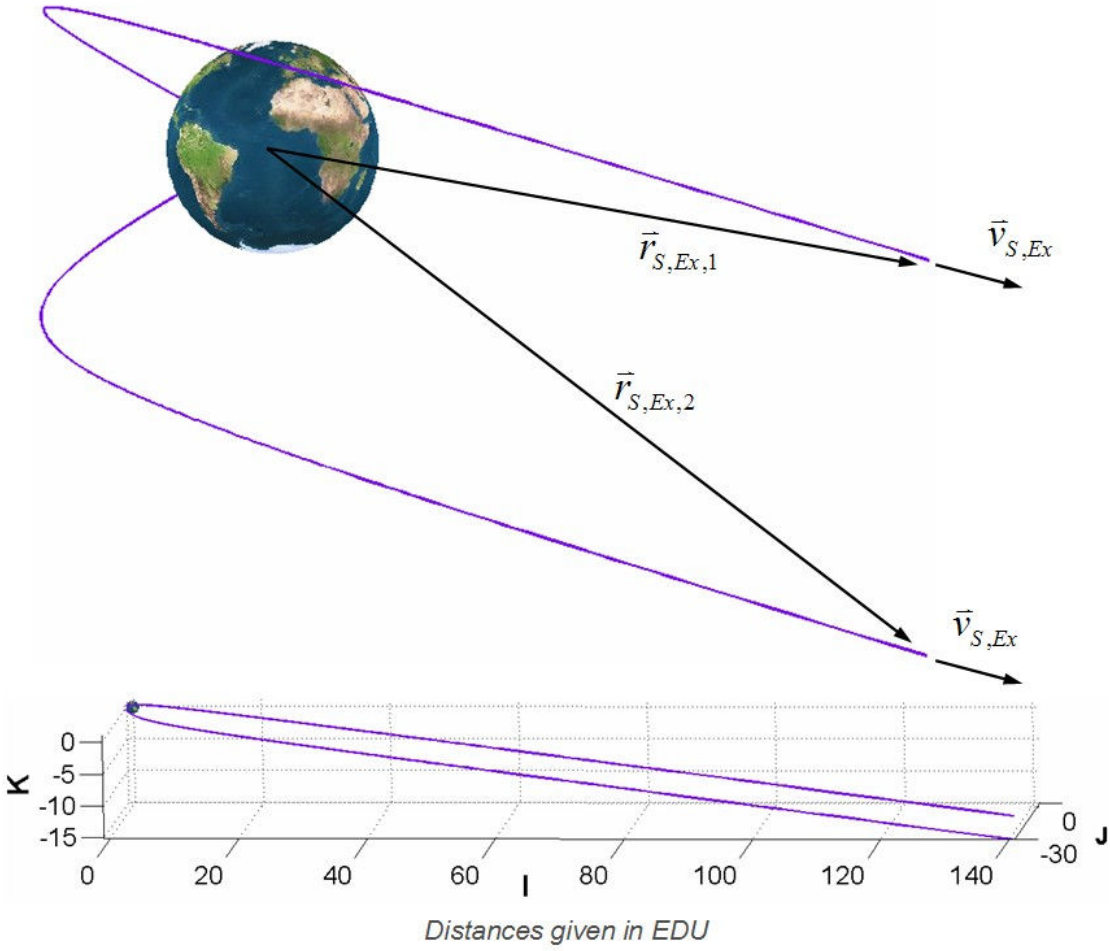

Figure 4.9 Trajectory Plots of Dual Departure Orbits for Sample Case

The trajectory plots confirm the close position proximity of the two departure orbits. At this stage, the selection of one or the other will not impact the trajectory matching or propellant usage calculations.

The departure orbit has now been completely defined based on the initial exit velocity vector and specified values for LEO orbit radius and departure inclination.

4.3.4. Departure Orbit Inclination Restrictions

In applying the previous section's formulation, it was discovered that there were several departure dates for which there was no satisfactory solution of the orbital elements. For these departure dates, though the ω value that yielded the smallest difference for **K** component velocity matching was found, that difference was unacceptably large. For example, the **K** component matching for the departure date of May 12, 2018 was in error by about 500 m/s for an inclination of 28.5°. As the ω matching is a function of i and guess values of ω, it was theorized that the specified inclination was insufficient for orienting the perifocal plane to provide the desired exit velocity component.

The implementation of the departure orbit was modified to check the magnitude of the difference discovered during ω matching. If the magnitude of the difference is greater than one meter per second, then the specified inclination is increased incrementally and the velocity component matching is iterated until the re-minimized ω yields a difference value that matches the tolerance. Figure 4.10 shows the ω solution behavior for different values of inclination on the departure date of May 12, 2018. The represented inclinations are the original LEO inclination of 28.5°, the incremented inclination value that first resulted in an acceptable ω solution (36.92° for this case) and an inclination beyond that point (40.0°).

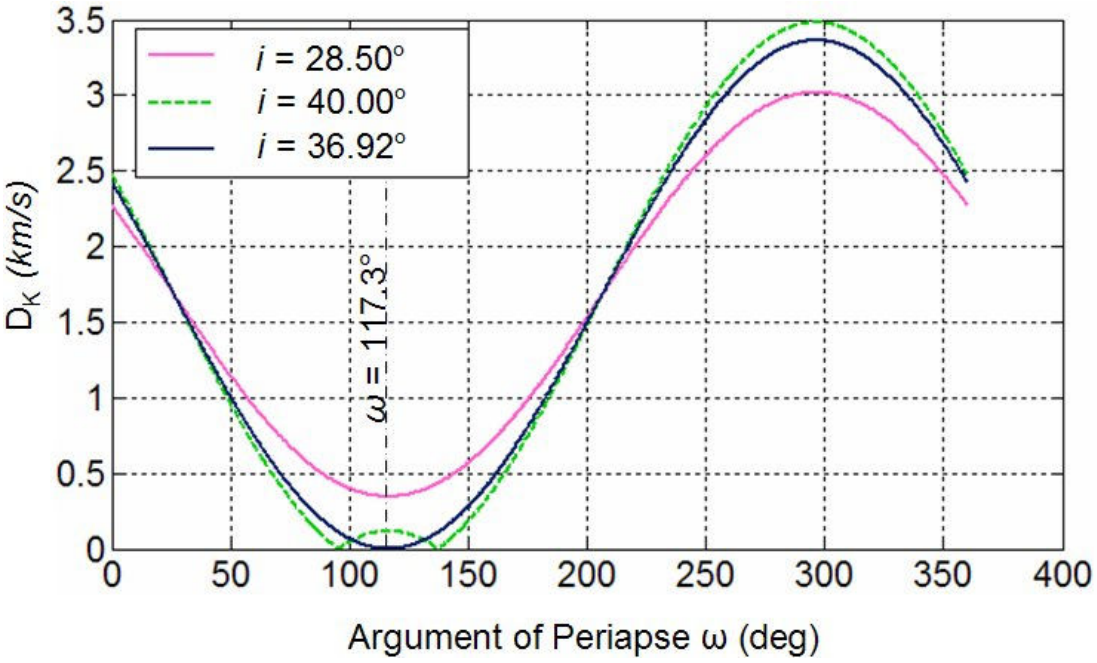

Figure 4.10 Argument of Periapse Values for Various Inclinations

The figure clearly shows that for an inclination of 28.5°, the minimum velocity component difference never reaches zero. Increasing the inclination to 36.92° does result in a zero value for the difference at a $\omega = 117.3°$. Unlike the general ω solution formulation in the previous section, there is only one ω solution for this inclination, not two. Larger inclinations (40.0°) increased beyond that required to just obtain a ω solution will again result in two solutions for ω. Increasing the inclination even further would shift the bottom of the ω curve lower and increase the separation distance between the two ω solutions.

After finding an acceptable value of ω, the solution of the right ascension Ω proceeds as before. Figure 4.11 plots the Ω curve for the single ω solution of the 36.92° inclination case and the dual Ω curves for the two ω values at the 40.0° inclination.

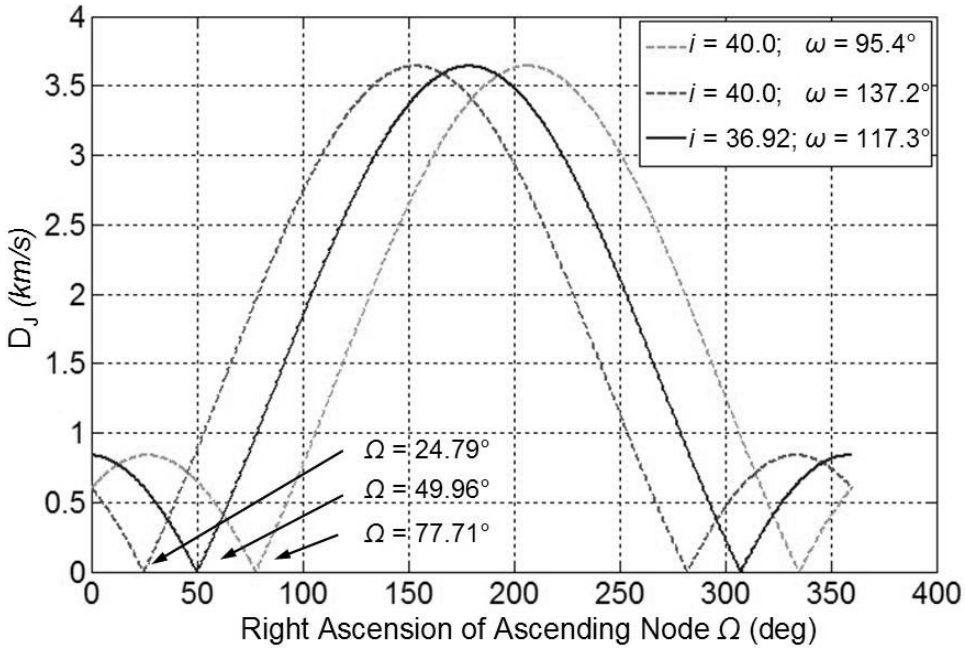

Figure 4.11 RAAN Values for Various Inclinations

The three Ω curves are of similar shape, shifted horizontally by their slightly different values of ω. The Ω values yielding the correct velocity component magnitude and direction are indicated on the figure. The orbital parameters of these three possible departure orbits for the May 12, 2018 departure are listed in Table 4.5.

Table 4.5 Orbital Parameters of Increased Inclination Departure Orbits

	$\boldsymbol{r}_{S,Ex}$	$\boldsymbol{r}_{S,Ex,1}$	$\boldsymbol{r}_{S,Ex,2}$	$\boldsymbol{v}_{S,Ex}$
	924,384 *km*	**924,384 *km***	**924,384 *km***	**2.800 *km/s***
I	559,370.67 *km*	563,797.73 *km*	556,669.62 *km*	1.7461 *km/s*
J	-483,005.04 *km*	-485,133.43 *km*	-479,412.79 *km*	-1.4014 *km/s*
K	-555,244.42 *km*	-548,874.7 *km*	-561,041.97 *km*	-1.6818 *km/s*
a (km)	-57,114.91	-57,114.91	-57,114.91	
e	1.1149	1.1149	1.1149	
i (deg)	36.92	40.0	40.0	
ω (deg)	117.318	95.417	137.163	
Ω (deg)	49.964	77.713	24.786	
v (deg)	152.0634	152.0634	152.0634	

The 36.92° inclination orbit is the first possible departure orbit for the May 12, 2018 case. Any higher inclination will provide two additional departure possibilities. The departure orbits for the 36.92° and the 40.0° inclinations are plotted in Figure 4.12 from LEO departure up until SOI exit.

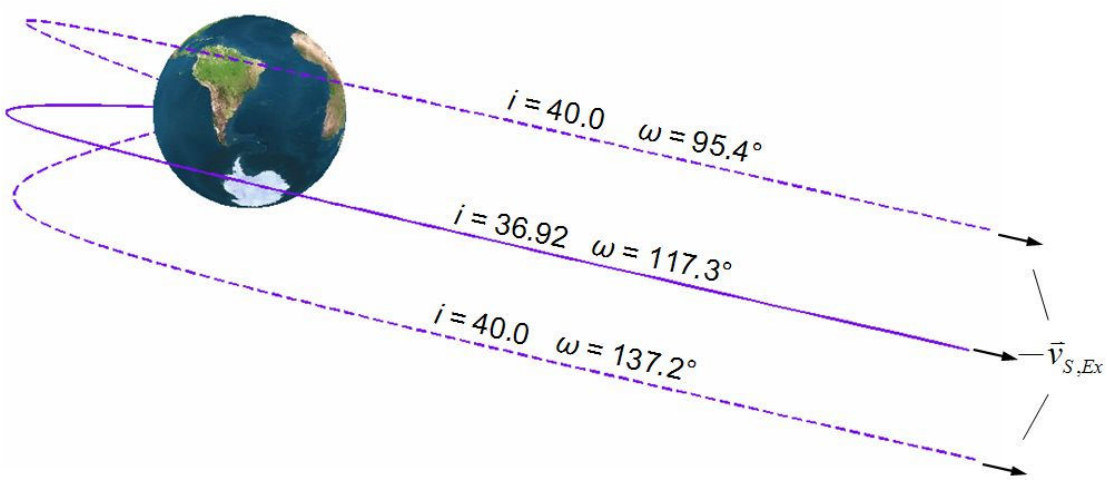

Figure 4.12 Trajectory Plots of Possible May 12, 2018 Departure Orbits

The figure demonstrates how the dual orbital possibilities of the higher inclinations relate to the single orbit possibility at the minimum inclination.

The inclination restriction may also be interpreted geometrically. The geometric representation of potential sphere of influence exit points facilitates both an understanding of departure orbit orientation possibilities and a visualization of the inclination restriction for allowable departure velocity vectors. At a specified inclination, the varying of the argument of periapse and the right ascension through all possible values will produce a host of departure exit points which define an exit surface with the radius of the SOI. The curve in Figure 4.13 is composed of all the possible exit points obtained by varying ω for a generic hyperbolic departure.

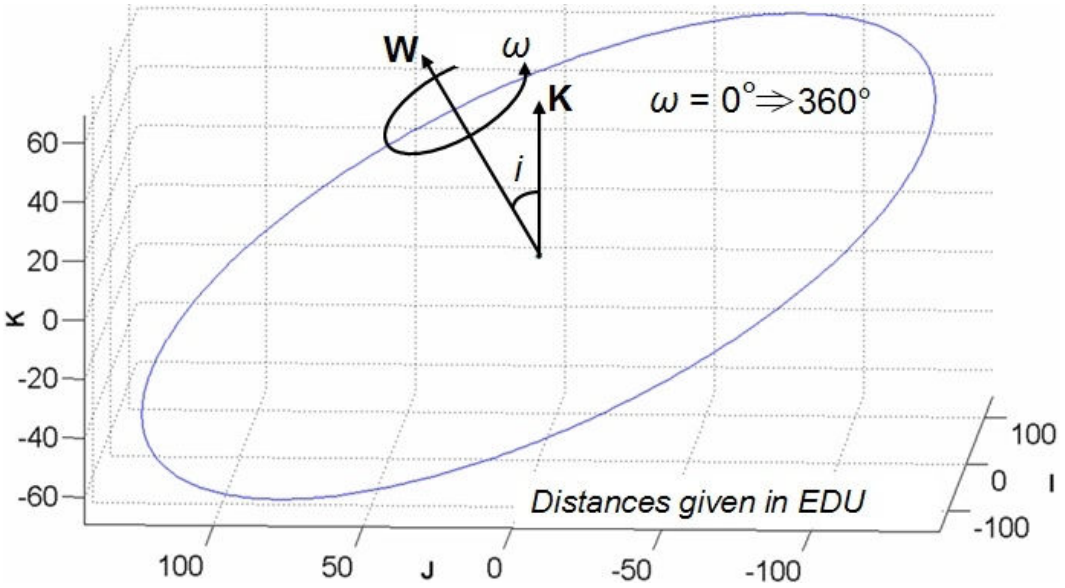

Figure 4.13 Possible Exit Points for Argument of Perigee Variation

The curve in the figure is for a specified inclination and some constant Ω. Changes in ω rotate the orbit about its **W** vector in the perifocal plane. The addition of Ω variation about the geocentric **K** direction in Figure 4.14 produces many such curves.

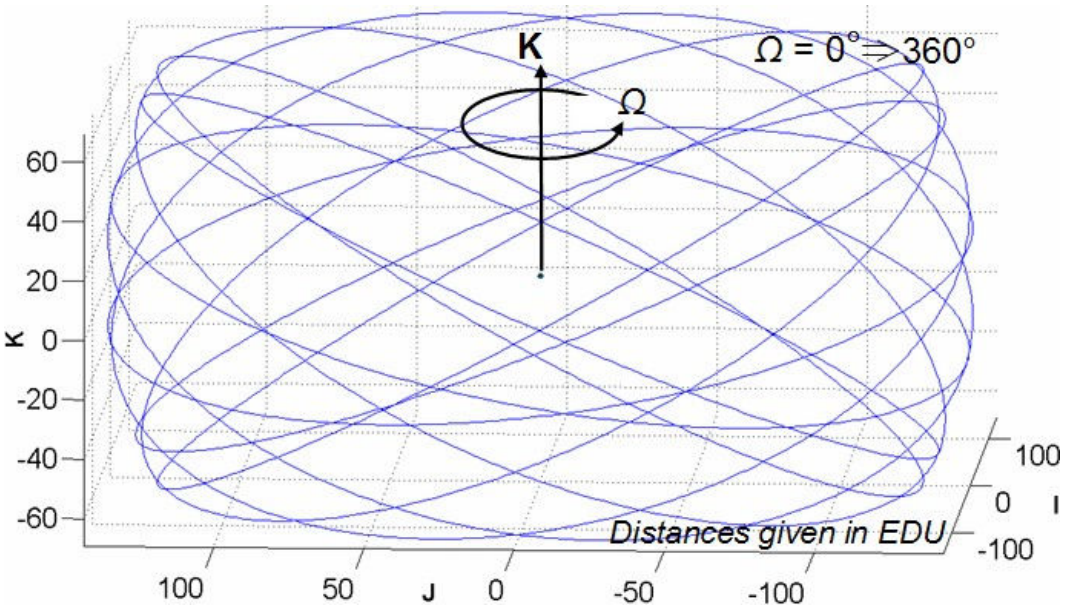

Figure 4.14 Possible Exit Points for Right Ascension Variation

When the exit points are plotted for all possible values of ω and Ω, they create an exit surface. The exit surface will be some portion of a spherical surface and is more extensive for higher inclinations. The exit surfaces for two different inclinations are shown in Figure 4.15.

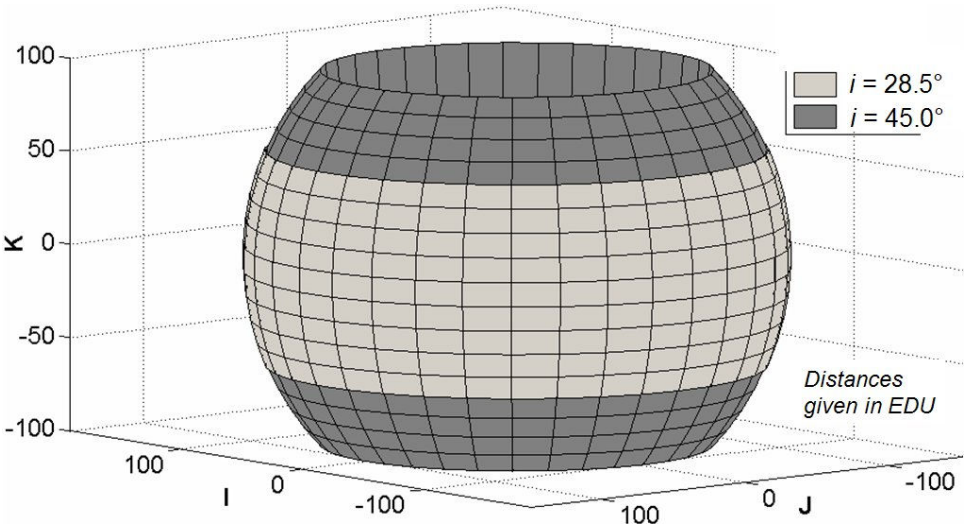

Figure 4.15 Surfaces of Possible Exit Points for Different Inclinations

The exit surface of the larger inclination includes the surface of the lower inclination but extends farther in the positive and negative **K** direction. In general terms, an inclination is valid if the desired geocentric departure vector may be drawn from the origin to some point on the surface. Neither inclination in the figure would be sufficient for an exit velocity vector nearly aligned with the vertical direction while both would be quite capable of exit vectors aligned anywhere near the horizontal **IJ** plane.

An additional consequence for those cases where the inclination must be increased is a modification in the calculation of the departure propulsion maneuver.

Two possibilities exist. If the LEO parking orbit is altered to be at the required inclination of the departure orbit, than the maneuver remains a simple collinear velocity difference. If the LEO parking orbit is in a different inclination than the departure orbit than the departure ΔV is now the result of vector subtraction. The case of the altered inclination parking orbit, though simpler in terms of maneuver calculation, will impact the amount of mass that can be placed in that orbit versus the baseline orbital inclination at the latitude of the launch site.

4.3.5. Departure Orbit Summary

In summary, after the hyperbolic departure orbit has been formulated in the perifocal plane, it is oriented into the geocentric coordinate system by finding the correct values for the angular orbital elements following the formulation presented. A specified inclination may or may not be sufficient for the extraction of the correct velocity vector. If acceptable, the inclination will yield two departure orbit possibilities, which despite being slightly separated in space position, will nonetheless have the same exit velocity vector. In cases where the inclination is insufficient to obtain the desired solution, the inclination is incremented until an acceptable value is attained. A single departure solution will therefore be found unless the inclination is incremented beyond the required minimum, in which case there will again be two departure solutions.

4.4. Arrival Phase: Mars-Centered

Continuing with the patched-conic approximation, the arrival segment begins on the Julian date of the spacecraft's entrance into the destination planet's sphere of influence and ends at the Julian date of the spacecraft's arrival at that planet. The destination planet for this study will be Mars throughout. Upon reaching the periapse of the arrival orbit, the spacecraft is initially assumed to be captured into a low altitude circular Mars orbit. This body of work is concerned primarily with the departure phase of the interplanetary trajectory. The abort scenarios that will be presented in later chapters will require exact knowledge of the spacecraft position and velocity throughout the entire departure phase. That level of position accuracy is not needed for the areocentric arrival orbit. The methods of the previous section for the determination of the hyperbolic orbit could be applied to the arrival orbit with minor changes; however, the present work will formulate a simpler form of the arrival phase.

4.4.1. Inbound Hyperbolic Orbit

Though exact position data along the inbound arrival orbit is not needed for this study, the orbit must be approximated sufficiently to calculate the propellant required for the Mars orbit insertion (MOI) burn. The solution begins with the same type of information that the departure orbit began with, namely the radius of the appropriate sphere of influence, and the infinity velocity vector at the sphere; though the velocity vector is entering the planet's SOI in this case instead of exiting. The radius magnitude of the final assumed circular Mars orbit must also be provided. The

magnitude of the capture ΔV is then calculated following the process contained in Eqs. (4-6) to (4-15). A schematic of the arrival phase showing the various position and velocity vectors is sketched in Figure 4.16.

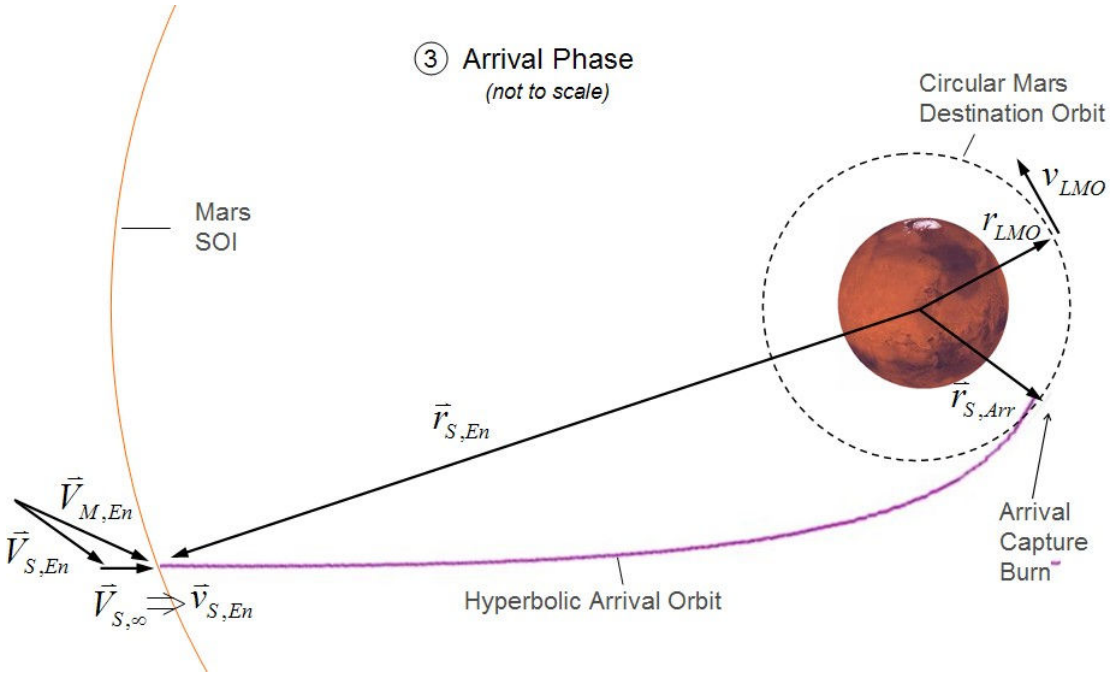

Figure 4.16 Arrival Phase Position and Velocity Vectors

Much of the work of the departure phase section was concerned with obtaining appropriate values of the exit position vector. The corollary entrance position vector for the arrival phase, $\boldsymbol{r}_{S,En}$, is not calculated in this abbreviated treatment of the arrival phase trajectory. Without that position, the trajectory patch at the Mars SOI is therefore not exact, but the simplification will not significantly affect the accuracy of the departure trajectory patch, which is the phase of greatest import to this investigation.

4.5. Trajectory Continuity at Interface

The final step in the formulation of the patched conic approximation is to ensure that the various trajectory phases match up and are continuous across the sphere of influence division. Achieving the desired continuity in position and velocity will require an iterative process. Time must also be consistent. For example, the Julian date of the Earth SOI exit, JD_{Ex}, must differ from the Julian date of LEO departure, JD_{Dep} by the same amount as the flight time of the hyperbolic departure orbit from LEO departure to SOI exit. This requires iteration since the velocity vector used to initially determine the departure orbit came from the point-to-point approximation which used the Earth position and velocity values for JD_{Dep}. Subsequent iterations are needed to improve upon that estimate using the values as they are on JD_{Ex}. The process of converging on the complete patched transfer trajectory is outlined below. The focus is on the accuracy of the departure phase, as the arrival phase was not fully patched.

1. For a specified JD_{Dep} and total time of flight TOF_{Tot}, calculate the interplanetary trajectory using the point-to-point two-body assumption. This will result in values of the spacecraft departure and arrival velocity vectors centered on the origin of the planets from which the $\Delta \boldsymbol{V}$ vectors for departure and arrival may be calculated.
2. Switch to the patched conic approximation and calculate the planetary spheres of influence.

3. Transform the $\Delta \boldsymbol{V}$ vectors from heliocentric coordinates to geocentric and areocentric coordinates. These $\Delta \boldsymbol{V}$ vectors are then assumed to be the infinity velocity vectors $\boldsymbol{v}_{S,Ex}$ and $\boldsymbol{v}_{S,En}$ respectively.
4. Using the magnitudes for the respective spheres of influence and periapse radii, compute the hyperbolic departure and arrival orbits in perifocal coordinates. Also calculate the departure and arrival ΔV magnitudes.
5. Calculate the departure and arrival times of flight TOF_{Dep}, TOF_{Arr} and use them to compute the exit and entrance Julian dates JD_{Ex} and JD_{En}. (Note, this analysis neglects the arrival trajectory patching therefore $JD_{En} = JD_{Arr}$.) The JD_{Dep} and JD_{Arr} remain the same and consequently so does the TOF_{Tot}, though the transfer time of flight TOF_{Trans} is the TOF_{Tot} minus the departure flight time TOF_{Dep}.
6. For the departure phase, determine the orbital elements that allow the hyperbolic orbit to yield back the infinity velocity vector $\boldsymbol{v}_{S,Ex}$. Use these values to compute the exit position vector $\boldsymbol{r}_{S,Ex}$.
7. Re-compute Earth position and velocity vectors from the Earth ephemeris using JD_{Ex}.
8. Compute the heliocentric exit position vector $\boldsymbol{R}_{S,Ex}$ by vector addition of $\boldsymbol{R}_{E,Ex}$ and $\boldsymbol{r}_{S,Ex}$.
9. Compute the interplanetary transit phase using the point-to-point approximation between $\boldsymbol{R}_{S,Ex}$ and $\boldsymbol{R}_{M,Arr}$ using the velocities $\boldsymbol{V}_{E,Ex}$ and $\boldsymbol{V}_{M,Arr}$ and the transfer time of flight TOF_{Trans}. Re-calculate the $\Delta \boldsymbol{V}$ vectors.
10. Return to step 3 above and iterate until $\boldsymbol{r}_{S,Ex}$ stops changing, then exit.

The above process requires only a handful of iterations to converge on a continuous trajectory. The formulation retains the same departure date and total time of flight throughout the application of the two different trajectory approximations. Comparing the converged trajectories to those of the first iteration reveals only minor differences, indicating that only small errors are introduced if the trajectory is not iterated after the first execution through to step 9.

This chapter has presented the method for determining an interplanetary transfer trajectory for a specified set of planets, departure date, and total time of flight. In addition to the point-to-point initial trajectory assumption, the patched conic approximation was added to provide detailed orbital elements and position date of the departure orbit suitable for use with the abort modes to be presented later.

Chapter 5. Earth-Mars Transit Trajectories

The work of this chapter utilizes the general trajectory methods that have been presented in previous chapters and apply them to the solution of specific Earth-Mars trajectories as part of an integrated manned Mars mission analysis. The attributes and requirements of the resulting trajectory classes are presented along with a tabulation of the resulting launch opportunities. Selection criteria are discussed for the identification of likely trajectory types for use in manned Mars exploration missions. These candidate trajectories are used as the basis from which to ascertain and quantify the departure phase abort requirements in the following chapters.

5.1. Mars Transfer Parameters and Characteristics

Constructing an interplanetary trajectory simply requires the positions and velocities of the planet of origin at departure and of the destination planet at arrival (Figure 4.1). Using planetary ephemerides, interplanetary transfer opportunities may therefore be uniquely identified by provision of the departure and arrival dates or equally by providing the departure date and time of flight. Trade studies of various interplanetary trajectories are often performed assuming point-to-point transfers following the description of the previous chapter. Trade studies of departure date and transit flight time are executed to establish opportunistic launch windows. The determined dates of opportunity will vary depending on propulsion type, mission architecture, and propulsive maneuver allocation. The launch parameters and results are typically portrayed in a "pork chop" plot[41] so called because of the distinctive shape of the delta V contours. The total delta V requirements for a Mars transfer in

2018 are shown in Figure 5.1. The total delta V for the presented example is the sum of the initial and final delta V requirements assuming propulsive departure and arrival maneuvers.

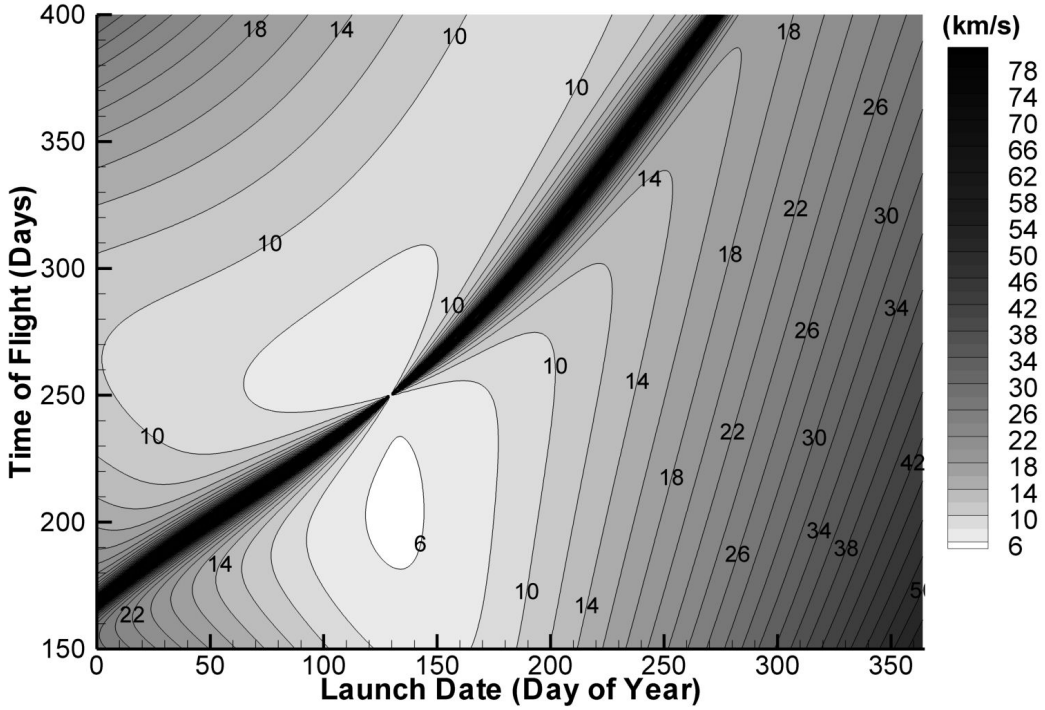

Figure 5.1 2018 Mars Departure Launch Window: Total Delta V

The plot shows a drastic difference in the amount of required delta V depending on the launch date and flight time. There are two regions of minimal delta V separated by a narrow band of extremely high velocity requirement. Understanding for the existence of this steep region may be gained by investigating the inclination changes the spacecraft executes to get on and off the transfer plane (Figure 5.2) as well as the interplanetary heliocentric transfer angle (Figure 5.3).

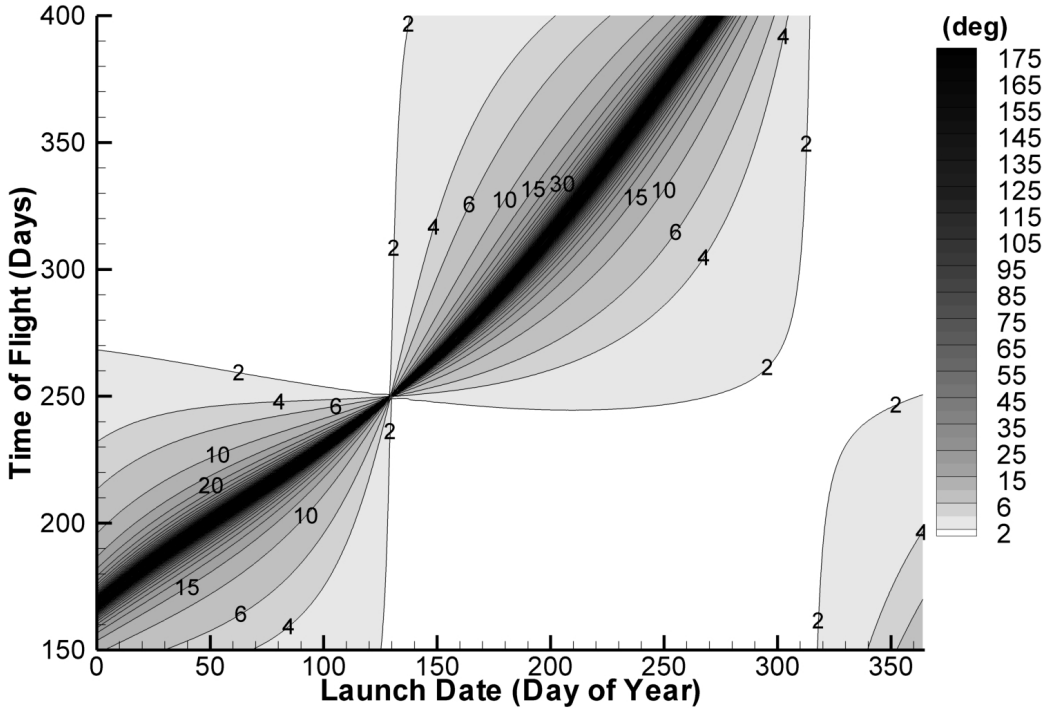

Figure 5.2 2018 Mars Departure Launch Window: Total Inclination Change

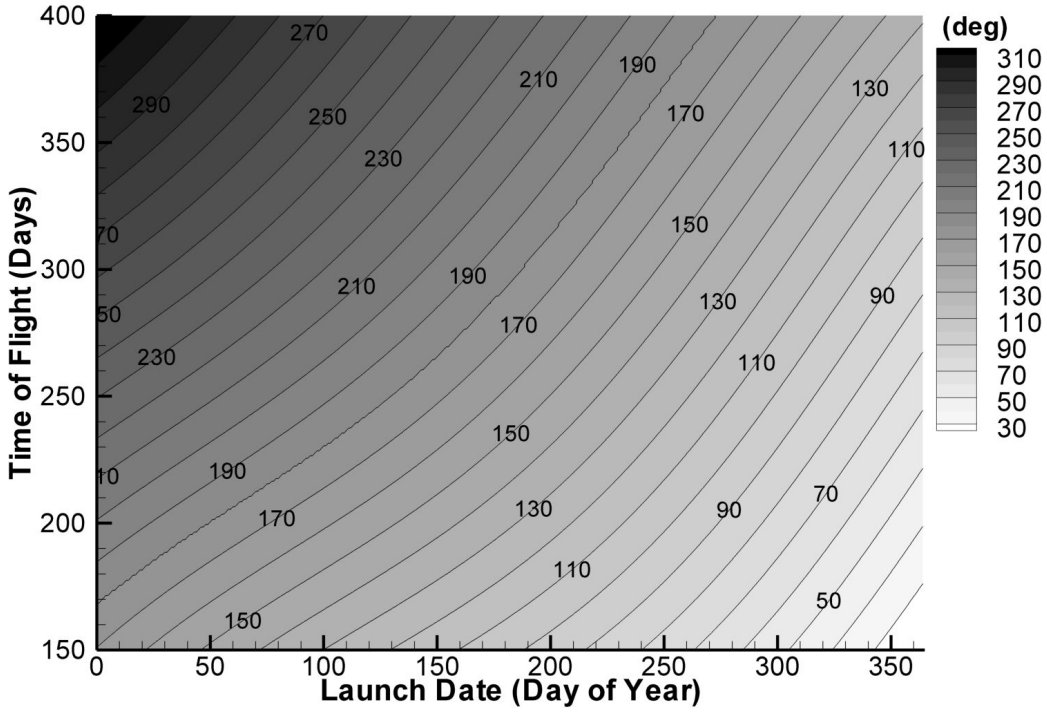

Figure 5.3 2018 Mars Departure Launch Window: Interplanetary Transfer Angle

Figure 5.2 shows that the regions of greatest inclination maneuvering match those of highest delta V requirement. Correlating this trend with Figure 5.3 reveals that the periods of greatest inclination change, and hence greatest delta V, occur when the transfer angle is nearest 180°. One result of the two-body gravitation assumption is that all orbital motion proceeds in the orbital plane. The transfer orbit plane for the interplanetary rendezvous problem is aligned using three points; the Sun and the positions of Earth at departure and Mars at arrival. Given that planetary orbital planes are different from one another, the transfer plane is inclined with respect to both in order to contain the three points thus requiring inclination change maneuvers on both ends of the transfer. This situation can be exacerbated when the planets are on opposite sides of the sun (~180° transfer angle). The only plane connecting Earth and Mars in that situation is perpendicular to the Earth's orbital plane (Figure 5.4).

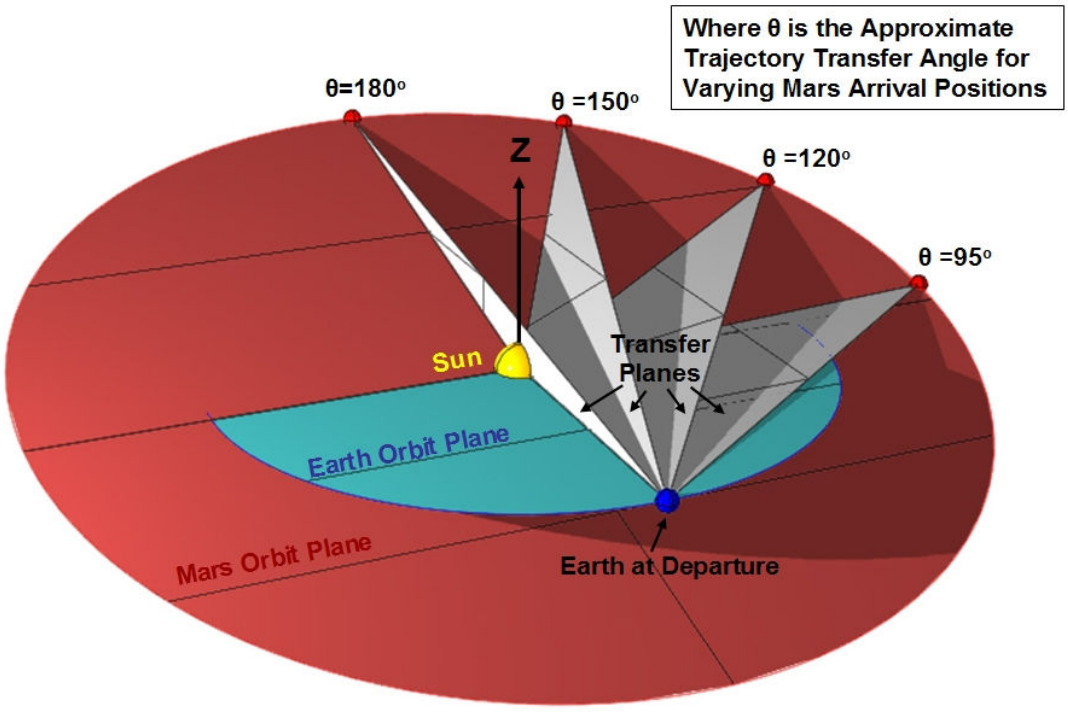

Figure 5.4 Transfer Plane Orientation Schema

There is one exception to the near perpendicular transfer for the 180° transfer angle case which occurs when Mars crosses the plane of Earth's orbit. At that moment, a 180° transfer orbit may be connected between the Earth and Mars that lies in the Earth's orbital plane requiring no outbound inclination change and a small inclination change to match Mars inclination at arrival. This phenomenon is evidenced by the small passage that divides the wall of high delta V in Figure 5.1. Even when this exception occurs, it does not necessarily represent the global delta V minimum. Combined effects from non-circular planetary orbits and total inclination minimization can result in delta V optimums in other parts of the trade space as is the case in Figure 5.1 where the minimum occurs on May 12, 2018 with a flight time of 204 days.

The situational sketch of the inclination differences in Figure 5.4 is exaggerated for clarity. In reality, the difference between the Mars and Earth orbital planes is only 1.9°. The result of such a small actual difference is that the required inclination changes are fairly small for most of the trade space as is documented by Figure 5.2. However, regardless of the magnitude of the inclination difference, any approximate 180° transfer between two non-coplanar orbits will require a nearly perpendicular transfer orbit. These drastic inclination effects and their influence on mission delta V requirements provide strong incentive to perform mission trades utilizing full three-dimensional planetary ephemerides rather than simplified two-dimensional approximations. Indeed, as has been shown, an exact Hohmann type

(180°) transfer between two planets is, except for the special case noted, the most propellant intensive transfer for a given launch date.

A final observation from the data is obtained by analyzing the transfer angles. When matching a trajectory for any two position vectors it is recalled that there are two possible solutions; the "long" and the "short" trajectory paths (Figure 3.7). The upper regions of Figure 5.1 are of trajectories with transfer angles greater than 180° while the lower regions are of transfer angles less than 180°. Therefore, as discussed in Chapter 3, the upper region represents "long" trajectory and the lower region "short" trajectory solutions to Lambert's problem. These areas are also referred to as being either Type I (short) or Type II (long) trajectories. For this investigation, the selection between trajectory path types is made by choosing the path whose orbital motion is in the same direction as the orbital motion of the planets. The direction check is accomplished by comparing the signs of the vertical components of the cross products of the planet's and spacecraft's position and velocity vectors.

The contours of the previous figures are for the 2018 departure opportunities. The Earth-Mars alignments of the year 2018 are beneficial from the standpoint of achieving an opportunity with a small value of delta V. Opportunities of the preceding and following years are not as advantageous in terms of minimizing total delta V. The planetary angular alignment of the two planets repeats every synodic period (approx 2 $1/7^{th}$ years). With each synodic period, the planets return to the same relative spatial position but these positions advance by $1/7^{th}$ of a circle each synodic period in inertial space[31]. The inertial positions therefore repeat every seven synodic periods, approximately every 15 years. Launch window contours for the

years 2003 and 2018 will thus be quite similar. Further, years with minimal delta V launch opportunities occur approximately every other year, repeating with the synodic period. As mentioned, the alternating "off-years" exhibit higher values of delta V. However, these off-years are sometimes utilized for certain mission architectures that incorporate more exotic maneuvering (e.g. Venus swing-by) than the straightforward dual-maneuver transfer. To illustrate the propulsive differences, the total delta V requirements for point-to-point dual-burn Mars transfers in the year 2017 are shown in Figure 5.5. Additionally, the total inclination changes and transit transfer angles are presented in Figure 5.6 and Figure 5.7 respectively.

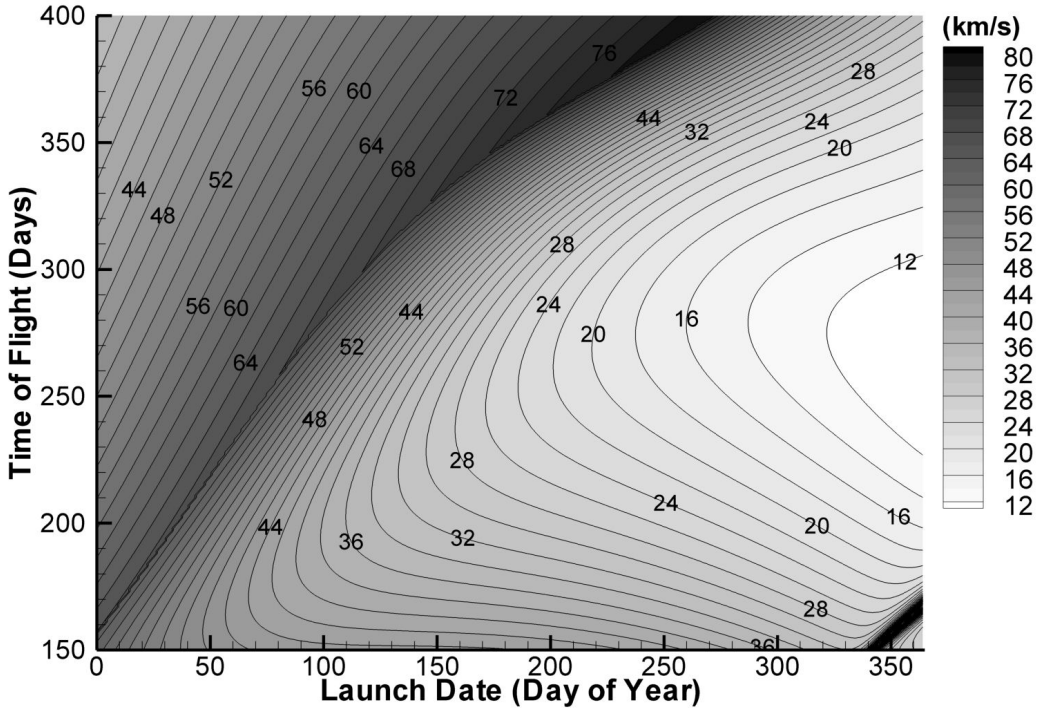

Figure 5.5 2017 Mars Departure Launch Window: Total Delta V

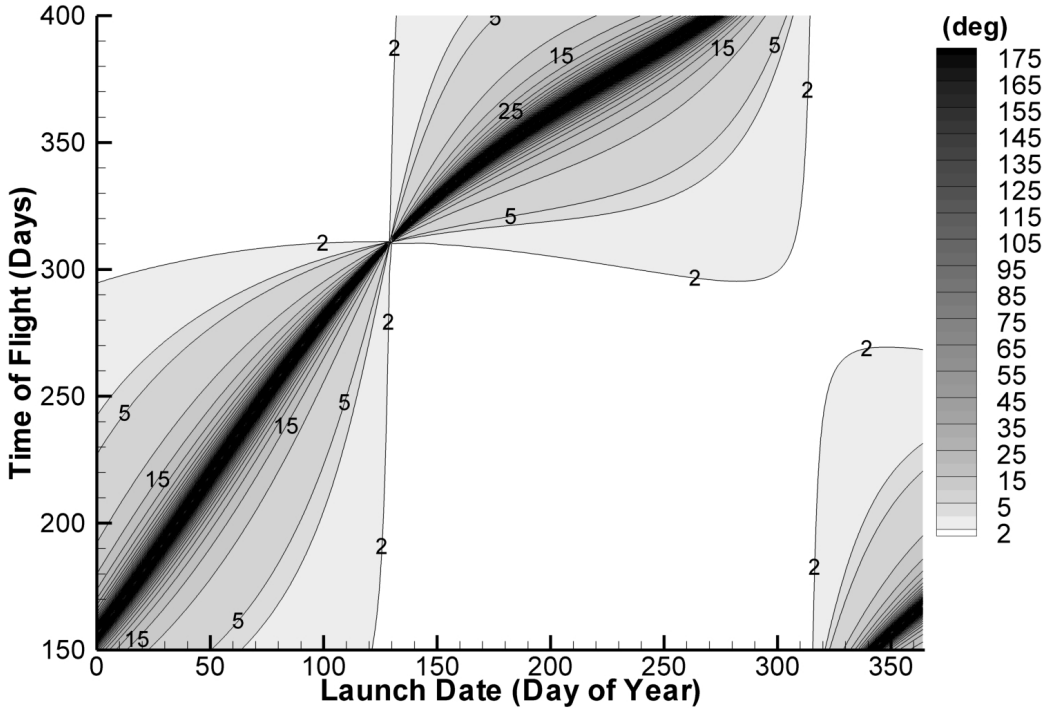

Figure 5.6 2017 Mars Departure Launch Window: Total Inclination Change

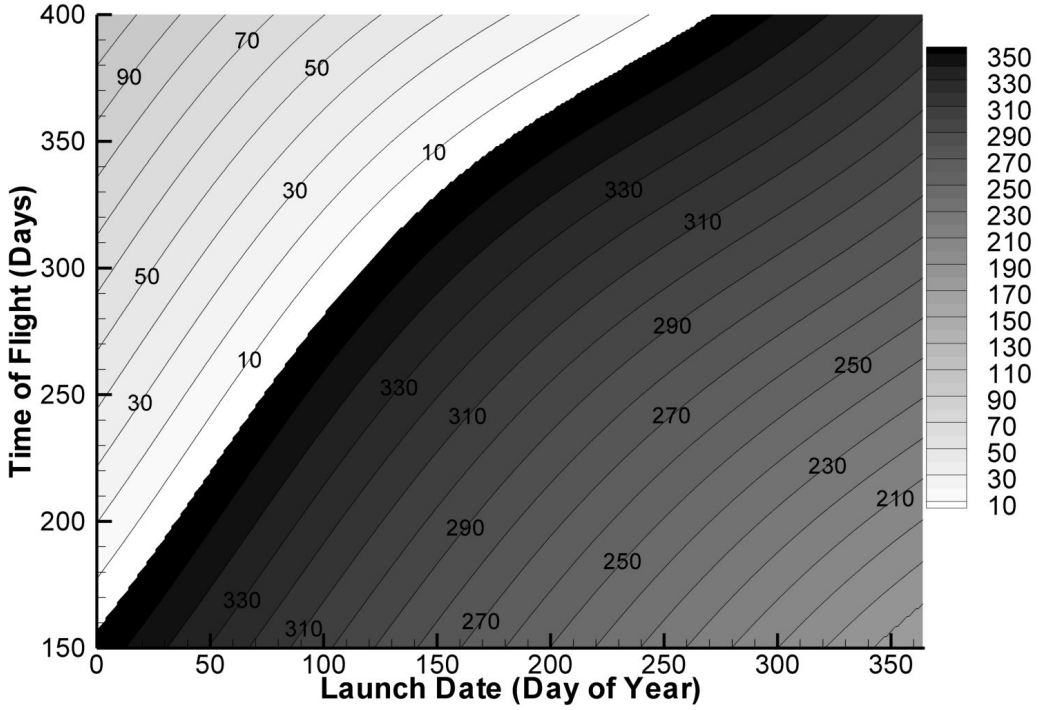

Figure 5.7 2017 Mars Departure Launch Window: Interplanetary Transfer Angle

Figure 5.6 shows inclination change requirements that follow the same trend observed for the 2018 plot; however, Figure 5.7 proves that these high-inclinations result from 0° transfers, the opposite alignment case to the previously discussed 180° transfers but identically the root cause of the high inclination changes. The resulting orbits for the extremely small and/or very large angle transfers have very high delta V requirements and are not mission practical. However, the right side region of Figure 5.5 shows delta V contours that match up with those on the left of Figure 5.1 and though they are higher, there are still realistic launch opportunities in this region depending on the mission and architecture setup, some of which will be shown in the next section.

5.2. Round-Trip Trajectory Options

The determination of realistic Mars transfer trajectories necessitates an examination of the entire mission scenario, not just the departure opportunities. Manned missions must be round trips. Due to the planetary motions of Earth and Mars, the selection of an outbound transfer trajectory to Mars will in part determine the available inbound return trajectories back to Earth as well as dictate the length of the stay time at Mars. An example proving these effects is given by Boden and Hoffman[42] who state that Hohmann outbound transfers require that Mars be leading the Earth by 44.3° at the time of launch while inbound transfers from Mars to Earth require that Mars be leading the Earth by 75°. However, for Mars arrivals via approximated Hohmann transfer, the Earth will be leading Mars by 75° upon arrival,

resulting in a 455 day layover until the proper return alignment is possible. Finding advantageous round-trip trajectories creates a double-rendezvous problem where the parameters of the first rendezvous (Earth to Mars) will influence the parameters of the second rendezvous (Mars to Earth). There are several classes of trajectories that could find application for Mars missions including ballistic, cycler, and low-thrust. The focus of the current research endeavor is aimed towards manned Mars missions and will not be considering the longer flight time trajectories offered by low-thrust propulsion. There are three major types of ballistic trajectories: the conjunction class, the opposition class, and free-return trajectories. The conjunction and opposition trajectories derive their names from whether at arrival the Earth is moving into conjunction or opposition with the Sun and Mars. There have been several excellent technical publications that have summarized the available trajectory options. The most widely referenced of these papers are those of Hoffman[43] and Soldner[44] with additional work by Lineberry and Soldner[45], Walberg[46], and most recently Landau and Longuski[47]. A summary of the attributes of the different classes is next discussed.

5.2.1. Conjunction Class Trajectories

The conjunction class trajectory is the most straightforward and consequently most common interplanetary trajectory type. Both the outbound and inbound trajectories are near-Hohmann transfers. As a result of the near double-Hohmann setup, the global minimum delta V transfers for each two year launch windows are always conjunction class trajectories.[45] A sketch of a typical conjunction class mission profile is shown in Figure 5.8.

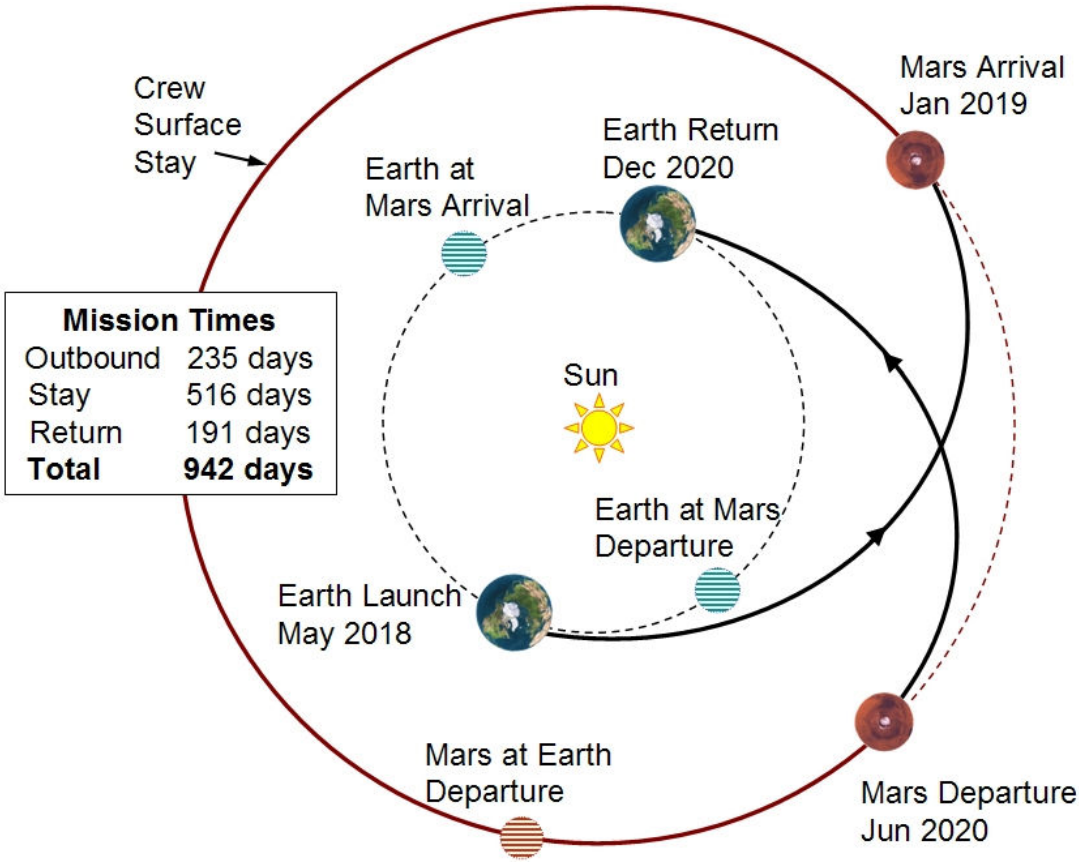

Figure 5.8 Conjunction Class Mission Profile

The typical trajectory characteristics[45] of a conjunction class transfer are the intersection and apparent symmetry of the outbound departure and inbound arrival transfer trajectories. Additionally, the transfer trajectories are bounded by the orbits of Earth and Mars themselves. Upon arrival at Mars, the planets are out of phase for a low energy transfer back to Earth necessitating a stay time from between 300 and 500 days until the correct alignment occurs. Conjunction class missions are therefore characterized by their long-duration surface stays. Combined with typical one-way transfer times of between 150 and 200 days, the conjunction class missions experience total mission times from Earth departure until Earth return on the order of 1000 days, approximately three years. These are the longest nominal round-trip times

for any considered trajectory class. The total delta V requirements for this mission class assuming propulsive Earth departure and Mars capture as well as propulsive Mars departure are typically between 7 to 9 km/s. Several proposed mission architectures use conjunction trajectories including direct, semi-direct, and stop-over missions.

5.2.2. Opposition Class Trajectories

Opposition class trajectories are another common trajectory type that has been widely analyzed. Compared to the conjunction class, the opposition class has higher energy trajectories and correspondingly higher delta V requirements. A sketch of an opposition class mission profile is represented in Figure 5.9.

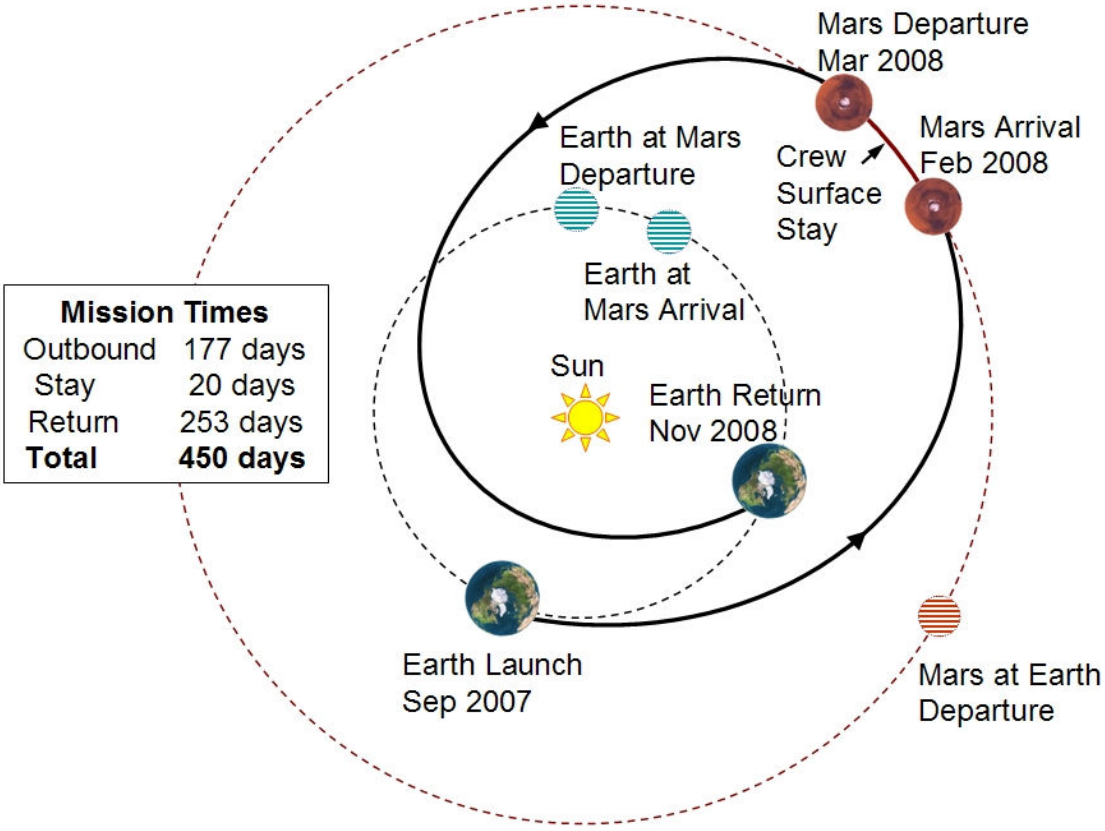

Figure 5.9 Opposition Class Mission Profile

The trajectory characteristics are much different than for the conjunction class. The opposition outbound departure and inbound return transfer orbits are very different from each other and one leg is of significantly longer duration than the other. Opposition trajectories are referenced[45] as either Option 1 or Option 2 to designate whether the longer trip time occurs during the inbound return or outbound departure. Typically, one leg of the round-trip appears to be similar to that of a conjunction mission, while the other leg has a trajectory that cuts inside the Earth's orbit as far as the orbit of Venus. In Figure 5.9 the outbound departure orbit of the Option 2 opposition trajectory appears like a minimum energy conjunction class orbit, but arrives on Mars *shortly* before an upcoming return trajectory opportunity. This scenario results in brief Mars stay times on the order of 30 to 60 days. For the example case, the return orbit must pass within the orbit of Venus to pick up velocity and catch up to the Earth. With transfer times of approximately 250 days for the trajectory legs, the opposition class missions have round-trip times on the order of 500 to 600 days, a much shorter total trip time than a conjunction mission. The total delta V requirements for an opposition mission range from between 12 and 20 km/s. Much trajectory work[43-45] has been undertaken to reduce the high propulsive costs of opposition missions by utilizing a gravitational swing-by of Venus on either the outbound and/or inbound leg of the mission. Besides reducing the amount of required delta V, the Venus swing-by can possibly extend the Mars stay time for a total of two months. The sprint class missions are a subset of the opposition class.

5.2.3. Free-Return Trajectories

Free-return trajectories[31,48] gained fame during and since the Apollo Moon program and have been investigated numerous times for application to future manned Mars missions. The extolled benefits of this trajectory stem from its primary attribute; that once embarked upon it will return to a proper Earth interface in the absence of nominally planned capture burn at Mars which is omitted in the event of certain system failures, creating a free (non-propulsive) return. The free-return trajectories account for shaping of the trajectory due to gravitational interaction with Mars. There are many ways to construct a Mars free-return trajectory. Illustrated in Figure 5.10 is a free-return trajectory that completes two complete heliocentric revolutions before arriving back at Earth.

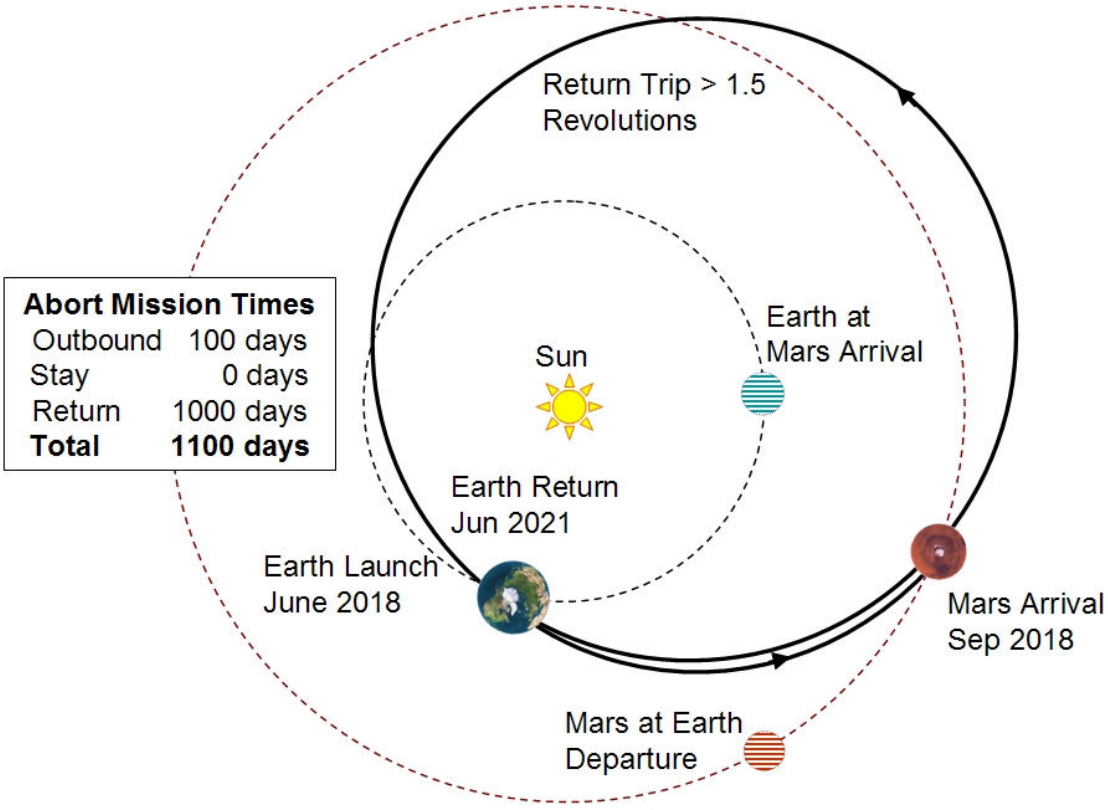

Figure 5.10 Free-Return Class Abort Mission Profile

The trajectory in the figure executes a nominal transfer to Mars and, in the absence of the MOI burn, slingshots around the planet and embarks on the return trajectory shown. The spacecraft will remain on that orbit for over 1.5 orbital revolutions until phasing with the moving Earth is matched. A crew on such a free-return completes two complete orbits of the sun and travels between Earth and Mars orbital distances twice before returning after a total flight time of three years. There are other free-return trajectory opportunities that use different multiples of Earth phasing. Additionally there has been research into enabling lower delta V free-returns that perform a Venus flyby[32,49]. Landau[47] has stated that the 2:3 resonance free-returns are more advantageous than those utilizing a Venus flyby when the requirements are averaged over entire synodic periods. As has been shown, Mars free-returns entail very long round-trip times that may even exceed the total duration of the nominal mission but which still may be advantageous in the event of certain aborts. Obviously, the safe return of the crew utilizing this trajectory class requires life-support operations that are successful for multiple years as well as a long duration spaceflight that exceeds the length of the longest in-space mission exposure that has yet been experienced.

5.2.4. Cycler Trajectories

Cycler trajectories[26-30] are those which transfer continually between the Earth and Mars. They typically use gravity assists at one or both encounters to shape the trajectory for the next encounter. Ideally, there would be no additional propulsive event after the insertion burn to create this orbit class. The primary mission benefits

arise out of the placement of a transfer habitat or logistics into cycler orbits that could then be used repeatedly by many flights. A major hurdle of such trajectories is the high-energy hyperbolic rendezvous required to embark or disembark from the trajectory. These dockings are especially troublesome when the rendezvous fails as the manned spacecraft is now located on a high-energy escape orbit. Such traits do not benefit initial manned Mars missions greatly and more detailed analysis of cycler trajectories was not undertaken for this investigation.

5.3. Launch Opportunities

This section presents the dates and propulsive requirements for actual transfer trajectories from among the different trajectory classes that have been discussed. The specific dates and orbital data of these trajectories will be needed to construct realistic outbound departure phase trajectories for use in the abort calculations of the following chapters. The computational code created to carry out this investigation was extensively and successfully validated against the trajectory data contained in the following tables. In presenting the delta V data, a more accurate estimate was employed than the point-to-point vector subtraction used for the contour plots at the beginning of this chapter. More realistic estimates for delta V are obtained by defining the altitude of the periapse for the departure and arrival hyperbolas and assuming propulsive requirements sufficient to switch between the escape and entry orbits and a circular orbit at the same altitude. Using the known quantities of V_∞ and r_{SOI} to determine the orbital energy (Eq. 4.6), the periapse velocity may be determined for a specified periapse altitude as shown for an Earth orbital case.

$$v_P = \sqrt{v_\infty^2 - \frac{2\mu_E}{r_{SOI}} + \frac{2\mu_E}{r_P}} \tag{5.1}$$

Figure 5.11 compares the resulting periapse velocity as a function V_∞ for both Earth and Mars hyperbolic trajectories at a set periapse altitude. Conversion between V_∞ and V_P does not depend on whether the hyperbolic is a departure or an arrival orbit.

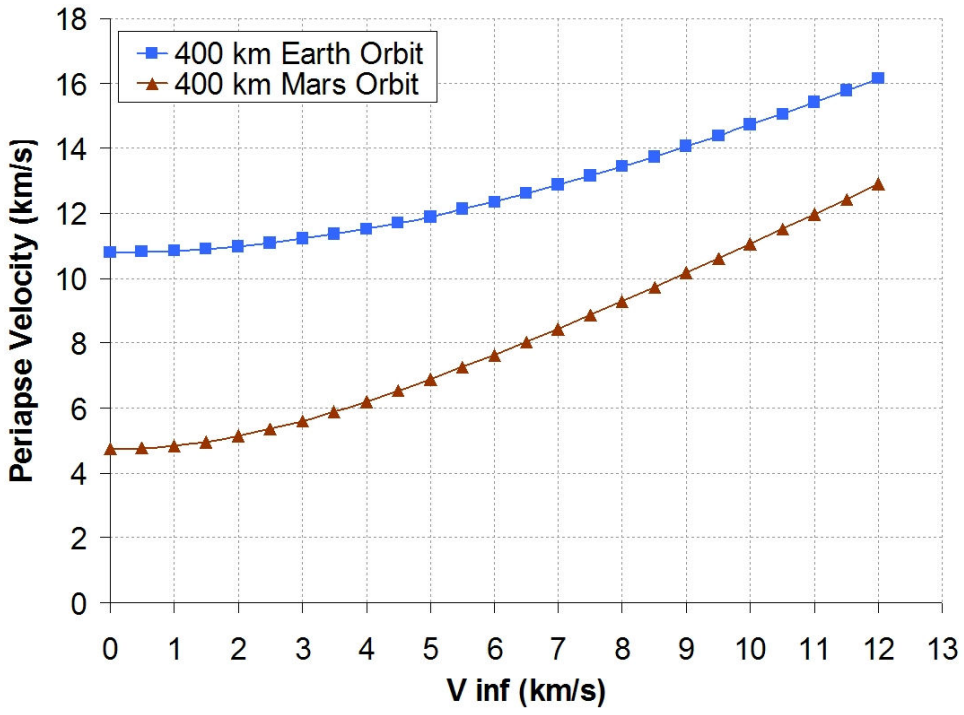

Figure 5.11 Periapse and Infinity Velocities for Earth and Mars Hyperbolas

The figure shows that the gravitational influences of the planet cause the periapse velocities to be higher than the velocities at the sphere of influence interface with the greater acceleration occurring for Earth with its greater mass. The delta V (TMI maneuver for the Earth departure case) is simply the difference between the periapse velocity and the circular orbital speed. The Mars MOI and TEI maneuvers are

similarly calculated when correct values for the gravitational parameter and sphere of influence radius are used.

$$\Delta v_{TMI} = \sqrt{v_\infty^2 - \frac{2\mu_E}{r_{SOI}} + \frac{2\mu_E}{r_P}} - \sqrt{\frac{\mu_E}{r_P}} \tag{5.2}$$

This is the basis for the delta V values that will be listed in trajectory opportunity tables of this section. Figure 5.12 shows the delta V calculations for different values of V_∞ for both Earth and Mars hyperbolic orbits.

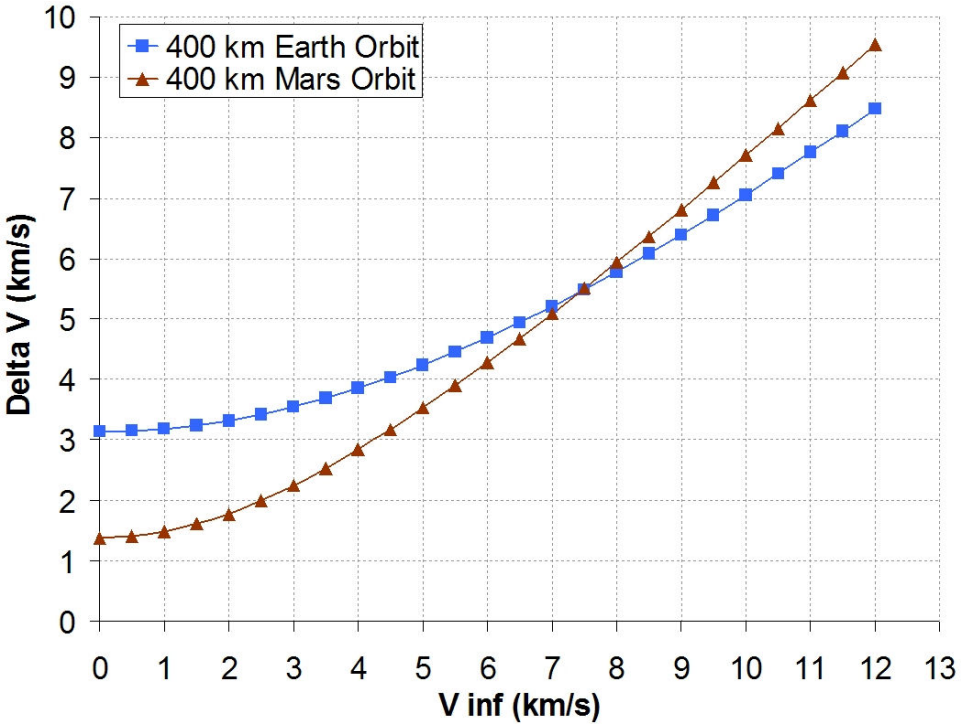

Figure 5.12 Delta V and Infinity Velocities for Earth and Mars Hyperbolas

The circular orbit speed for a low Earth orbit is approximately 7.6 km/s while the orbital velocity for a similar low-altitude Mars orbit is only 3.3 km/s. The figure shows that for smaller values of V_∞, the required delta V amounts are smaller for

Mars orbits. This trend is reversed for higher velocity orbits where it requires less propellant to match the higher velocity of a low Earth orbit than the low Mars one.

Some of the data to be presented in the following tables is referenced using the parameter *C3* instead of delta V. For elliptical and hyperbolic orbits, *C3* is expressed by the following equation.

$$C3 = -\frac{\mu}{a} = 2\xi \tag{5.3}$$

This expression can be employed to convert C3 into orbital energy from which delta V values may be calculated for any given periapse altitude via Eq. 4.6. The orbital data for the various trajectory classes is now presented.

5.3.1. Conjunction Class Opportunities

The typical conjunction class missions are those which correspond to minimum values of total delta V similar to those presented in the 2018 contour plot in Figure 5.1. As such, the minimum delta V may occur in either the Type I or Type II trajectory region. The dates of opportunity and propulsive data[43] for this mission class assuming minimization of the departure delta V are tabulated in Table 5.1.

Table 5.1 Earth-Mars Conjunction Opportunities, Minimum Departure Velocity

Launch Date	C3 TMI (km^2/s^2)	Outbound Flight Time (days)	C3 MOI (km^2/s^2)	Mars Stay Time (days)	C3 TEI (km^2/s^2)	Return Flight Time (days)	Total Mission Duration (days)
06/07/2003	8.81	201.7	7.32	550.7	13.56	192.3	944.7
09/01/2005	15.45	401.9	12.30	285.6	10.20	283.1	970.6
09/22/2007	12.75	368.5	7.95	307.6	7.86	296.9	973.0
10/14/2009	10.27	327.5	6.10	339.8	6.78	332.5	999.8
11/08/2011	8.95	297.6	7.57	391.8	5.79	335.3	1024.7
01/01/2014	8.78	328.8	19.79	382.7	5.42	300.2	1,011.7
03/21/2016	7.99	305.3	28.80	417.7	6.09	212.4	935.4
05/17/2018	7.74	235.1	10.63	515.4	11.43	191.2	941.7

The minimum delta V trajectory opportunities can vary widely in departure energy and outbound and return times of flight from one year to the next, but remain relatively constant in the total mission duration. The duration of the Mars stay time also fluctuates by as much as 250 days across the opportunities. Observing that greatly reduced times of flight would be available for minimal increases in delta V over the global minimum, it seems extremely unlikely that any mission would pursue options with transits that are 300 days or more long.

A similar option, and almost certainly better from an integrated mission point of view with humans in the loop is to constrain the acceptable trajectories to those occurring in the Type I region only. The opportunity data[42,45] for these cases are listed in Table 5.2.

Table 5.2 Earth-Mars Conjunction Opportunities, Type I Minimum Energy

Launch Date	ΔV TMI (m/s)	Outbound Flight Time (days)	ΔV MOI (m/s)	Mars Stay Time (days)	ΔV TEI (m/s)	Return Flight Time (days)	Total Mission Duration (days)	ΔV Total (m/s)
04/03/2001	3639	200	2532	545	2108	205	950	8278
06/08/2003	3574	204	2095	547	2647	192	943	8316
08/20/2005	3963	217	2038	492	2703	214	923	8704
10/06/2007	4199	248	2032	437	2278	262	947	8509
11/08/2009	4035	278	1988	374	2064	270	922	8087
11/28/2011	3672	252	2532	418	1989	259	929	8193
01/17/2014	3832	224	2794	458	1941	237	919	8567
03/11/2016	3739	204	2677	529	1983	212	945	8399
05/11/2018	3530	204	2230	553	2466	190	946	8227
07/27/2020	3807	207	2031	517	2746	203	927	8584

The data now show much lower and more consistent times of flight and Mars surface stay durations from year to year. The delta V increase over the global minimum is usually quite small. Considering an integrated spacecraft with resources for human

life support, the increase of 1 km/s delta V may easily be more beneficial than providing material, power, and consumables to run a life support system for an extra 100 days.

5.3.2. Opposition Class Opportunities

The standard opposition class trajectories occur during the alternate years between the years of the above conjunction opportunities. These particular opposition class opportunities are straightforward transfers without any gravity assist maneuvers. Data[42,45] for Option 2 trajectories of this class are presented in Table 5.3.

Table 5.3 Earth-Mars Opposition Opportunities

Launch Date	ΔV TMI (m/s)	Outbound Flight Time (days)	ΔV MOI (m/s)	Mars Stay Time (days)	ΔV TEI (m/s)	Return Flight Time (days)	Total Mission Duration (days)	ΔV Total (m/s)
08/27/2000	7692	262	4437	40	5401	168	470	17,531
10/05/2002	7276	251	4595	40	4209	169	460	16,079
11/06/2004	7889	236	4899	40	3404	174	450	16,192
12/13/2006	9421	219	5352	40	3133	201	460	17,907
01/19/2009	11790	207	5795	40	2972	233	480	20,557
03/27/2011	13053	221	5217	40	4812	209	470	23,081
06/06/2013	11142	247	4757	40	6244	183	470	22,143
07/31/2015	8844	264	4467	40	5085	176	480	18,396
09/15/2017	7488	260	4454	40	4556	170	470	16,498
10/24/2019	7576	242	4781	40	3585	168	450	15,943

The delta V requirements are much larger than for the conjunction opportunities and the Mars stay time and total mission duration are much smaller. The outbound, return, and total mission times remain fairly consistent across the dates of opportunity. The Earth return velocity for this class can be considerable and it is possible that an additional propulsive maneuver may be needed in some cases to slow to an acceptable approach speed.

The high delta V situation may be aided by using a Venus gravity assist during either the outbound or return flight legs. The resulting opposition class trajectory data[42,45] for transfers utilizing a Venus flyby are contained in Table 5.4.

Table 5.4 Earth-Mars Opposition Opportunities, Venus Fly-by

Launch Date	ΔV TMI (m/s)	Venus Swingby	Outbound Flight Time (days)	ΔV MOI (m/s)	ΔV TEI (m/s)	Return Flight Time (days)	Total Mission Duration (days)	ΔV Total (m/s)
04/01/2001	3635	Inbound	201	2538	4248	345	586	10,422
08/22/2002	3820	Outbound	302	4744	3134	261	603	11,704
06/09/2004	4131	Outbound	344	4429	2639	271	655	11,198
08/27/2007	4600	Inbound	188	4341	4030	340	568	12,972
01/17/2009	4208	In & Out	330	3339	3367	367	737	11,342
11/28/2010	4426	Outbound	330	3502	2494	303	673	10,422
11/21/2013	3692	Inbound	281	2464	4419	311	632	10,575
10/26/2015	4865	Inbound	279	3136	4810	261	580	12,811
04/06/2017	4181	Outbound	359	3780	2531	246	645	10,502
06/09/2020	4164	Inbound	190	2707	3961	364	594	10,832

All of the data in the table are for 40 day Mars surface stays. The total delta V requirements have dropped drastically and are usually within 2 km/s of the conjunction class propulsive requirements. A side effect of the flyby is the general increase in total mission duration over the nominal opposition class trajectories.

5.3.3. Free-Return Opportunities

The selection of resonance matching and presence of Venus flybys results in many different free-return options. One of the most standard returns in the literature is for 3-yr duration aborts similar to those of Figure 5.10. The mission parameters for both the nominal and abort cases must be presented for each launch date of opportunity. Table 5.5 tabulates the trajectory data[44] for a typical free-return trajectory profile.

Table 5.5 Earth-Mars Free Return Opportunities, 3 yr Aborts, 1000-Day Class

	Launch Date	ΔV TMI (km/s)	Outbound Flight Time (days)	Mars Arrival V_∞ (km/s)	Mars Stay Time (days)	ΔV TEI (km/s)	Earth Return V_∞ (km/s)	Return Flight Time (days)	Total Mission Duration (days)
Abort	11/24/2011	3.836	190	6.786	0	0	7.073	949	1139
Nominal	11/24/2011	3.836	190	6.786	512	0.986	7.023	220	922
Abort	01/01/2014	3.672	181	6.933	0	0	3.450	902	1083
Nominal	01/01/2014	3.672	181	6.933	555	1.069	7.341	180	916
Abort	03/02/2016	3.687	150	6.940	0	0	3.412	942	1092
Nominal	03/02/2016	3.687	150	6.940	635	1.699	7.456	120	905
Abort	06/05/2018	4.287	100	7.008	0	0	5.460	1000	1100
Nominal	06/05/2018	4.287	100	7.008	566	2.175	6.845	120	886
Abort	07/05/2020	4.217	139	5.974	0	0	8.488	1013	1152
Nominal	07/05/2020	4.217	139	5.974	630	2.180	7.458	150	919
Abort	09/06/2022	4.051	181	4.734	0	0	9.238	965	1146
Nominal	09/06/2022	4.051	181	4.734	540	1.684	7.009	190	911
Abort	10/12/2024	4.025	194	5.455	0	0	9.072	951	1145
Nominal	10/12/2024	4.025	194	5.455	515	1.352	7.183	210	914
Abort	11/13/2026	3.983	183	7.196	0	0	9.220	965	1148
Nominal	11/13/2026	3.983	183	7.196	516	1.068	7.168	220	919
Abort	12/14/2028	3.791	180	7.537	0	0	6.386	957	1137
Nominal	12/14/2028	3.791	180	7.537	541	0.999	7.242	200	921

The mission data appears very similar to the Type I conjunction class data in terms of total mission durations and Mars stay time. The departure delta V is also similar, though generally higher than the conjunction class delta V resulting in slightly shorter outbound flight times. The negative consequence of the free-return selection is the increased arrival velocity at Mars which will translate into larger MOI delta V than the conjunction case.

5.4. Trajectory Class Comparison for Manned Missions

The trajectories presented may be applied to any sort of Mars mission, but for the purposes of this investigation, it is necessary to identify which trajectory classes or types are the most advantageous for initial manned exploration missions. The human element is the most important part of any manned mission and this section will

analyze how the attributes of the different trajectory classes impact the human crew. Some of the resulting impacts will depend on the particular spacecraft hardware and mission architecture which is an optimization problem beyond the scope of the present work. Instead, the general influence of the different scenarios and their impact on mission goals and safety are discussed.

5.4.1. Propulsive Capture vs. Aerocapture

Spacecraft may be captured into orbit or atmospheric entry through propulsive means or an aerocapture maneuver. Most studies assume an aerocapture maneuver for the Earth return phase of an interplanetary trajectory and many assume the same at Mars in an attempt to reduce mission delta V. A trajectory that is optimized assuming an aerobraking maneuver at Mars will yield a higher approach velocity at Mars than one assuming propulsive capture[44]. Assuming the heat shield is capable of the entry heat load, it would appear that the best conjunction missions from the standpoint of minimum mission delta V are those that minimize the departure delta V for Type I trajectories. Free-return trajectories will almost surely employ aerocapture as their high Mars arrival velocities would lead to larger MOI delta V maneuvers. Importantly, selection of the Mars aerocapture mode increases the amount of available spacecraft delta V capability left for the execution of departure phase aborts.

5.4.2. Departure and Arrival Velocities

Directly pertinent to the previous discussion of capture methods is the analysis of the arrival and departure velocity magnitudes. The elimination of the arrival delta V, as would occur for a Mars aerocapture, provides freedom for the further reduction

of flight time or departure delta V optimization. Figure 5.13 presents the velocity breakdown as a function of time of flight for the transfers on May 12, 2018 (132nd day of the year).

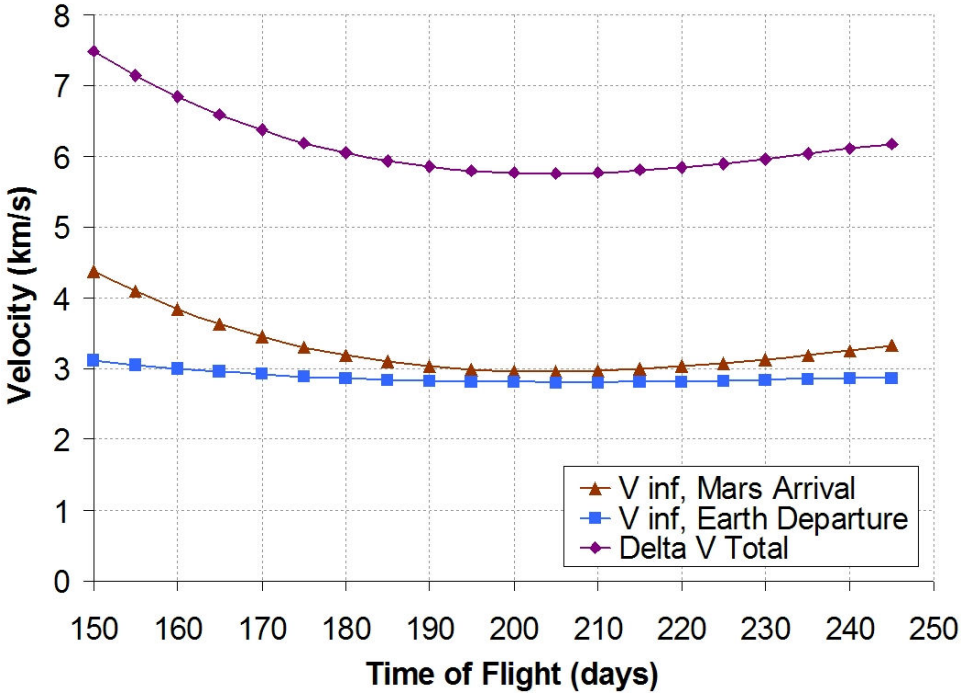

Figure 5.13 Departure and Arrival Velocity Breakdown, May 12, 2018

As shown, in the absence of an arrival burn, the total flight time can be reduced from the 200+ day optimum to around 150 days while only minimally impacting the magnitude of the departure velocity. This modification does; however, increase the arrival velocity at Mars[44,45]. Additionally, the return launch window opens on the same date, so the outbound transfer days saved by the faster transit get added to the duration of the surface stay. The values of Earth departure and Mars arrival delta V for the entire 2018 launch windows are shown in Figure 5.14 and Figure 5.15. Figure 5.14 clearly shows the flat response to shorter flight times around launch day 132.

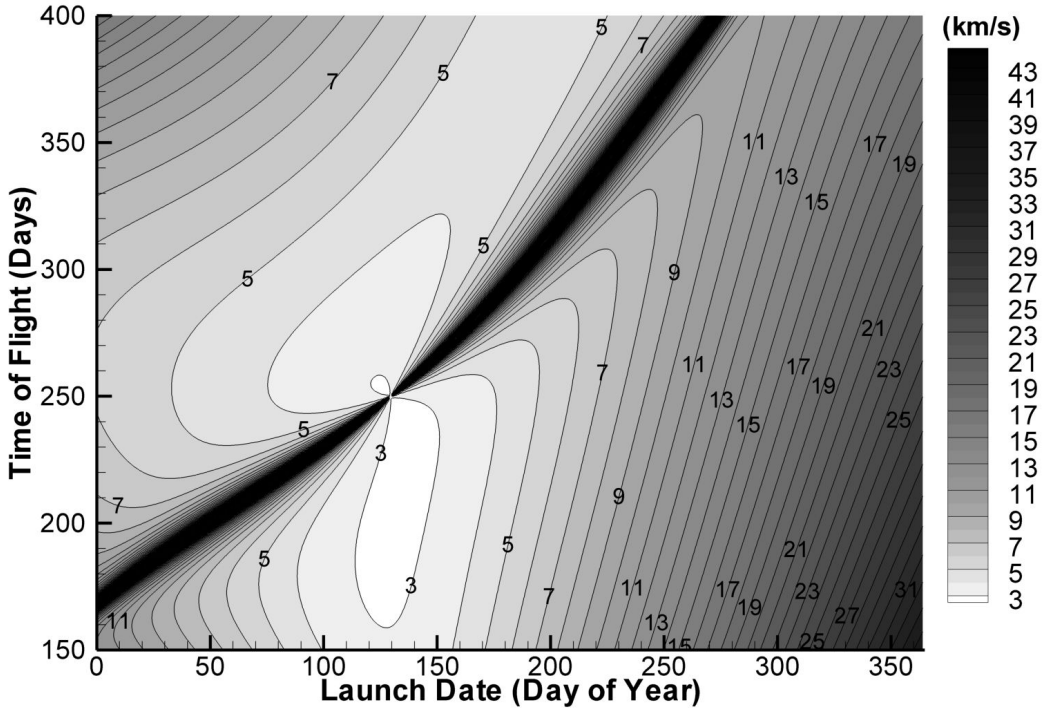

Figure 5.14 2018 Mars Departure Launch Window: Required Departure Delta V

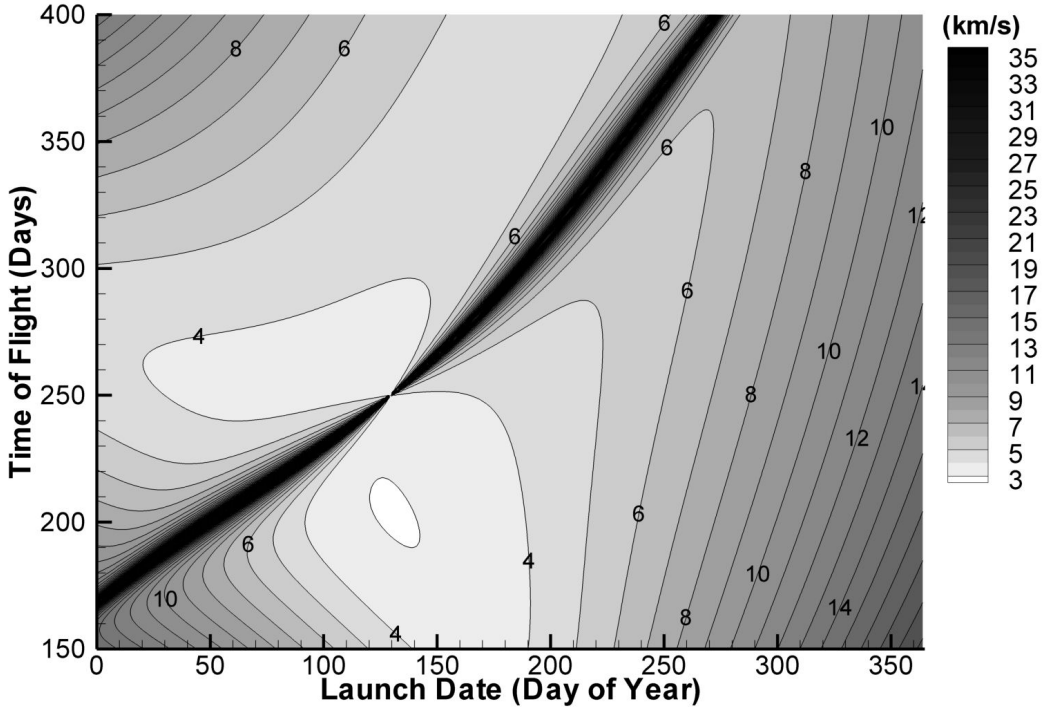

Figure 5.15 2018 Mars Departure Launch Window: Required Arrival Delta V

5.4.3. Propulsive Requirement Variation

The selection of the best trajectory class is complicated by the intrinsic variance in the class characteristics and requirements across different spatial and inertial synodic cycles. A particular class's propulsion requirements may double from one launch opportunity to another. For a given spacecraft or architecture to have a useful service outlook, or consistent abort capability, its performance must be designed to meet the most stringent requirements expected. Figure 5.16 presents the total delta V requirements for five candidate trajectory classes. The total delta V for each class is given for both the all-propulsive and Mars aerocapture (no MOI burn) options. The data presented are the ranges between the upper and lower bounds of the required delta V values across a 15-year inertial synodic period.

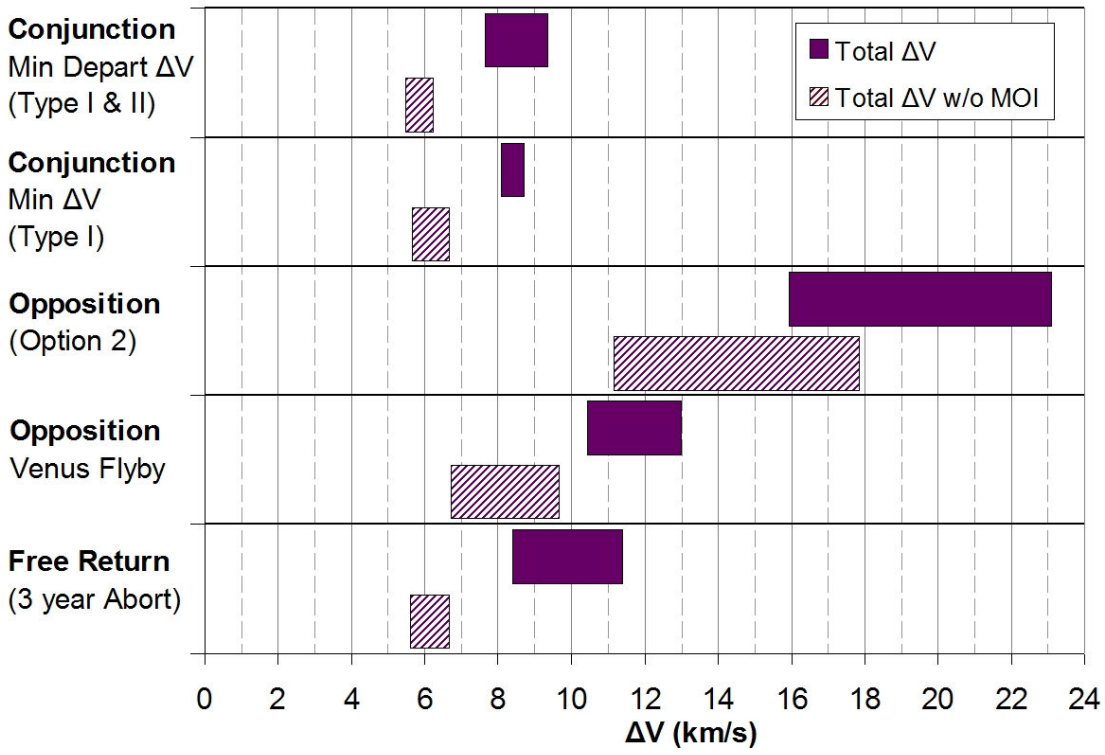

Figure 5.16 Total ΔV Ranges Over 15-Year Inertial Period

The length of the bars in the figure corresponds to the variation between the best and worst case delta V scenarios, e.g. longer bars correspond to greater disparity. Of the trajectory classes represented, the conjunction trajectories exhibit the least variability across different launch windows and the lowest actual values of total delta V. The free-return class displays similar characteristics though with more variation in total delta V. This greater breadth is a consequence of the increased Mars arrival velocities that can arise for the free-return class which increases the required delta V variability for the propulsive capture only and not for the aerocapture option as evidenced in the figure. The two opposition class trajectory classes show both larger delta V magnitudes and variability across launch windows compared to the other classes. A spacecraft architecture sized for 7 km/s delta V could successfully execute a conjunction or free-return aerocapture class trajectory for any launch opportunity while a standard opposition class would have to be sized for 18 km/s delta V to enable its continuous availability. In terms of mission delta V requirements, the opposition trajectories are outpaced by the conjunction and free-return trajectory classes.

Additional information can be gleaned by breaking up the total delta V results into constituent ranges for Earth departure, Mars arrival, and Mars departure delta V as done in Figure 5.17.

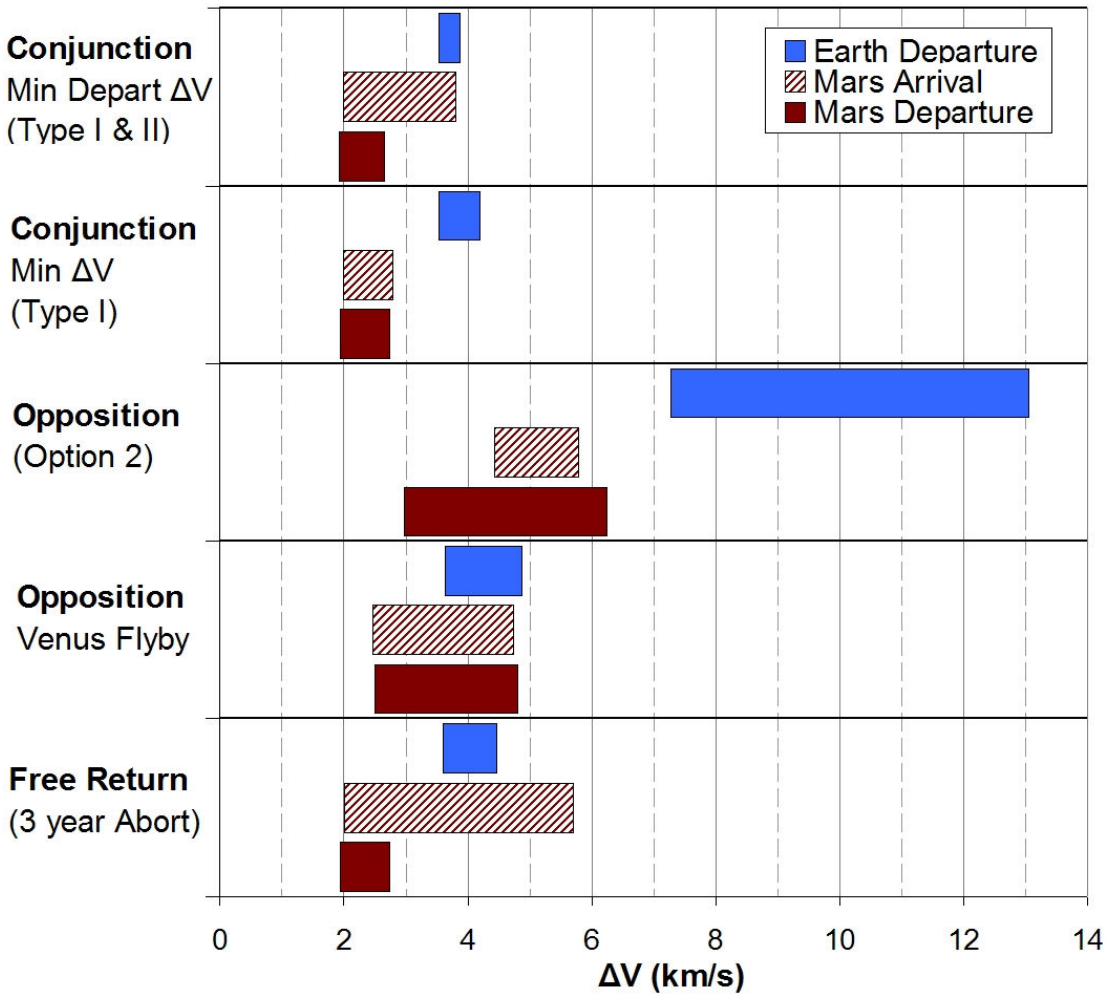

Figure 5.17 ΔV Breakdown Ranges Over 15-Year Inertial Period

The conjunction and free-return trajectories have the lowest and least variable Earth departure and Mars departure delta V of the five classes while the Option 2 opposition trajectory has the highest. The Mars arrival delta V requirements for the free-return class have the greatest variability though are typically lower than the opposition class Mars arrival delta V. The large variation becomes unimportant if the maneuver is performed via aerocapture, assuming captures up to 6 km/s are feasible. Each segment of the opposition Venus flyby class is more competitive with the conjunction and free-return classes than the standard opposition trajectory, though its

total delta V is much higher than the conjunction trajectories. Of the conjunction class, the Type I only trajectory exhibits the least amount of variance.

5.4.4. Mission Time: Surface Stay vs. In-Space Duration

Mars missions are risky endeavors regardless of safety precautions taken; it is the nature of exploration in an untamed frontier. Consequently, it is generally advisable to reduce the in-space exposure time. Figure 5.18 presents the total mission durations of the various trajectory classes as well as the corresponding duration of the in-space exposure.

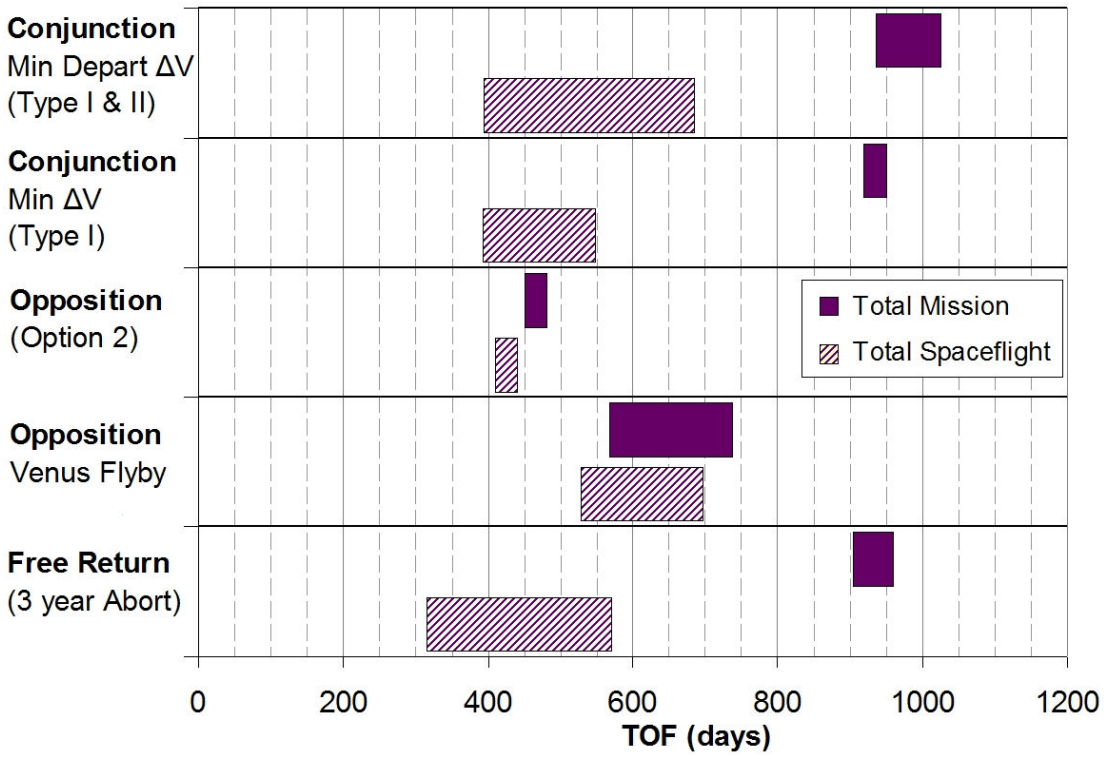

Figure 5.18 Mission Time of Flight Ranges Over 15-Year Inertial Period

The opposition class trajectories have approximately half the total mission length of the conjunction and free-return classes. The desire to minimize total mission time led NASA in the past to select opposition class trajectories in its 90-day report on Mars exploration[8]. This selection; however, greatly increases the propulsive requirements of the mission and reduces the effective payload mass delivered to Mars. Further, it is at best misleading to make a selection based solely on smallest total mission time. Radiation and microgravity deconditioning are two of the highest risk factors a human crew will be exposed to during a Mars mission. Both of these risks are pronounced during in-space transit but are moderately mitigated on the surface of Mars by the planet's gravity and atmosphere. It would likely then be desirable to minimize the total in-space exposure time of the astronauts. To this effect, it is noted that depending on the opportunity, the in-space duration exposure is approximately the same across the trajectory classes. The nominal free-return has the possibility for the least in-space time; however, the abort option, if exercised, would result in at least a 1000 day space exposure. The high delta V requirements of the opposition classes do not result in lower in-space exposure times, just decreased total mission times. Further, opposition trajectories cut into the orbit of Venus thus greatly increasing the radiation exposure to the Sun.

Figure 5.19 displays the times of flight for the various trajectory classes broken down by mission segment.

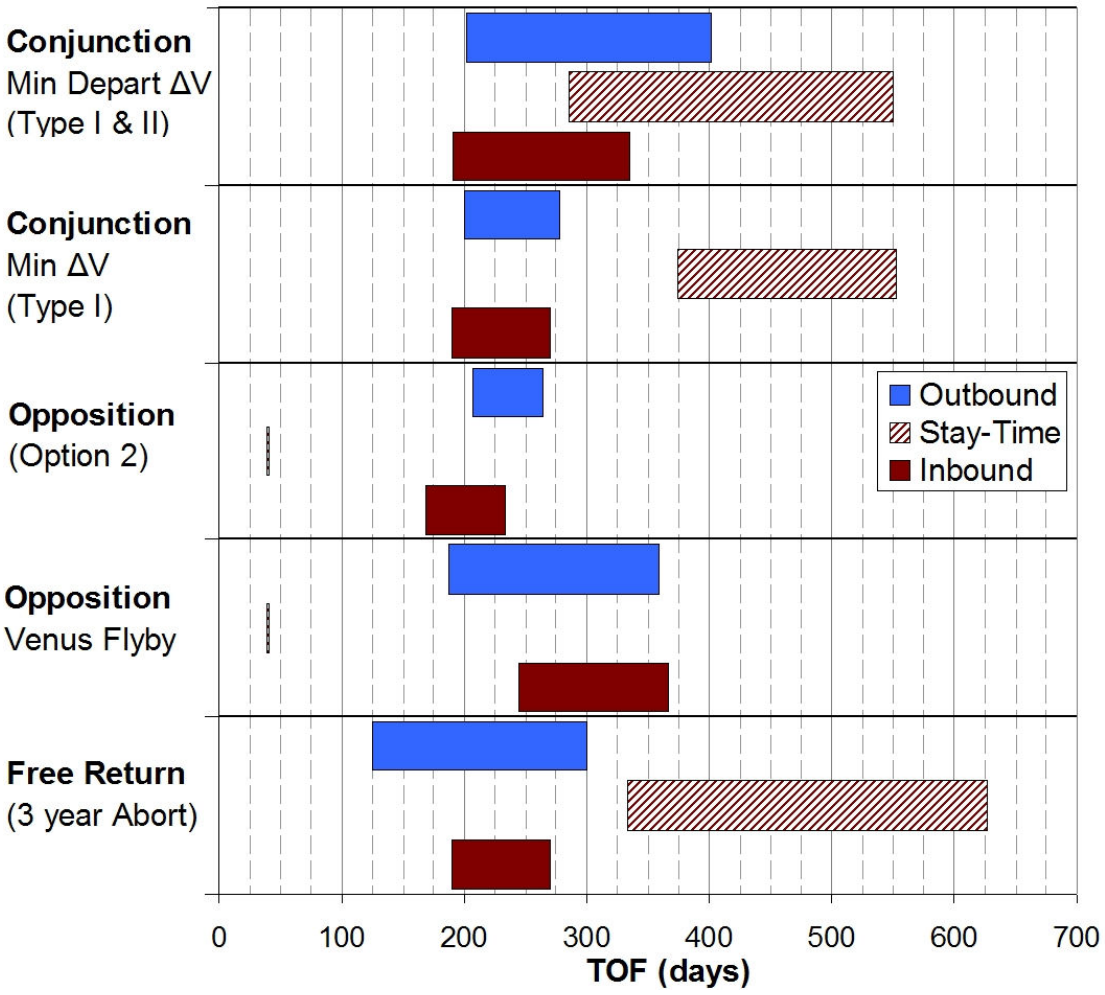

Figure 5.19 Time of Flight Breakdown Ranges Over 15-Year Inertial Period

The figure highlights the drastic differences in surface stay time between the conjunction and opposition trajectory classes. While there is great variation in the conjunction stay duration, the stay is typically at least ten times the length of the consistently short opposition stay times. The shortest and least variable transfer times belong to the Type I conjunction and standard opposition class. The majority of the conjunction mission is on the surface of Mars while the opposition mission spends most of its total mission in space. The long surface stays have been both criticized and applauded depending on the author's vision for Martian exploration. Zubrin[8]

praises the long-duration surface stay because it allows time for accomplishing the whole purpose of the mission, the exploration of Mars. Zubrin likens the opposition trajectory to a family traveling on a vacation to Hawaii that spends ten days in transit flying from one airport to the next with half a day at the beach, weather permitting. Though the conjunction mission commits the crew to a long duration surface stay, it does allow them to potentially accomplish significantly more than could be done on an opposition mission while providing minimal in-space exposure and delta V requirements. Free-return trajectories have similar attributes in terms of in-space transfer time and surface stay for a nominal mission. In the event of an emergency; however, the free-return would relegate the crew to a three year exposure to microgravity and interstellar radiation. The prudence and nominal transfer attributes of the free-returns plus the minimal propellant cost difference compared to the conjunction class makes them a logical contender though it is difficult to imagine a large number of failure possibilities that would rule out a Mars landing while still permitting three years of power and life support. Depending on the setup of the mission architecture, it will likely be better to abort to the Martian surface[9] for many of the possible interplanetary or Mars arrival phase failure scenarios.

5.4.5. Trajectory Selection

In summary, the most advantageous transfer trajectories in terms of life sciences and mission objectives appear to be the Type I conjunction class and similar free-return trajectories. These trajectory types minimize human environmental risk and propellant requirements while increasing opportunity for productive work at the exploration destination. Selection of propulsive or aerocapture options may further

improve these classes and may significantly impact the feasibility of a departure phase abort capability. Specific orbital data on the three selected trajectory classes for the baseline launch opportunity date of each opportunity year across the fifteen-year inertial period are presented in Appendices D1, D2, and D3.

Chapter 6. Earth Atmospheric Entry Aborts

The previous chapters have developed and validated a suite of general trajectory classes for application in manned Mars exploration. Methods were developed for the accurate position and velocity determination of the departure, transfer, and arrival trajectory phases. The transfer opportunities have been characterized over one complete 15-year inertial period to determine the maxima and minima of the resulting departure and arrival velocities of the various trajectory classes as well as the ensuing times of flight. The goal of the work contained in the present chapter is to discover and develop realistic departure phase abort options which will return the crew to the Earth's surface in the event of an outbound emergency. The investigated contingency plan consists of a direct abort to atmospheric entry. The availability and requirements of this abort mode are investigated for each of the representative trajectory classes. The results are calibrated according to the metrics of required abort propulsive delta V and abort time of flight.

6.1. Abort Trajectories to Atmospheric Entry

An abort to atmospheric entry has the advantage of directly returning the crew to the Earth's surface without delay. Additionally, it is possible, and desirable, to execute the abort trajectory such that once embarked upon it will deliver the crew to the proper atmospheric interface without any further propulsive maneuvers. Historically, direct aborts to atmospheric re-entry have been the principal contingency

plans for human spaceflight. During the Apollo program, in-transit emergency plans called for either a propulsive turnaround or free-return Moon flyby, both of which would eventually lead to the placement of the crew capsule into the narrow atmospheric entry corridor. Direct entry aborts are even more accessible to the Space Shuttle being that it is already located in a low-Earth orbit. Such Earth surface returns were the only practical abort options available to either program. The advantages of this abort mode extend to application during the departure phase of future Mars transfer trajectories, but come at a much higher propulsive cost due to the higher energy of the outbound escape trajectory versus orbital or even trans-lunar velocities. The atmospheric entry abort mode was selected as the baseline departure phase contingency plan for this investigation. Besides the dual attractions of direct Earth return and single-burn abort initiation, the straightforward return to the Earth's surface would be the preferred recovery option from the perspective of the human crew. Any other considered abort modes will be judged by whether they provide any additional capability or safety attributes versus the direct abort to Earth atmospheric entry.

6.1.1. Entry Corridor Requirements

The entry abort mode performs an aeroentry, meaning that the spacecraft decelerates from a hyperbolic or elliptical approach orbit utilizing the planetary atmosphere. While any number of trajectories could be created that intersect the atmosphere, acceptable approach trajectories must meet the limitations imposed by spacecraft and human factors realities. Three of the principal constraints are the crew's maximum deceleration limit[50], the vehicle aerodynamic performance[51], and

the integrated heat load capabilities[52] of the heat shield. The addition of these and similar competing criteria define an acceptable entry corridor[53, 54]. Delivering the spacecraft to the proper entry corridor requires that the Earth approach trajectory, for either a nominal or abort return, provide the proper entry velocity and orientation. Arriving at too shallow of an entry angle could lead to the spacecraft skipping out of the atmosphere while too deep of an arrival could easily exceed the heating capability of the vehicle. The Apollo capsule successfully executed many atmospheric entries over the course of the testing and mission phases of the Moon program. Table 2.1 summarizes the entry angle and velocity data[55] collected during Apollo.

Table 6.1 Summary of Entry Conditions for Apollo Missions

Apollo Flight	Inertial Entry Velocity at 400,000 ft.		Inertial Entry Angle
Mission / Vehicle	*(km/s)*	*(ft/s)*	*(deg)*
AS 202	8,690	28,512	-3.53
Apollo 4/017 AS 501	11,139	36,545	-6.93
Apollo 6/020 AS 502	10,007	32,830	-5.85
Apollo 8/103 AS 503	11,040	36,221	-6.48
Apollo 10/106 AS 505	11,069	36,314	-6.54
Apollo 11/107 AS 506	11,032	36,194	-6.48
Apollo 12/108 AS 507	11,008	36,116	-6.50
Apollo 13/109 AS 508	11,037	36,211	-6.49
Apollo 14/110 AS 509	11,025	36,170	-6.37
Apollo 15/111 AS 510	11,002	36,096	-6.51
Apollo 16/112 AS 511	11,000	36,090	-6.49

Starting with Apollo 7, all of the Apollo flights were manned missions. As seen from the table, the entry velocities and angles show very little variance for these manned flights. The fastest re-entry was experienced during the validation program by the Apollo 4 capsule. The data show deeper entry angles for faster velocities, so arranged to avoid skipping off the atmosphere at arrival. The re-entry characteristics of the planned CEV capsule have yet to be determined, but will likely require a very similar

entry corridor as the Apollo spacecraft. Material advances may allow for a slightly hotter re-entry than was possible during Apollo. The baseline entry interface requirements to be used in the current abort study assumed an 11 km/s entry velocity at an entry angle of -6.5°. Trades of the effect of various entry velocities on the abort propellant requirements will be shown in a later section. An actual re-entry corridor constraint that was not addressed by the present investigation was the targeting of the entry injection required for achieving a specific surface landing location.

6.1.2. Determination of Earth Entry Aborts

The atmospheric entry abort mode and all other abort modes in this study are candidate contingency trajectories available for use during the Earth departure phase of an interplanetary Mars transfer. The requirements for executing these aborts will be calculated for abort initiation anywhere along the outbound trajectory. The departure trajectory begins from a LEO parking orbit and proceeds on a hyperbolic escape trajectory until crossing the Earth gravitational sphere of influence (Figure 4.6). For a given spacecraft position along its outbound trajectory there are a host of possible atmosphere-intersecting abort orbits that could be constructed. These possible abort trajectories are varied primarily as a function of time of flight and trajectory transfer angle θ_{Trans}. The abort trajectory is begun by a propulsive maneuver which terminates the escape trajectory and starts the spacecraft on an abort path that will carry it to an atmospheric interface. The trajectory profile for an Earth atmospheric entry abort is presented in Figure 6.1.

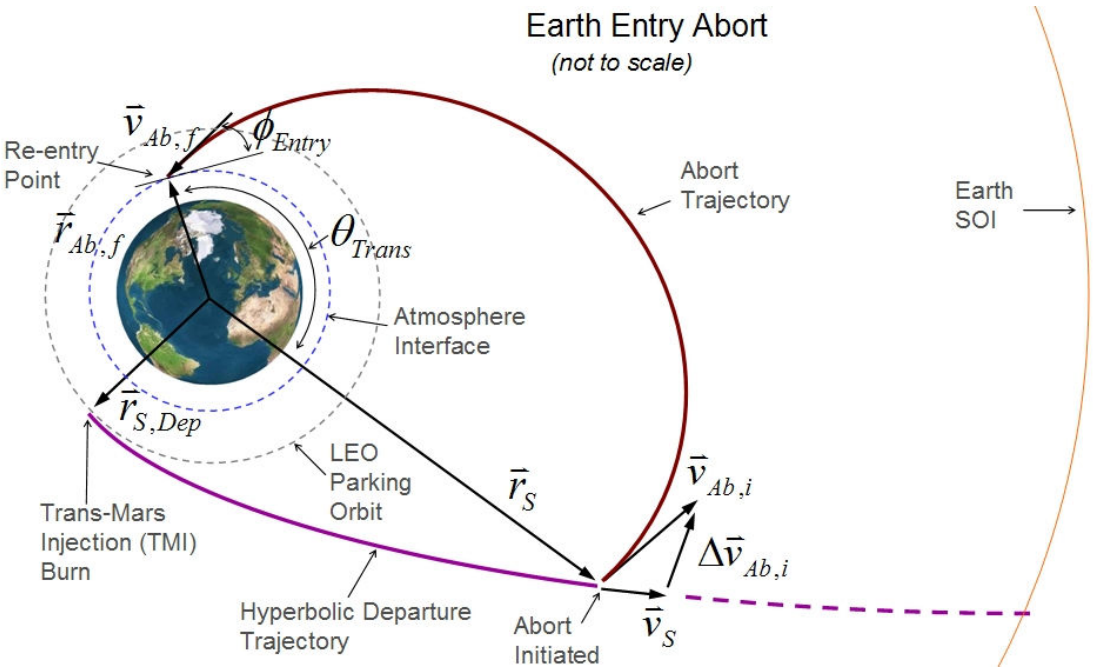

Figure 6.1 Earth Atmospheric Entry Abort Profile

Both the position and velocity vectors of the spacecraft, $\boldsymbol{r_s}$ and $\boldsymbol{v_s}$, are known at the point of abort initiation. To solve the orbit for a specified time of flight using the universal variables approach to Lambert's problem will require a final position vector $\boldsymbol{r_{Ab,f}}$ in addition to the known initial position. Assuming an Apollo type entry corridor, the assumption is made that the magnitude of the final position vector will correspond to an altitude of 400,000 ft (~122 km). From the figure it is noted that, given both the vector $\boldsymbol{r_S}$ and the assumed magnitude $r_{Ab,f}$ and assuming the vectors were two dimensional (coplanar), the vector $\boldsymbol{r_{Ab,f}}$ could be determined for a specified value of the transfer angle θ_{Trans}. With both position vectors defined, an orbital solution could then be found for the desired time of flight. Applying this method to the actual three dimensional position vectors will require rotation of the geocentric coordinates into the two-dimensional coordinates of the abort orbital plane. The abort

orbit is assumed to be coplanar with the plane of the original departure orbit. The orbital plane contains the position and velocity vectors $\boldsymbol{r_s}$ and $\boldsymbol{v_s}$. The specific angular momentum vector $\boldsymbol{h_S}$ is perpendicular to both of these vectors and is obtained from the cross product.

$$\vec{h}_S = \vec{r}_S \times \vec{v}_S \tag{6.1}$$

The angular momentum vector is always perpendicular to the orbital plane. The unit vector of the angular momentum will be useful later to define the orientation of the orbital plane.

$$\hat{h}_S = \frac{\vec{h}_S}{\left|\vec{h}_S\right|} \tag{6.2}$$

Transforming the position vector into a two-dimensional form requires successive rotations of the geocentric coordinates into the orbital plane. The same orientation could equally be achieved by aligning the **K** coordinate with the direction of the angular momentum. The transformation is illustrated in Figure 6.2.

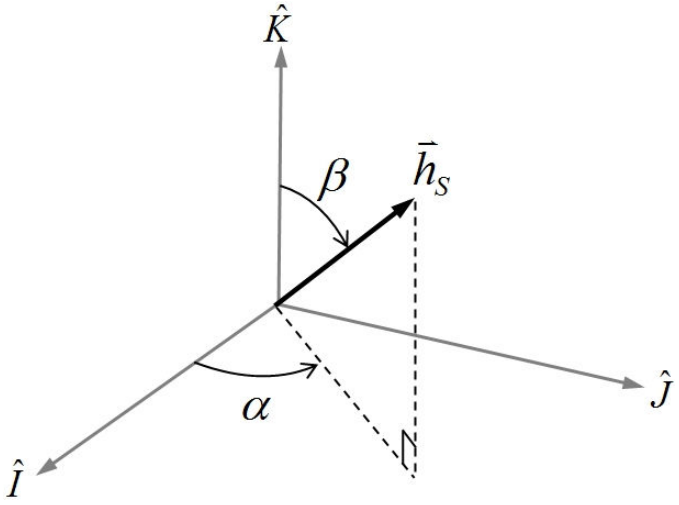

Figure 6.2 Geocentric Coordinate Transformation to Orbital Plane

The alignment setup requires a positive rotation about the **K** axis through the angle α followed by a positive rotation about the **J** axis through the angle β. The angles α and β are given by the following equations.

$$\alpha = \tan^{-1}\left(\frac{\hat{h}_{S,J}}{\hat{h}_{S,I}}\right) \tag{6.3}$$

$$\beta = \left(\frac{\pi}{2}\right) - \tan^{-1}\left(\frac{\hat{h}_{S,K}}{\sqrt{\left(\hat{h}_{S,I}\right)^2 + \left(\hat{h}_{S,J}\right)^2}}\right) \tag{6.4}$$

The **K** axis rotation matrix is then:

$$ROT3(\alpha) = \begin{bmatrix} \cos(\alpha) & \sin(\alpha) & 0 \\ -\sin(\alpha) & \cos(\alpha) & 0 \\ 0 & 0 & 1 \end{bmatrix} \tag{6.5}$$

The **J** axis rotation matrix using angle β is given by the following:

$$ROT2(\beta) = \begin{bmatrix} \cos(\beta) & 0 & -\sin(\beta) \\ 0 & 1 & 0 \\ \sin(\beta) & 0 & \cos(\beta) \end{bmatrix} \tag{6.6}$$

The spacecraft position at abort initiation can now be transformed into a two-dimensional vector and unit vector.

$$\vec{r}_{S,2D} = ROT2(\beta) \cdot ROT3(\alpha) \cdot \vec{r}_S \tag{6.7}$$

$$\hat{r}_{S,2D} = \frac{\vec{r}_{S,2D}}{\left|\vec{r}_{S,2D}\right|} \tag{6.8}$$

For positive rotations in the two-dimensional plane through a positive angle θ, the following rotation matrix is used.

$$ROT(\theta) = \begin{bmatrix} \cos(\theta) & -\sin(\theta) & 0 \\ \sin(\theta) & \cos(\theta) & 0 \\ 0 & 0 & 1 \end{bmatrix} \tag{6.9}$$

Rotating the two-dimensional unit vector of the initial position through a specified value of θ yields the two-dimensional unit vector of the final abort position.

$$\hat{r}_{Ab,f,2D} = ROT(\theta) \cdot \hat{r}_{S,2D} \tag{6.10}$$

The two-dimensional final abort position vector can then be obtained with the assumed magnitude of $r_{Ab,f}$.

$$\vec{r}_{Ab,f,2D} = r_{Ab,f} \cdot \hat{r}_{Ab,f,2D} \tag{6.11}$$

This position may then be transformed back into the original **IJK** coordinate system using the transposes of the rotation matrices and reversing the rotation order.

$$\vec{r}_{Ab,f} = ROT3^{T}(\alpha) \cdot ROT2^{T}(\beta) \cdot \vec{r}_{Ab,f,2D} \tag{6.12}$$

This is the final position vector that was needed in order to run the universal variables solution to Lambert's problem. Obtaining it required an assumption of its magnitude and its angular separation in the orbital plane from the known initial position vector. Running the universal variables solution for a chosen time of flight and the two position vectors, $\boldsymbol{r_S}$ and $\boldsymbol{r_{Ab,f}}$, returns the initial and final abort velocity vectors, $\boldsymbol{v_{Ab,i}}$ and $\boldsymbol{v_{Ab,f}}$. If the determination of $\boldsymbol{r_{Ab,f}}$ has been done correctly then the angular momentum of the cross product of $\boldsymbol{r_{Ab,f}}$ and $\boldsymbol{v_{Ab,f}}$ should match that of Eq. 6.1. Finally, an expression is required to determine the entry flight path angle of the resulting approach velocity vector.

$$\phi_{Entry} = \left(\frac{\pi}{2}\right) - \cos^{-1}\left(\frac{\vec{r}_{Ab,f} \bullet \vec{v}_{Ab.f}}{\left|\vec{r}_{Ab,f}\right| \cdot \left|\vec{v}_{Ab,f}\right|}\right) \tag{6.13}$$

Now that an abort trajectory has been created the propellant requirements for its execution may be calculated. The delta V required to initiate the abort is simply the vector difference of the required initial abort velocity and the original spacecraft velocity.

$$\Delta\vec{v}_{Ab,i} = \vec{v}_{Ab,i} - \vec{v}_S \tag{6.14}$$

To this point in the entry abort mode development, there has been no constraint imposed on the magnitude or direction of the final abort velocity $\boldsymbol{v_{Ab,f}}$. However, as discussed in the previous section, acceptable atmospheric entry trajectories will be limited to a narrow range of allowable entry angles and a maximum entry velocity $\boldsymbol{v_{Entry}}$. For abort trajectories that satisfy the corridor angle requirement but whose approach speeds are above the limit, an additional propulsive maneuver will be required to reduce that speed below the maximum allowable entry speed. The magnitude of this extra maneuver is calculated as follows.

$$\Delta v_{Ab,f} = \left|\vec{v}_{Ab,f}\right| - v_{Entry} \tag{6.15}$$

If the approach velocity satisfies the entry limit, then the above delta V is simply zero. The total abort delta V magnitude for the atmospheric entry abort mode is now calculated

$$\Delta v_{Ab,Tot} = \left|\Delta\vec{v}_{Ab,i}\right| + \left|\Delta\vec{v}_{Ab,f}\right| \tag{6.16}$$

To characterize abort behavior and optimize the required delta V amounts the above method is implemented thousands of times during the analysis of a single outbound escape trajectory. Solutions are run for many possible times of flight for

each incremental abort initiation position along the outbound track. For a given abort initiation point and particular time of flight, the delta V requirements are calculated for the suite of possible $\boldsymbol{\theta_{Trans}}$ values. Solutions that do not meet the entry angle requirement are discarded. Of the remaining possible solutions, the one with the minimal value of total abort delta V is returned for each time of flight case. It is possible that for some input times of flight there may not be trajectories that match the entry angle requirements. Of the remaining viable solutions, those that do not require the additional propulsive braking maneuver to match the entry velocity constraint would be preferred due to the advantages of having a single-burn abort initiation.

6.2. Analysis of Entry Abort Results

The above described process was employed to determine the requirements of the resulting entry aborts for a selected baseline departure trajectory with the objective of determining the solution behavior of the different abort parameters. The May 12, 2018 conjunction Type I minimum energy trajectory was selected as the baseline transfer trajectory for this and all other abort modes in this study. For each time of abort initiation along the outbound trajectory departing on that date, entry abort solutions were found for abort times of flight up to 330 hrs (approximately two weeks). Entry aborts with return flight times that were shorter than the elapsed mission time at the point of abort initiation were not searched. The total propellant delta V requirements for executing these entry aborts are represented in Figure 6.3. As seen in the figure, for a given time of abort initiation, the required delta V

decreases for longer abort times of flight. Data show that entry aborts with 330 hour flight times or shorter are possible provided that the spacecraft retains an approximately 4 km/s delta V capability. This is a large amount of delta V, of the same order as the just completed departure TMI burn maneuver. If lesser reserve capability exists for a particular spacecraft or architecture, long time of flight aborts may still be obtained for this case for much of the outbound transfer for a propellant cost of approximately 2.5 km/s. Figure 6.4 represents the ratio of the initial delta V required to start the abort and the final delta V (if needed) at Earth arrival for matching the entry corridor velocity requirement. For those abort solutions which met the entry corridor velocity requirements there was no need for a final delta V maneuver. This is a desirable situation in that the abort may be entirely executed with a single propulsive maneuver. For those aborts that do require a final burn, the failure of that maneuver to execute will lead to the spacecraft entering the atmosphere at a higher than desired velocity. Figure 6.4 shows that single burn entry aborts become impossible for later times of abort initiation. Figure 6.5 and Figure 6.6 represent the initial and final abort delta V amounts. Figure 6.6 confirms the occurrence of final delta V maneuvers for later times of abort initiation though these burns never require more than 0.4 km/s. Given the small amounts of final delta V, when utilized, the similarity between Figure 6.3 and Figure 6.5 is not surprising.

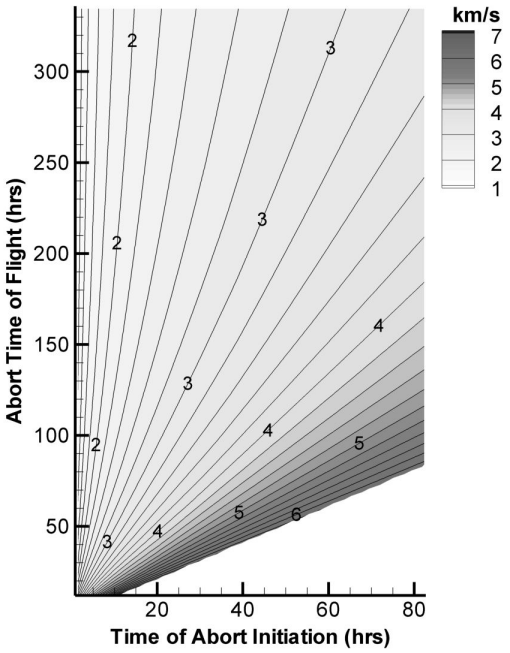

Figure 6.3 Entry Abort Total Delta V

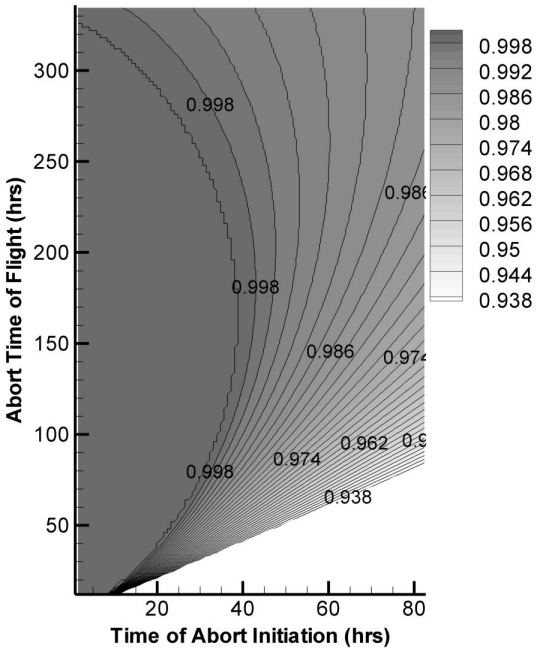

Figure 6.4 Entry Abort Delta V Ratio

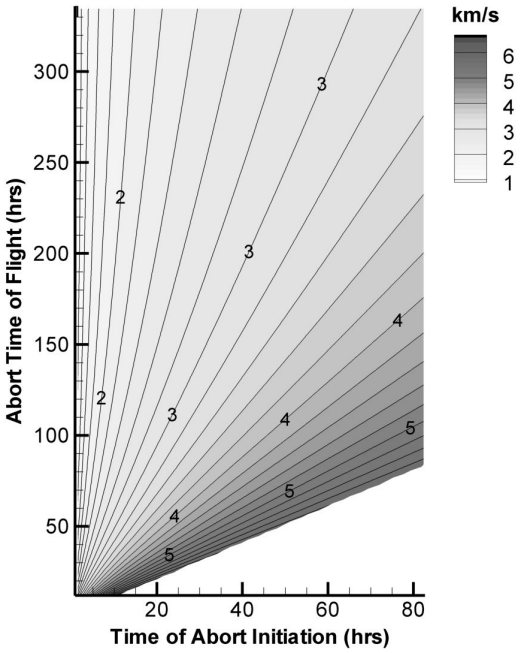

Figure 6.5 Entry Abort Delta V Initial

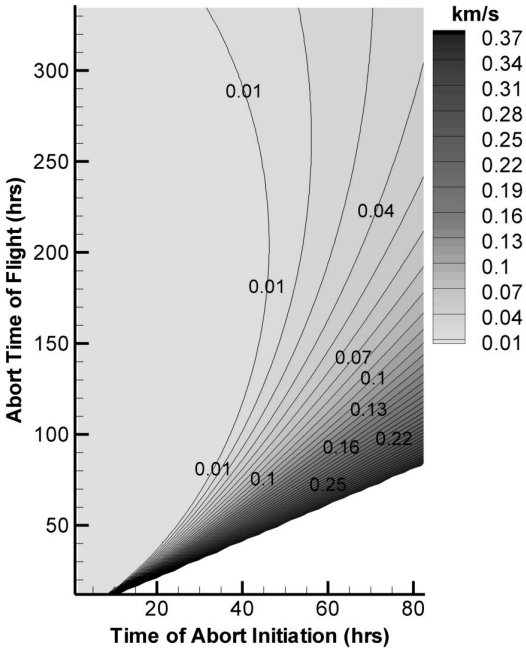

Figure 6.6 Entry Abort Delta V Final

Further understanding of the entry abort mechanics is gained by visualizing the geometries of the abort trajectories. Figure 6.7 shows the abort trajectories in increments of 30 hours for an abort maneuver initiated 20 hours into the mission.

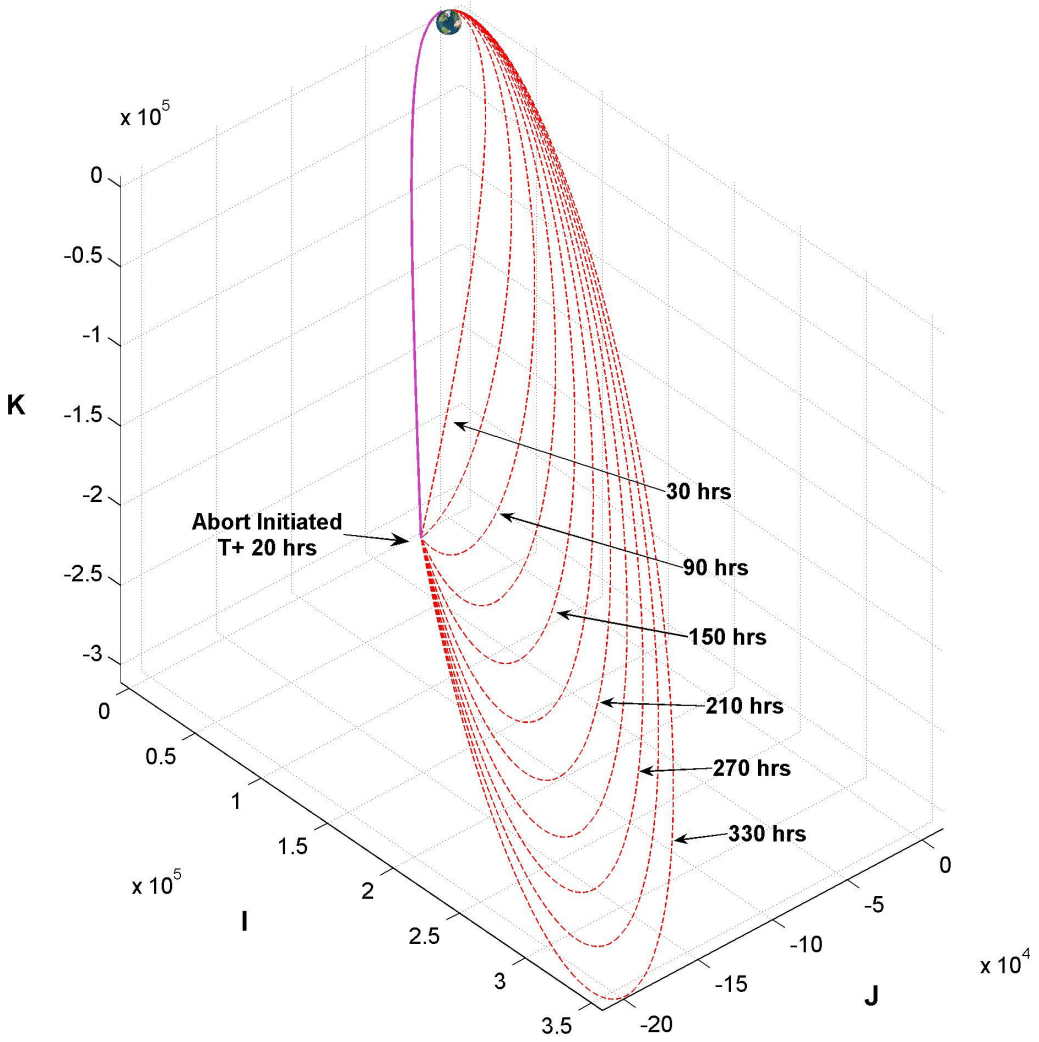

Figure 6.7 Entry Abort Trajectories by Times of Flight at T+ 20 hrs

As shown by the figure, the short 30 hour duration abort trajectory is a hyperbolic return trajectory very similar to the abbreviated hyperbolic exit trajectory. The longer abort duration trajectories become less energetic. For an abort duration of approximately 90 hours, the abort initiation maneuver essentially cancels any outward

velocity and the spacecraft simply falls back towards the Earth. The longer duration aborts decrease the outbound velocity to a degree sufficient to terminate the escape speed, but the spacecraft continues traveling in an outward direction until being eventually decelerated by the Earth's gravity at which point the spacecraft falls back in towards the planet. Figure 6.8 shows trajectories for an abort initiated after 50 hours.

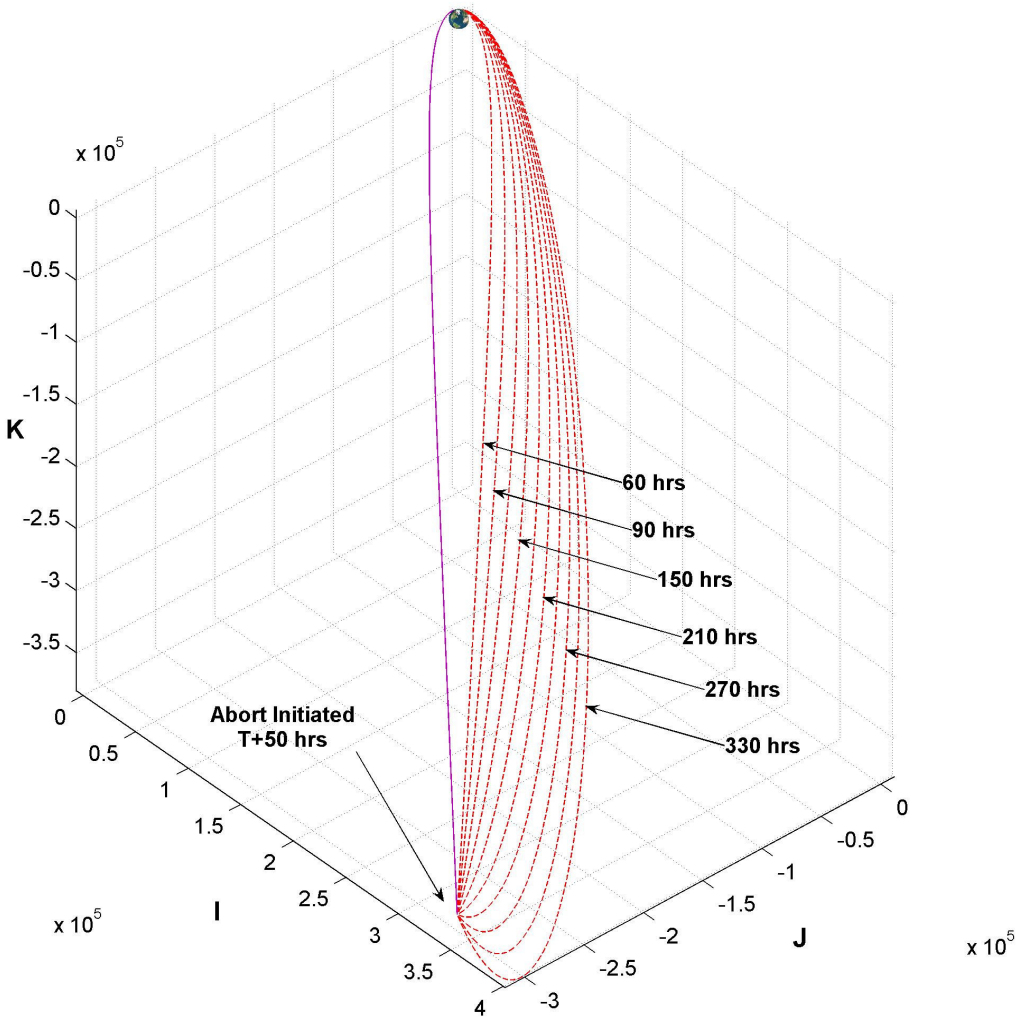

Figure 6.8 Entry Abort Trajectories by Times of Flight at T+ 50 hrs

Similar phenomena are observed at this later time of abort initiation, though the maintaining of the same abort time of flight expectations causes a greater number of the return possibilities from the farther initiation point to return more directly to Earth. The consequence is a larger abort initiation delta V for a 60 hour return abort initiated at T+ 50 hours than at T+ 20 hours as evidenced in Figure 6.5.

These geometric observations aid in the understanding of the abort trajectory's specific orbital energy as given by Figure 6.9. Positive energy values correspond to hyperbolic trajectories while negative energies are elliptic orbits. For the abort initiation after 20 hours, the energy first decreases then increases for increasing abort times of flight with a minimum near 90 hours time of flight. This is consistent with the previous geometric observation. Figure 6.10 documents the resultant abort transfer angles. The constant entry angle requirement drives the variety of abort orbits across a range of transfer angles in the attempt to match the entry corridor. Figure 6.11 presents the best entry angle match possible from the determined abort trajectories. As shown, the desired -6.5° entrance angle is achievable for nearly every situation except for aborts which occur in the first few hours of the outbound flight. In the case of an emergency during the transit of this narrow region, the initiation of the abort could simply be delayed until a mission time of approximately 10 hours when an entry abort with the required entry angle becomes available. The resulting arrival velocity at atmospheric interface for all the abort cases is shown in Figure 6.12. These velocities follow the same trend as the specific orbital energy.

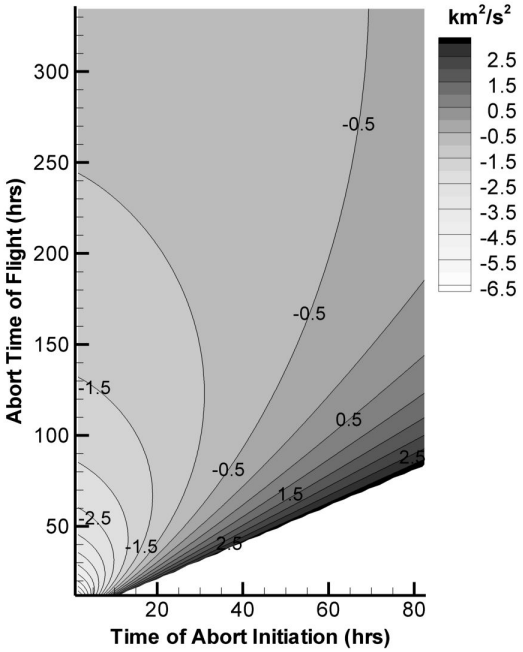

Figure 6.9 Entry Abort Specific Energy

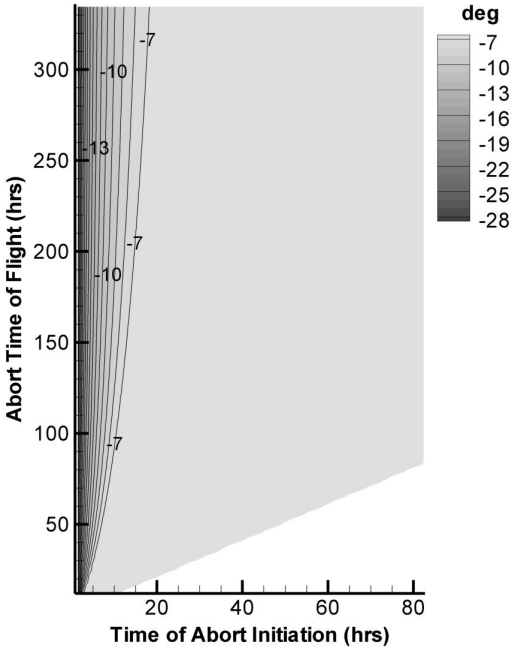

Figure 6.11 Entry Abort Entry Angle

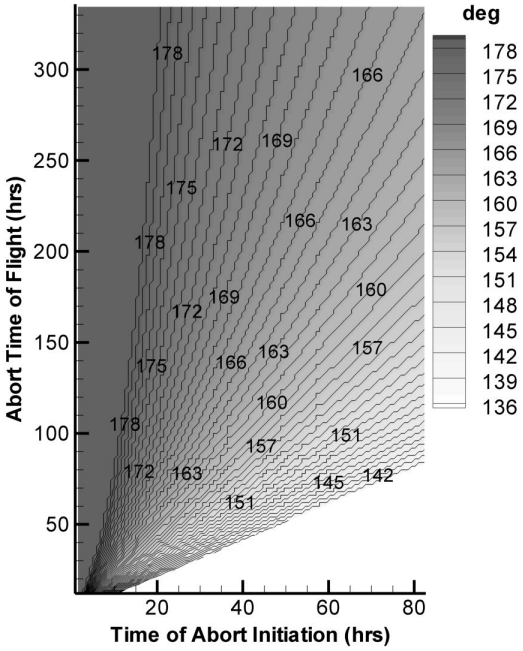

Figure 6.10 Entry Abort Transfer Angle

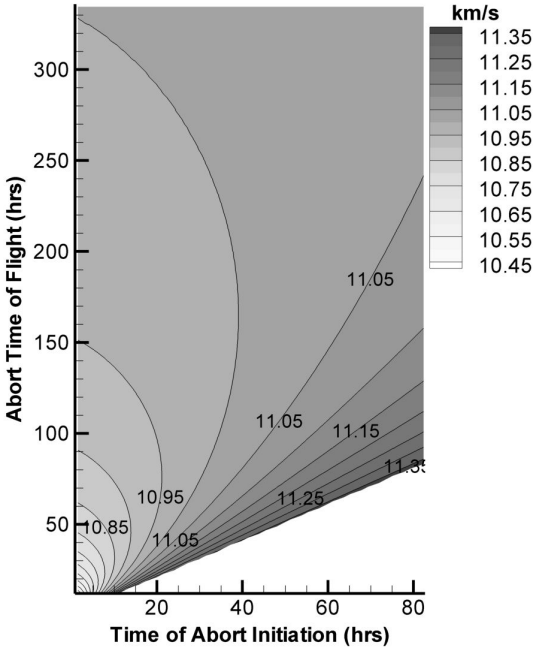

Figure 6.12 Entry Abort Arrival Velocity

Figure 6.13 provides a zoomed in detail of the various abort trajectories at the point of atmospheric entry for the T+ 20 hr abort initiation case. In matching the entry angle, the transfer angles are increased for increasing abort flight duration as verified by Figure 6.10.

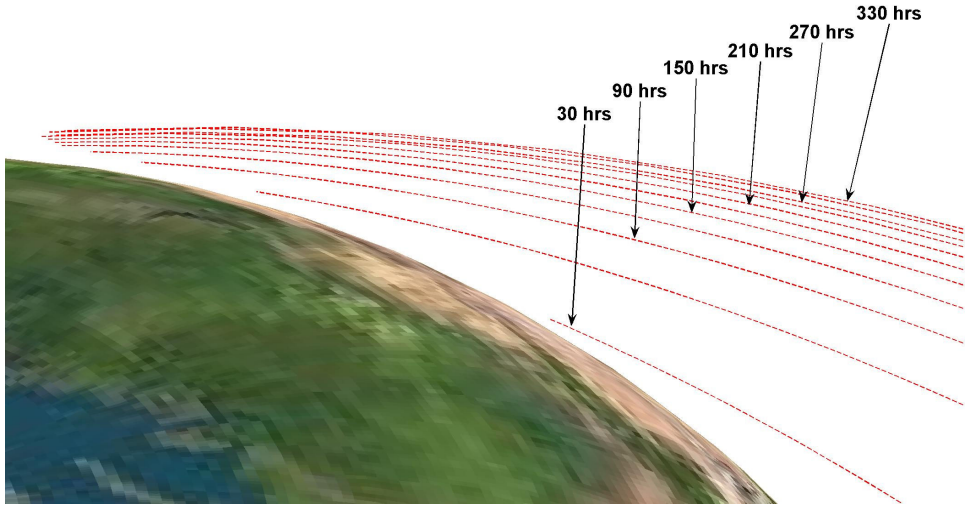

Figure 6.13 Entry Abort Trajectories: Detail of T+ 20 hrs Abort Entry Points

During the abort setup, it was theorized that a moderate reduction in abort delta V might be realized if the entry spacecraft was able to withstand entry velocities higher than the assumed 11 km/s. However, the data results of Figure 6.6 exhibited only occasional need for a final propulsive maneuver to reduce the entry velocity of the spacecraft below the maximum allowable entry velocity. Figure 6.14 shows the results of a trade study of allowable entry velocities from 10 km/s up 11.5 km/s for the baseline mission. The presented results for the 150 hour duration abort show that less delta V is required for faster entry limits. However, assuming the 11 km/s case is within current capability, there are only slight savings for higher entry velocities. Permitting even higher velocities is not a significant enabler of this abort mode.

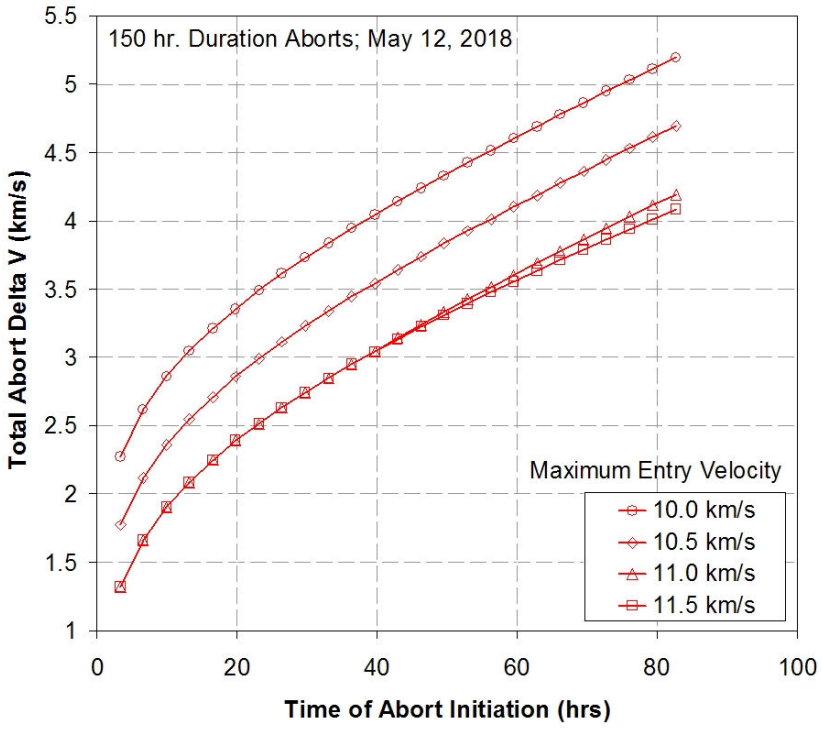

Figure 6.14 Sensitivity of Delta V to Maximum Allowable Entry Velocity

6.3. Entry Abort Results 2018-2033

As discussed previously in Chapter 5, a given planetary angular alignment repeats every synodic period, though the same positional alignment in space repeats with the inertial period. As a result, while specific interplanetary transfer setups recur every synodic period the particular requirements for the execution of that transfer vary across the inertial period. Consequently, if the utilized spacecraft is expected to accomplish the specified transfer during any year of opportunity then the design and sizing of that spacecraft must be set by the launch year with the most extreme requirements. This same schema will apply to the estimation of the abort capabilities of the spacecraft. The analysis of the abort requirements for a certain departure in a

single year is insufficient to determine the true requirements if the capability is desired during any launch opportunity. The detailed abort data and geometries of the previous section were for but a single departure date and a specified trajectory type. Determining the true abort design requirements necessitates the assessment of other possible Mars transfers and trajectory classes across multiple years. Entry abort solutions were therefore obtained for the best launch dates for each of the three trajectory classes across a fifteen year inertial period. Abort delta V requirements for abort flight times of 150 and 250 hours were extracted for each solution. This data reduction was necessary in order to identify trends in the massive amount of data generated by all the solutions. Figure 6.15 compares the required abort delta V for each of the three trajectory classes during the year 2024 for a 150 hour abort flight.

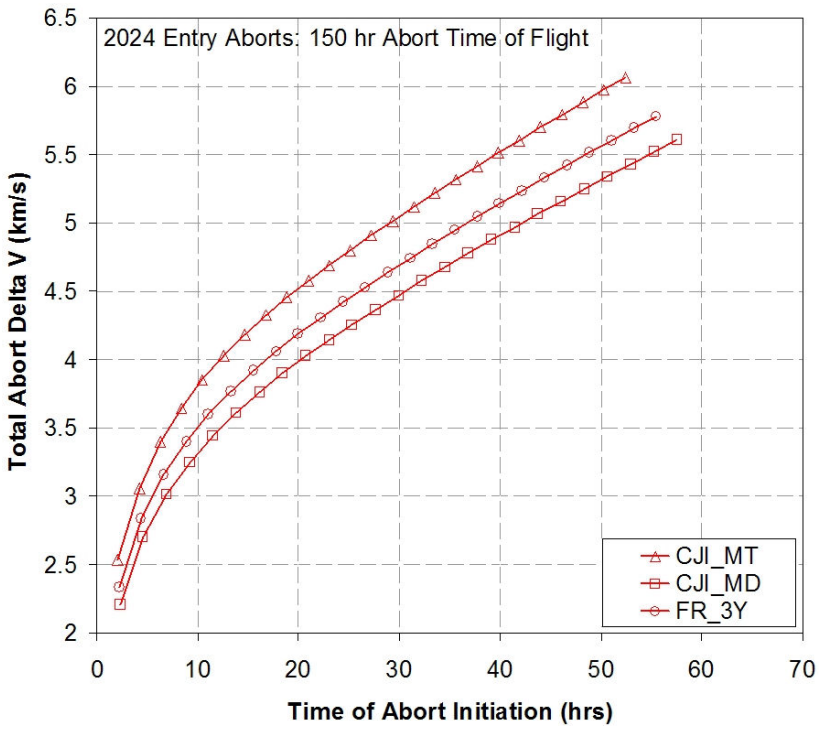

Figure 6.15 Example Entry Abort Requirements by Trajectory Class

Maintaining the same abort time of flight causes the abort delta V requirement to increase as the departure phase progresses. Entry abort delta V requirements are primarily a function of outbound velocity. As such, the minimum departure velocity trajectory class (CJI_MD) has the lowest required delta V of the three represented. Also, slower departure velocities equate to longer duration departure phases also seen in the figure. The three trend lines will shift year-to-year as the trajectory requirements and launch dates of the three classes vary. It would be extremely useful to establish the best and worst case requirements for each trajectory class. Figure 6.16 shows these extrema for both 150 and 250 hour abort durations for the conjunction minimum total delta V (CJI_MT) trajectory class which has a 2018 minimum and a 2024 maximum departure velocity.

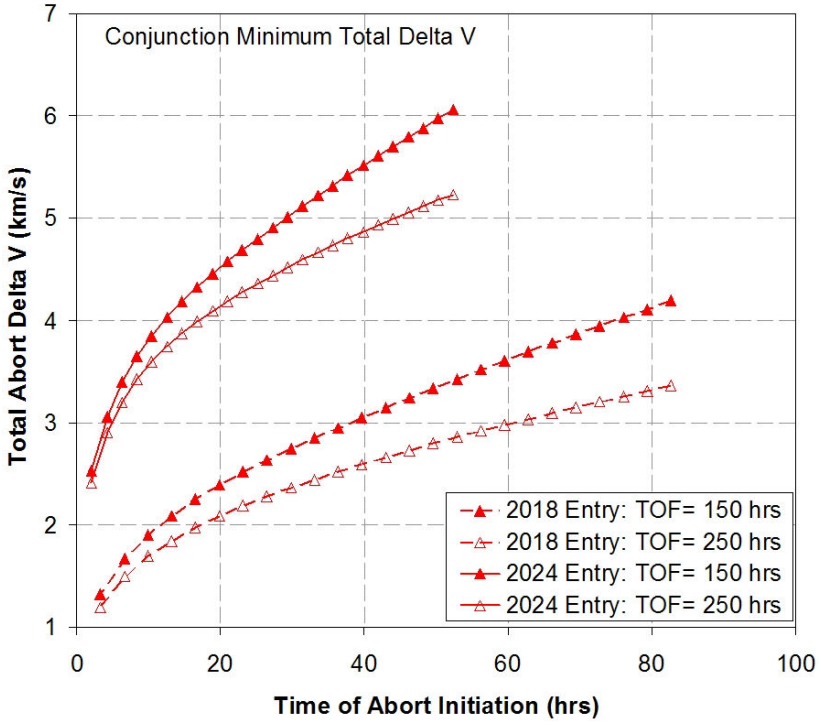

Figure 6.16 Requirements Extrema for Selected Entry Abort Durations: CJI_MT

As shown, the maximum and minimum abort delta V amounts required for a 150 or 250 hour abort to entry differ by as much as 2 km/s for this trajectory class. Additionally, the duration of the defined departure phase ranges between approximately 50 and 80 hours. The high propellant cost of the 150 hour abort, up to 6 km/s, means that aborts from this trajectory class will likely be of longer duration in practice. A 5 km/s delta V capability would be required to allow a spacecraft flying this trajectory to execute a 250 hour long abort to entry maneuver for all outbound opportunities. The maximums and minimums for the conjunction minimum departure delta V (CJI_MD) trajectory class trajectory class are similarly shown in Figure 6.17.

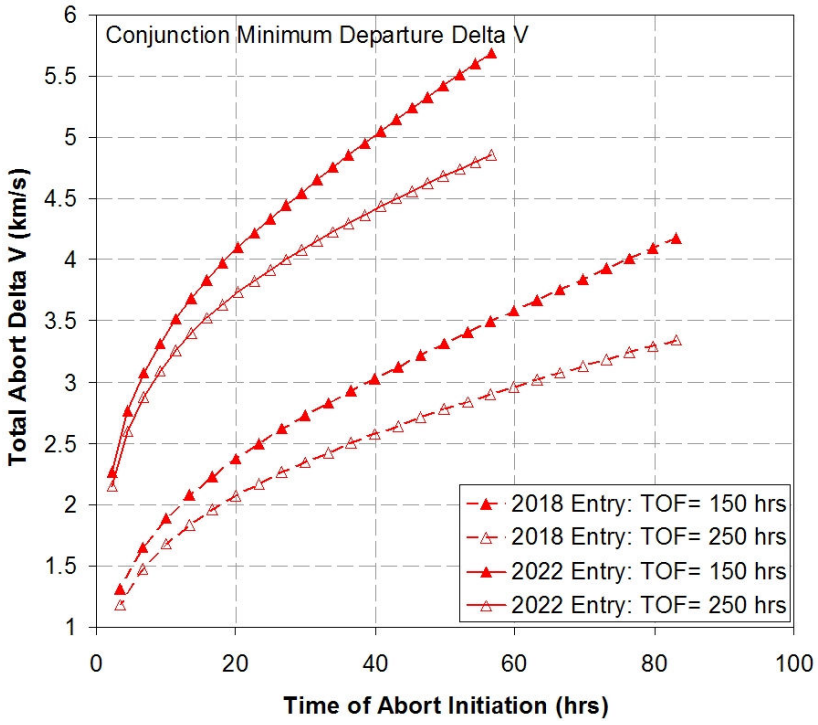

Figure 6.17 Requirements Extrema for Selected Entry Abort Durations: CJI_MD

The minimum of this conjunction minimum departure (CJI_MD) trajectory also occurs in 2018 but the maximum shifts to 2022. The slower outbound velocity of the conjunction minimum departure trajectory results in a small reduction (~0.4 km/s) in the maximum required delta V versus the conjunction minimum total (CJI_MT) trajectory. The differences between the extrema are also smaller (~1.5 km/s) while the shortest departure phase is several hours longer. Figure 6.18 presents the extrema for the free-return class transfer trajectory.

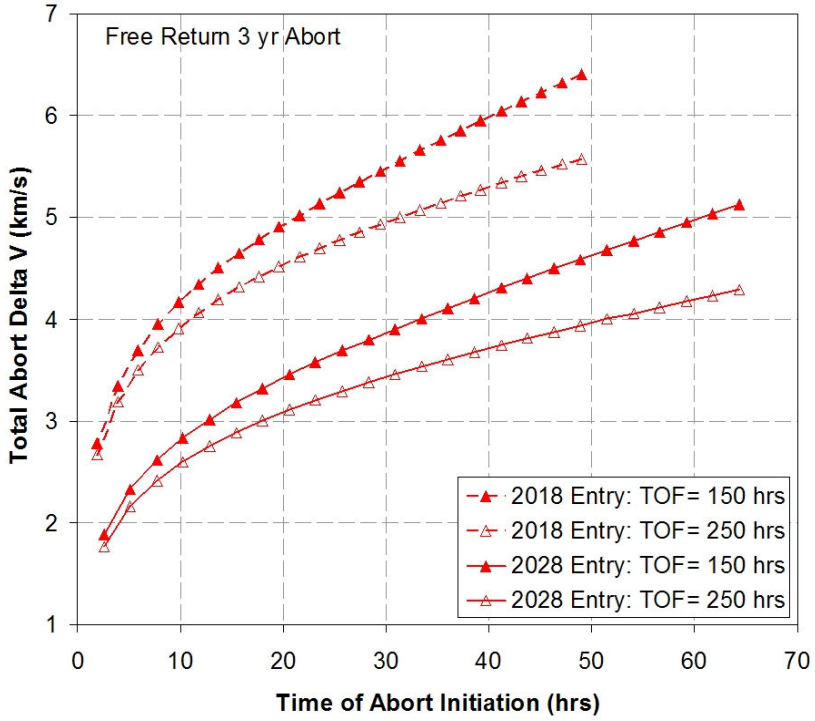

Figure 6.18 Requirements Extrema for Selected Entry Abort Durations: FR_3Y

The free-return trajectories were run for launch opportunities from 2018 up through 2028 using opportunity data from Soldner[44]. Interestingly, the maximum abort requirements for the free-return trajectory occur in 2018, the year the other classes

shared minimums. The minimum of the investigated free-return opportunities occurred in 2028. The resulting departure phase durations range from between 50 and 65 hours and have higher entry abort delta V requirements than the other trajectories. The extrema of the three trajectory classes for a 250 hour abort durations are compared together in Figure 6.19.

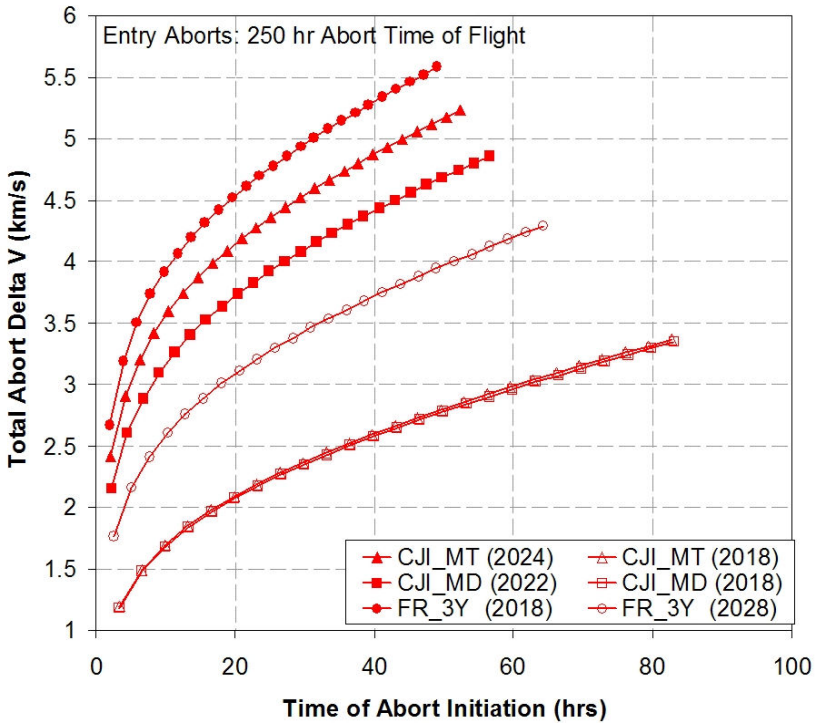

Figure 6.19 Comparison of Requirements Extrema by Trajectory Class

The data show that the maximum delta V requirements for a 250 hour abort from a free-return (FR_3Y) trajectory are the highest of the three classes while the conjunction minimum departure trajectory (CJI_MD) has the lowest. For the minimum delta V case, the free-return entry abort requirements are much higher than the others by a difference of approximately 1 km/s while the two conjunction class minimums are nearly identical and occur on the same year, 2018.

The objective of the present chapter was to investigate the requirements trends for the performance of an Earth entry abort from the various trajectory scenarios. The entry abort data presented in this section for the extracted 150 and 250 hour sample cases demonstrate the variability in required abort delta V across the inertial period and the resulting differences between trajectory classes. Designing in a continual 250 hour entry abort capability into a given spacecraft would entail the budgeting of approximately 5 km/s of post-TMI abort delta V. This large amount can be mitigated slightly by selecting abort times of flight longer than 250 hours. Additionally, permitting allowable entry velocities higher than the assumed 11 km/s can provide small reductions for some abort scenarios Nevertheless, it appears that for aborts on the order of 330 hours (two weeks) or less, 4 km/s or more of delta V capability must exist if the entry abort mode is to be enabled for every flight opportunity. Later chapters will move beyond this survey of requirements variation and determine the suitability of this abort mode for specific interplanetary architectures.

Chapter 7. Earth Orbit Aborts

The previous chapter established the abort to atmospheric entry as the baseline contingency plan for emergency crew recovery during the outbound departure phase. However, the nature of some emergencies, such as a damaged heat shield, may preclude the execution of an entry abort. This chapter investigates the potential of returning the spacecraft to a low-Earth orbit instead of the Earth's surface. Possible abort modes include the placement of the spacecraft in its own orbit or rendezvousing with another existing orbital asset. The objective of the chapter is to develop the methodology for the performance of these aborts and analyze the design space to establish the propulsive requirements for their execution.

7.1. Abort Trajectories to Earth Orbit

In the decades since the Apollo program, mankind had become increasingly experienced in operating satellites and space stations in low-Earth orbit. The current or planned existence of on-orbit assets capable of supporting human life opens up additional possible abort havens for other human spacecraft. These Earth orbit abort mode options were not really possible for previous human missions. Depending on the mission orbit and inclination, maneuvering the Shuttle to intercept another on-orbit human-rated asset such as the ISS is nearly always impossible given the remaining propulsive capabilities of the vehicle. During the Apollo and Gemini programs there simply were no other on-orbit assets. The future utility of low-Earth orbit as a viable abort destination is more limited than that of an Earth entry abort.

There are a number of reasons for this, the first of which is the required abort delta V. LEO circular orbital velocity is approximately 7.6 km/s, this is much lower than the 11 km/s allowed for Earth entry and will require a greater amount of delta V to decrease the approach velocity. The delta V impact could be mitigated by targeting a higher energy elliptical orbit with a low-altitude periapse but this would render rendezvous with on-orbit assets in supposed circular LEO orbits impossible. The rendezvous problem is a second complication to a LEO abort; targeting the moving position of an orbiting asset is more difficult than just achieving its same orbit. However, the spacecraft may be aborted to a LEO orbit without directly rendezvousing with another orbital asset; it could hold there to await rescue. For many emergency scenarios, the abort to entry abort is likely the desired abort mode. There are; however, possible emergency situations where the LEO abort mode would be superior to that of Earth entry. The most obvious one of these is in the case of a damaged re-entry heat shield which might rule out an atmospheric entry by the affected spacecraft. While likely not the preferred Earth-return abort mode in many cases, the flexibility of the spacecraft to leverage on-orbit assets enhances the comprehensive safety strategy that is desired for a human-carrying spacecraft by providing multiple and overlapping abort options.

7.1.1. Determination of LEO Aborts

The abort profile of the LEO abort mode is very similar to that of the Earth entry mode discussed previously. The LEO abort mode profile is shown in Figure 7.1.

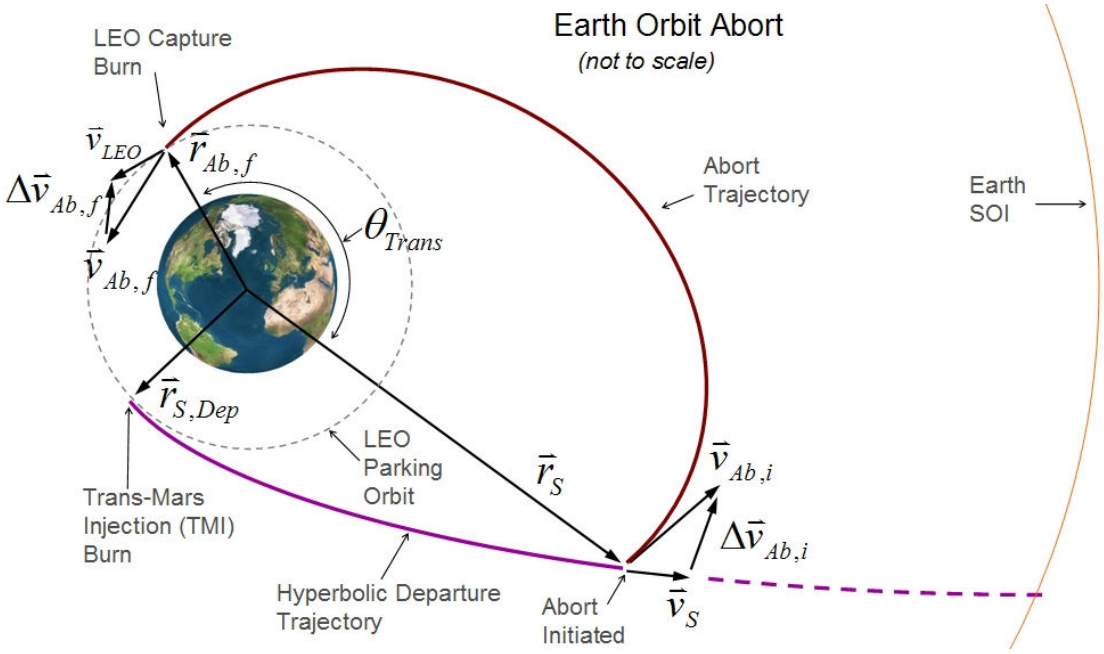

Figure 7.1 Earth Orbit Abort Profile

As shown by the figure, the LEO abort mode position and velocity setup at the point of abort initiation is identical to that of the Earth entry abort mode, though the final abort positions and velocities are different given that the LEO abort mode is targeting an Earth orbit instead of a lower altitude atmospheric interface. The solution of the LEO abort mode also will require a final position vector which is obtained via the same method as for the entry abort mode with three exceptions. First, the magnitude of the desired orbital altitude is much larger than for the atmospheric entry altitude. Second, an abort to LEO will be always be a two-burn abort, one to start the abort trajectory and one to circularize into the desired orbit. Lastly, a LEO abort need not satisfy any of the entry corridor constraints that were applied to the entry abort mode. Thus, for a particular abort initiation point and time of flight, the returned abort

trajectory will be the one for the transfer angle θ_{trans} which returned the least total abort delta V.

Establishing the 2nd propulsive maneuver will require the determination of the velocity vector direction of the circular orbit speed at the final position of the abort trajectory. For a circular orbit, the orbital velocity is always perpendicular to the position vector. Thus, the unit vector of the circular orbit velocity is obtained by rotating the arrival unit position vector of Eq. 6.10 a further 90°.

$$\hat{v}_{LEO,2D} = ROT\left(\frac{\pi}{2}\right) \cdot \hat{r}_{Ab,f,2D} \tag{6.17}$$

The two-dimensional circular orbit velocity vector is then simply the multiplication of this unit vector by the magnitude of the circular velocity.

$$\vec{v}_{LEO,2D} = \sqrt{\frac{\mu_E}{r_{Ab,f}}} \cdot \hat{v}_{LEO,2D} \tag{6.18}$$

This velocity can then be transformed into the **IJK** coordinate system using the transposes of the rotation matrices and reversing the rotation order.

$$\vec{v}_{LEO} = ROT3^T(\alpha) \cdot ROT2^T(\beta) \cdot \vec{v}_{LEO,2D} \tag{6.19}$$

The circularization delta V is then simply the vector subtraction of the circular orbit velocity and the final abort velocity vectors.

$$\Delta\vec{v}_{Ab,f} = \vec{v}_{LEO} - \vec{v}_{Ab,f} \tag{6.20}$$

The total abort delta V for the Earth orbit abort is the summation of the abort initiation delta V and the circularization delta V and is calculated via Eq. 6.16.

This methodology is applied to determine the orbit abort requirements for every incremented point of the outbound escape orbit in the same fashion as was previously done with the entry abort mode. The following sections present the orbit

abort trajectory requirements for the various Mars transfer trajectory classes and years of opportunity.

7.2. Analysis of LEO Abort Results

The orbit determination process was engaged to determine the requirements of the Earth orbit aborts for a selected baseline departure trajectory with the objective of determining the solution behavior of the different abort parameters. The May 12, 2018 conjunction Type I minimum energy trajectory was again the utilized baseline transfer trajectory. For each time of abort initiation along the outbound trajectory departing on that date, LEO abort solutions were found for abort times of flight up to 330 hrs (approximately two weeks). LEO aborts with abort times of flight that were shorter than the elapsed mission time at the point of abort initiation were not searched. The total propellant delta V requirements for executing these LEO aborts are represented in Figure 7.2. The delta V trends of the figure are very similar to those observed for the entry abort case in Figure 6.3; principally, decreasing delta V for longer abort flight times. Despite the similarity in trend, the magnitudes of the orbit aborts are, as was expected, much larger than comparable entry aborts (approximately 3 to 4 km/s more). LEO aborts with 330 hour flight times or shorter are achievable for this setup if the spacecraft retains an approximately 6 km/s delta V capability. This is a larger delta V amount than a comparable entry abort or even the initial TMI escape burn maneuver. Figure 7.3 represents the ratio of the initial delta V required to start the abort and the final delta V required to achieve orbit. If the final burn maneuver fails to occur, the spacecraft will slingshot past Earth. If the

inbound abort orbit was hyperbolic then the spacecraft would once again be on an outbound escape orbit, placing the crew in the undesirable necessity of aborting from their previously failed abort attempt. Figure 7.4 and Figure 7.5 represent the initial and final LEO abort delta V quantities. The abort initiation delta V amounts of Figure 7.4 correspond almost exactly to the entry abort initiation delta V magnitudes of Figure 6.5. The real differences between the entry and orbit abort modes are the maneuvers and constraints at the end of the abort trajectory. The actual abort paths for the orbit abort mode from the point of abort initiation up through Earth approach are extremely similar to those of Figure 6.7 and Figure 6.8 which were for the entry abort mode; hence the resemblance in the abort initiation requirements of Figure 7.4 and Figure 6.5. Given the similarity of the abort initiation maneuver, the additional 3 to 4 km/s delta V of the orbit abort must therefore arise primarily from the final abort termination burn into Earth orbit. The actual delta V values for this maneuver are contained in Figure 7.5. As shown, the required final delta V magnitudes for a given abort flight time are quite high for aborts initiated during the first few hours of the mission then decrease until increasing again slightly for later times of abort initiation. The two principal parameters of the abort trajectory that influence the severity of this maneuver are the arrival velocity magnitude and direction. Arrivals with higher velocities and/or large flight path angles will require larger propulsive maneuvers to enter onto the desired LEO orbit. Unlike the entry abort solutions; there is no need for these orbit aborts to match a particular entry orientation. The analysis program is therefore free to tradeoff these two parameters finding the arrangement with the lowest delta V for each particular initiation point and abort flight time scenario.

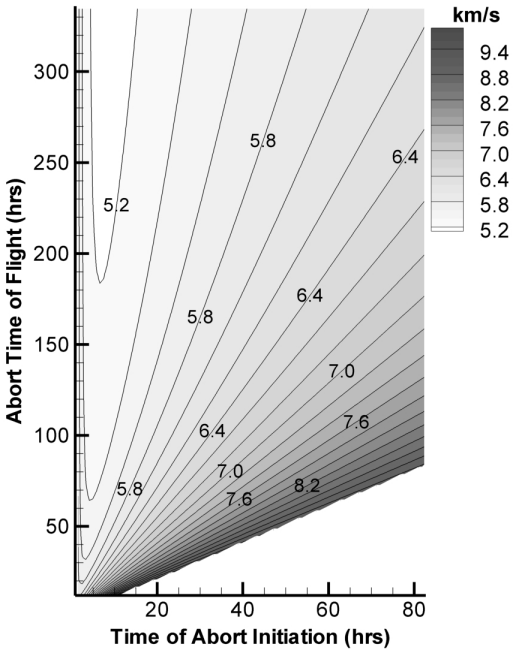

Figure 7.2 LEO Abort Total Delta V

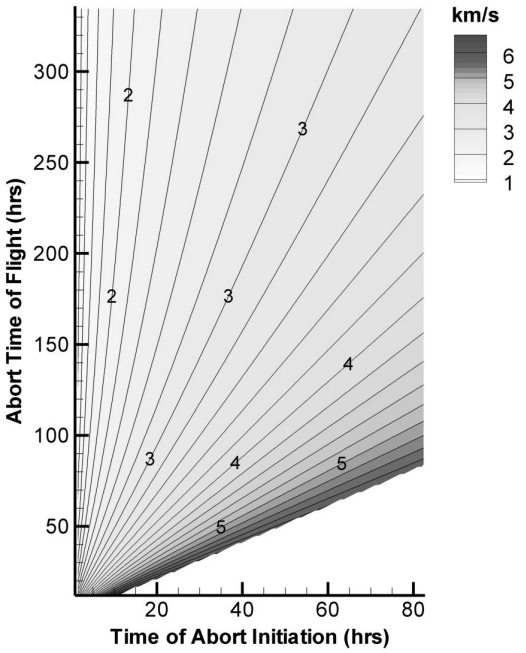

Figure 7.4 LEO Abort Delta V Initial

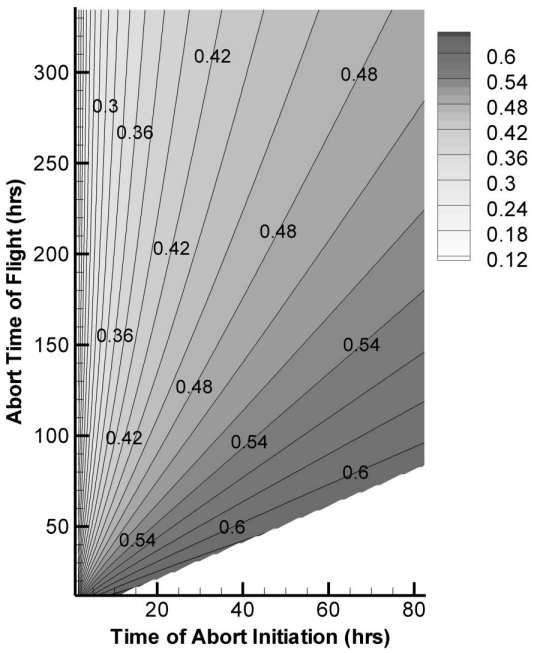

Figure 7.3 LEO Abort Delta V Ratio

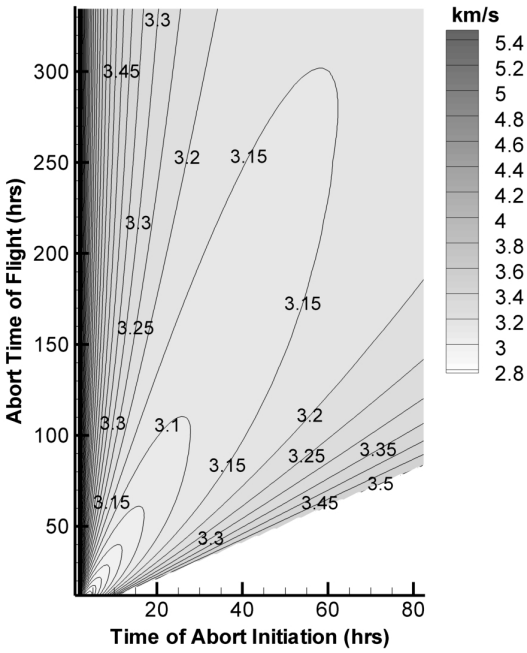

Figure 7.5 LEO Abort Delta V Final

The specific orbital energy of the orbit aborts are given in Figure 7.6. The energy trends closely mirror those seen for the entry aborts in Figure 6.9 as was expected given the similarity in the abort paths. As mentioned, the analysis program investigates a large number of possible transfer angles for each abort scenario and keeps the one with the lowest resulting abort delta V. These optimum abort transfer angles are shown in Figure 7.7 for all of the abort scenarios. The transfer angle data show a strong preference for angular transfers approaching 180°. This tendency is much more pronounced than for the entry abort case of Figure 6.10 since the entry/arrival angle was unconstrained for the orbit abort case. The arrival angles for the orbit abort case are presented in Figure 7.8. For the majority of the investigated abort envelope, the resulting arrival angles have been driven to small values. This behavior confirms the benefit of delta V reduction for near-tangent arrivals into the desired LEO orbit thus reducing the magnitude of the final delta V maneuver. Larger entry angles are selected for aborts initiated during the first 20 hours of the mission. Figure 7.9 shows the magnitude of the arrival velocity at the end of the abort trajectory. This velocity is a function of the abort specific energy and therefore mirrors the trends of Figure 7.6. Coupling the arrival angle and arrival velocity data explains the decreasing-increasing behavior seen in the final abort delta V magnitudes of Figure 7.5. The fast arrival velocities seen in Figure 7.9 for shorter abort flights initiated later in the mission drives up the abort final delta V for those abort scenarios while the higher final delta V values for aborts initiated early in the mission are due to the higher arrival angles of those trajectories as verified by Figure 7.8.

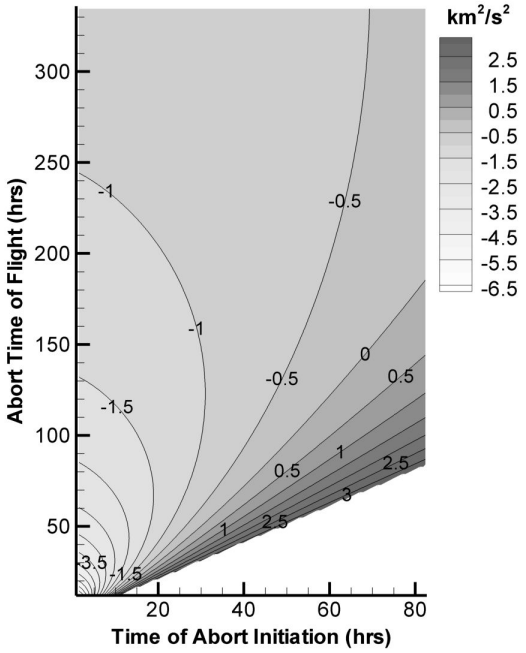

Figure 7.6 LEO Abort Specific Energy

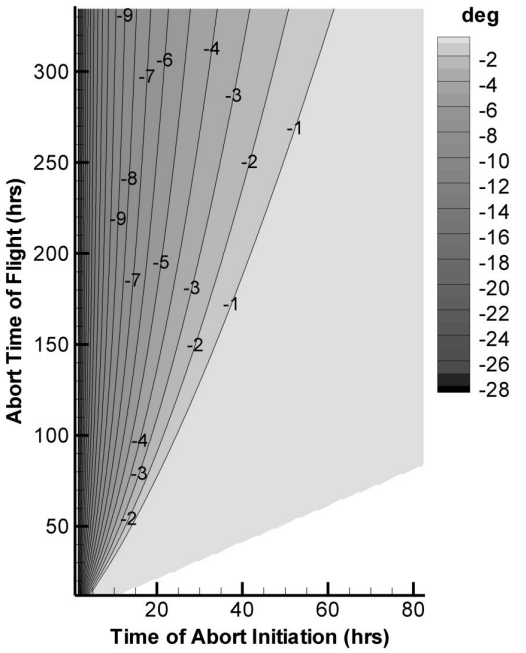

Figure 7.8 LEO Abort Arrival Angle

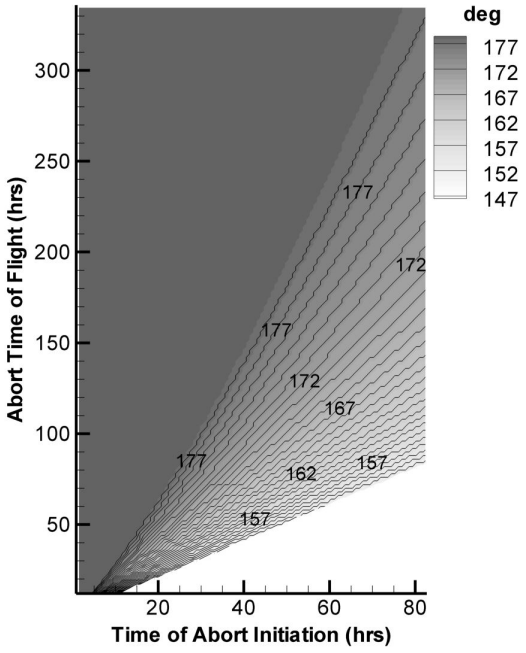

Figure 7.7 LEO Abort Transfer Angle

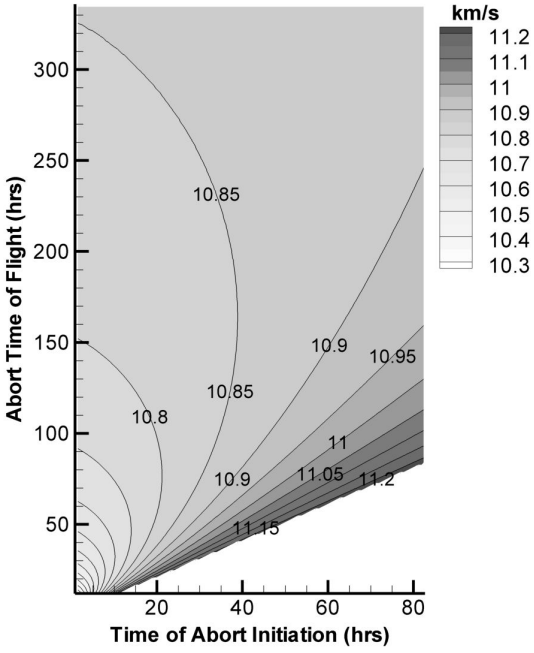

Figure 7.9 LEO Abort Arrival Velocity

Figure 7.10 supplies a zoomed-in detail of the various LEO abort trajectories at the point of orbit insertion for the T+ 20 hr abort initiation case. For abort flight times greater than 50 hours for this case, the resulting transfer angles are all about 180° with longer abort flight times arriving at steeper angles; very different results than the near constant arrival angles of the entry aborts in Figure 6.13.

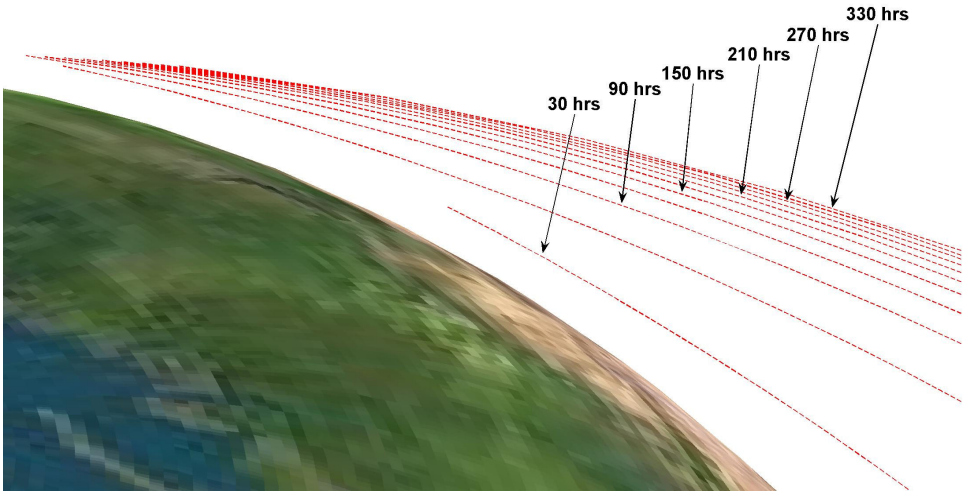

Figure 7.10 LEO Abort Trajectories: Detail of Abort Arrivals

7.3. LEO Abort Results: 2018 – 2033

As was done for the entry aborts of Chapter 6, evaluating the true LEO abort design requirements necessitates the assessment of other possible Mars transfers and trajectory classes across multiple years in addition to the baseline case considered in the previous section. LEO abort solutions were similarly found for the best launch dates for each of the three representative trajectory classes for the fifteen year inertial period. Abort delta V requirements for abort flight times of 150 and 250 hours were

extracted for each solution. Figure 7.11 presents the required LEO abort delta V magnitudes for each of the three trajectory classes during the year 2024 for a 150 hour abort flight.

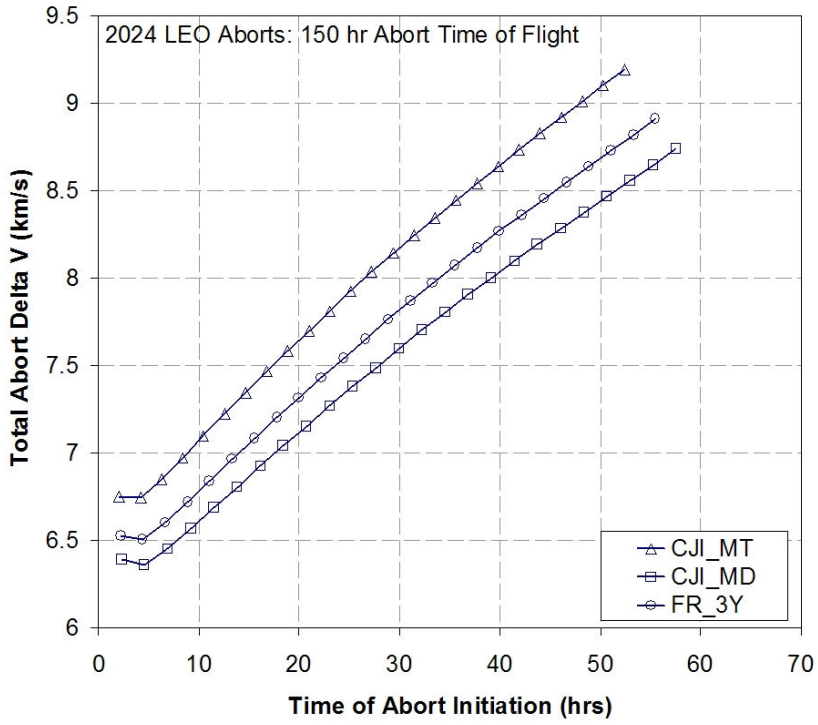

Figure 7.11 Example LEO Abort Requirements by Trajectory Class

LEO abort delta V requirements are a function of both the outbound velocity and the orbit insertion maneuver. The addition of the insertion delta V burn is the primary reason the LEO abort delta V quantities are so much larger than those required for the entry aborts of the previous chapter. The minimum departure velocity trajectory class (CJI_MD) has the lowest required abort delta V of the three considered trajectory classes for this year. With delta V requirements exceeding 9 km/s, a 150 hour abort to orbit is an infeasible abort option for most of the departure phase. The best and

worst case delta V requirements for the conjunction minimum total delta V (CJI_MT) trajectory class for both 150 and 250 hour abort durations are shown in Figure 7.12.

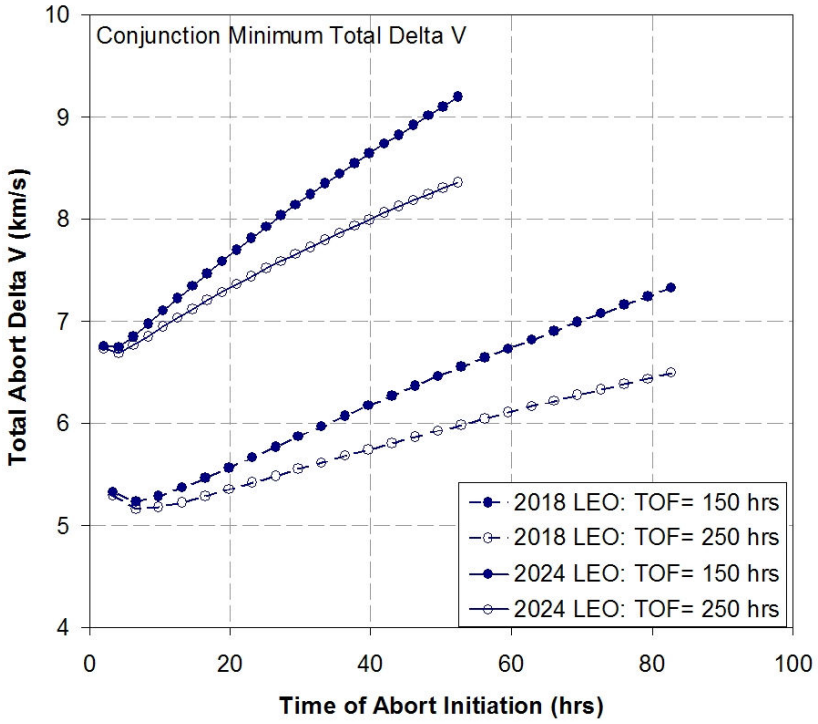

Figure 7.12 Requirements Extrema for Selected LEO Abort Durations: CJI_MT

As shown, the maximum and minimum abort delta V amounts required for a 150 or 250 hour abort to orbit differ by 2 km/s with departure durations ranging between approximately 50 and 80 hours. Approximately 8.5 km/s of delta V would be required to allow a spacecraft flying this trajectory to execute a 250 hour long orbit abort maneuver for all outbound opportunities; this is about 3.5 km/s more propulsive cost than was required for the matching entry abort case. The conjunction minimum departure delta V (CJI_MD) trajectory class is next considered. The maximum and minimum delta V trends for this trajectory occur in the years 2022 and 2018 respectively and are shown in Figure 7.13.

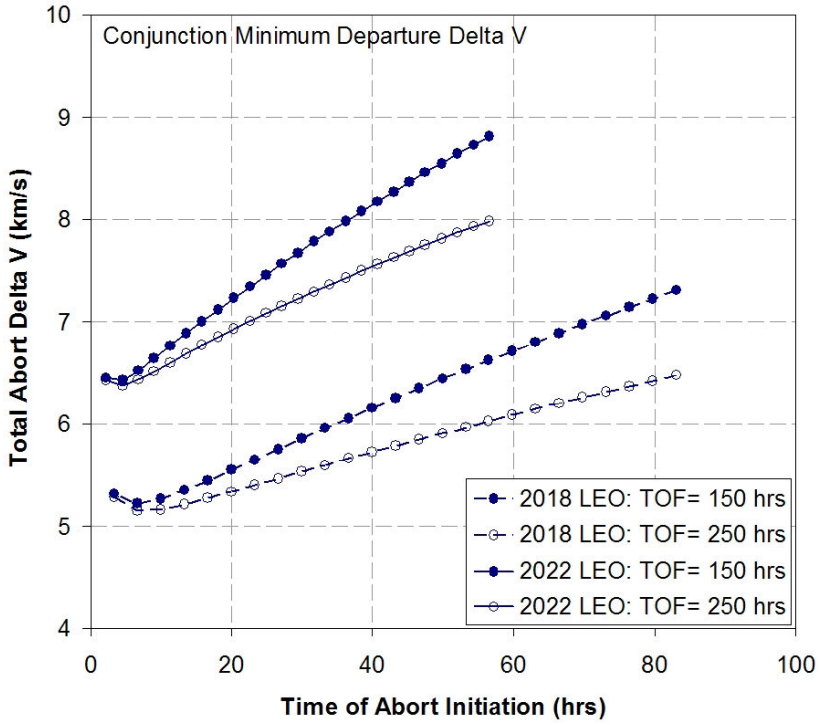

Figure 7.13 Requirements Extrema for Selected LEO Abort Durations: CJI_MD

A slower outbound trajectory reduces the cost of the abort initiation maneuver to embark on a specified abort return trajectory but does not reduce the magnitude of the insertion maneuver at the end of that abort trajectory into Earth orbit. The differences then between this trajectory class and the previous are solely attributable to the difference in outbound velocity profile. The savings provided by the minimum departure trajectory (CJI_MD) over the minimum total mission delta V trajectory class (CJI_MT) are of the same magnitude as for the entry abort cases; approximately 0.4 km/s less delta V. A 1.5 km/s delta V difference is likewise again noted between the extrema. Figure 7.14 presents the delta V extrema for the free-return class interplanetary transfer trajectory which are again higher than the other classes. The extrema of all three classes are compared jointly in Figure 7.15.

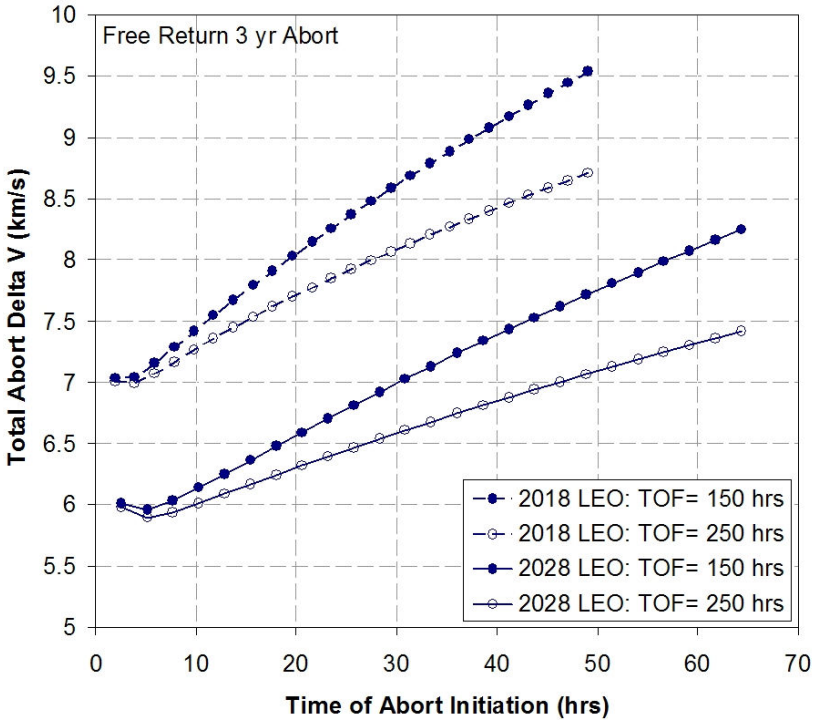

Figure 7.14 Requirements Extrema for Selected LEO Abort Durations: FR_3Y

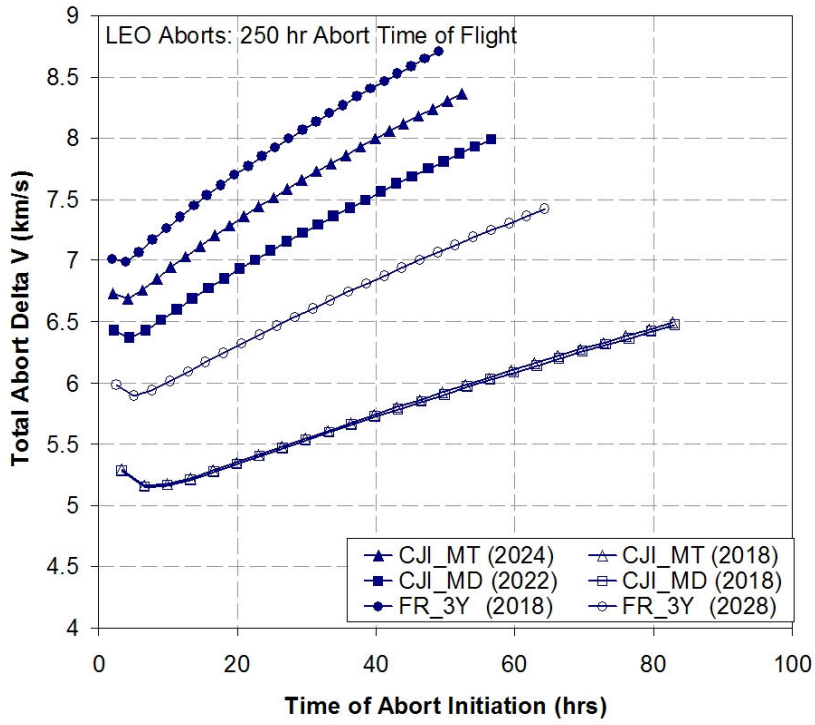

Figure 7.15 Comparison of Requirements Extrema by Trajectory Class

The results illustrate that the maximum delta V requirements for a 250 hour abort from a free-return (FR_3Y) trajectory are again the most extreme of all the considered classes while the conjunction minimum departure trajectory (CJI_MD) has the lowest. For the minimum delta V case years, the free-return entry abort requirements are also higher than the others by about 1 km/s.

The baseline orbit abort that has been developed and investigated to this point has been shown by the solution data to require large amounts of spacecraft delta V capability. These high requirements could render this abort mode infeasible in realistic application, though judgment will be deferred until the mode is applied to potential spacecraft architectures in the investigations that will follow.

7.4. Abort to Specific LEO Orbital Asset

To this point, the methodology and data of this chapter have been for the case of aborting the spacecraft to its own LEO orbit. The resulting orbit was of the same inclination as the original outbound departure trajectory. This section will investigate abort modes where the spacecraft is placed on an Earth return abort that will allow it to rendezvous with a specified Earth orbital asset such as the ISS. An abort to such an asset is in effect an abort to a specific LEO orbit instead of the most convenient one. Utilization of other orbital assets as possible safe havens becomes desirable in the situation of a failing spacecraft that is unable to execute an atmospheric entry. The remainder of this section will assume an abort to the ISS, though the encountered issues and mechanics would be analogous for abort to other orbits as well.

While desirable in certain circumstances, the feasibility of executing an orbital abort to the ISS or any other orbital asset is hampered by several difficulties that are not encountered when the spacecraft was simply aborted to its own LEO orbit. The first difficulty is the difference in orbital inclination between the plane of the departure orbit and that of the desired final LEO orbit; the ISS orbit in this case. The second primary difficulty arises from the orientation of the ISS orbit relative to the departure trajectory. The outbound trajectories of a Mars transfer vary greatly in direction and inclination for each trajectory class, launch date, and year of opportunity. Combined with the precession motion of the ISS orbit itself, the orientation of the ISS orbital plane with respect to the departure trajectory can vary considerably. Figure 7.16 shows several possible ISS orientations, differing by offset values of ISS right ascension ($\boldsymbol{\Omega}$) from the 2018 baseline departure's $\boldsymbol{\Omega}$.

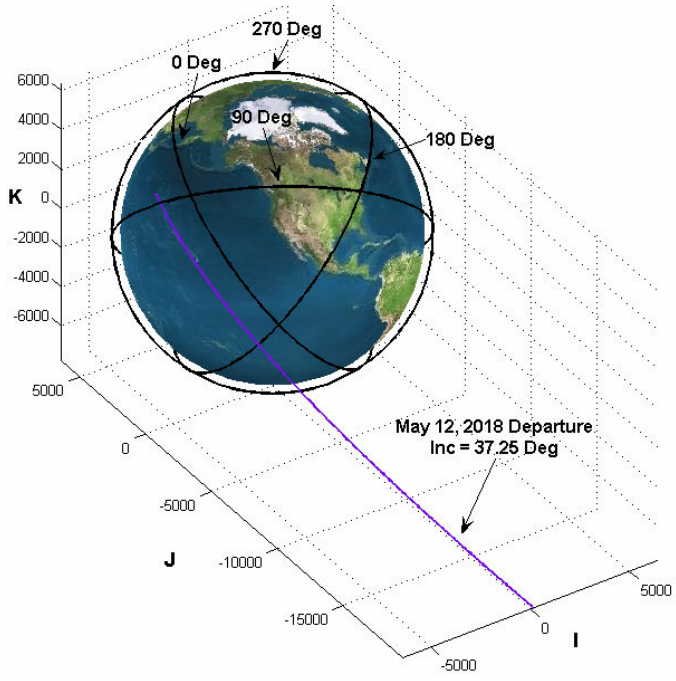

Figure 7.16 ISS Orbital Orientation for Right Ascension Offset

From inspection of Figure 7.16 it appears that many ISS orientations, especially those with orbital planes very nearly perpendicular to the departure direction, could result in abort trajectories with very steep arrival angles to the desired final ISS orbital direction thus drastically increasing delta V.

An analysis of the ISS abort mode was conducted for the 2018 baseline departure case for aborts initiated 20 hrs into the mission. From the specified starting point, abort solutions were run incrementally for possible ISS right ascension (RAAN) offsets from 0 through 360 degrees. For each offset value, aborts were constructed to all possible ISS positions along the offset ISS orbit and for multiple abort times of flight, up to 330 hrs duration. The ISS positions and times of flight with the lowest abort delta V values were kept for each offset increment. The same solution process was utilized a further two times with the gross assumption that the departure orbit inclination was first zero degrees and again assuming it was approximately the same inclination as the ISS. The delta V values for these three cases are plotted in Figure 7.17. The data show that, depending on the offset orientation, the required delta V for executing an ISS abort can be extremely expensive. For the zero degree inclination departure, the delta V requirements are the same for RAAN offsets separated by 180 degrees. Since right ascension is measured in the coordinate fundamental plane, aborts to ISS orbits differing by 180 degrees in right ascension are mirrors of each other geometrically and identical in terms of abort delta V magnitude. For the inclined departures, the minimum and maximum delta V values occur near the 40 and 165 degree offset positions respectively. Diametrically opposite offsets are no longer similar in delta V requirements for inclined departures.

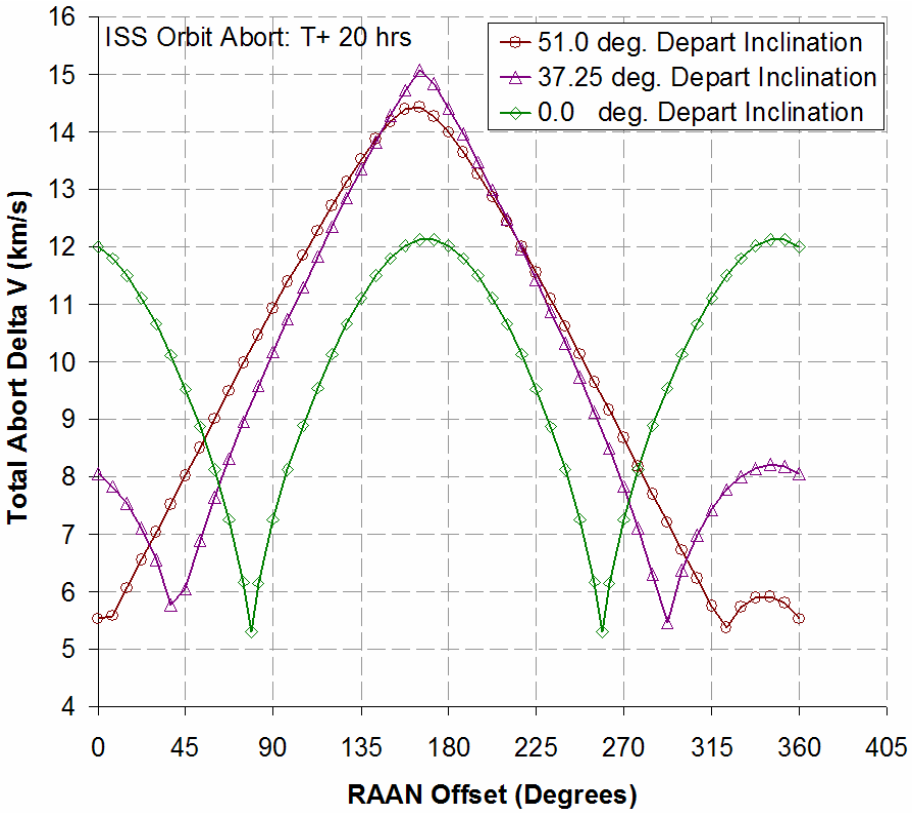

Figure 7.17 ISS Abort Delta V as Function of Inclination and Right Ascension

The high variability in the delta V requirements presents a problem for practical inclusion of the ISS abort mode as presently executed. The odds that the small range of offset conditions with the lowest delta V values will be the actual orientation conditions for any given departure are slim and the chance that optimal orientation would be consistently manifest for all departure opportunities is minute. Even when optimal alignment is achievable, the minimum delta V requirements are around 6 km/s, which is higher than for previous LEO or entry abort modes with 330 hr times of flight from the same abort initiation point.

Significant improvement in the required delta V is achievable if allowance is made for a three-burn rather than a dual burn abort methodology. The additional

maneuver converts the ISS abort from a single-leg trajectory transfer to a double-leg transfer. Inclination change maneuvers are very costly when executed close to the Earth, hence the reason for the large delta V values presented so far. A three-burn maneuver would allow the spacecraft to first intercept the ISS orbital plane at a far distance where the maneuver to match the ISS plane would be minimal. The first trajectory leg extends from the point of abort initiation until the point of intercept plane passage. The second leg of the transfer carries the spacecraft from the point of plane intercept until ISS rendezvous in LEO. The LEO rendezvous maneuver close to Earth now occurs entirely within the ISS plane, greatly reducing the inclination change maneuver required previously. The setup is shown in Figure 7.18 for the worst case RAAN offset of 165 degrees for both single and double leg aborts.

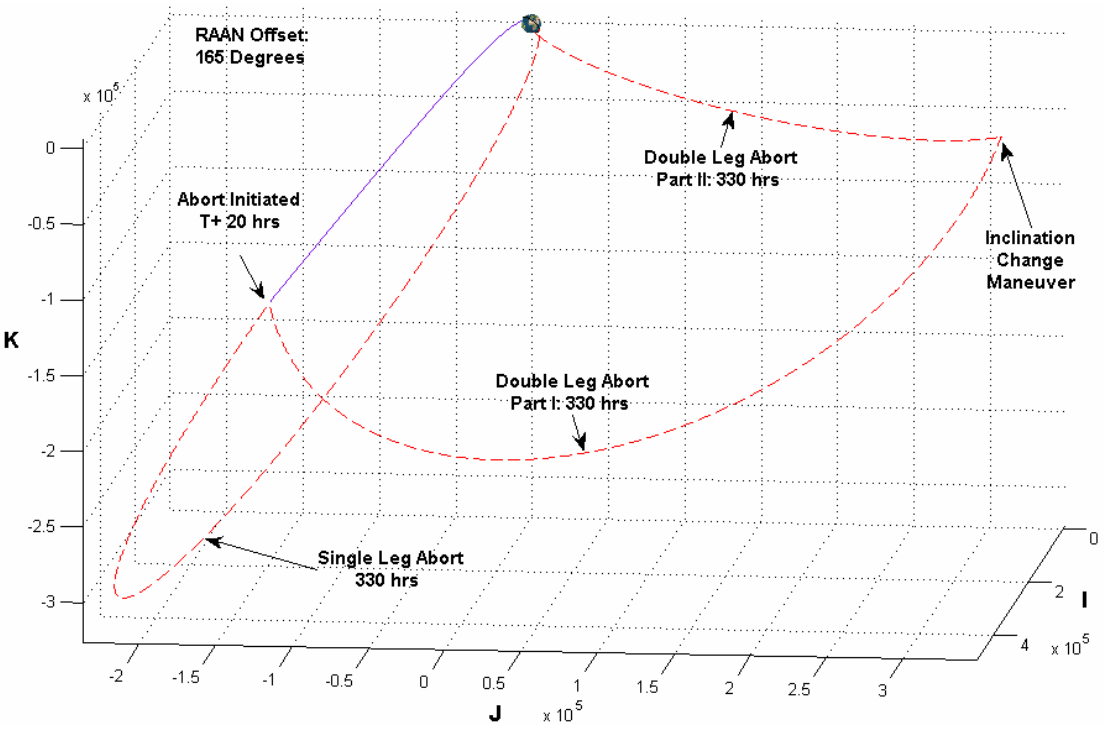

Figure 7.18 Single and Double Leg ISS Abort Trajectories: Worst Orientation

A consequence of targeting the remote point for the plane change with its attendant delta V benefits is an increase in the total time of abort duration; from 330 hrs to 660 hrs for the scenario considered. The delta V reduction that was achieved will be presented in a later figure. The three-burn ISS abort maneuver for the best case RAAN offset of 37.5 degrees is shown in Figure 7.19 for both single and double leg aborts.

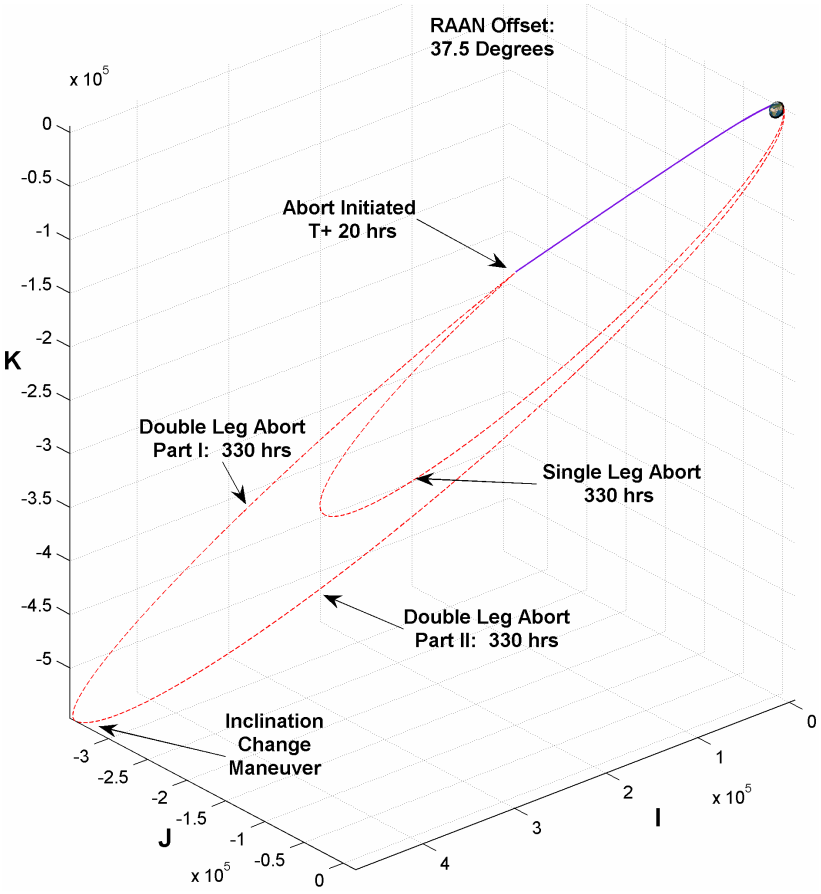

Figure 7.19 Single and Double Leg ISS Abort Trajectories: Best Orientation

The similarity of the single and double leg aborts for this case demonstrates that the planar orientation was already quite favorable. Figure 7.20 presents a zoomed in

detail of the Earth arrivals for both the single and double leg trajectories for the best and worst case RAAN offset arrival cases.

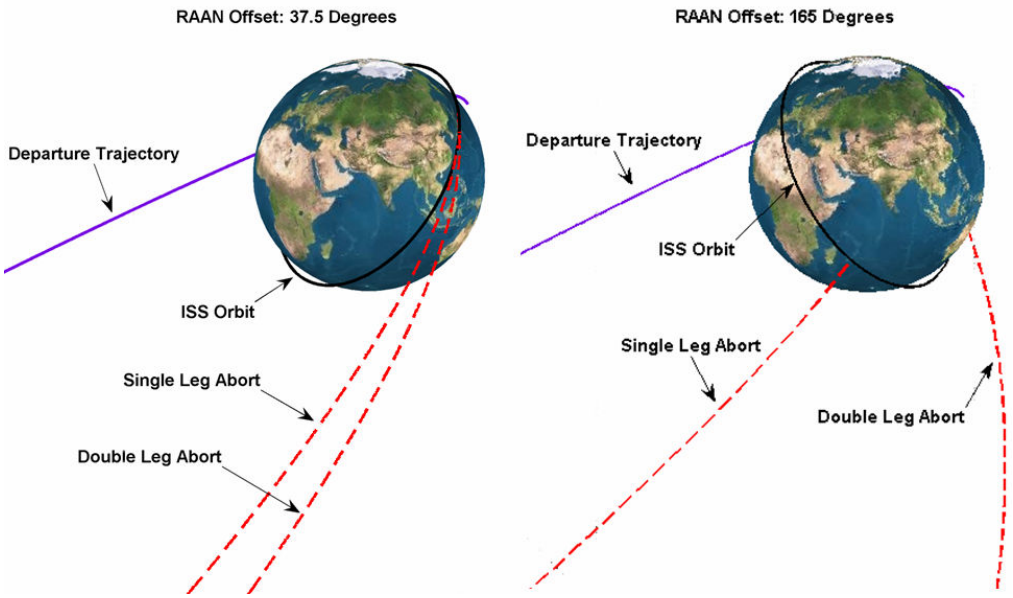

Figure 7.20 Single and Double Leg Abort Trajectories at ISS Arrival

The orbital motion during the second leg of the double leg abort, which is the portion shown in the figure, is always completely contained in the plane of the ISS orbit. The insertion burn into ISS orbit for the double leg aborts is therefore simply a braking maneuver to ISS orbital speed with no further inclination change. From the figure, it is noted that the single leg arrival for the best case offset arrives very nearly aligned with the double leg arrival indicating only a moderate inclination change is required to match ISS motion. Additionally, the angular point of arrival in ISS orbit is nearly identical for both abort arrivals with the best offset alignment. A very different situation exists for the worst case RAAN offset. The single leg abort has a much steeper arrival than the double leg abort. This situation illustrates why such high delta V values were obtained for many of the single leg aborts and highlights the

drastic reduction made possible by the double leg abort methodology. Figure 7.21 compares the differences in delta V requirements for ISS aborts from the baseline departure orbit (37.25 degree inclination) for both single and double leg ISS abort setups.

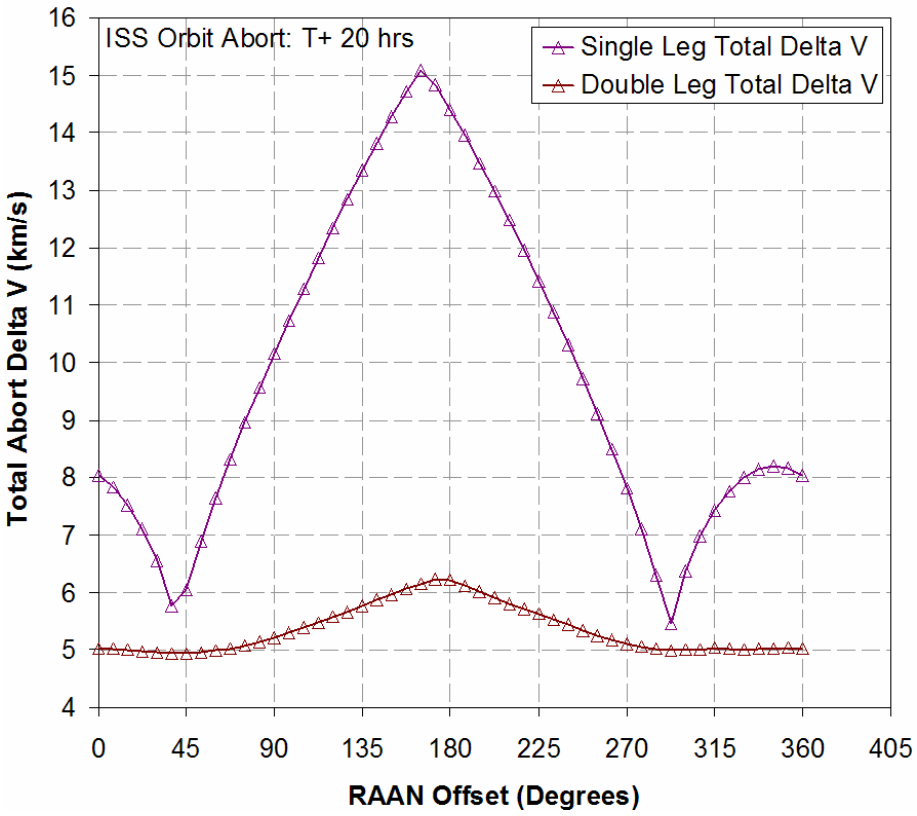

Figure 7.21 Single and Double Leg Abort Delta V for Right Ascension Offset

The figure makes evident the clear necessity of utilizing the double leg setup if an ISS abort mode is desired. For the worst case alignments, the double leg, three burn setup saves up to 9 km/s of delta V versus the single leg case. This savings is almost entirely due to the reduction in inclination maneuvering and not the doubling of the abort time of flight. In fact, doubling the allowable abort time of flight for the single leg aborts only results in a delta V savings of from one to two percent. For the two

single leg abort cases with optimal offsets, the extra benefit of matching the orbital plane at distance still reduces the required delta V by 1 km/s.

Based on the analysis of the ISS abort mode for the baseline 2018 departure trajectory and 20 hr abort initiation point, a broader investigation of ISS abort requirements for multiple trajectory classes and years of opportunity was not undertaken. Even with the addition of an extra maneuver and a doubling of the allowable abort time of flight, the ISS abort mode is more expensive than the straightforward orbital abort mode described at the first of this chapter and would only be preferred over an Earth entry or simple orbit abort mode in a very limited number of circumstances; i.e. having both a failing spacecraft and a broken heat shield. Nevertheless, the ISS abort study gives an insightful look into the non-obvious difficulties that arise in navigating between various orbits in the Earth neighborhood.

Chapter 8. Moon Aborts

The aborts investigated in the previous two chapters have all been Earth-return abort modes. If current exploration plans go forward, the next decades could see the establishment of habitation and other logistical emplacements on the Moon. The presence of such infrastructure could make the Moon's surface a viable safe haven destination for an aborted Mars spacecraft. This chapter presents the methodology for constructing moon aborts during the departure phase of an interplanetary Mars transfer trajectory. The propulsive requirements for performing these aborts are compared to those required for the Earth entry and orbit aborts previously developed. Additionally, an analysis of propulsive requirement variation with lunar position helps establish new launch dates and departure windows needed to enable the moon abort mode as a possible spacecraft abort option.

8.1. Lunar Abort Considerations

8.1.1. Lunar Safe Haven

The attractiveness of lunar orbit or lunar surface locations as abort safe havens is largely dependent on the extent of emplaced lunar logistical architecture. Supposing large-scale lunar habitation architectures with routine trans-Earth transportation elements are in place, then lunar aborts become more suitable provided that the propulsive requirements and flight times for executing such aborts are also advantageous versus an Earth-return abort. In the absence of such development, the

Moon cannot be considered a safe haven for the crew and Earth return aborts would remain the only acceptable contingency plans. In the case lunar aborts are executed, the crew must be transported from the Moon back to Earth by some other transportation system. Given the long abort times of flight seen in the implementation of the previous Earth-return abort modes, a lunar abort may be appealing if a shorter duration abort could be achieved for the same or less propellant cost. Such an attribute would be especially desirable in the case of a failing spacecraft that may be unable to sustain life support operations for the two week abort periods experienced by the Earth-return aborts.

8.1.2. Moon Orbital Motion

The inclusion of the Moon as part of an abort scenario modifies the problem setup through the inclusion of an additional gravitational body. The motion of the moon causes a more involved rendezvous setup than experienced with the Earth aborts. From a given abort initiation point, the moon position at abort arrival will be different for each investigated abort time of flight. Lunar orbital motion is affected by many perturbing influences arising from interactions with the Earth. The Moon's orbital speed with respect to the Earth is only 1 km/s. The combination of the long revolution period of the Moon with the fast heliocentric orbital velocity of the Earth results in a lunar orbital path that, when viewed in sun-centered **XYZ** heliocentric coordinates, never loops back upon itself. This situation, as shown in Figure 8.1, is a rare occurrence compared with other Solar System moons. The Moon's orbital plane is inclined approximately 5.1 degrees from the ecliptic and is not aligned with the Earth's equator. Indeed, the lunar inclination with respect to the Earth's equatorial

plane varies from between 18.3 and 28.6 degrees. Combining the inclination possibilities with the changes in Earth-Moon distance arising from the Moon's eccentricity creates a large variation of possible lunar positions. The geocentric lunar positions are plotted in Figure 8.2 for the duration of approximately five years.

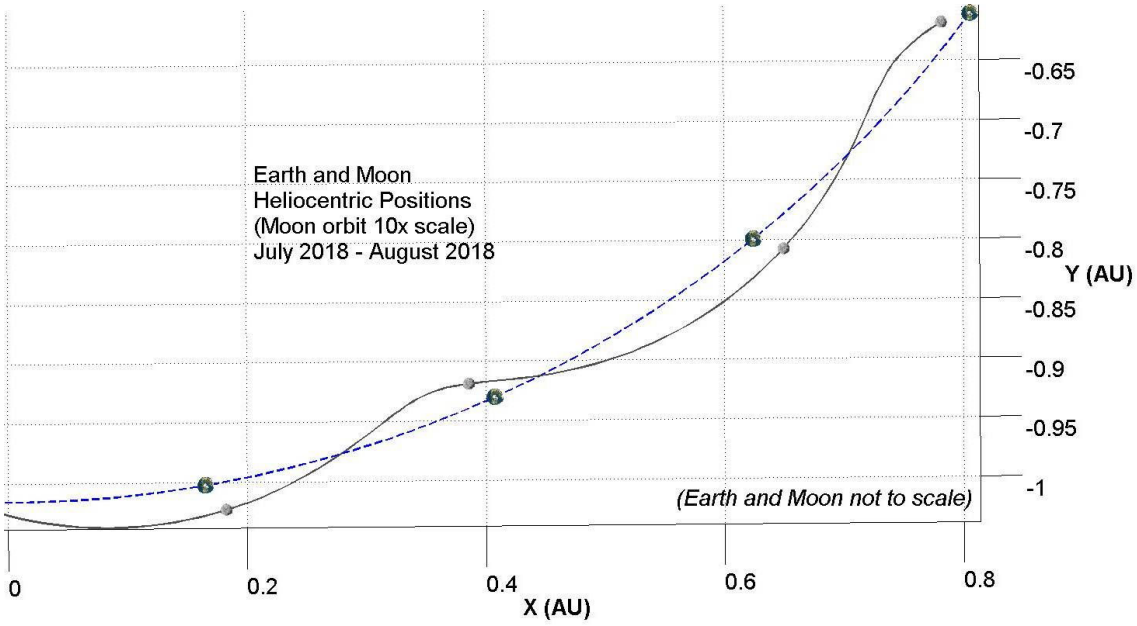

Figure 8.1 Lunar Orbital Motion (Heliocentric Position)

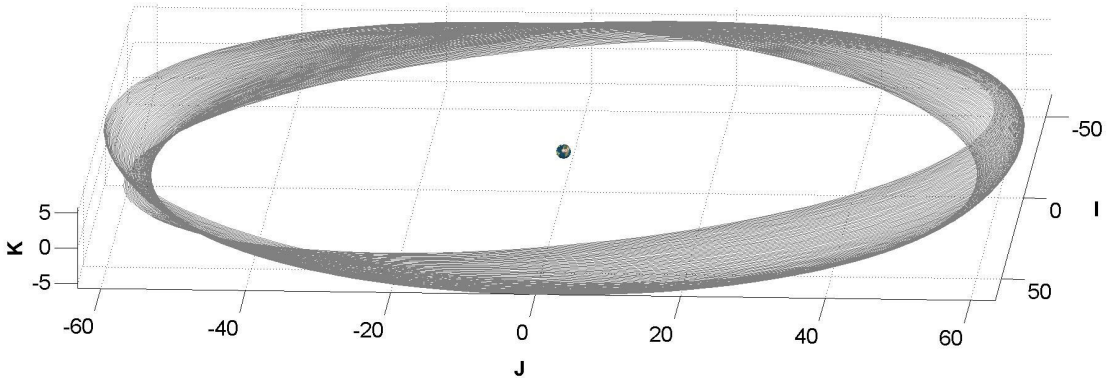

Figure 8.2 Lunar Orbital Motion (Geocentric Position)

The **IJK** positions seen in Figure 8.2 were generated using a lunar ephemeris as a function of Julian date. An analysis of the figure confirms the occasional possibility that an outbound Mars departure trajectory could experience a close pass of the Moon. Given the Moon's month-long orbit, a several day acceleration or postponement of the departure could open up a great number more potential lunar encounters. These permutation possibilities arising due to the intricacies of the Moon's orbital characteristics will be accounted for in the following sections.

8.2. Abort Trajectories to Lunar Orbit

Moon aborts are fundamentally different than the Earth-return aborts previously investigated in that the spacecraft will be progressing under the gravitational influence of both the Earth and the Moon to varying extents. The Earth is 81 times the mass of the Moon and will therefore dominate the majority of the abort trajectory. However, the final lunar arrival portions of the transfer will continue primarily under lunar influence. The patched conic approximation once again finds use in the solution of this orbital setup, though it is the Moon's gravitational sphere of influence which will be applied. Determining the abort requirements will necessitate evaluation of the abort trajectory not just during the geocentric transfer but also during the selenocentric arrival at the Moon.

8.2.1. Determination of Moon Aborts

The point of abort initiation is selected and incremented in the same manner as for the other abort modes with an initial abort propulsive maneuver which

terminates the escape trajectory and starts the spacecraft along an abort orbit. Using the time of abort initiation and selected abort trajectory time of flight, the lunar ephemerides are obtained for the date of lunar arrival and transformed into the lunar position and velocity vectors $\boldsymbol{r_{Moon,f}}$ and $\boldsymbol{v_{Moon,f}}$. A Lambert trajectory solution is then patched between the spacecraft position at abort initiation, $\boldsymbol{r_S}$, and the final lunar position which yields the initial and final abort velocity vectors $\boldsymbol{v_{Ab,i}}$ and $\boldsymbol{v_{Ab,f}}$. The abort initiation delta V is then the same as given in Chapter 6.

$$\Delta\vec{v}_{Ab,i} = \vec{v}_{Ab,i} - \vec{v}_S \tag{6.14}$$

Figure 8.3 shows the lunar abort profile for the geocentric portion of the abort up to lunar intercept. The difference between the final abort velocity vector and the lunar velocity vector will define the infinity velocity vector that enters into the lunar SOI.

$$\vec{v}_{S,\infty} = \vec{v}_{Moon,f} - \vec{v}_{Ab,f} \tag{8.1}$$

By transforming the infinity velocity into the Moon SOI and selecting an orbital distance for a low-lunar orbit (LLO) it is a straightforward process to obtain the perilune velocity of the arrival hyperbola. Assuming a circular lunar orbit, the orbital insertion delta V is then simply the vector magnitude subtraction of the perilune velocity and the circular orbit velocity at the specified LLO radius. The total abort delta V for executing the lunar abort mode is then simply the summation of the abort initiation and Moon orbit insertion propulsive maneuvers. The profile of the selenocentric portion of the abort trajectory is shown in Figure 8.4.

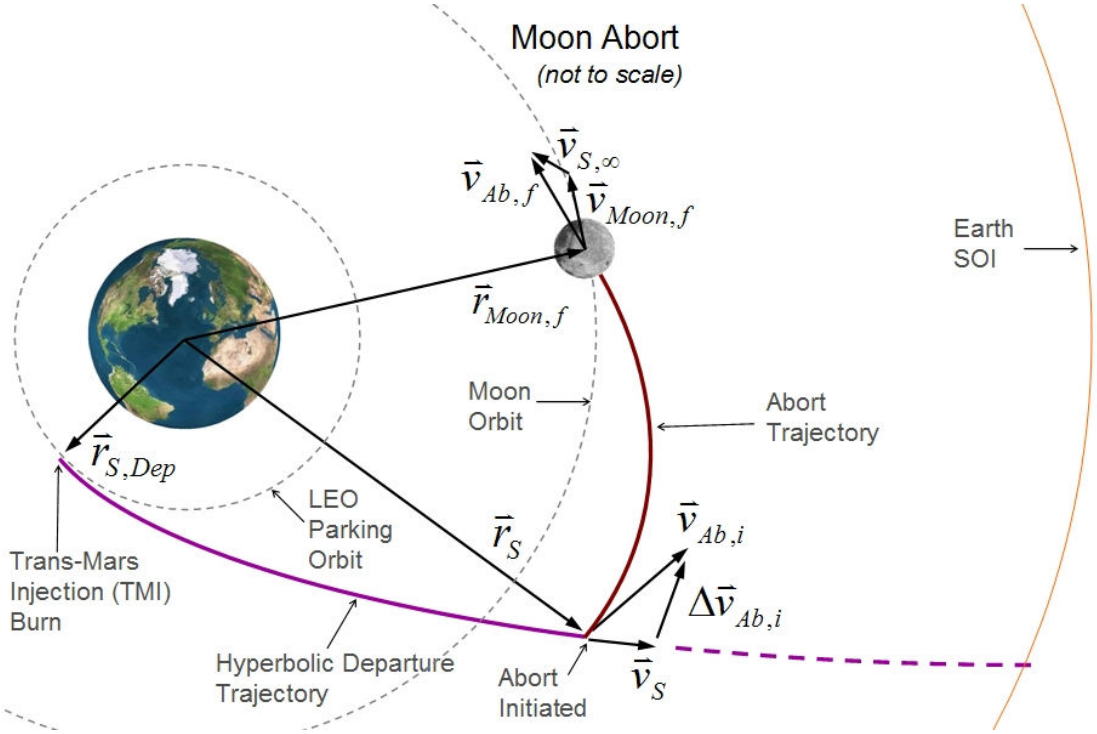

Figure 8.3 Moon Orbit Abort Intercept Profile

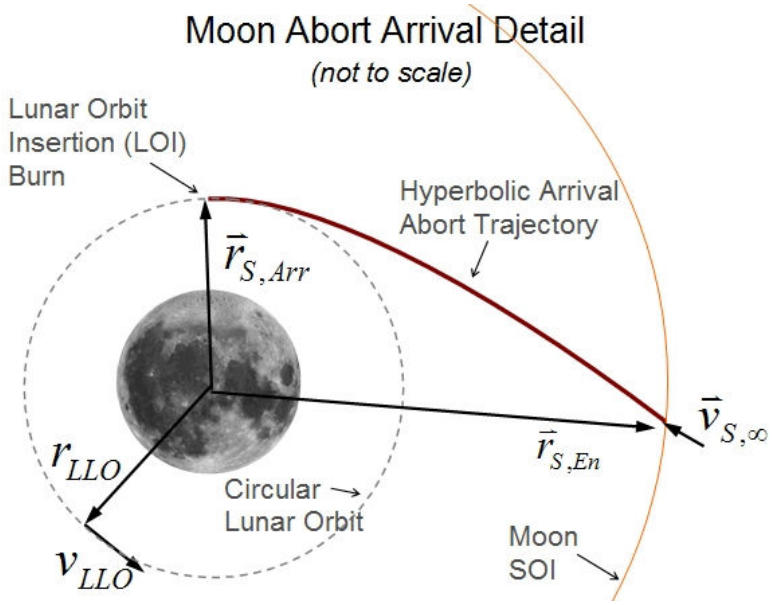

Figure 8.4 Moon Orbit Abort Arrival Profile

A small inaccuracy in lunar position has been introduced by this formulation because the trajectory interface at the lunar SOI was not iterated to be perfectly continuous as was done with the geocentric and heliocentric trajectory patching of Chapter 4. Given the small diameter of the lunar SOI and the resulting short duration selenocentric approach hyperbola, the approximation was judged to be acceptable, especially in light of the large numbers of analyzed lunar abort scenarios. It should be further noted that the limitations of the patched conic approximation become more pronounced when applied to the Earth-Moon system given the proximity and mass of the Moon.

A limit was placed on the allowable transfer angle for the Lambert solution between the abort initiation and lunar arrival positions. Only short trajectory (transfer angles less than 180 degrees) solutions were obtained. For the restricted abort times of flight limits of the investigation, it was generally preferable in terms of delta V requirements to prevent the long trajectory possibilities. A consequence of the short trajectory constraint is that abort trajectories are possible that encounter the Moon head-on. This head-to-head intersection is greatly moderated by the small orbital speed of the Moon.

The above described methodology results in the placement of the spacecraft in a low-lunar circular orbit. No attempt was made to target orbits of specific inclination or with particular surface access. No selection of lunar surface sites has yet been established. Achieving particular lunar orbits is essentially a function of lunar SOI entrance location and will not significantly alter the delta V requirements gleaned from the investigation as constituted.

8.3. Analysis of Lunar Orbit Results

The determination of the propulsive requirements for the lunar orbit abort mode followed the same process used for the previous Earth-return abort modes. The utilized baseline trajectory was once again the May 12, 2018 conjunction Type I minimum energy trajectory (CJI_MT). Lunar abort solutions were found for times of flight up to 330 hrs duration for each time of abort initiation along the outbound departure trajectory. During the investigation of the Earth-return abort modes, abort times of flight that were of shorter duration than the elapsed mission time were not considered. This constraint was placed to avoid return trajectories that arrived at Earth much faster than the departure trajectory had originally left. Since the Moon could conceivably lie close to the outbound path and not be encountered until many hours into the mission, such an abort time of flight restriction might prevent the discovery of advantageous abort scenarios and was therefore dropped from the lunar abort mode investigation. However, the allowance of very short time of flight abort trajectories will lead to high delta V results when the moon location at spacecraft arrival is not closely positioned to the outbound trajectory. The total propellant delta V requirements for executing the Moon abort mode on the baseline departure date are presented in Figure 8.5. The delta V requirements for the Moon abort mode are, for this case and alignment, slightly more expensive in terms of delta V than the entry abort mode but much more feasible than the orbit abort mode. The moon position for this opportunity at the point of abort initiation is approximately 90 degrees offset from the departure direction. Given this distant placement, it is no surprise that the

shortest abort flight durations have resulted in excessive propulsive cost. The general trends seen in the entry and orbit abort modes still appear for the lunar abort mode, namely decreasing delta V for longer duration aborts and increased delta V for later times of abort initiation with the same abort flight time. A unique trend seen for the lunar abort mode is the comparative reductions in delta V for aborts with times of abort initiation of approximately 20 hrs. For the baseline departure case, this corresponds to the approximate point in time when the departure trajectory has reached the same distance from the Earth as the Moon. Figure 8.6 shows the ratio of initial abort delta V and final lunar orbit insertion delta V. The abort initiation delta V requirements are represented in Figure 8.7 and the final abort delta V amounts are contained in Figure 8.8. Analyzing these trends it appears that the T+ 20 hr savings are a result of a delta V decrease in the abort initiation delta V. A likely basis for this trend is a reduction in the amount of velocity vector turning required to quit the exit hyperbola and turn onto the Moon abort trajectory when at or near the lunar orbital distance. The final delta V amounts of Figure 8.8 are divided into two regions where the upper region manifests approximately 1 km/s higher delta V than the lower region. This is an interesting trend since longer flight times usually result in lower delta V values. In the case of the moon abort for this departure opportunity, the upper region corresponds to abort trajectories with moon arrivals whose arrival velocity directions are to some extent in the opposite direction of the lunar orbital motion. These are the “head-on” arrivals described previously.

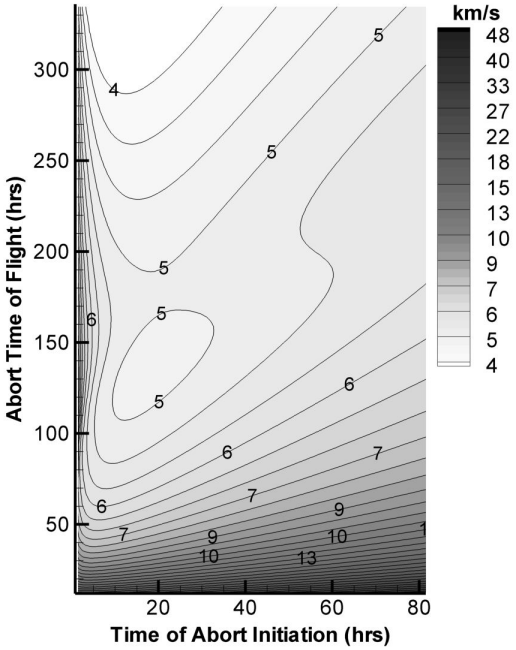

Figure 8.5 Moon Abort Total Delta V

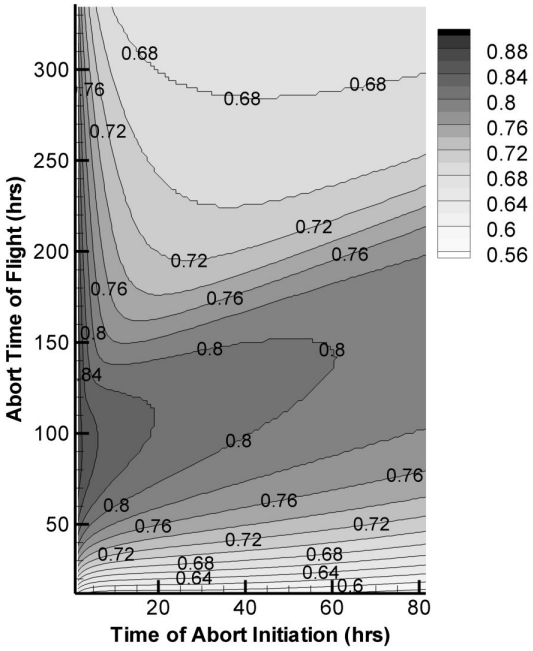

Figure 8.6 Moon Abort Delta V Ratio

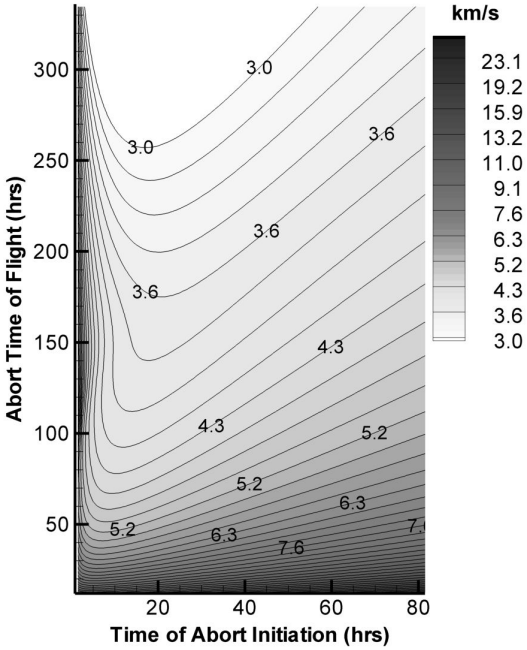

Figure 8.7 Moon Abort Delta V Initial

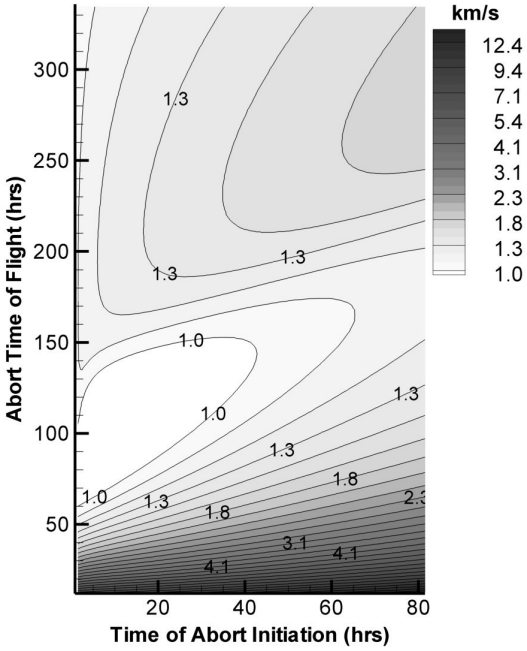

Figure 8.8 Moon Abort Delta V Final

The various abort trajectories for this opportunity for lunar aborts initiated 20 hrs into the mission are plotted in Figure 8.9. The figure clearly shows the variation in abort arrival position required for Moon rendezvous at diverse abort times of flight. The shorter abort times of flight for this case will not be practical; the 30 hr duration abort transfer requires ~10 km/s for example. For aborts initiated at T+ 20 hrs into the mission, the resulting abort trajectories become hyperbolic for abort flight times below ~100 hrs duration.

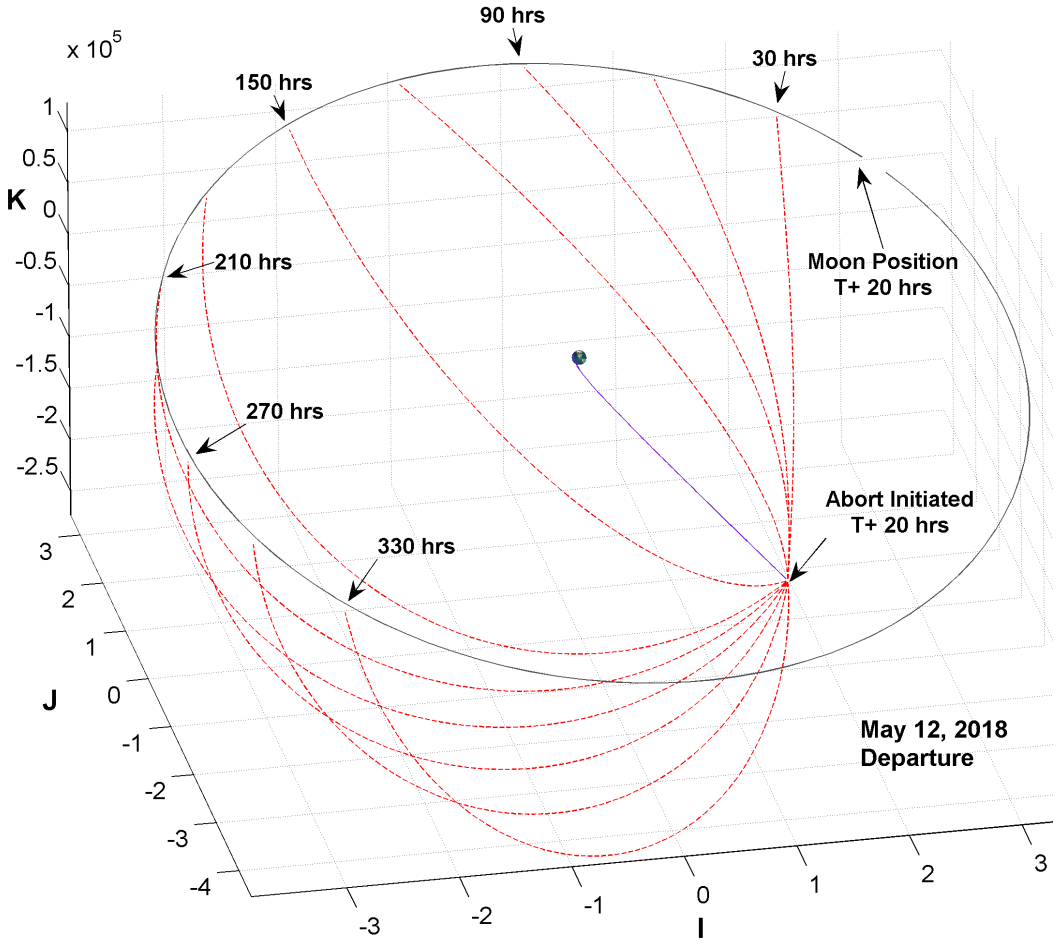

Figure 8.9 Moon Abort Trajectories by Times of Flight at T+ 20 hrs, 5/12/2018

The specific orbital energies of the lunar aborts are given by Figure 8.10. Positive energy values correspond to hyperbolic trajectories while negative values are elliptical orbits. Energies higher than 3 km^2/s^2 were not plotted in this representation. The energy data confirms that many of the shorter abort flights are hyperbolic for this departure case. Later abort initiations increase this trend. For example, aborts initiated at T+ 60 hrs will be hyperbolic transfers for all abort times of flight below ~250 hrs. Figure 8.11 presents the abort trajectory transfer angles. Allowing only short trajectory Lambert solutions results in transfer angles less than 180 degrees. The bottom region of the figure shows abort trajectories whose transfer angles approach the 180 degree limit as the abort time of flight is increased. The transfers in this region are those which are approaching the moon from the rear as confirmed by Figure 8.9. After reaching the angular limit the transfer angles then decrease for the top region of Figure 8.11 for the trajectories which have more frontal lunar approaches. Figure 8.12 shows the infinity velocities with which the spacecraft enters the lunar sphere of influence. For a specified circular LLO, the insertion delta V is a function of the infinity velocity; hence the trend similarity between Figure 8.12 and Figure 8.8. The boundary between the arrival regions of these figures matches up with the occurrence of the near 180 degree angular transfers of Figure 8.11. Figure 8.13 presents the actual arrival velocity at the lunar SOI as delivered by the transfer orbit. The variation in actual geocentric velocity shows the expected decreasing trend with increased time of flight abort orbits and also correlates exactly with the specific orbital energies of the transfer orbits seen in Figure 8.10.

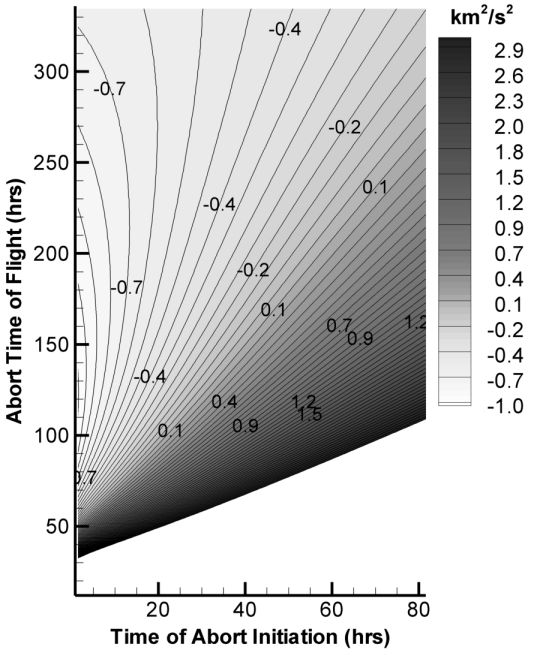

Figure 8.10 Moon Abort Specific Energy

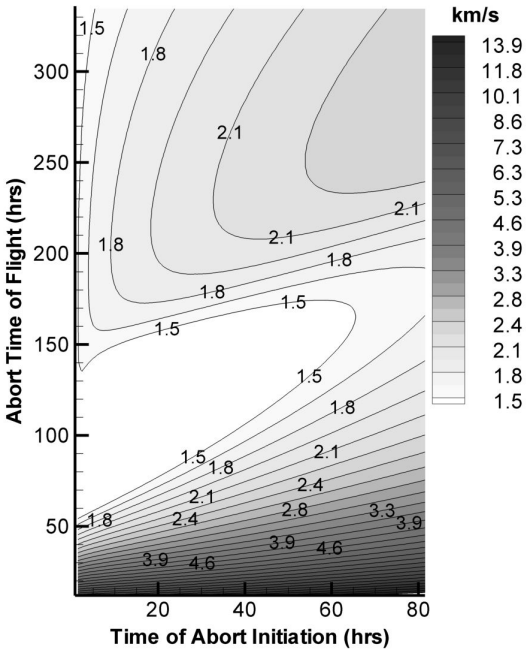

Figure 8.12 Moon Abort Infinity Velocity

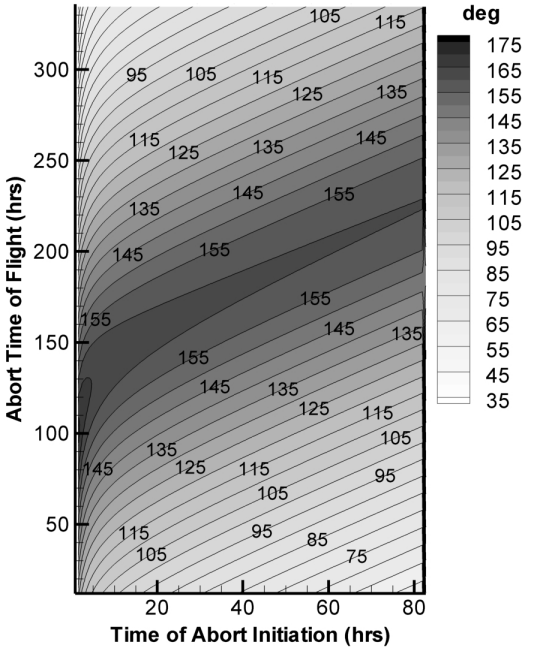

Figure 8.11 Moon Abort Transfer Angle

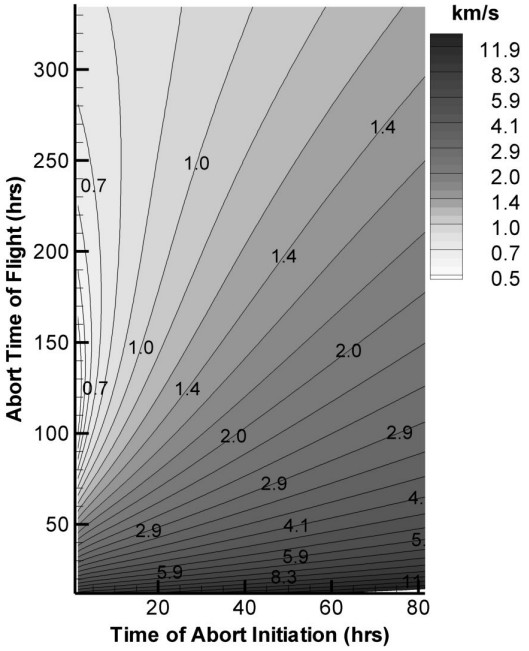

Figure 8.13 Moon Abort Arrival Velocity

Figure 8.14 provides a view of the resulting abort trajectories for an abort initiated near the end of the departure phase at T+ 60 hrs. The figure confirms the presence of the hyperbolic transfers that were indicated by the orbital energy data.

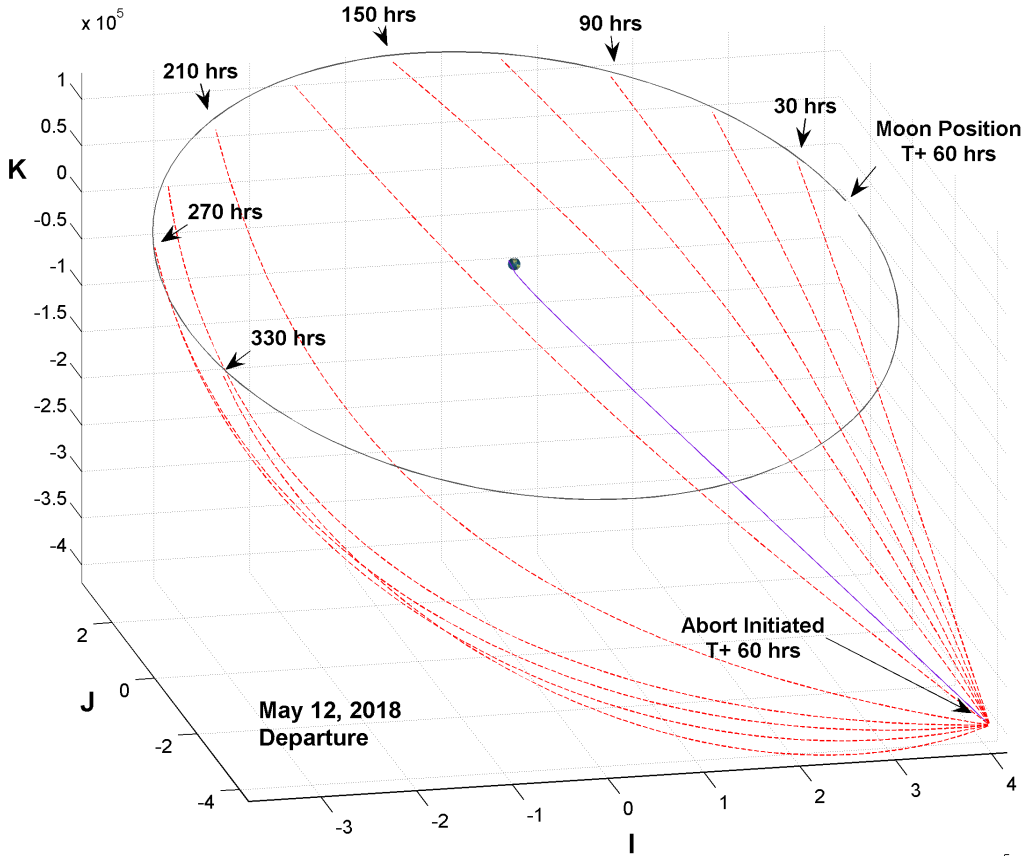

Figure 8.14 Moon Abort Trajectories by Times of Flight at T+ 60 hrs, 5/12/2018

8.3.1. Lunar Abort Variation with Lunar Year

The departure date of the baseline case was the optimum date for a conjunction Mars transfer in terms of delta V expenditure. However, as shown in Figure 8.9 and Figure 8.14, the position of the Moon on this particular date does not favor short abort times of flight. By inspection of these figures, it appears that

possible gains in the propulsive requirements of the lunar abort mode could be made if the departure occurred on a date roughly one week earlier than the date of the present baseline case. Figure 8.15 shows the resulting abort trajectories for the same 2018 abort initiation case as Figure 8.9 but for an earlier May 5th departure instead of the May 12th baseline departure date.

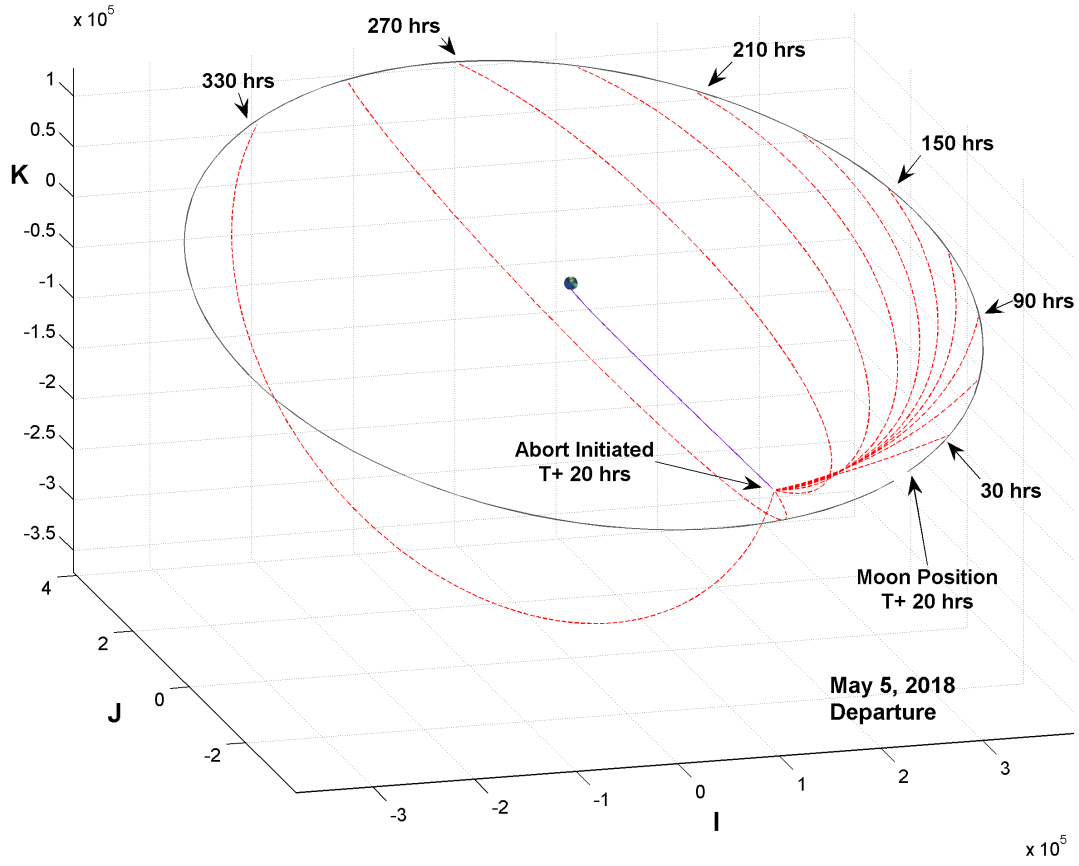

Figure 8.15 Moon Abort Trajectories by Times of Flight at T+ 20 hrs, 5/5/2018

As shown in the figure, the shorter duration abort flights now also traverse a much shorter distance for the investigated suite of abort flight times thus decreasing the amount of propulsive delta V for the shorter transfers of the moved up departure date. As an example, the 30 hr abort case delta V experienced a dramatic drop from ~8

km/s for the baseline departure date to ~4 km/s for the accelerated date; a delta V savings even when compared to the equivalent entry abort case. The data confirm that substantial variation in the lunar abort propulsive requirements occurs as a function of Moon position relative to the outbound departure trajectory. Identification of the most advantageous Moon position for enabling the Moon abort mode required running the abort cases for multiple Moon positions. Different Moon positions are achieved by analyzing different departure dates. Given that the baseline departure was the optimum Mars transfer for the year of opportunity, it is desirable that the modified departure dates remain as close as possible to the baseline date. The lunar sidereal period is 27.3 days. Modified departure dates were therefore investigated for transfers two weeks prior and two weeks following the baseline departure date to achieve analysis of a full lunar orbit. The schematic of Figure 8.16 identifies four of the position cases that were examined as part of this analysis. The corresponding delta V requirements for these cases are presented in Figure 8.17.

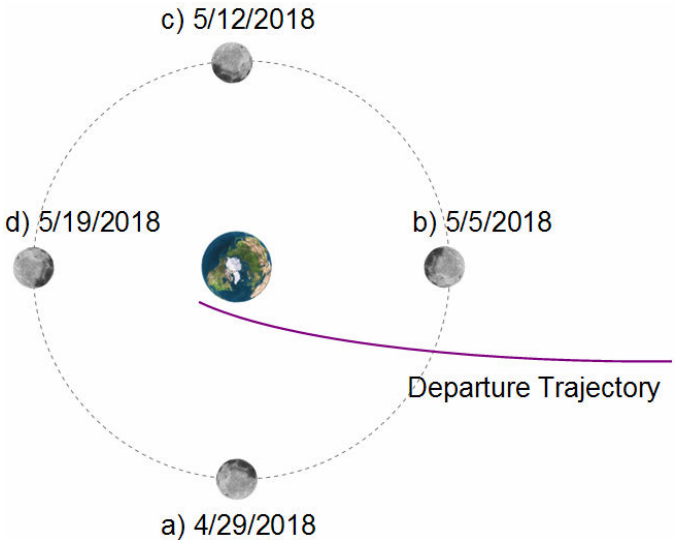

Figure 8.16 Variation in Moon Position Relative to Departure Trajectory

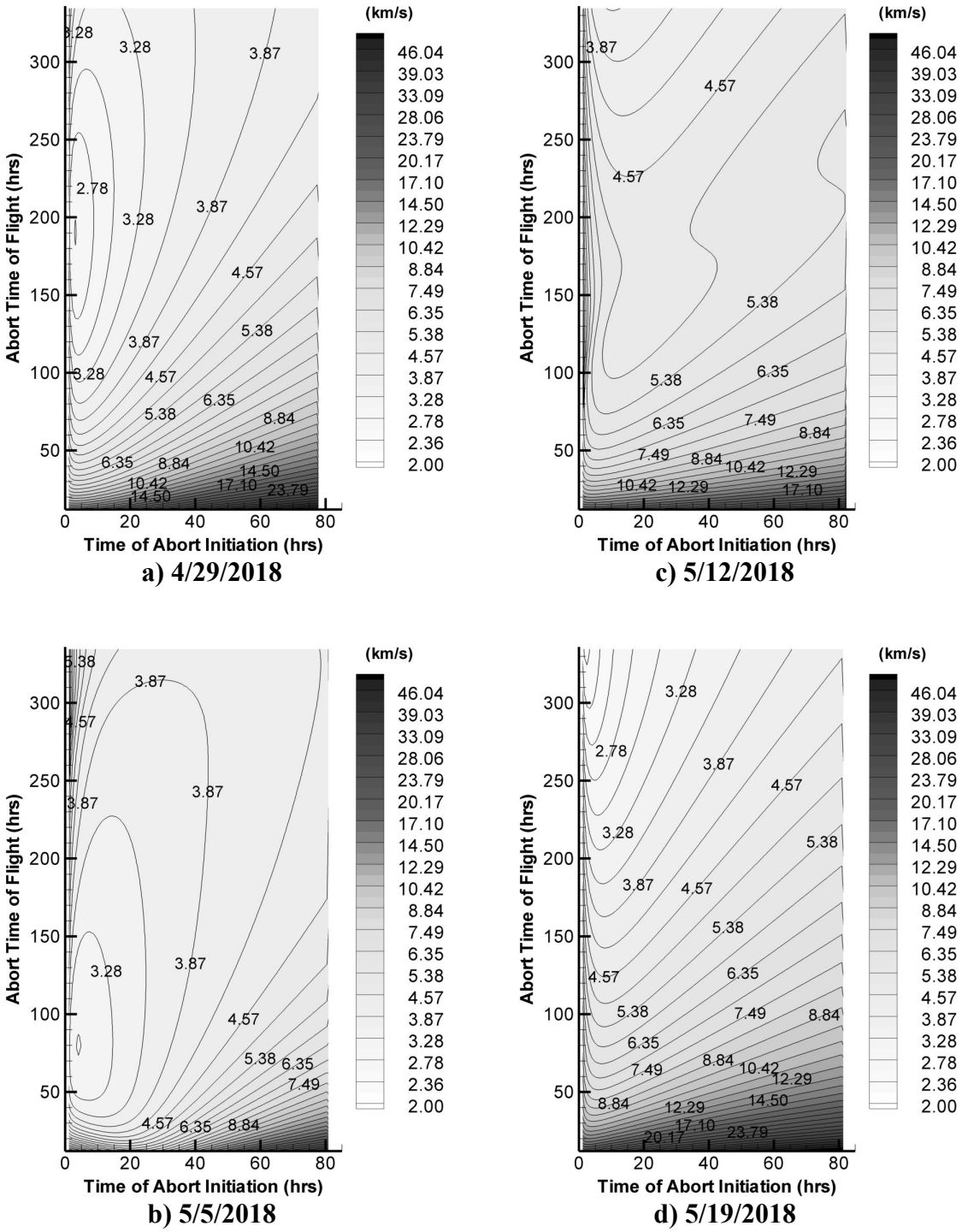

Figure 8.17 Moon Abort Delta V Variation with Moon Position

As seen from Figure 8.17, the regions of minimum lunar abort delta V all occur somewhere during the first 30 hours of the mission. However, the abort flight duration with the lowest delta V varies considerably; occurring at shorter abort flight durations for Moon positions which are aligned closely with the departure direction. A ~4 km/s delta V capability enables continuous access to the Moon abort mode at each point along the departure trajectory for any of the considered Moon positions. The resulting duration of the enabled abort will; however, fluctuate greatly with the different Moon positions.

While the prospect of obtaining very short duration lunar aborts (30-60 hrs) for the same propellant cost as a longer duration Earth return abort is attractive, the possibility only occurs for a very limited portion of the departure. For later times of abort initiation, such short flight times become infeasible regardless of lunar relative position. A more realistic assessment of the merits of a given positional arrangement is achieved by comparing the delta V requirements for an abort flight time that could be more realistically expected over a larger range of the possible initiation locations. As was done in the previous chapters, the delta V requirements for the Moon abort mode were extracted for abort times of flight of 150 hrs and 250 hrs. The requirements trends of the Moon abort mode for each of the four analyzed Moon positions of Figure 8.16 are presented in Figure 8.18 and Figure 8.19 for the 150 hr and 250 hr abort cases respectively. The data for the baseline position scenario is represented with filled in symbols in both figures.

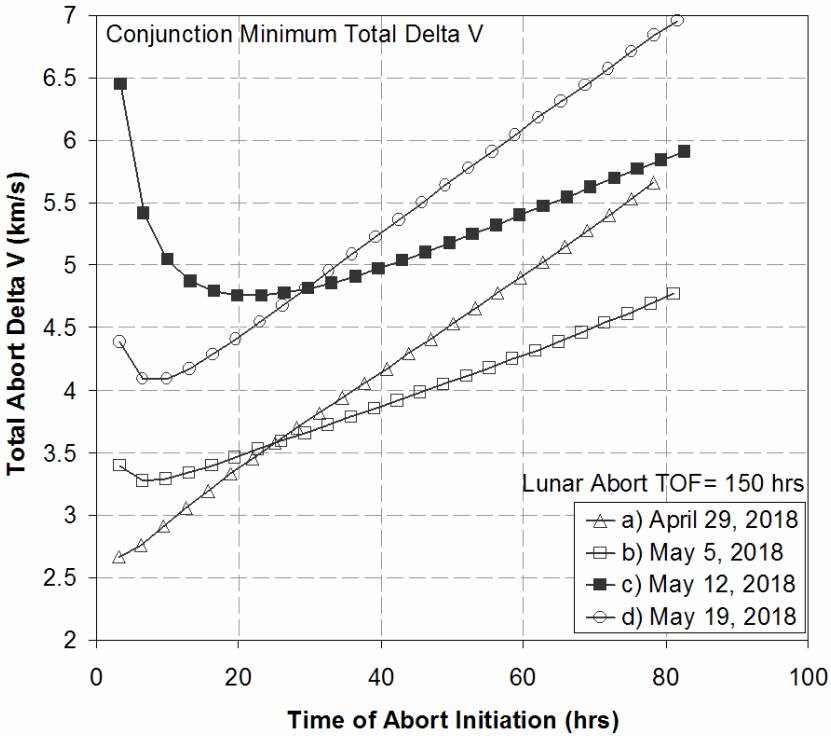

Figure 8.18 150 hr Moon Abort Delta V Variation with Moon Position

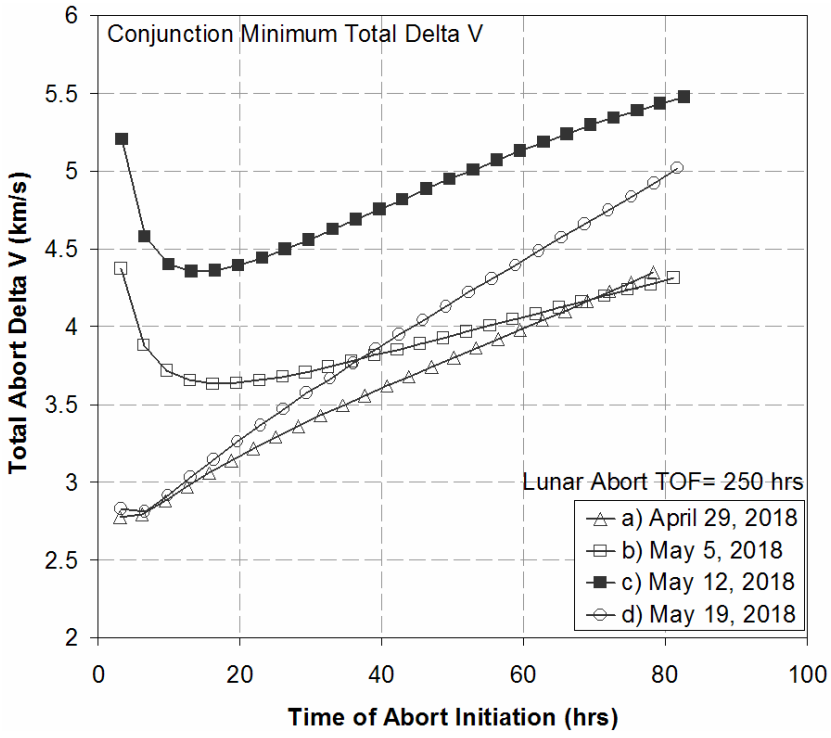

Figure 8.19 250 hr Moon Abort Delta V Variation with Moon Position

Considering the 150 hr abort case of Figure 8.18 it is observed that the baseline departure on May 12th, position c), is the least attainable of the four considered departure dates for early term abort initiations. Position d), which corresponds to the later May 19th departure date, becomes the most expensive in delta V for later abort initiations. The best overall position of the four departure possibilities is position b) which corresponds to the earlier departure of May 5th. Comparing all four trends illustrates the great variety in Moon abort requirements as a function of lunar alignment with total variations approaching 4 km/s for some abort scenarios. The 250 hr abort case of Figure 8.19 also shows improved capability for the non-baseline lunar positions. For this longer abort flight time, position a) provides the lowest overall delta V requirements. However, position b) once again becomes competitive for the second half of the departure phase. Considered together, the data indicates a preference for Moon positions that are roughly aligned with or are moving into alignment with the direction of the outbound transfer.

8.3.2. Comparison of Entry, LEO, and Moon Abort Modes

Before a requirements comparison of the Moon abort mode with the entry and LEO abort modes can proceed, the effects of the accelerated or delayed launch dates must be taken into account. The alteration of the launch date compared to the baseline case modifies the attributes of the entire interplanetary Mars transfer. The specific requirements of the entry and LEO abort modes will therefore be altered to some degree. Given that the lunar alignment modulates at a much faster rate than the Earth-Mars alignment, it is conceivable that the resulting requirements changes to the interplanetary transfer that result from a slightly different departure date could be

acceptable if substantial improvement in the lunar abort mode could be obtained in consequence. The entire astrodynamic setup of this problem is integrated and the actual influence on the transfer trajectory can only be discovered by re-working the entire mission trajectory and transfer phases. The investigation proceeded to obtain the requirements of the entry and LEO abort modes on the modified launch dates. The entry and LEO abort data for the original baseline departure date remain unchanged. Figure 8.20 combines the baseline entry and LEO abort data of the previous chapters with the baseline Moon abort delta V amounts. Data are presented for both of the investigated abort flight times. The figure once again highlights the drastic increase in abort requirements of the LEO abort mode versus the entry abort mode. The Moon abort makes gains compared to the required LEO delta V amounts but is more expensive than the entry abort mode requirements. It must be remembered that the baseline departure date in any year of opportunity was selected based on minimization of transfer requirements. The Moon position on that date is wholly arbitrary and, depending on the year, may be favorably or unfavorably aligned for abort utilization. The baseline year for the investigated trajectory class happens to exhibit a poor Moon alignment for facilitating feasible aborts. Figure 8.21 presents the reworked requirements for the three abort modes for the moved up departure date of May 5th, 2018. The Moon abort mode requirements have now dropped closer to those for the entry abort mode averaging approximately an additional 1 km/s of delta V. The entry abort mode requirements for the accelerated launch date have increased by ~50 m/s versus the baseline; a minimal tradeoff between attempting to satisfy both interplanetary transfer requirements and abort requirements.

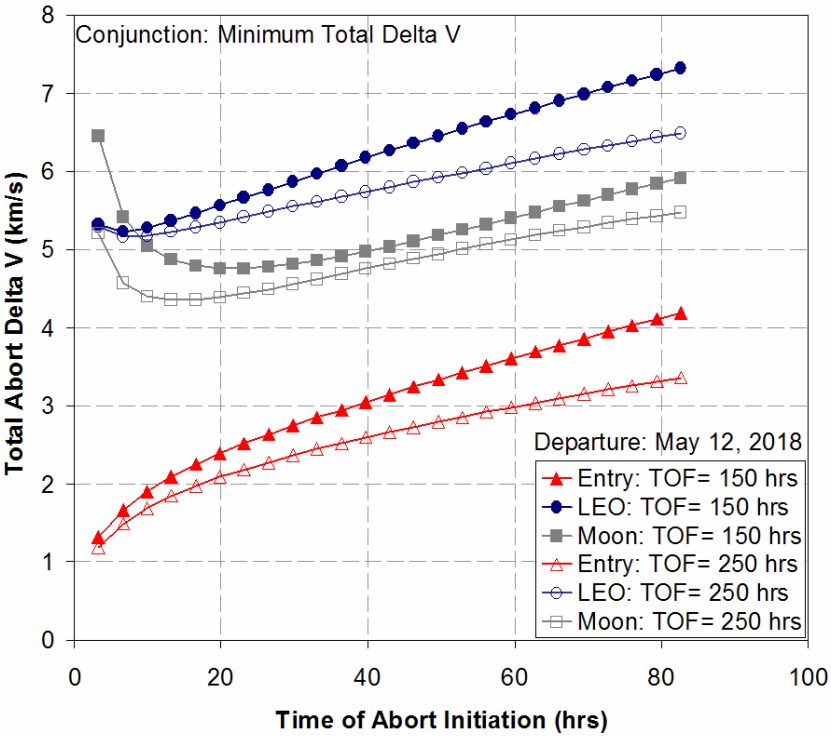

Figure 8.20 Abort Modes Requirements Comparison: May 12, 2018

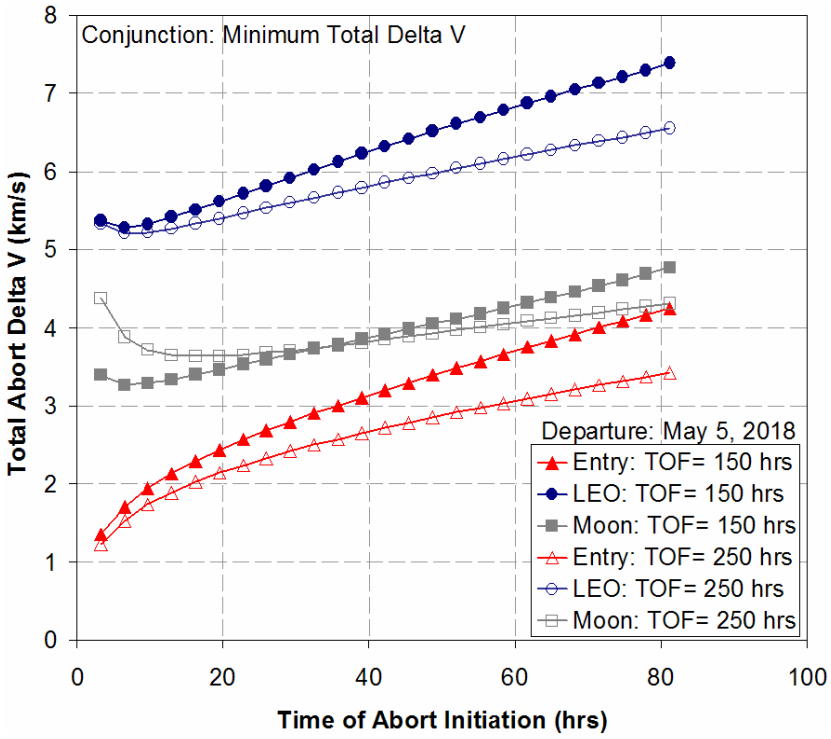

Figure 8.21 Abort Modes Requirements Comparison, May 5, 2018

The mean values of the abort delta V requirements of all three abort modes for the four considered departure dates are listed in Table 8.1 for both 150 hr and 250 hr abort flight times.

Table 8.1 Mean Delta V Variation by Abort Mode for Selected Flight Times

	Mean Delta V *(km/s)*: TOF= 150 hrs			Mean Delta V *(km/s)*: TOF= 250 hrs		
Abort Mode:	Entry	LEO	Moon	Entry	LEO	Moon
April 29, 2018	3.209	6.412	4.170	2.723	5.964	3.588
May 5, 2018	3.101	6.303	3.943	2.613	5.852	3.932
May 12, 2018	3.048	6.250	5.264	2.561	5.799	4.881
May 19, 2018	3.083	6.284	5.401	2.595	5.834	3.917

The median abort requirements values were also computed but not included as they were nearly identical to the mean values presented in the table. These averaged values confirm the previous observation concerning aligned Moon preference during departure.

The physics of the abort modes are primarily a function of outbound velocity hence the preferred Moon position for minimizing abort delta V should remain approximately the same for aborts of similar flight duration. The actual delta V requirements will, of course, increase as the outbound velocities are increased. All the data analyzed in this section has been for varying Moon positions matched to the CJI_MT trajectory class for 2018. Additional abort classes and years were not run for this part of the investigation due to the large number of solutions required for each trajectory class and opportunity year if Moon position is standardized, essentially generating large amounts of data while providing little additional insight. Moon abort results of one class are only comparable to one another when they share identical Moon location setup. Optimization of the lunar position influence on the Moon abort

mode will be accounted for in the architecture abort capability optimization that will be presented in a later chapter of this investigation. The analysis in this chapter has shown that Moon aborts are achievable for a slight additional delta V compared to Earth entry aborts and depending on alignment and year of opportunity may provide additional possibilities for short abort duration recoveries for the same propellant cost as much longer Earth-return options. The value added by this capability will be investigated as part of the architecture evaluation later in this work.

Chapter 9. Manned Mars Mission Architectures

The preceding chapters have characterized the required propulsive energy as a function of abort time of flight necessary for the execution of the conceived departure phase abort modes. The critical question remains as to whether one or more of these abort modes are achievable by likely Mars spacecraft designs. This chapter presents several of the principal candidate Mars transportation architectures that are under consideration for manned Mars missions. The objective of this presentation is not to rank the architectures but rather to identify the positioning, interaction, and capabilities of the various spacecraft elements with primary emphasis on the piloted transfer vehicles utilized for crew transport during the departure phase.

9.1. Selected Split Mission Architectures

According to Donahue and Cupples[56], the architecture consists of the choice of trajectory type, mission duration, mission frequency, fleet size, payload requirements, abort modes, required precursors, and vehicle reuse options. As applied to Mars, such architecture development began in the 1940's with the publication of Wernher von Braun's *Das Marsprojekt* study. For the next several decades, the principal architectures consisted of unrealistically massive LEO-assembled Mars spacecraft that were capable of executing a single flight, "all-up" mission. Studies from the last several decades have been configured differently, incorporating a "split" mission profile where the cargo and piloted elements are separated. A key benefit of this setup is the ability to transfer cargo on the most energy efficient trajectories regardless of flight duration, a freedom that is not

permissible for the human crew. Split mission architecture possibilities are numerous, but all result in reduced launch mass versus the all-up options. When choices of transfer trajectory, propulsion type, *in-situ* resource utilization (ISRU), and aerocapture options are also included, the number of potential architectures increases dramatically. Compiled by Griffin[57] et al, Figure 9.1 shows several of these branching possibilities for many of the principal architectures of the past three decades.

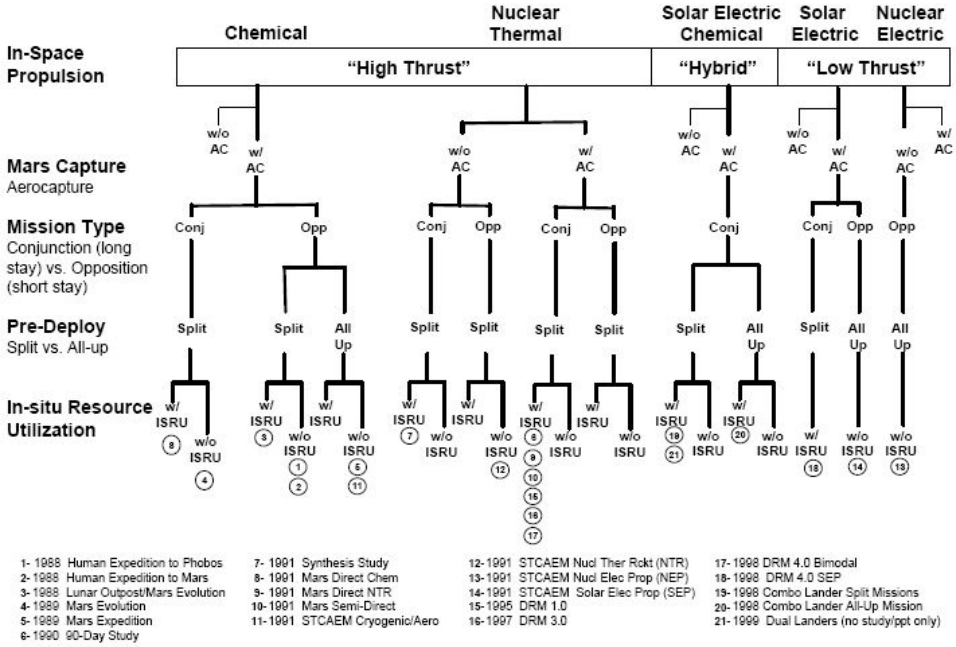

Figure 9.1 Mission Design Options for Mars Studies (Griffin[57])

When evaluating departure phase abort capability, it is the piloted segments of these split architectures which are to be analyzed. Desirable flight times for manned missions are not achievable for the low thrust architecture options. Further, for the reasons presented in Chapter 5, the present investigation focused only on conjunction

type mission trajectories. The next sections describe the Mars mission architectures that were included in this present study.

9.1.1. 1990 Mars Direct Architecture

The introduction of the Mars Direct architecture in 1990 represented a fundamental shift in focus away from the massive "all up" spacecraft architectures that had been prevalent in previous decades. As advocated by Zubrin and Baker[8], the architecture heavily emphasized ISRU on Mars for the creation of the rocket propellant required for the return trip home. Both Earth and Mars orbital rendezvous situations were eliminated in favor of a direct surface-to-surface transfer. This type of transfer necessitated the creation of a launch vehicle capable of placing 47 metric tons directly on an interplanetary trajectory. The envisioned launcher would be derived from existing shuttle hardware in order to save on development costs. The plan called for the launch of an unmanned, combination ascent stage and return habitat vehicle with an ISRU plant to the Mars surface one opportunity ahead of the planned human arrival. After a successful aeroentry and landing, this vehicle would use hydrogen feedstock brought from Earth in its ISRU plant to create the methane and oxygen rocket fuel with which to fuel the empty ascent/return vehicle. Once completed, the way would be open for the arrival of the human crew on the next launch opportunity. The piloted combination transfer/surface habitat also performs an aeroentry and lands close by the fueled ascent/return vehicle. Upon completion of the mission, the crew boards the ascent/return vehicle for the flight back to Earth. The Mars Direct vision advocates the repetition of this cycle every year of

opportunity as a means to rapidly establish multiple outposts on the planet's surface. Figure 9.2 illustrates the various mission sequences of the Mars Direct architecture.

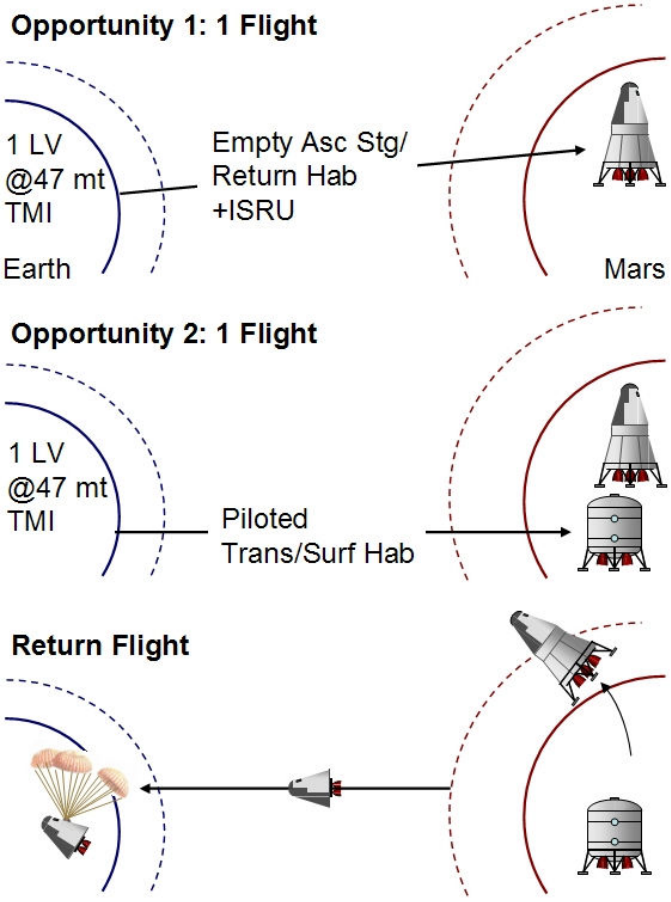

Figure 9.2 Mars Direct Architecture Mission Sequence Diagram

The Mars Direct architecture benefits from mass reductions gained through its use of ISRU and non-propulsive Mars capture. Operations are also simplified given the absence of any orbital rendezvous and the fact that, once the launch vehicle is developed, only two flights are required to support each human expedition team. There are several difficulties that need to be overcome as well. First, the 3-yr duration of the manned mission imparts a large reliability expectation of the utilized habitats and hardware. The pre-deployed ascent/return vehicle would need to be

reliable for an even longer duration. There are very few abort options available when using the Mars Direct architecture. The manned transfer habitat has minimal propulsive capability and would be unable to execute any propulsive aborts. The architecture was conceived with an "abort to Mars surface" philosophy given the pre-emplaced surface assets. However, in the event of the failure of those assets during the crew's half year long outbound flight, there would be no abort options available. This hazard can be mitigated by the utilization of a Mars free-return trajectory which would return the crew to Earth; however, this option is only available if the transfer habitat, or some portion thereof, is capable of performing a high velocity Earth atmospheric entry or at the very least an Earth aerobraking maneuver to capture into orbit to await rescue. As originally constituted, the Earth entry vehicle in this architecture is part of the pre-deployed ascent/return vehicle and not available to the crew in the event the Mars landing does not take place.

9.1.2. 1998 Design Reference Mission Version 3.0

The attributes of the Mars Direct plan initiated the analysis of a wave of similar architecture possibilities throughout the 1990's. As these architectures sought to improve upon the deficiencies of Mars Direct, several of its benefits were compromised, most particularly the prohibition against Mars and Earth orbital operations. The NASA Design Reference Mission (DRM) was a culmination of these efforts. The standard reference mission currently in use is the 1997 DRM modified as Version 3.0 in 1998[58]. The purpose of the reference mission is to provide the exploration community with a standard by which an equal comparison of mission

approaches and technology concepts can be evaluated. The reference mission does not necessarily advocate itself as the optimal solution.

The DRM 3.0 architecture is also a split mission with a pre-deployed surface lander that comprises the ISRU plant and ascent vehicle. However, unlike Mars Direct, the return habitat and TEI propulsion elements have been removed from the lander and incorporated into a separate vehicle that is pre-deployed to Mars orbit. Unlike Mars Direct, these assets are not launched directly from the Earth's surface onto the interplanetary transfer. In an effort to eliminate the need for the development of a large launch vehicle, the 1998 DRM 3.0 plan calls for separate launches of the mission payloads and the required TMI propulsion elements into LEO orbit. Each Mars flight would therefore entail two Earth launches and one LEO rendezvous. Since 1998 DRM 3.0 calls for two payload flights to Mars in the first year of opportunity there will be four launch vehicles required, each capable of placing 80 metric tons into a LEO orbit to await docking. The architecture assumes Nuclear Thermal Propulsion (NTP) for the TEI stages. NTP with its higher specific impulse helps reduce the amount of initial mass in low-Earth orbit (IMLEO). After the docking of the payload and TMI elements, the mission departs LEO. Upon Mars arrival, the fueled TEI stage/return habitat is aero-captured into a low-Mars orbit (LMO) and the empty ISRU ascent stage is landed on the Martian surface where it begins propellant production. On the next opportunity, two Earth launches will place the transfer/surface habitat payload and its TMI stage into LEO orbit. If the habitat is launched unmanned, a third flight will be required to deliver the human crew. Upon Mars arrival, the manned trans/surface habitat performs an aero-entry and lands near

the now-full ascent stage. Upon completion of the mission the crew transfers to orbit aboard the ascent stage and rendezvous with the TEI stage/return habitat and proceeds to Earth. Figure 9.3 illustrates the various mission sequences of the 1998 Design Reference Mission Version 3.0.

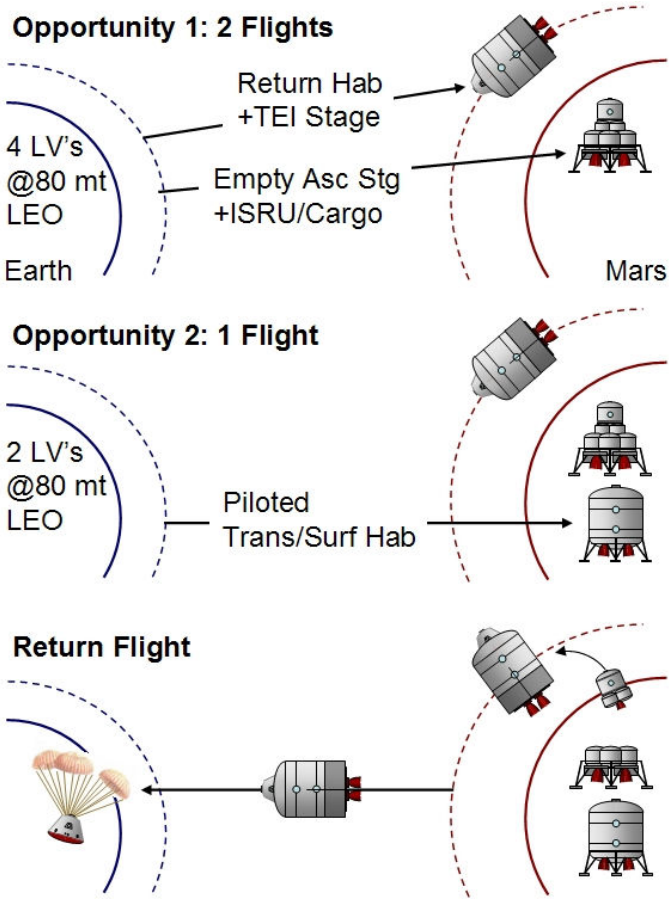

Figure 9.3 1998 DRM 3.0 Architecture Mission Sequence Diagram

As described, the 1998 DRM 3.0 architecture necessitates an orbital rendezvous at both Earth and Mars. Additionally, the ISRU benefit is reduced moderately as the fuel for the TEI stage is now delivered to orbit initially instead of being locally produced as was done with Mars Direct. A benefit of the architecture is the reduction in the size of the payload mass manifested on each launch vehicle; assuming that

multiple medium launches are superior to the development of a heavy-lift launcher. Additional contingency options at Mars are also enabled since the transfer habitat could rendezvous with the fueled TEI stage/return habitat vehicle and return to Earth without requiring a surface landing.

Both the Mars Direct and 1998 DRM 3.0 architectures were baselined assuming methane/oxygen propulsion for the ascent and TEI stages. The selection of methane propulsion on the Mars end of the mission was based on long-term storability issues in the case of 1998 DRM 3.0 and available ISRU propellant in the case of Mars Direct.

9.1.3. 1999 Design Reference Mission

A 1999 revision[56] to the Design Reference Mission called for the combination of the Earth departure and return functions into a single vehicle. This change resulted in a piloted vehicle capable of performing a round-trip Mars transfer independently. An additional change was the elimination of aerobraking for the Mars-orbit capture (MOC) of this vehicle into Mars orbit. The round-trip spacecraft utilizes NTP propulsion for all three major propulsion events: TMI, MOC, and TEI. During the first mission opportunity, this architecture deploys an empty ISRU ascent vehicle to the Martian surface and a surface habitat which aerobrakes into LMO. Four Earth launches are required to enable these two Mars transfers. Upon Mars arrival on the second opportunity, the crew boards the surface habitat in orbit and uses it to descend to the surface. After mission completion, the ascent vehicle is utilized to transfer the crew back to the transfer vehicle left in LMO. Figure 9.4 illustrates the mission sequences for the 1999 DRM architecture.

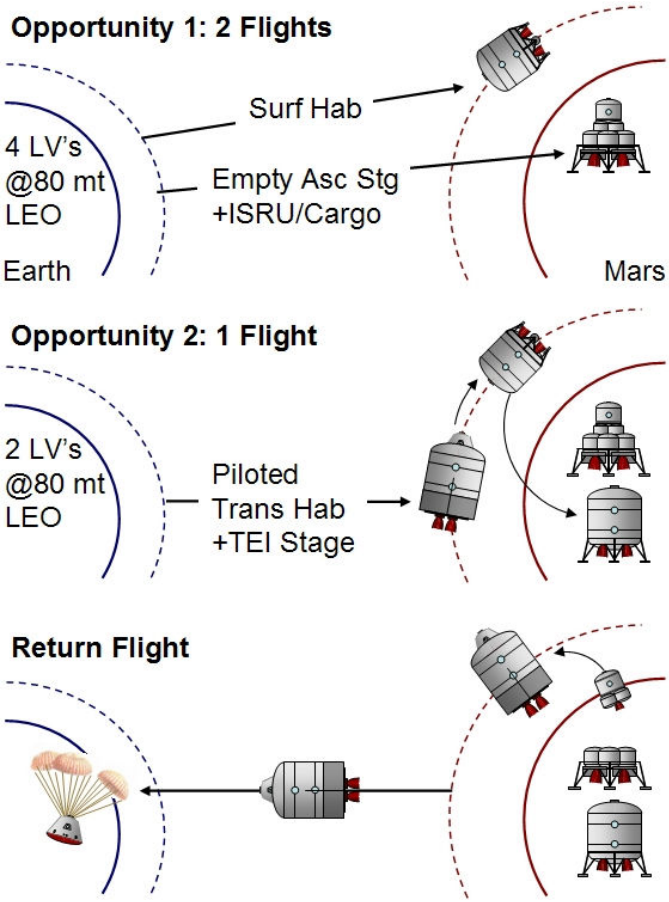

Figure 9.4 1999 DRM Architecture Mission Sequence Diagram

The 1999 DRM architecture no longer employs the "abort to Mars surface" philosophy that characterized Mars Direct. The round-trip capable transfer stage opens up the possibility of propulsive aborts back to Earth independent of the pre-deployed assets. Such contingency ability mitigates the requirement to fly a Mars free-return trajectory. The reliance on Mars aerobraking and ISRU has become less prominent. Similar to the 1998 DRM 3.0 architecture, the 1999 DRM has baselined both LEO and LMO orbital rendezvous operations.

A modification of the 1999 DRM was proposed by Donahue and Cupples[56] that would transform the architecture from NTP to an all-chemical version and re-

introduce the aerocapture maneuvering for the piloted transfer vehicle. The focus of these changes was the elimination of the additional technological development of NTP before a Mars mission could be undertaken. The reduced performance of the chemical TMI stages required that two of them be launched for every payload module. This modification also re-introduced aerocapture as the MOI method for the piloted transfer vehicle. The modified architecture now requires eight LEO payload flights instead of the original six due to the need to double up the lower performance chemical TMI stages for the heavier payload transfers.

9.2. Architecture Elements for Manned Departure Phase

The abort capabilities that have been described throughout this work are desired attributes of the manned spacecraft elements contained in the presented architectures. A characterization of the departure phase abort capabilities of a given architecture will therefore focus on the vehicle elements and resources that are actually present or accessible to the crew during Earth escape. This section discusses the determination and utilization of these capabilities.

9.2.1. Abort Philosophy: Abort Options vs. Mission Success

The current abort philosophy for the majority of the Earth-Mars transfer, espoused to some degree by all three of the considered architectures, envisions scenarios where the manned spacecraft is aborted to the surface of Mars in the event of a failure. Such a philosophy leverages resources and pre-deployed surface assets, arguing that the Martian surface is the safest place for the human crew for many

emergencies. This "safe on Mars" philosophy has the added benefit of perhaps permitting a continuation of the mission. By the time a spacecraft has embarked upon an interplanetary transfer, a great deal of expense and effort has already been spent to lift the various elements from the Earth's surface and impel them on the escape orbit. Abort options that could continue to at least partially fulfill mission goals would avoid wasting the already expended effort and expense. Subject to the type of failure, this abort philosophy can be difficult to realize during the departure phase. For most of the mission, the rationale for aborting to the Martian surface is the conveyance of the crew to the most accessible surface haven in terms of time and propulsive requirements. During the departure phase, the Earth is a much more quickly attained refuge. Though the high departure abort propulsive expenditure would indicate a preference for continuance to Mars instead, the frightening prospect of committing the crew to a six month voyage in a spacecraft that has already experienced a failure versus a two week abort flight home clearly indicates Earth as the ideal haven for these cases.

Potential departure phase failures that were identified in previous chapters are associated with either the TMI propulsion event or the spacecraft cooperative system operation shortly following full initialization. The departure abort requirements developed in the previous chapters assumed aborts which occurred after the termination of the TMI burn where the spacecraft would be traveling at its maximum departure energy. In the event of a propulsive failure resulting in a partially complete TMI maneuver, the various abort modes would be correspondingly more accessible than their full-velocity counterparts. The abort options include atmospheric entry and

Earth or Moon orbit depending upon residual delta V amounts. As stated, the abort requirements were generated for post-TMI failures. For failures that occur during the TMI maneuver, additional propulsive capability may be available depending on the architectural setup and burn execution method of the TMI stage(s). Zubrin and Weaver[59] have shown how a dual engine and/or dual stage TMI setup may allow for the execution of an orbital abort or even the continuation of the outbound mission depending on the nature and timing of the TMI failure. It appears that these strategies may prove beneficial in mitigating mission risk associated with TMI failure. For post TMI failures, especially including the spacecraft system failures described previously, the need for departure phase abort options remains in effect.

9.2.2. Departure Characteristics of Baseline Manned Elements

The various architectures all have a slightly different vehicle and propulsion composition for the manned vehicle elements. In the Mars Direct and 1998 DRM 3.0 plans, the crew travels aboard a transfer habitat that directly descends to the surface of Mars and continues to serve as their surface habitat. In the 1999 DRM, the crew rides aboard a vehicle that is the transfer habitat for both outbound and return trajectories. The first two employ aerocapture at Mars with varying amounts of descent propulsion while the third utilizes a NTP propulsion system for Mars Orbit Insertion (MOI) and Trans-Earth Injection (TEI). The differences in scale and composition lead to vehicles that vary greatly in their ability to perform a post-TMI departure phase abort. Table 9.1 presents a brief description of the departure phase manned vehicle elements for each of the three candidate architectures.

Table 9.1 Manned Architecture Elements During Departure Phase

	Mission Architectures		
	Mars Direct	1998 DRM 3.0	1999 DRM
Depart Vehicle Type	Trans/Surf Hab	Trans/Surf Hab	Trans/Return Hab+TEI
Entry Capable ECRV	No	No	Yes
ECRV mass *(kg)*	n/a	n/a	5800
Propulsion Type	CH4/OX	CH4/OX	NTP
Specific Impulse *(s)*	379	379	900
Delta V Amounts (km/s)			
Midcourse	0.1	0.1	0.1
MOI	0.1	0.1	2.5
Descent	0.5	1.0	n/a
TEI	n/a	n/a	1.7
Total Post-TMI	0.7	1.2	4.3

Also contained in the table is an estimation of the various propulsive delta V maneuvers planned for the vehicle. For all three transfer vehicles, a midcourse propulsive maneuver of 100 m/s has been bookkept. Whether by aerocapture or propulsive capture, all three vehicles are placed on a highly elliptical, 250 km by ~33,000 km orbit. The Mars Direct and 1998 DRM 3.0 architecture differ in the amounts of propulsive capability they reserve for Mars surface descent after aeroentry and parachute deployment. In their baseline configurations, only the 1999 DRM spacecraft, with a post-TMI delta V capability of 4.3 km/s, is able to realistically achieve the different abort modes that have been developed. It should be noted that the representative values quoted here from the corresponding references are approximations and vary with launch opportunity, assumed transfer trajectory class, and mass assumptions. Another issue with the Mars Direct and 1998 DRM 3.0 architectures is a lack of a vehicle component that is capable of withstanding an Earth atmospheric entry, an Earth Crew Return Vehicle (ECRV). In these two architectures, the designated ECRV vehicles were pre-deployed to Mars with the first

opportunity cargo flight and are therefore unavailable to the crew during the departure phase of the manned flights that embark on the second interplanetary opportunity. These spacecraft would be confined to LEO and lunar orbit abort modes if sufficient delta V capability was present.

9.2.3. Enhancement of Manned Element Abort Capability

In their present incarnation, several of the different manned transfer craft are severely limited in their ability to achieve the departure phase abort modes due to either a lack of propulsive reserve and/or entry capability. In seeking to realize an abort capability, solutions were desired that provided abort options that would not adversely compromise or scale the mass of the vehicle. In the case of the 1999 DRM such capability was naturally inherent given the design and allocation of the crew transfer vehicle. For a given propellant amount, the delta V potential is a function of the mass to be accelerated. For the transfer/descent stages that compose the piloted elements of the Mars Direct and 1998 DRM 3.0 plans there are several thousand kilograms of propellant aboard to execute the descent delta V maneuvers highlighted in Table 9.1. In the case of a departure phase abort, the majority of the habitat mass that composes these landers would not be needed. Conceivably, these vehicles could be designed with a smaller integrated crew capsule that, along with the engines and propellant, could be detached from the remainder of the habitat in the case of a departure phase emergency. This lifeboat vehicle would be much less massive than the original habitat and a much greater delta V capability could be realized for the same propellant amount. The Earth-entry capable lifeboat would only need to be designed to provide bare minimum crew support for durations of two weeks or less.

The lifeboat mass penalty could be offset greatly if it was responsible for many of the habitat's functions during nominal operations, such as communications, command and control systems, life support and any other functions that would be required of either vehicle. Assuming a 7 metric ton crewed lifeboat capsule, the existing engines and propellant of the Mars Direct trans/surf habitat would be capable of providing approximately ~2 km/s of delta V in such a configuration. The 1998 DRM 3.0, which has a more generous descent propellant allocation, would be capable of ~3 km/s of delta V with this setup. Such a plan for the provision of a lifeboat is far superior to the alternative of simply designing an additional fueled emergency vehicle and adding it to the outbound stack. The first is a creative re-configuration of already planned resources and is hopefully achievable within original mass allocations while the additional mass penalty represented by the alternative option wrecks havoc on the balance and launch requirements of the entire architecture. The existence of such a lifeboat version of the vehicle could prove beneficial for addressing other foreseeable contingencies during other mission phases.

Chapter 10. Departure Abort Capability of Candidate Architectures

The goal of this chapter is to ascertain the extent of the departure phase abort capability that may be achievable for each of the three system architectures described in the previous chapter. Earlier chapters have investigated many possible classes of trajectories for Earth-Mars transfers. Because all trajectory classes are not equally applicable to the particular sizing of a given architecture, results will only be generated for the most applicable transfer classes for each investigated architecture. Each of the candidate architectures are reviewed to establish which abort modes are possible with a specified trajectory class and given departure opportunity and subsequently to determine the resulting return time-of-flight characteristics of these feasible aborts. Combining these results allows for the determination of feasible abort regions of the departure phase as well as exclusion zones where such aborts are not achievable. The analysis of this data facilitates a comparison of architectures and the identification of architecture attributes and propulsive potentials necessary to attain sufficient departure phase abort capability.

10.1. 1999 Design Reference Mission

The previous chapter established that the departure-phase system elements of the 1999 Design Reference Mission architecture had the largest post-TMI residual

delta V capability of the three representative architectures considered. A larger delta V available correlates with a more extensive abort capability but is not the only contributing factor. The magnitude of the relative departure velocity also plays a major role and is the primary reason abort capabilities will differ between trajectory classes and years of opportunity. The attributes of a given architecture aid in the selection of likely transfer trajectory classes. The manned vehicle elements of the 1999 DRM architecture are propulsively captured into Mars orbit. Consequently, optimization of the 1999 DRM architecture will show an aversion to higher Mars approach velocities. A review of the Mars arrival velocities presented in Figure 5.17 indicates that the minimum total delta V conjunction trajectory (CJI_MT) would be the most likely trajectory choice for this architecture followed by the minimum departure delta V conjunction trajectory (CJI_MD). The high magnitude and yearly variability of the Mars arrival velocity inherent in the free-return (FR_3Y) class makes it an unattractive choice for an all-propulsive architecture such as the 1999 DRM. The free-return also becomes less relevant for such an architecture because propulsive aborts during the interplanetary transfer or Mars arrival trajectory phases are achievable options and result in greatly reduced return flight times.

10.1.1. 1999 DRM: Achievable Aborts for Baseline Opportunities

The departure abort requirements and resulting abort flight times are derived assuming the spacecraft successfully completes the TMI burn maneuver, an assumption that considers the spacecraft traveling at its full departure velocity profile and consequently constitutes a worst-case velocity scenario. Failures occurring at

some previous point during the departure burn maneuver would result in slower velocities with a corresponding decrease in abort requirements.

The first step in determining the abort capability is to compute the delta V requirements for the entry, LEO, and Moon abort modes across a range of possible abort times of flight for every point along a given outbound trajectory. For each point of abort initiation, data are saved for the abort trajectory possibility with the shortest abort time of flight whose delta V requirement is equal to or less than the available spacecraft delta V. The 1999 DRM architecture has a residual post-TMI delta V capability of 4.3 km/s. For several points of abort initiation there may not be any aborts with low enough delta V requirements and no abort is feasible. The achievable aborts for this architecture for the minimum total delta V (CJI_MT) trajectory class for the 2018 departure opportunity are shown in Figure 10.1

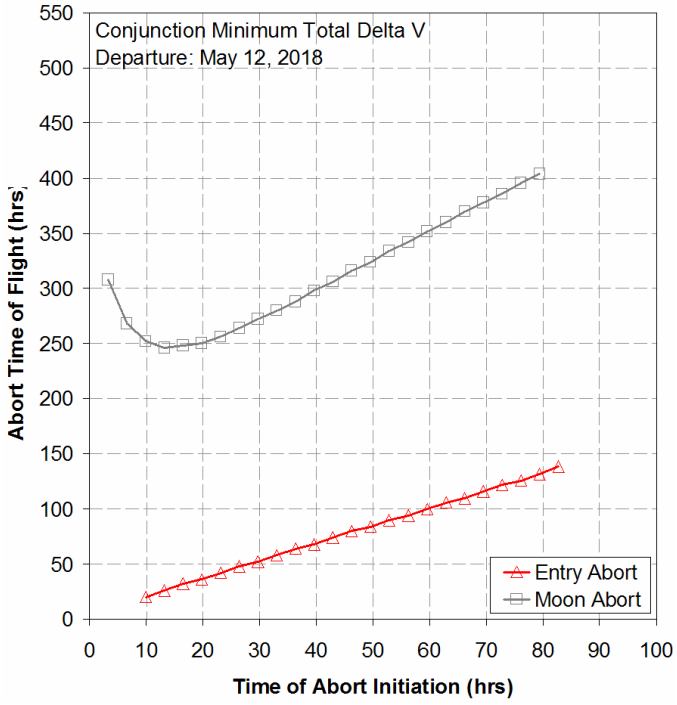

Figure 10.1 1999 DRM (CJI_MT): Achievable Aborts for 2018 Departure

The figure shows the resulting times of flight for both entry and Moon aborts that are available to this architecture. For this date of departure, the achievable Moon aborts are of much longer duration than the entry abort possibilities; however, both abort modes are accessible for the majority of the outbound transfer. Conspicuously absent is the LEO abort mode whose delta V requirements exceeded the available delta V for all investigated possibilities up to abort flight durations of three weeks (504 hrs). The baseline 2018 CJI_MT transfer is the minimum of the 15-year inertial period for this trajectory class and thereby constitutes the most favorable departure year for achieving abort capability. The fact that the LEO abort mode is inaccessible to this departure opportunity implies that it will never be available at any year of opportunity for the given amount of delta V available. The presented Moon aborts are a result of lunar position on the baseline departure date. A following section will investigate the effect of departure date variance to achieve more beneficial lunar alignments.

Throughout this work, the entry abort mode has been established as the baseline for comparison and, when possible, is considered the preferred abort mode. The other trajectory class possibility for the 1999 DRM architecture is the minimum departure velocity conjunction class (CJI_MD). This trajectory class will prove to be applicable to all three candidate architectures and will therefore serve as a point of comparison. The entry abort capabilities of the 1999 DRM architecture were next ascertained for both the minimum departure and minimum total conjunction trajectory classes for the best and worst case departure years of opportunity for each class. The resulting entry aborts for these four cases are presented in Figure 10.2.

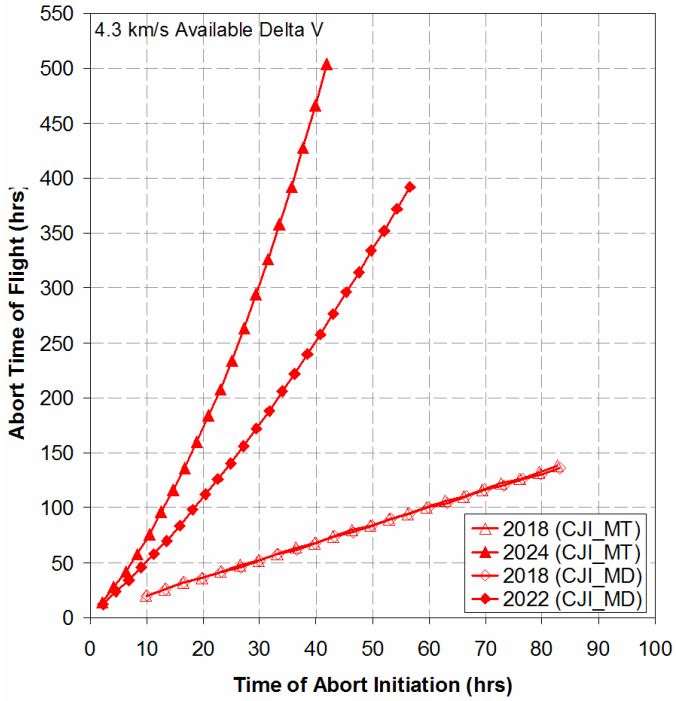

Figure 10.2 1999 DRM: Achievable Entry Aborts for Trajectory Class Extrema

The figure establishes the best and worst case aborts of the 1999 DRM architecture for each of the two trajectory classes. Both classes share inertial period minimums in the year 2018 and have very similar abort capabilities for those departures. The opportunity years for the inertial maximums with their faster departure velocities show entry abort results that, while still achievable for the majority of the outbound departure, are often between four to six times longer duration than the achievable aborts during the minimum years. If the worst case abort time of flight of three weeks is deemed acceptable, then the 4.3 km/s post-TMI delta V capability is sufficient to enable entry aborts of this duration or less for the minimum total (CJI_MT) trajectory class during any year of opportunity. The similar minimum departure (CJI_MD) class is likewise enabled but with maximum abort times of flight of 17 days (~400 hrs) or less.

10.1.2. 1999 DRM: Optimization of Moon Abort Mode

Chapter 8 illustrated how the Moon abort characteristics could vary as a function of lunar position. The entry abort capabilities of the previous section were computed for the baseline departure dates that were selected based on criteria of the interplanetary transfer. The purpose of the present section is to characterize the achievable Moon aborts that result for possible lunar positions during a complete lunar year. Accelerating or delaying the baseline launch date may provide great improvement in the Moon abort mode. Such a shift does; however, alter the characteristics of the interplanetary transfer. For comparison, the achievable Moon aborts for departure dates ranging from two weeks prior through two weeks following the baseline departure date were analyzed in increments of two days. The average Moon abort time of flight and resulting total transfer delta V for each investigated alignment are shown in Figure 10.3 for the 2018 CJI_MT trajectory class.

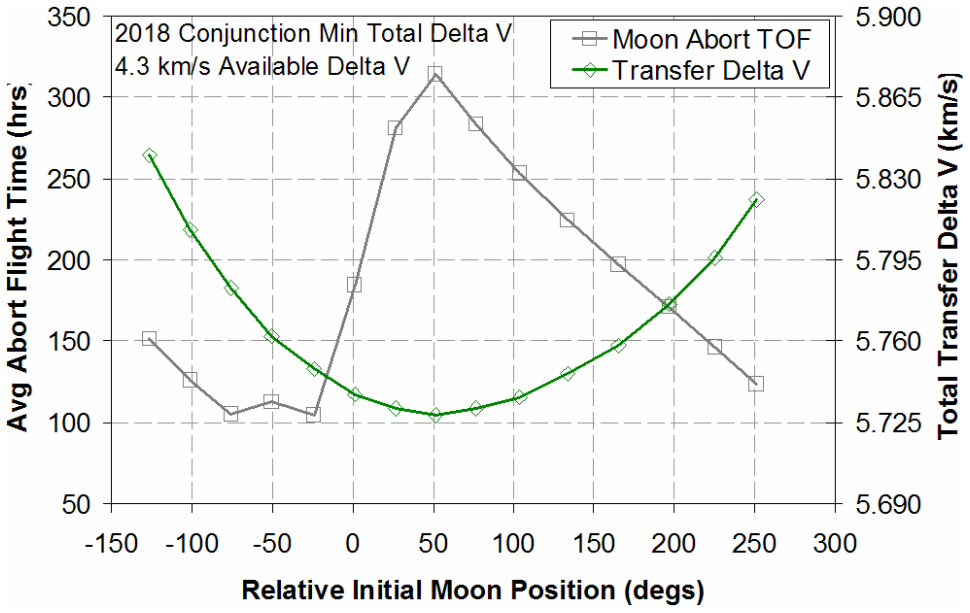

Figure 10.3 1999 DRM (CJI_MT): 2018 Abort/Transfer Requirement Variation

The lunar positions are measured in the fundamental plane of the geocentric **IJK** coordinate system relative to the position vector at the point of Earth sphere of influence exit. Locating the minimum of the total transfer delta V curve in the figure identifies the baseline date of departure and corresponds to a relative lunar position that is leading the departure position vector by approximately 50 degrees. For the case under consideration, that relative position also corresponds to the longest average abort time of flight for the Moon aborts achievable with the 1999 DRM architecture. The maximum values of the transfer delta V curve in the figure indicate an increase in the total transfer delta V of less than 2.5 percent for departure dates ranging from two weeks prior through two weeks following the baseline departure date. If the improved Moon abort enabled by the switch in departure date is desirable, the small increase in total delta V should be acceptable. The figure shows that drastically shorter Moon aborts are obtainable for lunar positions between approximately -25 degrees and -75 degrees. The same investigation was carried out for both the minimum total (CJI_MT) and minimum departure (CJI_MD) trajectory classes for years of inertial minimums and maximum. Figure 10.4 illustrates the average Moon abort time of flight trends for the 1999 DRM architecture for the years of transfer extrema for the minimum departure trajectory class. The trend shows that the more demanding year (2022) exhibits both longer and shorter time of flight trends than 2018. This trend is largely spurious however, because for much of the departure phase, the Moon abort mode is unachievable resulting in an average that is heavily skewed towards a handful of achievable points. While sparse, these achievable points do indicate the most advantageous lunar alignment for obtaining as much of a Moon

abort mode as possible. The preferred lunar alignment occurs once again at approximately the -50 degree position.

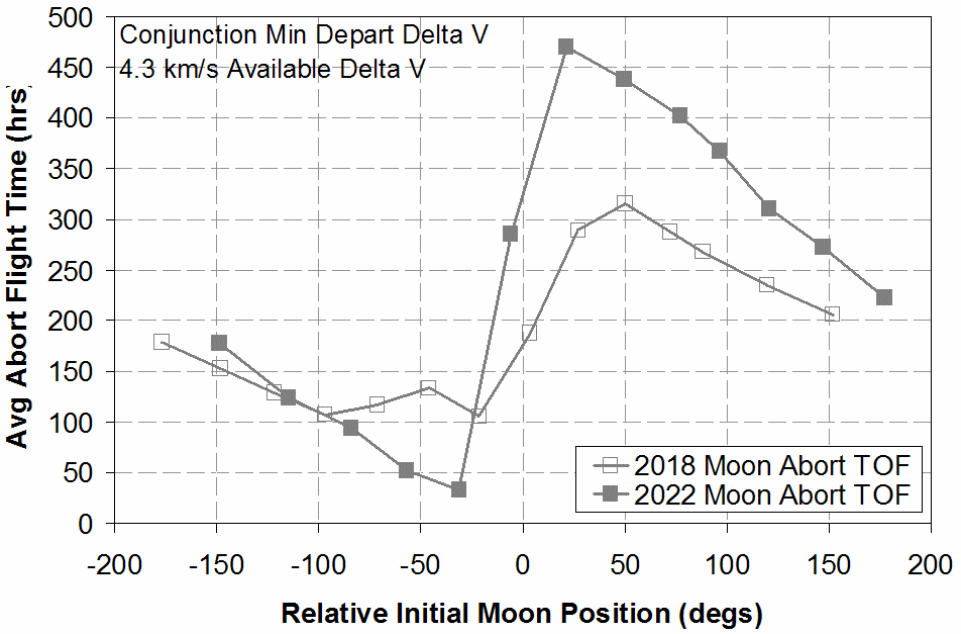

Figure 10.4 1999 DRM (CJI_MD): Extrema Abort/Transfer Variation

The baseline departure for each trajectory class was next altered to achieve the lunar alignment situation described and the abort capabilities of the abort modes were once again calculated. Figure 10.5 and Figure 10.6 present the abort capabilities for the entry and Moon abort modes at these improved lunar positions for the years of inertial minimum and maximum for both the minimum total (CJI_MT) and minimum departure (CJI_MD) trajectory classes respectively.

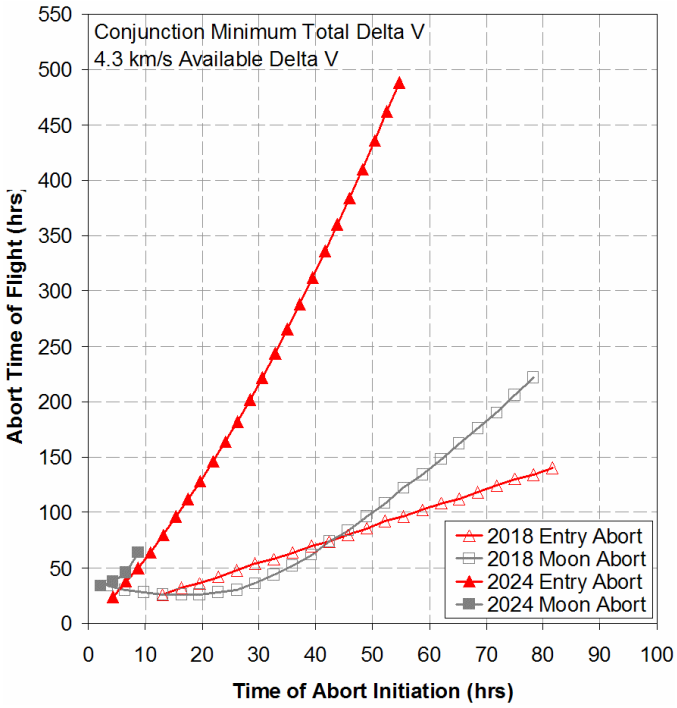

Figure 10.5 1999 DRM (CJI_MT): Abort Results for Improved Moon Position

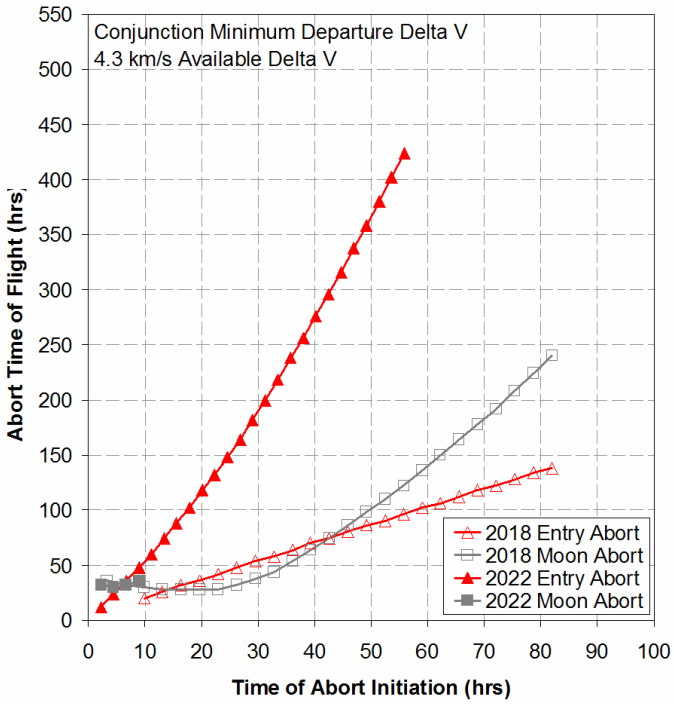

Figure 10.6 1999 DRM (CJI_MD): Abort Results for Improved Moon Position

The results of both figures report almost no change in the magnitude or trends of the achievable entry aborts; they retain essentially the same capability as on the baseline departure date. There has, however, been a drastic change in the achievable Moon aborts. For the inertial minimum case of 2018, both trajectory classes can achieve Moon aborts that have comparable abort flight times as the entry aborts; initially even lower and higher later. Comparing the 2018 Moon abort capability of Figure 10.5 with the original Moon abort capability of the baseline departure date in Figure 10.1 graphically illustrates the advantage of shifting the opportunity date to achieve a more favorable lunar alignment. However, the extent of the Moon abort mode nearly disappears when considering the faster departure velocities corresponding to transfer in the years of inertial maximum. The Moon abort capability in 2024 and 2022, the maximum years for the minimum total and minimum departure trajectory classes respectively, is available for only the first 10 hours of the outbound departures. Since the 1999 DRM architecture had the highest post-TMI delta V capability of the three considered architectures, it is anticipated that the Moon abort mode will be even less accessible to the other architectures.

10.2. 1998 Design Reference Mission Version 3.0

The manned elements present during the departure phase of the 1998 DRM 3.0 architecture consist of a transfer/surface habitat that, after arriving at Mars, will perform an aero-entry and descend to the planet's surface. The delta V capability of the habitat is designed at approximately 1.2 km/s. The previous chapter described how the module might be re-configured as a lifeboat in the event a departure abort

becomes necessary by discarding as much habitat mass as possible such that the available propellant amount would be sufficient to provide ~3 km/s delta V capability to the small remaining Earth return vehicle. In the absence of such a lifeboat configuration, the architecture will have no departure phase abort capability with only 1.2 km/s available. This study assumes the lifeboat configuration of this architecture. The lack of a propulsive maneuver at Mars indicates that the minimum departure delta V (CJI_MD) trajectory class would be preferred over the minimum total delta V class (CJI_MT). The Mars free-return trajectory class (FR_3Y) is applicable since the vehicle will have no inherent ability to perform a propulsive abort during the interplanetary or Mars arrival trajectory phases. This need is mitigated moderately by this particular architecture as a fueled Earth-return vehicle is already pre-deployed to Mars orbit and an aerobraking and docking could be conceivably arranged.

10.2.1. 1998 DRM 3.0: Achievable Aborts for Baseline Opportunities

The abort capabilities of the 1998 DRM 3.0 architecture were ascertained for both the minimum departure (CJI_MD) trajectory class and three-year free-return (FR_3Y) class assuming the lifeboat available delta V of 3 km/s. With less available delta V than the previous architecture, the LEO abort mode is similarly impossible. The achievable entry aborts for both classes during the years of their respective inertial maximums and minimums are plotted in Figure 10.7.

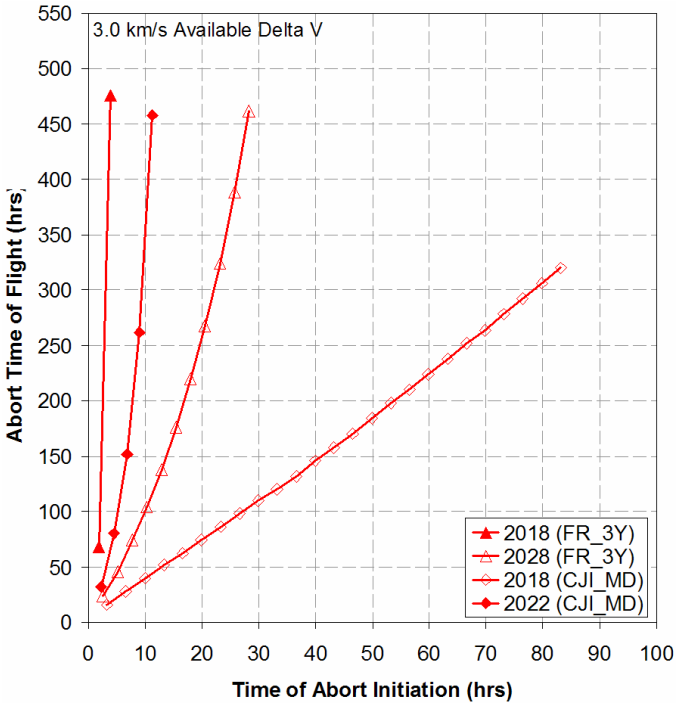

Figure 10.7 1998 DRM: Achievable Entry Aborts for Trajectory Class Extrema

The entry abort profile of the minimum departure class at the 2018 opportunity is similar to that achieved by the previous 4 km/s architecture though shifted to higher abort times of flight and is available throughout the departure phase. The 2028 inertial minimum of the free return is much less accessible, lasting for less than half of the outbound transfer before quickly exceeding the three week abort time of flight limit. The available entry aborts for both classes at their respective inertial maximums are drastically less accessible, with aborts from the minimum departure class feasible for just the first ten hours of the departure and those of the free-return class feasible for but four hours. The higher departure velocities of the free-return cases enable only limited capability during the year of inertial minimum and almost no capability during the inertial maximum year. The minimum departure class achieves a moderate entry abort capability for the inertial minimum year.

10.2.2. 1998 DRM 3.0: Optimization of Moon Abort Mode

As done for the first architecture, an optimization of lunar position was performed for the 1998 DRM 3.0 architecture to determine preferred lunar position and the resulting Moon abort capability. The achievable Moon aborts for each case are combined to present an average abort time of flight. These achievable Moon abort averages are presented in Figure 10.8 for both the 1998 DRM 3.0 and 1999 DRM architectures employing the minimum departure delta V (CJI_MD) trajectory class.

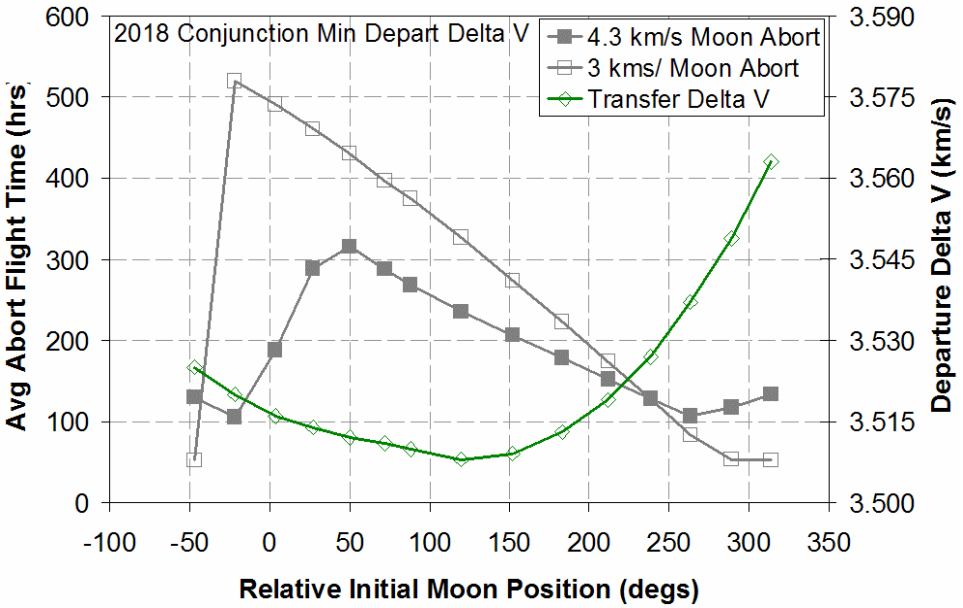

Figure 10.8 2018 Abort/Transfer Requirement Variations

The data for the 3.0 km/s available delta V corresponding to the 1998 DRM 3.0 architecture is once again slightly spurious as presented abort times are often averages of only a handful of achievable Moon aborts. However, the data confirm an optimal lunar alignment from approximately –50 (+315) degrees through -75 (+290) degrees. The baseline departure case corresponds to the minimum point of transfer delta V at

approximately 120 degrees. The maximum variation in that optimal delta V is less than 1.5% for accelerated or delayed launch dates of up to two weeks. The resulting achievable entry and Moon aborts for the maximum and minimum inertial years of the minimum departure trajectory class for the 1998 DRM 3.0 architecture are shown in Figure 10.9.

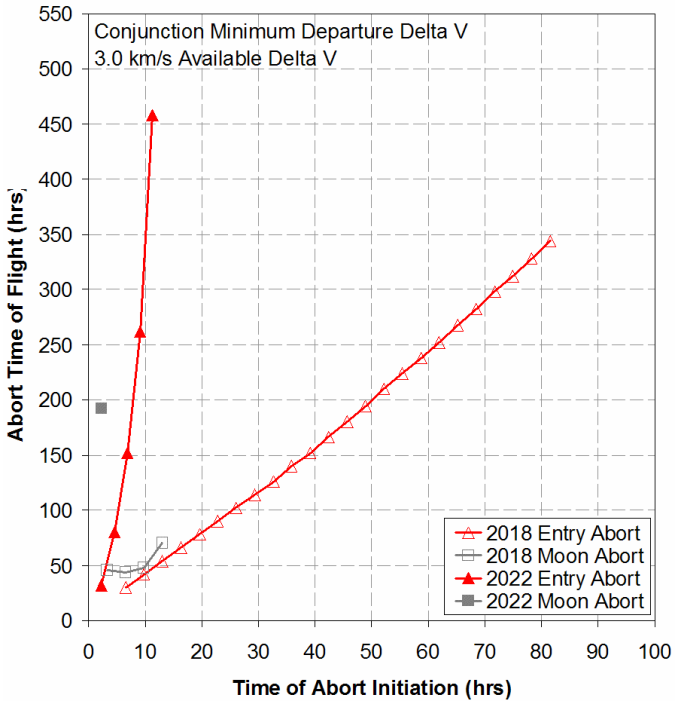

Figure 10.9 1998 DRM (CJI_MD): Abort Results for Improved Moon Position

As previously seen, there is little change in the resulting entry aborts arising from the shift in launch dates to optimize lunar opportunities. The Moon aborts for the minimum year of 2018 are available for less than the first 15 hours of the mission and are no improvement in abort time of flight versus the corresponding 2018 entry abort. The 2022 departure opportunity reveals virtually no achievable Moon aborts, save a single occurrence of those sampled for this investigation. The results indicate that a 3 km/s delta V capability is insufficient to achieve any practical Moon abort capability.

A lunar abort mode optimization was not performed for the free-return class trajectory cases for this or any other architecture case. The trajectory analysis code created to perform the investigations in this work does not presently have the ability to determine free return opportunities and was therefore not suited for analyzing free-return options across a range of departure dates for which no trajectory data was available. The free-return departure dates and transfer characteristics that have been employed are those identified by Soldner[44].

10.3. Mars Direct

The departure phase present spacecraft assets of this architecture are virtually the same as those of the 1998 DRM 3.0 architecture but are of lesser propulsive capability due to less conservative Mars descent delta V assumptions. Configuring the departure assets in a lifeboat configuration as described in the previous section could enable an Earth return vehicle with a 2.0 km/s post-TMI delta V capability. The minimum departure (CJI_MD) and free-return trajectory classes are once again applicable.

10.3.1. Mars Direct: Achievable Aborts for Baseline Opportunities

Given the results presented thus far, nearly no significant abort capability is expected for an architecture with such minimal delta V available. The achievable entry aborts are presented in Figure 10.10 at both the maximum and minimum inertial years of opportunity for the free-return and minimum departure delta V trajectory classes.

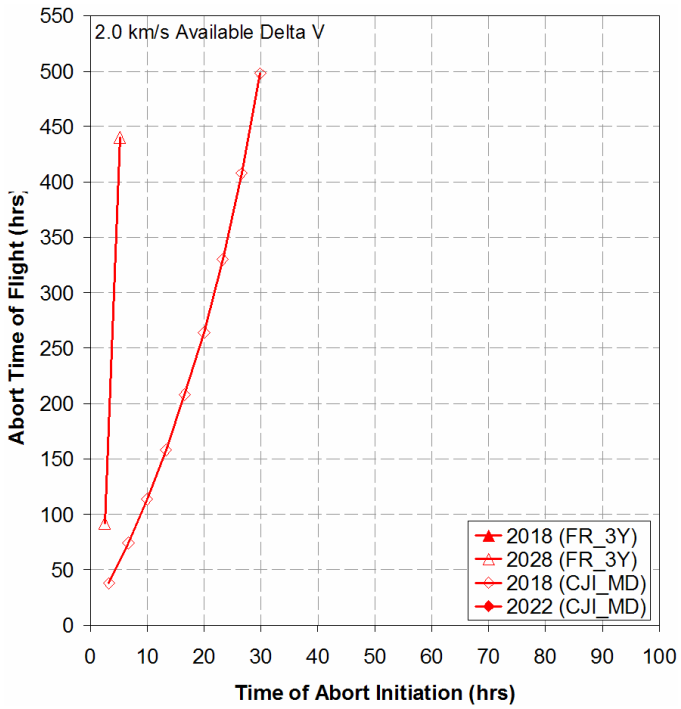

Figure 10.10 Mars Direct: Achievable Entry Aborts for Trajectory Class Extrema

There are no available entry aborts for either year of inertial maximum. The minimum departure case for the 2018 opportunity has a weak initial abort capability achieved through long duration flight times. The few data points of the free-return class do not constitute much of a realistic abort option.

10.3.2. Mars Direct: Optimization of Moon Abort Mode

The optimization of lunar position produced no realistic abort options for this architecture. A few sporadic single-point solutions were discovered for various lunar alignment scenarios for the 2018 minimum departure case but could hardly be considered as representative of a real Moon abort capability.

10.4. Comparison of Architecture Capabilities

This section combines the results of the previous architecture sections in order to present a comparison of abort capabilities. Of special interest are the regions of the departure transfer where a departure phase abort is feasible or infeasible. Figure 10.11 displays the feasibility regions for each of the analyzed architecture and trajectory cases during the years of inertial minimum transfers. The lengths of the bars in the figure correspond to the total duration of the departure phases of each case; each feasible region displays its duration in hours.

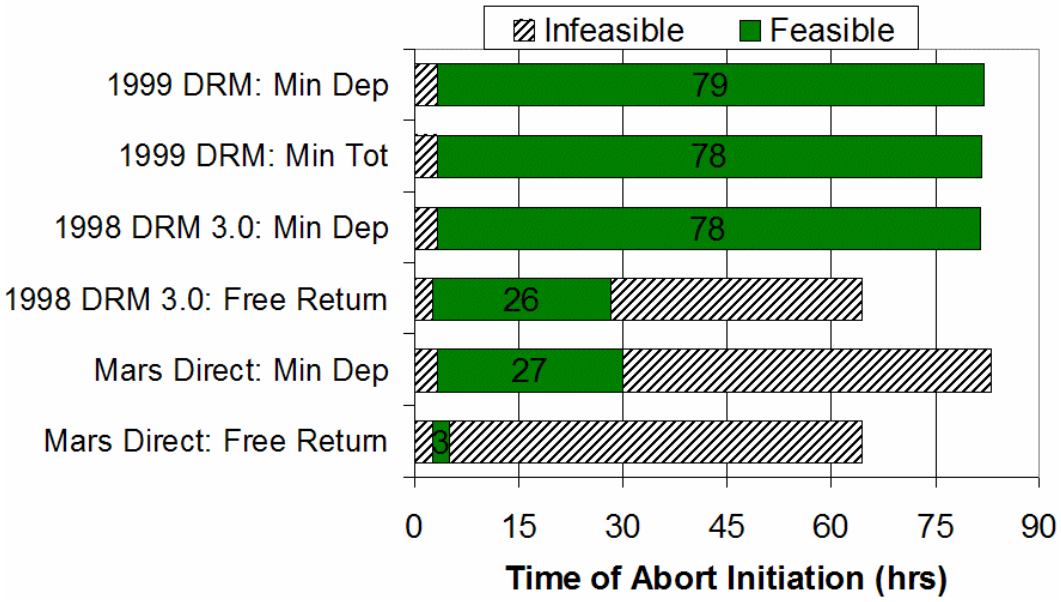

Figure 10.11 Architecture Abort Capability Comparison (Inertial Minimum)

The feasible aborts presented consist primarily of the entry abort mode, though the Moon abort mode is also feasible for both the 1999 DRM and 1998 DRM 3.0 architectures during inertial minimums as has been shown. The 1999 DRM with its larger delta V potential is capable of performing a departure phase abort across the majority of the transfer. The exclusion zones at the beginning of each bar are partly

the result of quickly changing angles and velocities near the Earth departure and partly a result of the distribution of the analysis sampling points. The free-return trajectory class exhibits larger exclusion zones compared to the minimum departure trajectory class for the same opportunities and architectures. While the feasibility regions of the minimum departure trajectory cases for the 1999 DRM and 1998 DRM 3.0 architectures are similar, it must be remembered that the higher delta V potential of the 1999 DRM results in lower abort times of flight. When there are large regions of infeasibility, they occur during the latter half of the departure resulting in feasible regions that are only achievable during the first day of the mission. The same feasibility regions are plotted in Figure 10.12 for the years of inertial maximum.

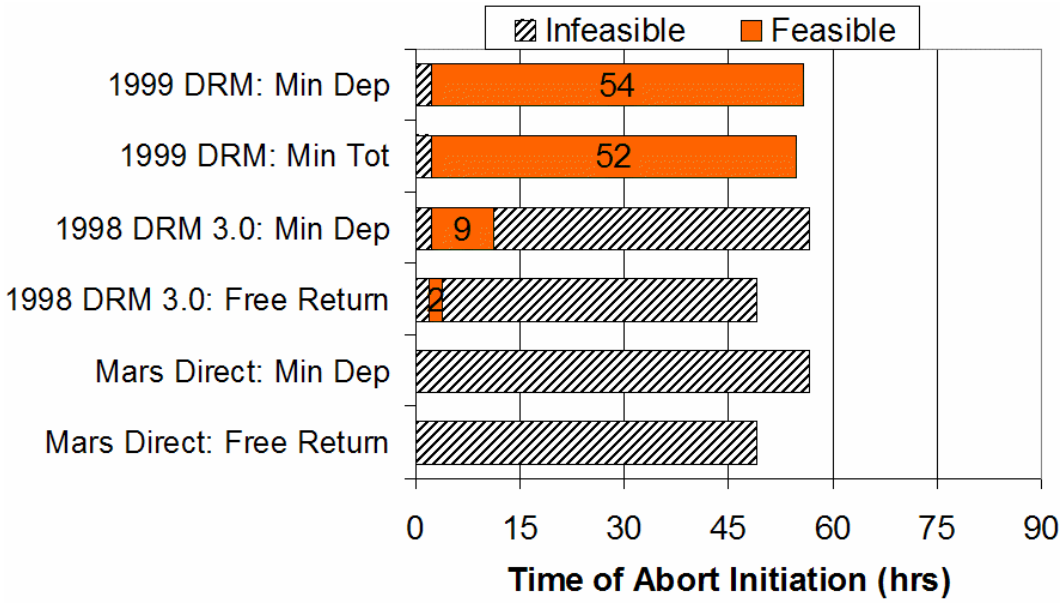

Figure 10.12 Architecture Abort Capability Comparison (Inertial Maximum)

The 4.3 km/s 1999 DRM architecture is the only one to retain any significant abort capability for its year of inertial maximum. The 3.0 km/s 1998 DRM 3.0 architecture achieves a minimal capability of 9 hours for the minimum departure case and the

Mars Direct attains none. It is interesting to note that an increase of only 1.3 km/s over the 3 km/s case would increase the abort feasibility from 9 hours to 54 hours and virtually eliminate the infeasible exclusion zone. If significant abort capability is required at the year of inertial maximum then only the 1999 DRM architecture or other architecture with a delta V capability in excess of 4 km/s is acceptable.

The comparisons of this chapter have utilized the years of inertial maximums and minimums to illustrate the best and worst case abort capability results for the various architectures and trajectory classes. While these extracted cases establish the bounds of the achievable abort capabilities, it would be prudent to determine where approximately each of the intermediary opportunities would stand in relation to those bounds before making any generalized conclusions regarding the preferred cases. Figure 10.13 plots the spacecraft infinity velocity at the sphere of influence exit for all three considered trajectory classes at each year of opportunity.

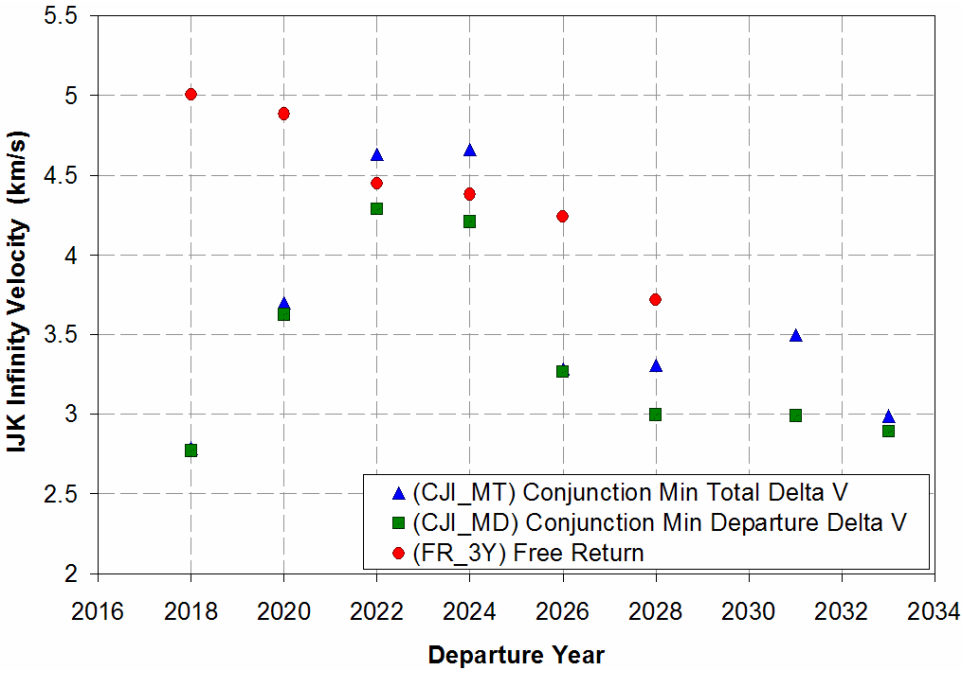

Figure 10.13 Variation of IJK Infinity Velocity by Trajectory Class 2018 to 2033

Comparing the intermediary infinity velocities with those of the maximum and minimum departures permits an estimation of the degree in similarity that could be expected between the abort capability of the intermediate year and that of one of the bounds. The minimum departure velocity class trajectories represented the greatest degree of abort capability for each of the architectures. The variation in infinity velocity for this transfer class indicates that a majority of the opportunity years would yield abort capabilities similar to those of the inertial minimum scenario. In effect, the minimum departure class results for the minimum inertial year could be roughly expected for five of the eight launch opportunities during the course of all launch opportunities of the fifteen year inertial period. The same trend is evidenced to a lesser extent by the minimum total delta V trajectory class. The free-return class varies in an approximately linear fashion with no dwell in the ranges of minimum velocity. These results are very encouraging for the minimum total delta V and minimum departure delta V trajectory classes because the longer duration feasible regions of Figure 10.11 could be expected to hold approximate for more than half of all launch opportunities.

Chapter 11. Summary and Conclusions

This chapter summarizes some of the principal findings of the departure phase abort investigation and provides recommendations for trajectory classes, abort modes, and architecture selection based on the results. Finally, possible research avenues are proposed for future work in developing robust departure phase abort capability.

11.1. Summary

An analysis of the failure behavior exhibited by historical manned spacecraft programs indicated the definite possibility of a manned Mars mission experiencing a major systems failure during the Earth escape maneuver and departure phase transit. A review of the available government and industry literature indicated that, although a great number of thorough investigations have been carried out into interplanetary and Mars arrival abort trajectories and contingency options, there had been no detailed formulation and analysis of possible abort options during the Earth departure phase segment of the Earth-Mars transfer. Given the importance of achieving a continual abort capability, the present work developed achievable departure phase aborts to contribute to the available mission suite of abort options. A primary goal of the investigation was to analyze, and judge these developed departure phase abort modes in the context of integrating them with the extensive and detailed transfer trajectory and spacecraft architecture work and results that have been previously accomplished thus improving the accuracy and usefulness of the abort results.

11.2. Conclusions

11.2.1. Interplanetary Transfers

The construction of full three-dimensional Earth-Mars transfer trajectory models was required by the need to know the actual orientation and position of the Earth departure phase trajectory in time and space. The inclusion of realistic elliptical and inclined planetary orbits introduces variation into the problem which results in unique launch opportunities that vary with both synodic and inertial periods.

The investigation considered five candidate trajectory classes for application to the manned Mars transfer. Of these, the two opposition trajectory classes were found to have excessively large fluctuations in the amount of mission required delta V when analyzed across the range of an entire inertial period. These types of trajectories also exhibited some of the highest departure velocities of all the considered classes, an attribute that would greatly reduce departure phase abort capability. Additionally, the opposition class permits only short duration Mars surface stays and is not as conducive to assumed mission scope and goals as the long duration stays enabled by the conjunction class trajectories. The remaining three classes were retained for further application in determining the abort requirements of the various departure abort modes and for use in evaluating candidate architectures. Two of these were conjunction types which minimized either total mission delta V or departure delta V while the third was a 2:3 resonance free-return trajectory class transfer. Of the three, the free-return class displayed the highest average values of

departure velocity while the minimum departure class had the lowest. Breaking out the Earth departure and Mars arrival velocity trends, both the minimum departure delta V and free-return trajectory classes exhibit greater variation in the magnitude of the Mars arrival velocity than the minimum total delta V trajectory class. This attribute suggests incorporation of architectures utilizing propulsive capture at Mars more likely for the minimum total delta V class and Mars aerocapture architectures more likely for the minimum departure velocity and free-return trajectory classes.

11.2.2. Departure Phase Abort Modes

The three departure phase abort modes that were developed and analyzed as part of this activity were: aborts to atmospheric entry, aborts to low-Earth orbit, and aborts to Moon orbit. The requirements for the execution of the three abort modes were determined for all three trajectory classes at each possible combination of abort initiation location and abort flight times of up to two weeks.

The entry aborts were obligated to match an entry corridor requirement defined as having a velocity of less than 11 km/s and an entry angle of approximately – 6.5 degrees. Comparing the entry abort results across the range of possible trajectory classes at both minimum and maximum inertial years of opportunity revealed substantial fluctuations in required delta V over a range of example abort flight times. Enabling an entry abort capability with abort flight times of two weeks duration or less across all opportunities would require approximately 5 km/s delta V.

The orbital abort mode was an investigation done in two parts. First, the requirements for delivering the manned spacecraft to the most convenient low-Earth parking orbit, and then the requirements for enabling a rendezvous of the spacecraft

with another existing Earth orbital asset. The first option aborts the spacecraft to a circular orbit of specified altitude and at the same inclination as the departure orbit. Achieving such a capability consistently across the range of investigated trajectory classes and abort flight times required a delta V capability of at least 6 km/s. The second option is a complicated one given the almost certain mismatch between the inclinations and right ascensions of the departure orbit and desired rendezvous orbit. An optimization of this scenario concluded that this option is only realistically achievable with the application of a dual-leg transfer where the spacecraft first matches the desired orbital plane at some distant point and then proceeds in to rendezvous. Requirements for achieving this second option are approximately the same as for the first option, but require twice the abort flight duration. The principal reason for the higher cost of the orbital abort mode with respect to the entry mode is the propulsive braking of the spacecraft down to the desired orbital velocity, a speed that is of much lower magnitude than the 11 km/s permitted for atmospheric entry. Given the high cost of executing these orbital aborts, it could be beneficial to consider an aerobraking deceleration should the orbit mode be desirable.

The final abort mode considered aborts to lunar orbit. Utilization of this abort mode presupposes a significant amount of previous logistical development of lunar orbit and surface assets sufficient to warrant their inclusion in a list of possible abort safe havens. Moon aborts are targeting problems where from a given point of abort initiation, lunar position will be significantly changed for different abort times of flight. The resulting abort requirements show behavior that is more intricate than that of the Earth return abort modes and is further complicated by the possibility of launch

date modification to optimize lunar abort capability. In general terms, the Moon abort mode requires approximately the same amount of delta V as the entry abort mode for optimized lunar positions and is occasionally cheaper during the beginning half of the departure phase and typically more expensive towards the end of the departure.

Of the three considered trajectory classes the free-return class requires the largest delta V to enable any of the abort modes while the minimum departure delta V trajectory class requires the least. The years of inertial maximum for the free-return class are of substantial departure velocity and are rather prohibitive to achieving extensive departure abort capability. The minimum total delta V and minimum departure delta V trajectory classes are reasonably similar in terms of abort requirements and the selection between the two is a question of which is better suited to a particular architecture.

11.2.3. Architecture and Trajectory Selection

The investigation considered three candidate architectures which were selected to represent relevant Mars transportation scenarios that are still being actively considered as well as to provide options with a diverse range of post-TMI delta V potentials from which to draw abort capability conclusions. Each architecture was investigated to determine the achievable abort capability with the respective amount of residual delta V. The 1998 DRM 3.0 and Mars Direct architectures were analyzed in an assumed lifeboat configuration to maximize the delta V potential of their respective propellant amounts.

The 4.3 km/s 1999 DRM architecture effectively achieves a robust departure phase abort capability regardless of departure year, though shorter abort flight times result from the opportunity years of slower departure velocity. The entry abort mode is available throughout the departure phase for either the minimum total or minimum departure trajectory class even on the years of inertial maximums. The optimized Moon abort mode is also widely available, sometimes at a moderately shorter time of flight.

The 3.0 km/s 1998 DRM 3.0 architecture exhibits strong abort capability for the cases utilizing the minimum departure delta V trajectory class during the minimum inertial year. The capability dwindles significantly for the year of inertial maximum where there are great ranges of infeasibility. The minimum departure class also enables a limited Moon abort capability for this architecture during the inertial minimum, but the mode becomes unrealistic for faster departures. The free-return trajectory class exhibits almost no feasible abort capability for the 1998 DRM 3.0 architecture during the maximum inertial year.

The 2.0 km/s Mars Direct architecture has insufficient delta V, even in the lifeboat configuration to achieve any realistic abort capability beyond that of a severely limited set of achievable entry aborts during the year of inertial minimum.

An analysis of the velocity variation of the three different trajectory classes at the intermediary years of opportunity reveals that many of the minimum departure and minimum total delta V trajectory class opportunities are of comparable departure velocity as the minimum inertial opportunity year. It can therefore be assumed that

these intermediate years of opportunity can be expected to achieve similar abort capability as the capable minimum inertial year opportunity.

In conclusion, at least 4.0 km/s of post-TMI delta V capability is required of a Mars bound spacecraft in order to enable a comprehensive departure phase abort capability that is accessible across the fifteen year inertial period with resulting abort flight durations of less than three weeks. The abort modes available with such a propulsive ability are primarily entry aborts, though overlapping Moon aborts are typically achievable as well especially during the first two days of the departure transfer. It is recognized that this value exceeds the inherent post-TMI delta V capability of the majority of proposed architectures, especially those of the split-mission type that assume Mars aerocapture. It has been suggested in this work that such spacecraft retain an ability to be reconfigurable as lifeboats in the case of emergency by discarding unneeded transfer stores, descent hardware, and excess habitat and retaining all available propellant. Thus modified, the delta V capability could be increased to higher values. A 3.0 km/s post-TMI delta V capability is sufficient to enable continuous abort capability for the minimum inertial year of the minimum departure delta V trajectory class. An evaluation of the intermediate years of opportunity indicates that similar abort capability is achievable for over half of all departure opportunities of this class. A fair amount of departure phase abort capability is therefore achievable without severe scaling up of the baseline architecture elements. Should a more propulsively capable architecture such as the 1999 DRM be selected, it would have an inherent departure phase abort capability.

11.3. Recommendations for Future Work

The present investigation considered three departure phase abort modes: entry aborts, LEO aborts, and aborts to Moon orbit. The selection of these modes was based largely on the desirability of returning to Earth, in the case of the first two, and achieving a possible safe haven in as timely manner as possible, in the case of the Moon abort. As indicated by the presented results, the achievable aborts for the available amounts of delta V are typically of several weeks duration. Given that achieving any extensive departure phase abort capability will require a spacecraft capable of maintaining the crew for a period of at least two weeks duration, it is possible to imagine other abort modes that may be achievable besides the three investigated in this study. For example, many proposed Moon and Mars architectures make use of logistical nodes located at either the Earth-Moon or Sun-Earth Lagrange points. The abort delta V requirements for traveling to one of these nodes may show gains versus those considered in this study and may additionally contribute to further evaluation of the architecture proposals that utilize such points. Even if there was no extensive emplaced logistics at such points, perhaps it would be beneficial to pre-position an Earth crew return vehicle (ECRV) there, one that could be available to any outbound Mars flight should the need arise. This type of arrangement would also mitigate the problem posed by the absence of an ECRV as is characteristic in the baseline Mars Direct and 1998 DRM 3.0 architectures.

Another avenue of research that could be pursued is a more detailed analysis of the lifeboat configuration of the Mars transfer habitats/landers that was proposed in this work. The propulsive characteristics of these vehicles are similar for many

architectures and, in light of the results just presented, lack sufficient delta V to accomplish a departure phase abort in their baseline configuration. Any methods that could extract more delta V from the available propellant would be beneficial.

Finally, achieving a departure phase abort capability may not entail returning the crew to Earth at all. It is exactly the stop-and-turn-around feature of these aborts that makes them so propulsively expensive. Many architectures envision two or more launches per launch opportunity in a sustained Mars exploration program, usually one crew vehicle and one cargo vehicle. From an energetics viewpoint, it would be much easier to arrange a rendezvous of these tandem outbound spacecraft in the event the manned one experiences a failure. Depending on the architecture, the companion cargo shipment is often composed of a viable habitat or crew return vehicle as well as power and propellant. The feasibility of such a "wingman" option that considered the total implications for transfer trajectories of the different elements and system redundancies would be a very interesting topic for a detailed Mars architecture assessment.

Appendix A: Planetary Ephemerides

Algorithms for the orbital elements of the first five planets of the Solar system are given below as taken from Meeus[38]. The reference epoch is J2000 and the elements are given in units of degrees where applicable or astronomical units. Methods were given in the planetary ephemerides section of the text for the conversion of longitude of periapse and mean longitude into argument of periapse and true longitude.

MERCURY

a = 0.387098310

e = 0.20563175 + 0.000020406*TT - 0.0000000284*TT**2 - 0.00000000017*TT**3

i = 7.004986 - 0.0059516*TT + 0.00000081*TT**2 + 0.000000041*TT**3

Ω = 48.330893 - 0.1254229*TT - 0.00008833*TT**2 - 0.000000196*TT**3

$\tilde{\omega}$ = 77.456119 + 0.1588643*TT - 0.00001343*TT**2 + 0.000000039*TT**3

λ = 252.250906 + 149472.6746358*TT - 0.00000535*TT**2 + 0.000000002*TT**3

VENUS

a = 0.723329820

e = 0.00677188 -0.000047766*TT + 0.0000000975*TT**2 + 0.00000000044*TT**3

i = 3.394662 - 0.0008568*TT - 0.00003244*TT**2 + 0.000000010*TT**3

Ω = 76.679920 - 0.2780080*TT - 0.00014256*TT**2 - 0.000000198*TT**3

$\tilde{\omega}$ = 131.563707 + 0.0048646*TT - 0.00138232*TT**2 - 0.000005332*TT**3

λ =181.979801 + 58517.8156760*TT + 0.00000165*TT**2 - 0.000000002*TT**3

EARTH

a = 1.000001018

e = 0.01670862 - 0.000042037*TT - 0.0000001236*TT**2 + 0.00000000004*TT**3

i = 0.0000000 + 0.0130546*TT - 0.00000931*TT**2 - 0.000000034*TT**3

Ω = 0.0

$\tilde{\omega}$ = 102.937348 + 0.322555*TT + 0.00015026*TT**2 + 0.000000478*TT**3

λ = 100.466449 + 35999.3728519*TT - 0.00000568*TT**2 + 0.000000000*TT**3

MARS

a = 1.523679342

e = 0.09340062 + 0.000090483*TT - 0.0000000806*TT**2 - 0.00000000035*TT**3

i = 1.849726 - 0.0081479*TT - 0.00002255*TT**2 - 0.000000027*TT**3

Ω = 49.558093 - 0.2949846*TT - 0.00063993*TT**2 - 0.000002143*TT**3

$\tilde{\omega}$ = 336.060234 + 0.4438898*TT - 0.00017321*TT**2 + 0.000000300*TT**3

λ = 355.433275 + 19140.2993313*TT + 0.00000261*TT**2 - 0.000000003*TT**3

JUPITER

a = 5.202603191 + 0.0000001913*TT

e = 0.04849485 + 0.000163244*TT - 0.0000004719*TT**2 - 0.00000000197*TT**3

i = 1.303270 - 0.0019872*TT + 0.00003318*TT**2 + 0.000000092*TT**3

Ω = 100.464441 + 0.1766828*TT + 0.00090387*TT**2 - 0.000007032*TT**3

$\tilde{\omega}$ = 14.331309 + 0.2155525*TT + 0.00072252*TT**2 - 0.000004590*TT**3

λ = 34.351484 + 3034.9056746*TT - 0.00008501*TT**2 + 0.000000004*TT**3

Appendix B: Lambert's Problem Solution Algorithm

$\mu = 1$

$\cos(\Delta\nu) = \left(\frac{\vec{r}_1 \bullet \vec{r}_2}{r_1 r_2} \right)$

if (DM = -1)

$A = -\sqrt{r_1 r_2 (1 + \cos(\Delta\nu))}$

else if (DM = 1)

$A = \sqrt{r_1 r_2 (1 + \cos(\Delta\nu))}$

end if

If (Δυ = 0) position vectors parallel
If (A = 0) cannot calculate orbit

Initialize

$z = 0$ $z_{up} = (2\pi)^2$ $z_{low} = -16\pi$ $C2 = \frac{1}{2}$ $C3 = \frac{1}{6}$

while $|\Delta t - \Delta t_0| > 0.000001$

if $|C2| > 0.000001$

$y = r_1 + r_2 + \frac{A(zC3 - 1)}{\sqrt{C2}}$

else

$y = r_1 + r_2$

end if

if (A > 0) and (y < 0) Determine lowest bound that does not yield negative y

$ys = 0$

$zs_2 = z_{up}$

$z = 0$

$C2 = \frac{1}{2}$

$C3 = \frac{1}{6}$

do

$$zs_1 = \left(\frac{1}{C3}\right)\left(1 + (ys - r_1 - r_2)\frac{\sqrt{C2}}{A}\right)$$

if $|zs_2 - zs_1| <= 0.000001$

$z_{low} = zs_1$

exit

end if

call FindC2C3(zs1,C2,C3)

$zs_2 = zs_1$

end do

$z_{low} = zs_1$

$z_{up} = (2\pi)^2$

$z_n = \left(\frac{z_{up} + z_{low}}{2}\right)$

call FindC2C3(zn,C2,C3)

if $|C2| > 0.000001$

$y = r_1 + r_2 + \frac{A(z_n C3 - 1)}{\sqrt{C2}}$

else

$y = r_1 + r_2$

end if

end if

if $|C2| > 0.000001$

$x = \sqrt{\frac{y}{C2}}$

else

$x = 0$

end if

$\Delta t = \frac{x^3 C3 + A\sqrt{y}}{\sqrt{\mu}}$

if $\Delta t <= \Delta t_0$

$z_{low} = z$

else

$z_{up} = z$

end if

$z_n = \left(\frac{z_{up} + z_{low}}{2} \right)$

call FindC2C3(zn,C2,C3)

$z = z_n$

end while

$f = 1 - \frac{y}{r_1}$

$g = A\sqrt{\frac{y}{\mu}}$

$\dot{g} = 1 - \frac{y}{r_2}$

$\vec{v}_1 = \frac{\vec{r}_2 - f\vec{r}_1}{g}$ resulting initial velocity vector

$\vec{v}_2 = \frac{\dot{g}\vec{r}_2 - \vec{r}_1}{g}$ resulting final velocity vector

---

FindC2C3(z,C2,C3) returns C2 and C3 for input value of z

if $z > 0.000001$

$C2 = \frac{1 - \cos\left(\sqrt{z}\right)}{z}$

$C3 = \frac{\sqrt{z} - \sin\left(\sqrt{z}\right)}{\sqrt{z^3}}$

else if $z < -0.000001$

$C2 = \frac{1 - \cosh\left(\sqrt{-z}\right)}{z}$

$C3 = \frac{\sinh\left(\sqrt{-z}\right) - \sqrt{-z}}{\sqrt{(-z)^3}}$

else

$C2 = \frac{1}{2}$

$C3 = \frac{1}{6}$

end if

return

Appendix C: Planetary Physical and Orbital Data[40]

	MERCURY	*VENUS*	*EARTH*	*MOON*	*MARS*	*JUPITER*	*SATURN*	*URANUS*	*NEPTUNE*	*PLUTO*
Mass (10^{24} kg)	0.33	4.87	5.97	0.073	0.642	1899	568	86.8	102	0.0125
Diameter (km)	4879	12104	12756	3475	6794	142984	120536	51118	49528	2390
Density (kg/m^3)	5427	5243	5515	3340	3933	1326	687	1270	1638	1750
Gravity (m/s^2)	3.7	8.9	9.8	1.6	3.7	23.1	9	8.7	11	0.6
Escape Velocity (km/s)	4.3	10.4	11.2	2.4	5	59.5	35.5	21.3	23.5	1.1
Rotation Period (hrs)	1407.6	-5832.5	23.9	655.7	24.6	9.9	10.7	-17.2	16.1	-153.3
Length of Day (hrs)	4222.6	2802	24	708.7	24.7	9.9	10.7	17.2	16.1	153.3
Dist to Sun (10^6 km)	57.9	108.2	149.6	0.384	227.9	778.6	1433.5	2872.5	4495.1	5870
Perihelion (10^6 km)	46	107.5	147.1	0.363	206.6	740.5	1352.6	2741.3	4444.5	4435
Aphelion (10^6 km)	69.8	108.9	152.1	0.406	249.2	816.6	1514.5	3003.6	4545.7	7304.3
Orbital Period (days)	88	224.7	365.25	27.3	687	4331	10747	30589	59800	90588
Orbital Velocity (km/s)	47.9	35	29.8	1	24.1	13.1	9.7	6.8	5.4	4.7
Orbital Inclination (deg)	7	3.4	0	5.1	1.9	1.3	2.5	0.8	1.8	17.2
Orbital Eccentricity	0.205	0.007	0.017	0.055	0.094	0.049	0.057	0.046	0.011	0.244
Axial Tilt (degrees)	0.01	177.4	23.5	6.7	25.2	3.1	26.7	97.8	28.3	122.5
Mean Temperature (C)	167	464	15	-20	-65	-110	-140	-195	-200	-225
Surface Pressure (bars)	0	92	1	0	0.01	?	?	?	?	0
Number of Moons	0	0	1	0	2	63	47	27	13	3
Ring System	No	No	No	No	No	Yes	Yes	Yes	Yes	No
Global Magnetic Field	Yes	No	Yes	No	No	Yes	Yes	Ys	Yes	?

Appendix D1: Baseline CJI_MT Trajectories

Deparure Year	**2018**	**2020**	**2022**	**2024**	**2026**	**2028**	**2031**	**2033**
Departure Month	5	7	9	10	11	12	2	4
Departure Day	12	25	19	26	13	21	12	16
Departure Julian Date	2458251	2459056	2459842	2460610	2461358	2462127	2462910	2463704
Orbit Periapse Altitude (km)	300	300	300	300	300	300	300	300
Orbit Apoapse Altitude (km)	300	300	300	300	300	300	300	300
Orbit Periapse Velocity (km/s)	7.726	7.726	7.726	7.726	7.726	7.726	7.726	7.726
Escape Periapse Velocity (km/s)	11.238	11.497	11.829	11.841	11.37	11.378	11.433	11.29
TMI Maneuver (km/s)	**3.512**	**3.771**	**4.104**	**4.115**	**3.645**	**3.652**	**3.707**	**3.565**
Escape Time of Flight (hrs)	82.69	64.66	52.73	52.42	71.84	71.33	68	77.85
IJK Infinity Velocity (km/s)	2.79	3.697	4.628	4.658	3.282	3.309	3.494	2.993
Departure Inclination (deg)	37.25	28.5	46.75	49.25	29.5	28.5	33.25	56
Transfer Time of Flight (days)	**204**	**205**	**234**	**262**	**271**	**231**	**208**	**198**
Arrival Year	2018	2021	2023	2025	2027	2029	2031	2033
Arrival Month	12	2	5	7	8	8	9	10
Arrival Day	2	15	11	15	11	9	8	31
Arrival Julian Date	2458455	2459261	2460076	2460872	2461629	2462358	2463118	2463902
Orbit Periapse Altitude (km)	500	500	500	500	500	500	500	500
Orbit Apoapse Altitude (km)	500	500	500	500	500	500	500	500
Orbit Periapse Velocity (km/s)	3.315	3.315	3.315	3.315	3.315	3.315	3.315	3.315
Approach Periapse Velocity (km/s)	5.532	5.352	5.369	5.332	5.483	6.235	6.199	5.737
MOI Maneuver (km/s)	**2.216**	**2.037**	**2.054**	**2.017**	**2.168**	**2.919**	**2.884**	**2.422**
Mars Infinity Velocity (km/s)	2.961	2.61	2.645	2.569	2.869	4.128	4.074	3.328

Appendix D2: Baseline CJI_MD Trajectories

Deparure Year	**2018**	**2020**	**2022**	**2024**	**2026**	**2028**	**2031**	**2033**
Departure Month	5	7	9	10	11	12	1	4
Departure Day	18	19	8	13	13	10	28	5
Departure Julian Date	2458257	2459050	2459831	2460597	2461358	2462116	2462895	2463693
Orbit Periapse Altitude (km)	300	300	300	300	300	300	300	300
Orbit Apoapse Altitude (km)	300	300	300	300	300	300	300	300
Orbit Periapse Velocity (km/s)	7.726	7.726	7.726	7.726	7.726	7.726	7.726	7.726
Escape Periapse Velocity (km/s)	11.234	11.473	11.699	11.67	11.366	11.291	11.29	11.264
TMI Maneuver (km/s)	**3.508**	**3.747**	**3.974**	**3.944**	**3.64**	**3.565**	**3.564**	**3.538**
Escape Time of Flight (hrs)	83.14	65.86	56.59	57.59	72.15	77.8	77.92	80.21
IJK Infinity Velocity (km/s)	2.773	3.622	4.285	4.203	3.267	2.996	2.99	2.891
Departure Inclination (deg)	28.5	28.5	46.25	50.75	28.5	28.5	34.5	55.75
Transfer Time of Flight (days)	**235**	**193**	**204**	**220**	**272**	**222**	**190**	**178**
Arrival Year	2019	2021	2023	2025	2027	2029	2031	2033
Arrival Month	1	1	3	5	8	7	8	9
Arrival Day	8	28	31	21	12	20	6	30
Arrival Julian Date	2458492	2459243	2460035	2460817	2461630	2462338	2463085	2463871
Orbit Periapse Altitude (km)	500	500	500	500	500	500	500	500
Orbit Apoapse Altitude (km)	500	500	500	500	500	500	500	500
Orbit Periapse Velocity (km/s)	3.315	3.315	3.315	3.315	3.315	3.315	3.315	3.315
Approach Periapse Velocity (km/s)	5.698	5.473	5.933	6.219	5.54	6.764	7.248	6.148
MOI Maneuver (km/s)	**2.382**	**2.158**	**2.618**	**2.904**	**2.225**	**3.448**	**3.933**	**2.833**
Mars Infinity Velocity (km/s)	3.26	2.85	3.657	4.104	2.976	4.89	5.541	3.995

Appendix D3: Baseline FR_3Y Trajectories

Deparure Year	**2018**	**2020**	**2022**	**2024**	**2026**	**2028**
Departure Month	6	7	9	10	11	12
Departure Day	5	5	6	12	13	14
Departure Julian Date	2458275	2459036	2459829	2460596	2461358	2462120
Orbit Periapse Altitude (km)	300	300	300	300	300	300
Orbit Apoapse Altitude (km)	300	300	300	300	300	300
Orbit Periapse Velocity (km/s)	7.726	7.726	7.726	7.726	7.726	7.726
Escape Periapse Velocity (km/s)	11.982	11.931	11.759	11.733	11.683	11.503
TMI Maneuver (km/s)	**4.256**	**4.205**	**4.033**	**4.007**	**3.957**	**3.777**
Escape Time of Flight (hrs)	49.05	50.19	54.73	55.51	57.12	64.36
IJK Infinity Velocity (km/s)	5.005	4.882	4.445	4.376	4.241	3.716
Departure Inclination (deg)	32.75	28.5	41.25	44.25	28.5	28.5
Transfer Time of Flight (days)	**100**	**139**	**181**	**194**	**183**	**180**
Arrival Year	2018	2020	2023	2025	2027	2029
Arrival Month	9	11	3	4	5	6
Arrival Day	13	21	6	24	15	12
Arrival Julian Date	2458375	2459175	2460010	2460790	2461541	2462300
Orbit Periapse Altitude (km)	500	500	500	500	500	500
Orbit Apoapse Altitude (km)	500	500	500	500	500	500
Orbit Periapse Velocity (km/s)	3.315	3.315	3.315	3.315	3.315	3.315
Approach Periapse Velocity (km/s)	8.455	7.611	6.66	7.203	8.542	8.899
MOI Maneuver (km/s)	**5.14**	**4.296**	**3.345**	**3.887**	**5.227**	**5.584**
Mars Infinity Velocity (km/s)	7.047	6.008	4.746	5.481	7.151	7.574

Bibliography

[1] Hyle, Charles T., Foggatt, Charles E., Weber, Bobbie D., "Apollo Experience Report; Abort Planning," NASA Technical Note, NASA TN D-6847, June 1972.

[2] Bush, George W., "President Bush Announces New Vision for Space Exploration Program," White House Office of the Press Secretary, January 14, 2004.

[3]Griffin, Michael D., "Prepared Statement of Michael D. Griffin," The Future of Human Spaceflight, Hearing before the Committee on Science, House of Representatives, 108th Congress, 1st Session, 16 October, 2003, Serial-No 108-29.

[4] Snead, J.M., "Architecting Rapid Growth in Space Logistics Capabilities," AIAA-2004-4068, 40th AIAA/ASME/SAE/ASEE Joint Propulsion Conference and Exhibit, Fort Lauderdale, Florida, July 11-14, 2004

[5] Carpenter, M. S., Cooper, L.G., Glenn, J.H., Grissom, V.I., Schirra, W.M., Shepard, A.B., Slayton, D.K., We Seven, Simon and Schuster, Inc., New York, NY, 1962.

[6] Jenkins, Dennis R., Space Shuttle: The History of the National Space Transportation System. The First 100 Missions, Published by Dennis Jenkins, Cape Canaveral, FL, April 2001, ISBN: 0-9633974-5-1.

[7] Chaikin, Andrew, A Man on the Moon; the Voyage of the Apollo Astronauts, Penguin Books Ltd., New York, NY, 1994, ISBN 0-670-81446-6.

[8] Zubrin, Robert, The Case for Mars, Simon and Schuster, New York, NY, 1997, ISBN: 0-684-82757-3.

[9] Garriott, Owen K., Griffin, Michael D.; et all, "Extending Human Presence into the Solar System: An Independent Study for the Planetary Society on Strategy for the Proposed U.S. Space Exploration Policy," Planetary Society, July 2004.

[10] Lovell, Jim; Kluger, Jeffrey, Lost Moon: The Perilous Voyage of Apollo 13, Houghton Mifflin Company, New York, NY, 1994, ISBN: 0-395-67029-2.

[11] Exploration Systems Mission Directorate, "Exploration System of Systems Programmatic Guidelines and Requirements Document," Revision E, ESMD-RQ-0021, NASA Headquarters, Washington D.C., 24 March 2005.

[12] Columbia Accident Investigation Board, "Report of the Columbia Accident Investigation Board," U.S. Government Printing Office, August 2003.

[13] Coyne, Kevin, "NASA Ejection Seats: Gemini Spacecraft," The Ejection Site, http://www.ejectionsite.com/, Accessed April 20, 2007.

[14] Brooks, C.G., Grimwood, J.M., Swenson, L.S., "Chariots for Apollo: A History of Manned Lunar Spacecraft," NASA History Series, NASA SP-4205, 1979.

[15] NASA, The First Man in Space, Soviet Radio and Newspaper Reports on the Flight of the Spaceship, Vostok, Compiled and Translated by Joseph L. Zygielbaum, Jet Propulsion Laboratory, California Institute of Technology, Pasadena, California, May 1, 1961.

[16] Clark, Philip, *The Soviet Manned Space Program*, Salamander Books, London, 1988. *ISBN*: 051756954X.

[17] Wade, Mark, "Encyclopedia Astronautica: Shenzou," Accessed April 19, 2007. http://www.astronautix.com/craft/shenzhou.htm

[18] Joels, K. M., Kennedy, G.P., Larkin, D., The Space Shuttle Operator's Manual, Balantine Books, New York, Revised Edition 1988, ISBN 0-345-34181-3

[19] Craft, J., Ess, R., Sauvageau, D., "Achieving Space Shuttle Abort-to-Orbit Using the Five-Segment Booster," AIAA 2003-5127, AIAA Joint Propulsion Conference, Huntsville, AL, July 21-23, 2003.

[20] Cucinotta, F.A., Manuel, F., Jones, J., Izsard G., Murray, J., Djojonegoro B., and Wear M., Space Radiation and Cataracts in Astronauts. *Radiation. Research.* 156, 460-466, 2001a.

[21]Titus, R.R., "A New Criterion for Mission Selection-Abort Capability," *AIAA Journal of Spacecraft,* Vol. 6, No. 4, April 1969, p 403.

[22] Rall, C.S., "Free-Fall Periodic Orbits Connecting Earth and Mars," Sc.D. Thesis, Department of Aeronautics and Astronautics, M.I.T., Cambridge, MA, Oct. 1969.

[23] Rall, C.S., Hollister, W.M., "Free-Fall Periodic Orbits Connecting Earth and Mars," AIAA Paper 71-92, January 1971.

[24] Hollister, W., "Castles in Space," Astronautica Acta, Vol. 14, 1969, pp. 311-316.

[25] Hollister, W., "Periodic Orbits for Interplanetary Flight," *AIAA Journal of Spacecraft and Rockets*, Vol. 6, No. 4, 1969, pp 366-369.

[26] Aldrin, E., "Cyclic Trajectory Concepts, " SAIC presentation to the Interplanetary Rapid Transit Study Meeing, Jet Propulsion Laboratory, October 1985.

[27] Byrnes, D.V., Longuski, J.M., Aldrin, E., "Cycler Orbit Between Earth and Mars," *AIAA Journal of Spacecraft and Rockets*, Vol. 30, No. 3, May-June 1993, p 334.

[28] Walberg, G., "How Shall We Go to Mars? A Review of Mission Scenarios," *Journal of Spacecraft and Rockets*, Vol. 30, No. 2, pp. 129-139, 1993.

[29] Bonin, G., "A Low-Energy Mission Architecture for Reusable Earth-Mars Cyclers," CMAS Mars Project, Carleton University, Ottawa, ON, 2005.

[30] Linder, N., Vasile, M., "Comparison between Cyclers and Stop-over Cyclers fro a Regular Earth-Mars Transportation System," Dynamics and Control of Systems and Structures in Space (DCSSS), 6th Conference, Riomaggiore, Italy, July 2004.

[31] Patel, M.R., Longuski, J.M., Sims, J.A., "Mars Free Return Trajectories," *Journal of Spacecraft and Rockets*, Vol. 35, No. 3, May-June 1998.

[32] Tartabini, P.V., "Abort Options for Potential Mars Missions," *Journal of Spacecraft and Rockets*, Vol. 31, No. 4, July-August 1994, p 543.

[33] Vallado, David A., Fundamentals of Astrodynamics and Applications, Second Edition, Microcosm Press and Kluwer Academic Publishers, 2001, ISBN: 1-881883-12-4.

[34] U.S. Naval Observatory Astronomical Applications Department, "Julian Date Converter", http://aa.usno.navy.mil/data/docs/JulianDate.html , Accessed July 2006.

[35] Bate, Roger R., Mueller, Donald D., White, Jerry E., Fundamentals of Astrodynamics, of the Department of Astronautics and Computer Science, United States Air Force Academy, Dover Publications, Inc., New York, 1971, ISBN 0-486-60061-0.

[36] NASA Human Spaceflight homepage, "Orbital Elements," http://spaceflight.nasa.gov/realdata/elements/graphs.html, Accessed July 2006.

[37] Wittmann, A., "The Obliquity of the Ecliptic," Astronomy and Astrophysics, vol. 73, no. 1-2, Mar. 1979, p. 129-131.

[38] Meeus, Jean, "*Astronomical Algorithms,"* Willmann-Bell, Inc., Richmond, VA, 1991, 477pp.

[39] Chapra, S.C., Canale, R.P., Numerical Methods for Engineers, 4th Edition, McGraw Hill, 2002, ISBN 0-07-243193-8.

[40] National Space Science Data Center, "Planetary Fact Sheets,", NASA Goddard Spaceflight Center, http://nssdc.gsfc.nasa.gov/ ,version 4.3.10, updated: 01 May 2006

[41] Matousek, S., Sergeyevsky, A.B., "To Mars and Back: 2002-2020 Ballistic Trajectory Data for the Mission Architect," AIAA-98-4396, AIAA/AAS Astrodynamics Specialist Conference, Boston, MA, Aug 10-12, 1998.

[42] Boden, Daryl and Hoffman, Stephen, "Chapter 9: Orbit Selection and Astrodynamics," Human Spaceflight: Mission Analysis and Design, Editors: Larson, Wiley and Pranke, Linda, McGraw-Hill, New York, NY, ISBN:0-07-236811-X.

[43] Hoffman, S.J., McAdams, J.V., Niehoff, J.C., "Round Trip Trajectory Options for Human Exploration of Mars," AAS 89-201, Advances in the Astronautical Sciences, vol. 69.

[44] Soldner, J.K., "Round-Trip Mars Trajectories: New Variations on Classic Mission Profiles," AIAA-90-2932, AIAA/AAS Astrodynamics Conference, Portland, OR, Aug 20-22, 1990.

[45] Lineberry, E.C., Soldner, J.K., "Mission Profiles for Human Mars Missions," AIAA-90-3794, AIAA Space Programs and Technologies Conference, Huntsville, AL, September 25-28, 1990.

[46] Walberg, G., "How Shall We Go To Mars? A Review of Mission Scenarios," AIAA-92-0481, 30th Aerospace Sciences Meeting and Exhibit, Reno, NV, January 6-9, 1992.

[47] Landau, D.F., Longuski, J.M., "A Reassessment of Trajectory Options for Human Missions to Mars," AIAA 2004-5095, AIAA/AAS Astrodynamics Specialist Conference and Exhibit, Providence, RI, August 16-19, 2004.

[48] Wolf, A.A., "Free Return Trajectories for Mars Missions," AAS 91-123, AAS/AIAA Spaceflight Mechanics Meeting, Houston, TX, February 11-13, 1991.

[49] Okutsu, M., Longuski, J.M.,"Mars Free Returns via Gravity Assist from Venus," *Journal of Spacecraft and Rockets*, Vol. 39, No. 1, January-February 2002, pp 31-36.

[50] Putnam, Z.R., Braun, R.D., Rohrshneider, R.R., Dec, J.A.,"Entry System Options for Human Return from the Moon and Mars," AIAA 2005-5915, AIAA Atmospheric Flight Mechanics Conference and Exhibit, San Francisco, CA, August 15-18.

[51] Johnson, J.E., Starkey, R.P., Lewis, M.J., "Aerodynamic Stability of Reentry Heat Shield Shapes for a Crew Exploration Vehicle," *Journal of Spacecraft and Rockets*, 0022-4650 Vol.43, No.4, (721-730), 2006.

[52] Korkan, K.D., Hanley, G.M., "Apollo Command Module Aero-Thermodynamic Characteristics at Hypersonic Earth Entry Velocities," AIAA 1965-491, American

Institute of Aeronautics and Astronautics Annual Meeting, 2nd, San Francisco, CA, July 26-29, 1965.

[53] Shapland, D.J., Price, D.A., Hearne, L.F., "A Configuration for Re-Entry from Mars Missions Using Aerobraking," *Journal of Spacecraft*, Vol. 2, No. 4, July-August, 1965.

[54] Strouhal, G., Curry, D.M., Posgay, R.G., "Definition of Entry Corridor Thermal Limits for Apollo Spacecraft," AIAA-1968-1144, Manned Spacecraft Center and TRW Systems Group, Houston, TX, 1968.

[55] Pavlosky, J.E., St Leger, L.G., "Apollo Experience Report – Thermal Protection Subsystem," NASA Technical Note, NASA TN D-7564, January 1974.

[56] Donahue, B. B., "Comparative Analysis of Current NASA Human Mars Mission Architectures," *Journal of Spacecraft and Rockets*, Vol.38, No.5, (745-751), September-October 2001.

[57] Griffin, B., Thomas, B. Vaughn, D., Drake, B., Johnson, L., Woodcock, G., "A Comparison of Transportation Systems for Human Missions to Mars," AIAA-2004-3834, 40th AIAA/ ASME/ SAE/ ASEE Joint Propulsion Conference and Exhibit, Fort Lauderdale, Florida, July 11-14, 2004.

[58] Drake, Bret G, Editor, "Reference Mission Version 3.0 - Addendum to the Human Exploration of Mars: The Reference Mission of the NASA Mars Exploration Study Team," NASA Special Publication NASA/SP 6107-ADD, June 1998.

[59] Zubrin, R.M., Weaver, D.B., "Practical Methods for Near-Term Piloted Mars Missions," AIAA-1993-2089, 29th AIAA/ ASME/ SAE/ ASEE Joint Propulsion Conference and Exhibit, Monterey, California, June 28-30, 1993.